UNCLASSIFIED
CONFIDENTIAL

WT-1401

This document consists of 202 pages.

No. 139 of 200 copies, Series A

OPERATION PLUMBBOB

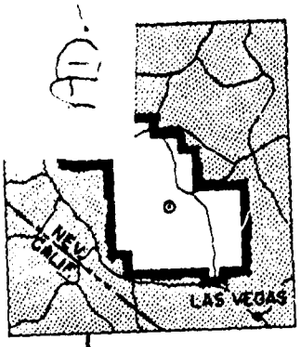

NEVADA TEST SITE
MAY-OCTOBER 1957

Project 1.1

Classification (~~Cancelled~~) (Changed to UNCL.
By Authority of TID 1400 32
By Angela Lawhon 7-23-96

BASIC AIRBLAST PHENOMENA (U)

Classification (~~Cancelled~~) (~~Changed to~~ Confirmed)
By Authority of W. Rugg DOE/NIC + DNI/OMA dtd 5 Feb 1999
By [illegible] Date 19 July 1999

Issuance Date: June 30, 1962

HEADQUARTERS FIELD COMMAND
DEFENSE ATOMIC SUPPORT AGENCY
SANDIA BASE, ALBUQUERQUE, NEW MEXICO

Statement A
Approved for public release;
Distribution unlimited.

[redacted]

Handle as Restricted Data in foreign dissemination. Section 144b, Atomic Energy Act of 1954.

This material contains information affecting the national defense of the United States within the meaning of the espionage laws, Title 18, U.S.C., Secs. 793 and 794, the transmission or revelation of which in any manner to an unauthorized person is prohibited by law.

[redacted]

Inquiries relative to this report may be made to

Chief, Defense Atomic Support Agency
Washington 25, D. C.

When no longer required, this document may be destroyed in accordance with applicable security regulations.

DO NOT RETURN THIS DOCUMENT

USAEC Division of Technical Information Extension, Oak Ridge, Tennessee

WT-1401

OPERATION PLUMBBOB—PROJECT 1.1

BASIC AIRBLAST PHENOMENA (U)

E. J. Bryant, Project Officer
J. H. Keefer

Ballistic Research Laboratories
Aberdeen Proving Ground, Maryland

ABSTRACT

Surface level overpressures and dynamic pressures were measured during 14 shots of Operation Plumbbob. The objectives were met in that useful information was obtained on (1) overpressure and dynamic pressure as a function of time and distance, (2) formation and history of precursor waveforms, (3) applicability of scaling laws for determining surface and near-surface pressure from high-altitude bursts, and (4) validity of the pressure-distance curve in the low-pressure region.

In these experiments, 223 overpressure-time gages and 57 dynamic pressure-time gages were used. These gages yielded 174 overpressure and 47 dynamic pressure records of good quality.

Shot Priscilla was the first test during which emphasis was placed on the high-pressure region. A sharp rising classical pressure-time wave was measured at 350 and 450 feet, and it was not until the third station at 650 feet that a precursor wave was observed. During Shot Priscilla, a good comparison was obtained between the predicted blast wave parameters and the measured values.

Nine shots were instrumented for precursor waveform information, and precursors were observed on six of the nine. All precursor-producing shots provided waveform data in the desired region above 50 psi.

Ten self-recording, low-pressure gages were used to make surface and near-surface overpressure measurements at five stations during Shot John. Seven gages gave good pressure-time records, two recorded peak pressure, and one failed to record.

Measurements in the low-pressure region (0.1 to 1 psi) showed large variations in maximum pressure and indicated that temperature and wind velocity can substantially change a shock wave when the pressure is weak and the travel time is long.

FOREWORD

This report presents the final results of one of the 46 projects comprising the military-effect programs of Operation Plumbbob, which included 24 test detonations at the Nevada Test Site in 1957.

For overall Plumbbob military-effects information, the reader is referred to the "Summary Report of the Director, DOD Test Group (Programs 1–9)," ITR–1445, which includes: (1) a description of each detonation, including yield, zero-point location and environment, type of device, ambient atmospheric conditions, etc.; (2) a discussion of project results; (3) a summary of the objectives and results of each project; and (4) a listing of project reports for the military-effect programs.

CONTENTS

[redacted]

[redacted]

[redacted]

Chapter 1

BASIC AIRBLAST PHENOMENA, SHOT PRISCILLA

1.1 INTRODUCTION

Basic measurements of airblast resulting from the detonation of nuclear weapons are necessary to evaluate blast damage to targets of military significance. As a result of measurements obtained during past tests of nuclear explosions, the pressure-time behavior of shock waves producing overpressures in the 5- to 100-psi range is fairly well known. To determine the considerations involved in designing structures to withstand damage at higher pressure limits than were set previously, there has developed a need for investigations of basic phenomena at pressure levels in excess of 100 psi.

1.1.1 Objectives. The primary objective of Project 1.1 was to obtain data on overpressure versus time and dynamic pressure versus time as a function of distance during Shot Priscilla. The pressure range of interest in this shot was from 5 to 1,000 psi for overpressure and from 1 to 650 psi for dynamic pressure.

Additional objectives were to: (1) obtain free-field blast measurements at specific locations as required by various organizations conducting equipment or structure tests during Shot Priscilla and (2) continue the evaluation of modifications in gage designs, instrument components, and measurement techniques.

1.1.2 Background. Basic blast measurements from atomic detonations are needed to properly evaluate blast damage to various types of structures of military significance. The blast measurements made during Operation Upshot-Knothole (References 1 through 3) were not sufficient to fully define the parameters most significant in causing damage. In particular, the occurrence of precursor phenomena and distorted waveforms made uncertain the relations between overpressure and dynamic pressure. During Operation Teapot (References 4 and 5) as well as in other operations, considerable information was gathered in the low- and intermediate-overpressure regions for devices of various yields. Within these regions from 5 to 100 psi, overpressure measurements are comprehensive. Although some uncertainty still exists concerning the relation between overpressure and dynamic pressure in the precursor zone, sufficient data was obtained during Operation Teapot (References 4 and 5) from dynamic-pressure measurements to permit predictions on an empirical basis. The test results of Operation Teapot indicate that the factors influencing precursor formation and flow characteristics behind blast waves are surface conditions, height of burst (HOB), and yield of the device.

Recently, emphasis has been placed on the design of structures capable of resisting blast pressures in excess of 100 psi. The requirement for an accurate understanding of the nature of blast waves of these intensities and the desire for accurate knowledge of the pressures acting on the test structures have necessitated measurements at pressures up to 1,000 psi. Plumbbob is the first operation where such measurements have been made.

In past tests, asymmetries in blast pressure contours have been noted (Reference 4), that is, a pressure indicated at a given distance along one radius from ground zero may not be found at

the same distance along another. This dictates the installation of individual gages at each structure to provide the true pressure-time histories required in the analysis of structural response.

Recently, a study has been conducted at the Ballistic Research Laboratories (BRL) by which an empirical method was devised for predicting the waveforms in the precursor zone. Although much data is already available for devising this prediction method, it is felt that gaps do exist and also that the method needs to be further verified. The capability of predicting waveforms becomes important in considering design of structures for withstanding the blast forces acting thereon.

1.1.3 Predictions of Blast Phenomena for Shot Priscilla. For this study, Shot Priscilla was assumed to be a 40-kt device detonated at 700 feet above the surface of Frenchman Flat. The shot characteristics and the scaling factors assumed are shown in Table 1.1. The atmospheric pressures of previous shots on Frenchman Flat indicated that the variation of pressure versus height of the National Advisory Committee for Aeronautics (NACA) standard atmosphere probably would be very near the atmospheric conditions occurring at shot time. Atmospheric temperatures were estimated on the basis of average temperatures for previous shots on Frenchman Flat.

The characteristics of the previous shots of interest are given in Table 1.2 for comparison.

Shot 10 of Operation Upshot-Knothole was scaled so that its A-scaled burst height of 204 feet was maintained, i.e., it was scaled to 40 kt at 740 feet height of burst. (A-scaling is the use of $W^{1/3}$ scaling to normalize all values to 1 kt at sea level.) Other shots were scaled to Shot Priscilla, assuming that the variation in their A-scaled burst height from 195 feet would not produce a significant change in the resulting curves. For pressures over an ideal surface and above 100 psi, the curves from Reference 6 were used. Below 100 psi the curve from the good-surface chart in TM 23-200 (Reference 7) was used for overpressure, and the curve from Reference 8 was used for dynamic pressure.

Figure 1.1 contains the estimated curve for peak overpressure versus distance for Shot Priscilla. The limits of experimental data from previous events are indicated. Data obtained during shots of yield approximately equal to Shot Priscilla was used to determine the curve. The predicted curve at less than 500 feet ground range in Figure 1.1 was estimated under the assumption that the pressure in the regular reflection region would be equal to less than the maximum reflected pressure at normal incidence of the free-air shock wave. Figure 1.2 shows a plot of the data used, as well as the ideal and the estimated curves.

Figure 1.3 shows the estimated curve for maximum dynamic pressure versus distance, the ideal curve as derived from the ideal overpressure curve, and a plot of previous data. The Teapot Shot 12 data essentially determined the curve. Teapot Shots 4 and 13 indicate that, for yields greater than Shot 12, dynamic pressures may be higher than ideal beyond the 4,000-foot ground range in Figure 1.3. The curve indicated by Shot 12 data was extended arbitrarily to ranges less than 1,500 feet.

The curve of the arrival time of the blast wave initial disturbance estimated for Shot Priscilla is shown in Figure 1.4 and the data used in deriving this curve is shown in Figure 1.5 scaled to 40 kt.

Figure 1.6 shows the estimated curve of the positive-phase duration based on data from previous shots. Also included in Figure 1.6 is the predicted curve of positive-phase duration obtained from TM 23-200.

1.1.4 Corrections of Dynamic Pressure Measurements. Plots of the dynamic pressure data indicated in Figure 1.3 represent the as-read values, and some of these data points contain to some degree the influence of dust present in the flow. A relative comparison between these values and the ideal dynamic pressure is not valid even if the influence of the dust in the flow was negligible. The ideal dynamic pressures define the free-stream conditions whereas the as-read values require corrections to take into account the compressibility resulting from the immersion of a body such as the pitot gage into the flow. For the condition when the blast wave

is dust-laden, compressibility corrections are also necessary for the air phase portion of the wave to indicate free-stream conditions. Hence, a more realistic comparison with the ideal values would be to use appropriate corrections to the as-read data.

It was realized that agencies taking dynamic pressure measurements had different types of gages and used different notations for the response parameters of the gage as well as different correction techniques for angle of flow and Mach compressibility to yield free-stream dynamic pressure. Correct comparison of this data was difficult.

After the completion of the field test phase following Operation Plumbbob, a conference was called (Reference 9) involving several agencies participating in nuclear field tests to resolve existing problems concerning the measurement and proper interpretation of dynamic pressure, particularly when the blast wave was dust-laden. The agencies represented were Headquarters Armed Forces Special Weapons Project (AFSWP) (now Defense Atomic Support Agency, DASA) Field Command, AFSWP; Naval Ordnance Laboratory (NOL); Stanford Research Institute (SRI); BRL; and Sandia Corporation (SC). Agreement was reached at this meeting to standardize the nomenclature for reporting of dynamic pressure data and to also apply the appropriate correction factors for each type gage used. The nomenclature agreed upon and response of each gage are given in Table 1.3 and Figure 1.7, respectively.

The correction factor for Mach compressibility and corrections for angle of flow, where applicable, are presented in this report for the BRL q-gages only. Further information about the treatment of data concerning the remaining gages can be obtained from Reference 10.

The as-read value from the BRL q-gage when no dust is present behind the shock wave is given by:

$$q'_c = (P_t - P_s)' \text{ for } M < 1 \tag{1.1a}$$

or

$$q'_c = (P_p - P_s)' \text{ for } M > 1 \tag{1.1b}$$

For the clean air case, the free-stream dynamic pressure is defined by:

$$q = \frac{1}{2}\rho u^2 \tag{1.2}$$

The relationships for determining the free-stream dynamic pressure behind a clean blast wave from the measurements taken expressed in terms of isentropic flow and normal shock wave equations (Reference 11) are:

For $M < 1$

$$\frac{P'_t}{P'_s} = \left(1 + \frac{\gamma - 1}{2} M^2\right)^{\gamma/\gamma - 1} \tag{1.3}$$

The value of q can be related to the static pressure P_s and to the Mach number M in accordance with the following relations:

$$q = \frac{1}{2}\rho u^2 = \frac{\frac{1}{2}\rho u^2}{C^2} \frac{\gamma P_s}{\rho} = \frac{\gamma M^2 P_s}{2} \tag{1.4}$$

Where: $C^2 = \frac{\gamma P_s}{\rho}$

To correct the q'_c value of Equation 1.1a use is made of Equations 1.3 and 1.4, yielding the following:

$$q = \frac{(P_t - P_s)'}{\frac{2}{\gamma M^2}\left[\left(1 + \frac{\gamma - 1}{2} M^2\right)^{\gamma/\gamma - 1} - 1\right]} \tag{1.5a}$$

or:

$$q = \frac{(P_t - P_s)'}{1 + 1/4\,M^2 + 1/40\,M^4 + \text{----}} \tag{1.5b}$$

Equations 1.5a and 1.5b are known as the pitot tube equations. Use of the latter two equations becomes superfluous, since it would suffice to use Equation 1.3 to obtain the Mach number and by Equation 1.4, using $\gamma = 1.4$, the q or free-stream dynamic pressure is derived directly. Another advantage for using Equation 1.4 is that, for supersonic flow, it is necessary to correct the total head pitot pressure P_p to the free-stream total pressure P_t prior to use of Equations 1.5a or 1.5b.

Hence: For $M > 1$

$$\frac{P_t}{P_p'} = \left[\left(\frac{2\gamma}{\gamma+1}\ M^2 - \frac{\gamma-1}{\gamma+1}\right)\right]^{\frac{1}{\gamma-1}} \left[\frac{1 + \frac{\gamma-1}{2}\ M^2}{\frac{\gamma+1}{2}\ M^2}\right]^{\gamma/(\gamma-1)} \tag{1.6}$$

and:

$$\frac{P_p'}{P_s'} = \left[\frac{\left(\frac{\gamma+1}{2}\ M^2\right)^{\gamma}}{\left(\frac{2\gamma}{\gamma+1}\ M^2 - \frac{\gamma-1}{\gamma+1}\right)}\right]^{1/(\gamma-1)} \tag{1.7}$$

Obviously, Equation 1.6 is not necessary when use is made of Equation 1.4.

In Summary, for $M < 1$, Equation 1.3 along with Equation 1.4 yields the free-stream dynamic pressure, and Equation 1.7 combined with Equation 1.4 yields the free-stream dynamic pressure for $M > 1$.

The above considerations are for the clean blast wave. When the blast wave is dust-laden, the free-stream dynamic pressure is defined by the combination of the airflow and momentum flux of dust, i.e.,

$$q_c^{*\prime} = q + \phi_d \tag{1.9}$$

The response of the BRL q-gage is given by:

$$q_c^{*\prime} = \left(P_t^{*\prime} - P_s\right) \text{ for } M < 1 \tag{1.10a}$$

or:

$$q_c^{*\prime} = \left(P_p^{*\prime} - P_s\right) \text{ for } M > 1 \tag{1.10b}$$

This may also be expressed by the following equation:

$$q_c^{*\prime} = (q_c + n\phi_d)' \tag{1.11}$$

Preliminary investigations of the dust registry coefficient n for the BRL q-gage shows the value to be small (Reference 12) lying between 0.12 and 0.21.

The problem of obtaining free-stream dynamic pressure in the presence of dust, therefore, is to measure separately the contributions to the dynamic pressure resulting from air alone and that resulting from dust. To realize this condition, at least two different gages are required, with known registry coefficients for both. With these two values known, the momentum flux could be determined and then from Equation 1.11, the air portion q_c would be known. Expressing the above mathematically would yield the following:

$$q^{*\prime}_{c_1} = q'_c + n_1 \phi_d \tag{1.12a}$$

and:

$$q^{*}_{c_2} = q'_c + n_2 \phi_d \tag{1.12b}$$

Combining the above results in:

$$\phi_d = \frac{q^{*\prime}_{c_1} - q^{*\prime}_{c_2}}{n_1 - n_2} \tag{1.13}$$

Now since q_c' is related to P_t and P_s in accordance to Equation 1.1a, e.g.,

$$P'_t \text{ (air)} = q'_c + P'_s \text{ for } M < 1 \tag{1.14}$$

the treatment for correcting the compressibility effect to obtain free-stream air dynamic pressure will be similar to that described.

Although Equation 1.14 is indicated to hold for the subsonic case, it is believed that it may be applicable for either the subsonic or supersonic case as pointed out in Reference 10.

When the flow is not parallel to the long axis of the q-gage body, corrections are required for the pitch and/or yaw angle of flow. For some gages, corrections are required when the flow is parallel. Wind tunnel tests of the SC gage (Reference 13) indicated corrections for zero angles of pitch and yaw as a function Mach number. Since the BRL q-gage is similar in shape, but somehwat larger in size compared to the SC gage, the same correction factors were applied to the BRL gage for zero angle of flow wherever applicable.

1.2 PROCEDURE

The main endeavor of Project 1.1 was made for the military-effect shot (Priscilla) of Operation Plumbbob. For this event, 38 self-recording gage installations at 16 stations along the main blast line were used. The station numbers, distances, and the numbers and types of gages used are given in Table 1.4. Additional installations of self-recording gages were provided to furnish blast data within the vicinity of the various project stations, as indicated in Table 1.5. Not all of the gages provided the various projects were for free-field blast phenomena—some were used for loading studies, and some were for special effects studies.

1.2.1 Selection of Gage Stations. The locations of the gage stations were dictated by requirements that a blast line be instrumented to give representative data concerning pressure-time histories and that the magnitude of overpressure in the vicinity of certain structures and project stations be measured.

The expected overpressure at any particular distance from ground zero was determined from the AFSWP composite curve of pressure versus distance (Reference 7) as well as the prediction curves discussed in Section 1.1.3 of this report, which were based on data obtained from numerous detonations over a desert surface and scaled to 1 kt at sea level.

Gages were installed at stations where new data concerning high pressures could be obtained. The gages at intermediate stations obtained data for correlation with previous test shots. Gages at the most distant stations were installed to detect the region in which the waveform makes the transition from precursor shape to classical shape. The station layout along the blast line for Shot Priscilla is shown in Figure 1.8.

1.2.2 Instrumentation. All of the instruments used by Project 1.1 to gather primary data for the project and supplementary data for other projects were self-recording gages. Two types were used: overpressure-time (P_t) gages and dynamic pressure-time (q) gages. With the exception of five dynamic pressure-time (q) gages, of an experimental model, all of the q-gages used on the test were essentially the same as used during previous operations (References 4 and 14).

The difficulties encountered and experience gained during the past operations led to many modifications of the gages for use during Operation Plumbbob. Figures 1.9 through 1.11 show the P_t-gage, q-gage, and the new prototype q-gage.

Pressure versus Time Gages. Some minor modifications were made to the P_t-gages. A new thermal link was designed in which the metal creep in the thermally sensitive solder is minimized.

The photo-initiation circuit was changed to keep the initiation circuit separate from any timing circuit. The initiation circuit was repackaged with circuit components potted. All changes were made to make the P_t-gage an even more reliable and accurate instrument while maintaining its portability and ease of installation and recovery.

In addition, the gages at the stations close to ground zero were modified to be initiated by a timing signal. The hard-wire initiation was used on one of the two gages on the first five stations on the blast line. The hard-wire-initiated gages are listed in Table 1.6 with a letter "B" after the station number. The signal for the gages was produced by the closure of a standard Edgerton, Germeshausen and Grier (EG&G) timing relay at -5 seconds and was used to close the electrically latching relay. The operation of the -5-second relay was duplicated by a second relay at -1 second.

The thermal initiator used during the P_t-gage during Operation Plumbbob operated similarly to the initiator used during Operation Redwing. However, to prevent premature initiation caused by creep in the solder material, the overlapped portion of the thermally sensitive link was modified so as to require actual separation of the two portions before initiation of the gage could take place.

The photo-initiation system, which was actuated by the sharp transient character of incident light from the detonation, employed a cadmium-sulfide cell, a transistorized amplifier, and a sensitive relay. In field use, a density-of-3 neutral filter was placed directly over the photocell to reduce the quiescent current and to eliminate pre-initiation caused by random pulses of light.

A schematic diagram of the complete photo-initiation circuit of the pressure-time gage is shown in Figure 1.12. To prepare the gage for recording, the activating microswitch SWI, which completes the ground return circuit and which is normally open, was closed. The amplifier circuit is an ordinary grounded emitter utilizing a CK722 PNP transistor. Prior to initiation, the transistor is biased nearly to cutoff by resistor R_1, which is connected to the positive terminal of the 45-volt battery. At zero time, light impinging upon the photocell reduces the resistance by a factor of approximately 10^6. As a result, a large negative pulse appears at Point A. This negative pulse, coupled through Capacitor C1 to the base of the transistor, causes the transistor to conduct heavily. This current surge closes the sensitive relay (RL-1), which is in series with the transistor collector and the negative side of the battery.

A pair of normally open contacts on RL-1 were used to latch the relay in the closed position by placing the battery voltage directly across the relay coil. The increased current, 5.6 ma, through the relay insured continuous contact closure, despite blast and ground shocks. The other set of relay contacts was used to apply voltage from the 8-volt mercury-cell source to the drive motor. This started the recording cycle, and the turntable continued to rotate a predetermined number of revolutions until the star cam opened the normally closed microswitch (SWII), which disconnected the motor and the transistor from their respective voltage supplies.

For protection against dirt and moisture, a portion of the amplifier circuit was potted in an epoxy resin.

The basic component common to the self-recording gages is a pressure-sensing capsule. Fundamentally, the new capsules used during Operation Plumbbob were similar to those used previously. Capsules with ranges from 0 to 5 psi up to 0 to 1,000 psi were used in the self-recording gages. The capsules with ranges from 0 to 800 psi and 0 to 1,000 psi were developed specifically for use during Operation Plumbbob.

The characteristics of the individual pressure capsule were known from the calibration curves supplied by the manufacturer. These curves showed the deflection of the stylus as a function of

the pressure. Laboratory calibration of a group of capsules selected at random showed the manufacturer's calibration curves to be sufficiently reliable to be used without further check.

The heart of the timebase in the pressure-time and dynamic pressure gages is the A. W. Haydon, Series 5600, chronometrically governed, dc motor (Reference 14).

A study was undertaken in BRL to determine the reliability of the motor under field conditions. Tests were performed to obtain turntable behavior, as a function of time, from the instant power was applied until it was removed and to study the effect of shock acceleration as great as 80 g.

The first tests determined the consistency of the length of time required for the motor to reach constant velocity. Oscillograph traces were made showing motor current, turntable rotation, and reference time for free motors and for motors loaded in the manner in which they were to be used. This data was then plotted as turntable rotation versus time (Figure 1.13 and 1.14). For the 3-rpm motors, the data shows that they attained full velocity in approximately 100 msec, exceeded their rated velocity, and then settled down to constant speed. Overshoot and oscillation were decreased by loading, but in no case lasted longer than 400 msec. The difference between the plot of total angular displacement versus time and a linear extrapolation to zero rotation of constant velocity never exceeded 20 msec after plus 50 msec from zero time. The time difference between the point of intersection of the extrapolated line with the x-axis and true zero as indicated on the plotted curve was 65 msec, with a standard deviation about this value of 11 msec. As a result of the test of 10-rpm motors, the data shows that the motors attained constant velocity in approximately 400 msec without exceeding the rated velocity or oscillating about this velocity prior to reaching constant speed. For these motors the time difference between the point of intersection of an extrapolated line of constant rotation with the x-axis and true zero, as shown on the plotted curve, was about 150 msec.

The second group of tests was made to determine the effect of shock on turntable velocity. Again, oscillograph traces were made of turntable rotation, motor current, and reference time while the gage was subjected to shock in a Barry 150 VD medium-impact-shock machine. The motors were tested under impacts as high as 80 g with a duration of 12 msec. Shock-acceleration tests were run in preference to vibration-acceleration tests, because the former more closely duplicated field conditions. The gages withstood impact shock of at least 50 g without appreciably affecting record accuracy. Deviations from the linear operation line did not exceed 5 msec under a shock of 50 g. At higher accelerations, the velocity oscillated after the instant of shock in some cases, and occasionally, the glass recording disk broke. Acceleration shock at 50 g or less, however, did not materially affect motor and turntable velocity.

Dynamic Pressure versus Time Gages. The dynamic-pressure gage was a modified model of the type used during Operations Redwing, Teapot, and Castle. The gages used during Redwing were recovered, cleaned and rebuilt. The gage nose section, which contains the capsules and recording elements, was filed and polished to remove most deep scratches and dents suffered during the tests. The main body of the gage was cleaned by sandblasting and refinished with baked enamel.

The major modification to the gage is the installation of the new-type pressure capsules. The turntable assembly was changed to bring about more nearly constant speed of rotation. This involved mounting the drive spindle on roller bearings. The spindle had previously been a running fit in the turntable housing. Because of the tendency of the spindle to bind, turntable rotation had been uneven. To reduce acceleration effects, the mass of the record disk retainer was reduced, and the diameter of that portion in contact with the glass disk was increased to furnish more support for the disk. A new method of mounting the relays, batteries, and other components was designed to prevent intermittent operation due to acceleration, to provide easier means of checking the gage circuits, and to provide for better protection against the elements.

Gage initiation was accomplished through the use of a photoelectric system backed up by a thermal initiator.

The photoelectric system for the q-gage was different from that system used on the P_t-gage. It contained a 918 phototube, a sensitive plate relay, an adjustable potentiometer, and a mechanical latching relay. The sensitive relay closes when the light becomes sufficiently intense to

allow 400 μa of current to pass. This closure completed the solenoid circuit of the latching relay, which closes the drive motor circuit. This circuit functioned properly on 23 of the 24 dynamic pressure gages used during Shot Priscilla.

The standard BRL q-gage was modified so as to make it possible to mount this gage on a standard contractor-installed mount. The base flange of the BRL self-recording q-gage is identical with the base flange on the electronic dynamic-pressure gages. The BRL q-gage and a standard contractor-installed mount are shown in Figure 1.15. Another modification was the relocation and redesign of the phototube holder and thermal link assembly. This modification in design completely sealed the electronic-initiation system from moisture.

Design of a New Gage for Dynamic Pressure versus Time. In designing a new dynamic-pressure gage, it was considered that the following features were desirable: (1) ability to be changed from a two-element P_s and P_t to a direct-reading dynamic-pressure gage, (2) simpler field servicing and installation, and (3) use of standardized pressure-time-gage components wherever possible ($3\frac{1}{2}$-inch P_t-gage recording disks, 3- and 10-rpm motors, and P_t-gage initiation system).

Five gages of an experimental model incorporating these features were built and used during Operation Plumbbob.

In design and construction, the new gage represents a radical departure from the BRL q-gage used during previous operations. The old gage consisted of a nose in the form of a pitot tube attached to and collinear with the cylindrical body that housed the battery pack and initiation circuits and that was used to support the tube on the field mount. The overall dimensions of the gage, including the pitot tube nose and body, were approximately 36 inches in length by $3\frac{3}{4}$ inches in diameter. All of the recording mechanism was contained within the pitot tube section. During tests, it was necessary to orient the axis of the gage body along a line toward the blast. With this orientation, the $3\frac{3}{4}$-inch gage-body diameter restricted the freedom of placement of gage components and the size of the recording disk.

The new gage has a cylindrical body oriented at right angles to the nose of the gage. This body houses the pressure-sensing capsules, drive motor, recording system, and standard P_t-gage, and it accommodates a $3\frac{1}{2}$-inch P_t-gage disk. Capsules and motors are interchangeable with P_t-gage components. Turntable bearings are the same as P_t turntable bearings. The photoelectric initiation system uses the same components with different mountings. The thermal initiator is the new, smaller, standardized plunger and link support.

The pitot tube assembly protrudes from the side of the cylindrical body and has a removable nose section. This permits conversion of the gage from a two-pressure, manual-subtraction-type gage to a direct-reading differential-pressure gage by the use of interchangeable gaskets at the junction of the nose and nose cone. In addition, the separable nose permits the use of extension noses when it is desirable to place the pressure inlets farther from the main body to avoid blast-wave reflections that would affect the accuracy of the pressure records obtained.

The main body and nose-cone assembly will be described together, since they are closely related. The main body is machined from a solid billet of duralumin. The outside is finish machined and the inside roughed out. The cavity for the insertion of the nose cone is precision bored. The nose cone is completely machined, with the cylindrical portion finished to 0.005 inch larger than the cavity in the body. To assemble the two pieces, the nose cone is soaked in dry ice and the main body heated to 200° F in an oven. This temperature difference of approximately 300° F is sufficient to allow the nose cone to be easily inserted into the main body. The resulting shrink fit forms a permanent fit between the two pieces, and welding or pin fastening is unnecessary. The finish machining of the interior of the main body and nose cone is completed with the two pieces assembled.

To keep the mass of moving parts to a minimum, the rotating parts, turntable, and record-blank keepers are machined from dural. The turntable bearings are 30-mm angular-contact bearings preloaded to minimize acceleration sensitivity. The motor and motor batteries are located in the lower end of the main body. The top portion contains the photoelectric initiation system with its battery supply and relays, the thermal initiator and switch, a master cutoff switch, and a timing switch. The timing switch is screw actuated and can be preset to cut off

the operation of the gage after completion of 2 revolutions or as many as 12. All covers and sections of the main body are sealed with O-rings to maintain a constant air pressure inside the gage.

In the field, the gage is secured in position by means of a dural flange bolted to the base of the gage. The flange is 6 inches in diameter and $\frac{3}{4}$ inch thick. Eight $\frac{3}{8}$-inch bolts on a $5\frac{1}{4}$-inch bolt circle are used to fasten the gages to the field mount.

All laboratory tests of the new q-gage were performed in the BRL 24-inch shock tube. The axis of the pitot tube lay along the axis of the shock tube, so that it was completely submerged in the airflow following the shock front. The gage was tested under a variety of conditions and pressures. The pressures varied between 5 and 30 psi side-on, and tests were conducted with both clean and dust-laden air. The gage was positioned with angles of yaw from 0° to 40°. Several tests were made with the extension pitot tube. A series of tests at various pressures were fired with the gage ported for direct dynamic pressure. Preliminary investigations of the shock-tube data showed good agreement in all cases between the dynamic pressures indicated and those expected. However, because of the questionable performance of this gage under field conditions, postshot investigations and analysis of the shock tube data did not seem to be warranted.

1.2.3 Installation of Gage Stations. Surveys for the blast lines were made by the civilian contractor. At stations where the peak overpressure expected was in excess of 35 psi, gage mounts for the P_t-gages were contractor installed. At the first six stations, the P_t-gage mounts were of the type designed to accommodate two of these gages. Mounts for the self-recording q-gage were contractor installed where the dynamic pressure was expected to be above 200 psi. These mounts were the AFSWP standard-design 3-foot q-gage tower for use in the high-pressure zones (Figure 1.16). At all other gage stations, the mounts were installed by project personnel. For the q-gage, this installation consisted of inserting the gage mount, pouring Cal-Seal (a quick-setting cement) around the mount, and leveling the mount so that the gage would be parallel to the ground and directed toward ground zero. A 3-foot gage mount with the new q-gage installed is shown in Figure 1.17. Ten-foot and 3-foot tower mounts for the q-gage were prefabricated. In all cases, the gage or gages required at a particular station were placed in their mounts and secured by project personnel.

1.2.4 Data Reduction and Presentation. Self-recording gage records scribed on a rotating disk present the record in polar coordinate form, and it is necessary to convert to rectangular coordinates. A Gaertner toolmaker's microscope with a rotating table was used for the conversion. The microscope was modified by the addition of digital read-out heads.

The information from the read-out heads on the microscope is converted to digital form by Telecordex equipment and then punched on IBM cards. These cards, representing readings taken at short intervals throughout the span of the record, together with cards representing calibration steps are used as input data for the EDVAC high-speed digital computer for linearizing both time and pressure values. The program coded for the EDVAC uses a straight-line equation, and the pressure values are calculated from a straight-line interpolation between the various calibration steps. The output data from the EDVAC is then punched on IBM cards, and these cards are fed to an Electronics Associate vari-plotter. The plotter has a 30- by 30-inch plotting table and can plot 6.6 points per inch. The plots of the pressure-time histories can be varied in size. After the points of the pressure-time plots are connected by straight lines, the records are reduced in size by photographic means for inclusion in the final report.

Photographs of the plots of the pressure-time history data are shown at the end of this chapter.

1.2.5 Dynamic Pressure Data Reduction. Similar procedures were used as described in Section 1.2.4 for reading records from the BRL q-gage disks. Several steps were taken to reduce the data from the records for purposes of calculating the free-stream dynamic pressures.

It should be brought out at the outset that it was hardly possible to separate the dust flow from the airflow for Shot Priscilla and also that appropriate corrections could be applied to the pressure measurements for yaw and pitch angles of flow. Lack of yaw and pitch gages as well as the unknown dust registry coefficient for the BRL gage precluded any such considerations.

There is reason to believe from the preliminary test for determining the dust registry coefficient (Reference 12) that the influence of dust on the pressure measurements is small. Furthermore, except for very close distances, as the distance from ground zero is increased, the air-to-dust mixture decreases, minimizing the influence of dust on the measurements. Hence, some scatter in the data can be expected.

From past tests, it was determined that the pitch and yaw records in the presence of a precursor indicated that flow became parallel to the gage axis within the first 30 to 50 msec. Within this period of time for most of the q-gage records within the precursor zone, the flow is not at its maximum value. It is believed that results derived were not seriously hampered by not using the correction factors for pitch and yaw angles of flow.

The initial step for calculating the free-stream dynamic pressure was to compute the Mach number from the ratio of total to static pressure using either Equations 1.3 or 1.7. Wherever possible the surface overpressure measurements were substituted for the q-gage side-on pressure measurements. In case this could not be done, then a correction for zero angle of flow was applied in accordance with that given in Reference 13 following the application of the initial step. The latter case required that an iteration process be used for computing a new Mach number. The new Mach number, along with static pressure, was substituted in Equation 1.4 yielding the calculated free-stream dynamic pressure. The data was processed as a function of time, and the BRL high-speed computer was used for the computation.

1.3 RESULTS

The performance of the gages utilized for the blast line instrumentation of Project 1.1 and free-field blast instrumentation for other projects was generally good. The failures of some of the self-recording pressure-time gages were due to premature initiation, failure of initiation, and high-acceleration effects (particularly on the q-gages). In spite of the premature initiation and failure of initiation, peak values of pressures from the gages were obtained. It can be assumed that, in the tabulation of results where neither the arrival time nor the positive duration data is given, only peak values were recorded on the gages. The q-gages at distances of 1,650 feet or less from ground zero were affected by ground accelerations, resulting in excessive hash and high-frequency oscillations on the records.

Ninety-seven self-recording gages were used to obtain pressure-time versus distance data for various flow phenomena from a nonclassical blast wave. Table 1.6 lists the gages used for each project and the type of record obtained.

The curves presenting the basic blast parameters versus distance included herein have been fitted by eye.

1.3.1 Blast Line Data, Project 1.1. The plots of the measured maximum values of overpressures as a function of distance for the main blast line and the free-field measurements taken for the various projects are shown in Figure 1.18. The tabulated results of the overpressure measurements are given in Table 1.7, along with the arrival time and positive duration values. When the time of arrival and positive duration are not given in the table, then the pressure indicated is peak only. The pressure-time histories are shown in Figures 1.19 through 1.27, which include all the free-field overpressure measurements taken.

The depression of the overpressure distance curve and waveforms of the pressure-time curves indicates the formation of a precursor as was expected in Shot Priscilla. The free-field measurements for the various projects were in the Frenchman Flat area west of ground zero. Generally, the small variation of the maximum pressure values between these scattered measurements and those of the main blast line indicates that the shock wave was symmetrical. This

is further borne out by the comparison of waveforms at the same distance from ground zero. A striking feature of the similarity between pressure-time records at an equivalent ground range is shown in Figures 1.22 and 1.23. Four P_t gages were located at a ground range of 1,040 feet, each gage separated along an arc by about 70 feet, the two end gages separated by about 240 feet. The differences in the waveforms at this ground range are in the high-frequency oscillation present on the record.

Plots of the as-measured difference between the total head pressure and the static pressure are shown in Figure 1.28. The calculated or corrected dynamic pressures are shown in Figure 1.29. Both figures show data obtained along the main blast line and for various projects. The tabulations of the maximum pressures for total, static, and dynamic (pressure difference and calculated) are given in Table 1.8 for the main blast line. The remaining tabulations of the same data for various projects are given in Tables 1.9 through 1.16. In the tables, only those values are reported for which pressure-time histories were obtained. The pressure-time plots are shown in Figures 1.30 through 1.50. In these figures the computed Mach number as a function of time is also shown. The static pressures reported in the tables and shown in the pressure-time figures are in most cases the ground baffle values unless otherwise noted.

In Figures 1.28 and 1.29 the subscript 10 adjacent to the symbols designating pressure values indicates measurements taken at a 10-foot elevation. All others are at the 3-foot elevation. A wide scatter of data occurs in the lower portion of the curves of Figures 1.28 and 1.29. The gage ranges for the total head and static pressure are similar, and because of the small pressure difference measured, a large variation can be expected because of reading errors as well as some oscillation on gage records.

An attempt was made to smooth through the high-frequency oscillations of the corrected dynamic pressure-time curves. The smoothing of the pressure-time curves is indicated by the dashed lines.

Although a record was inscribed on the q-gage disk at 850 feet, the wave was so distorted from acceleration effects that any value reported would be questionable. The new q-gage results do not compare favorably with those from the old gage. The maximum values are lower and duration times are shorter. The latter however, could be attributed to the fact that the motor did not achieve maximum speed.

The arrival time measurements from the main blast line are not representative, since in some cases the gages initiated by signal wire did not respond in the manner expected and therefore are misleading. However, by taking all the data obtained from various projects and plotting, a reasonably accurate curve has been constructed (Figure 1.51). Except for the points from the main blast line, the data does not show too great a variation.

The positive duration curve is given in Figure 1.52. Again, as in the case of the arrival time data, all of the positive duration points are given in one curve. The spread of the data is small, and the curve can be assumed to be reasonably accurate. Correction factors for arrival times and positive duration were made in accordance with that given in Reference 14. The motor of the self-recording gage requires 400 msec to establish its rated rpm. Correction factors of 65 msec for the 3-rpm motor and 150 msec for the 10-rpm motor were added to the arrival times obtained from the record. A nonlinear correction factor was applied to both time of arrival and positive duration where the true time of arrival was less than 400 msec.

1.3.2 Free-Field Blast Data For Various Projects. The free-field blast measurements taken for each project are given in Tables 1.9 through 1.16. A better proportion of pressure-time records was obtained from these gages than from the gages along the main blast line (Table 1.7).

Good pressure-time records were obtained for Project 1.7. The greatest variation in the maximum overpressure at equivalent ground ranges occurs at the 1,360-foot station: one gage records a pressure of 40 psi and the other 60 psi. However, an inspection of the waveforms (Figure 1.23) indicates that the selection of the 40-psi point resulted from the fact that the peak of that record was cut off. At the two closer stations, 760 feet and 1,040 feet, the

maximum overpressures are in better agreement (Figure 1.22).

Table 1.10 indicates that no pressures were recorded for three of the gages. These gages were inside the structures, and it can be assumed that no excess pressure above ambient entered into the structure. A small pressure was detected in the plenum chamber of Structure F3.3-9019.2, as indicated in Table 1.11. The purpose and scope of these measurements are given in the reports prepared by the projects for which these measurements were taken.

The instrumentation provided Projects 4.3/33.2 and 6.1 resulted in separate blast lines. The blast line for Project 4.3/33.2 consisted of P_t-gages and q-gages extending from 2,030 feet out to 6,120 feet from ground zero. This line was parallel to the main blast line and approximately 300 feet south. The results from these gages are given in Tables 1.14 and 1.15.

The blast line for Project 6.1 was in a northeasterly direction from ground zero, and it consisted of P_t-gages only. The range for location of these gages extended from 1,250 feet out to 5,320 feet (Table 1.16). Except for Project 6.1, the free-field blast data taken for the other projects has been plotted in Figures 1.18 and 1.28. A separate overpressure versus distance curve was drawn for the values obtained for Project 6.1, and it is shown in Figure 1.53. The empirical data of Figure 1.53 is very similar to that shown in Figure 1.18.

1.4 DISCUSSION

Although the data on overpressure versus time is not as complete as would be desired, a representative amount has been obtained, which leads to a better understanding of the magnitudes and waveforms of the pressure within a precursor zone. Certain characteristics of the pressure waveform, such as the inconsistencies in the magnitudes of maximum overpressure at equivalent ranges, although not resolved, can be attributed to several factors. These factors can be (1) acceleration effects due to ground motion, and (2) blast per se, (3) overshoot of the pressure capsule, and (4) turbulent flow created by the thermal layer ahead of the blast wave, and (5) presence of dust behind the blast wave. The latter, of course, is not experimentally verified. Inspection of the pressure-time waveforms points out the difficulty in the arbitrary selection of the maximum overpressure value, which, in effect, also contributes to the inconsistencies.

The sharp rise of the pressure front at the first two stations, 350 and 450 feet on the main blast line, implies that the precursor did not form as yet. At the next station, 650 feet, the pressure waveform is distorted; hence, the precursor was formed in the region between 450 and 650 feet. Typical precursor waveform patterns are observed as far as the 4,000-foot station. At the last station, 5,000 feet, the pressure wave has a sharp rise and is a classical-type shock. The precursor zone, therefore, extended along the main blast line from approximately 450 feet out to 5,000 feet. On the other hand, the pressure waveforms obtained for Project 4.3/33.2 indicate a clearing up of the precursor at 3,939 feet, which is a classical-type shock wave. This anomaly is not readily explainable. The pressure magnitude at 4,000 feet along the main blast line is the same as the value at 3,939 feet of Project 4.3/33.2. Also, the positive duration and the time of arrival for both these stations are of the proper magnitude at least within the experimental error. It is highly unlikely that the difference in ground range between these two stations should indicate large variation in pressure, time of arrival, or positive duration. The above anomaly leads to the belief that the shock was asymmetrical but not large enough to be observed except for the particular case above.

The relative merits of the outlined procedure given in Section 1.1.4 for determining the free-stream dynamic pressure are difficult to evaluate. The difficulty lies principally in the degree of the dust influence on the pressure measurements. Lack of additional instrumentation precluded separating the dust portion of flow from air. If the preliminary estimates of the dust registry coefficient n for the BRL q-gage can be believed, then the free-stream dynamic pressures as given are reasonably accurate. Further difficulty was encountered in the data reduction process. This arose when use was made of the ground surface pressure measurement for subtraction from the total head pressure to obtain the pressure difference. In some cases, the ground surface pressure time did not correspond to the total head pressure time. It was

then necessary, generally, to adjust the times of the total head pressure to correspond to the ground surface pressure time. Although there exists some question as to the validity of the calculated free-stream dynamic pressure, using the outlined procedure, the measurements taken during Shot Priscilla do increase the confidence for understanding the flow phenomena associated with precursor formation and also of being able to estimate the magnitudes of flow for dust and air combinations.

1.4.1 Predicted Maximum Overpressure Versus Distance Compared to the Measured Curve. The BRL- and AFSWP-predicted curves for overpressure versus distance as compared to the measured curves are shown in Figure 1.54. The measured curve compares favorably with the predicted curves. At the higher pressure values, over 300 psi, the measured curve is about the same as the AFSWP-predicted curve. The BRL-predicted curve overestimated the values. Below 300 psi, the largest variation in the measured curve is approximately 20 percent as compared to the predicted curves.

This favorable comparison between predicted maximum overpressure and measured maximum overpressure indicates that the state of knowledge concerning maximum overpressure is good, especially since Shot Priscilla was the first event in which overpressures above 200 psi were measured.

1.4.2 Predicted Curve of Peak Dynamic Pressure Versus Distance Compared to Measured Curve. The comparison of the predicted dynamic with measured dynamic pressure is shown in Figure 1.55. In this figure, the predicted values are given for the ideal or free-stream dynamic pressure and for the pressure difference between total and static pressure as measured from previous operations. Comparison of the as-measured difference with the predicted curve gives a less favorable agreement than was obtained with the overpressure-distance curves, except in the lower pressure region. The maximum difference between measured and predicted is in the center portion of the curve. The construction of the predicted curve was based on a limited number of data points, and use was made mainly of the SRI data. In retrospect however, an examination of the data points shown in Figure 1.3 indicates lower values of pressure from the BRL q-gage in the center portion of the curve. Since SRI data of past tests is above the BRL data, then the dust registry coefficient of the SRI gage may be higher than for the BRL gage, leading to higher values of pressure difference recorded. The BRL data of past tests is closer to the measured values of Shot Priscilla.

The corrected dynamic pressure or the calculated dynamic pressure versus distance approaches closer to the ideal curve than the uncorrected curve, but it is still about 50 to 100 percent higher. The extent of the dust influence, for Mach number calculations that are used for determining the corrected dynamic pressures as mentioned previously, is unknown. Any discussion concerning the calculated dynamic pressures at this time would be premature. To discuss the validity of the applied corrections, additional information is needed principally in the dust registry coefficient of the gages used for measuring the flow phenomena.

1.4.3 Comparison of Predicted Values of Time of Arrival and Positive Duration with Measured Values. Shown in Figure 1.56 is a comparison of the predicted time of arrival and positive duration curves with the measured curves of Shot Priscilla. Except at the closer ground distances, the comparison is reasonably good for both blast wave parameters. At closer ground distances the measured positive duration is shorter, and the time of arrival is longer than the predicted values. The predicted curve for positive duration, based on TM 23-200 (Reference 7), gives a better comparison with the measured curve than the BRL-predicted curve. The BRL curve was drawn higher in the range of 1,500 to 5,000 feet because of thermal action predicted from Teapot 12 and Upshot-Knothole 10 data.

Again as in the case of the overpressure-distance curve, the fair correlation between the measured and predicted curves for time of arrival and positive duration indicates that the knowledge about basic blast phenomena is reasonably good.

1.5 CONCLUSIONS

Shot Priscilla was the first test during which emphasis was placed on results from the high-pressure region. The overall free-field overpressure measurements yielded good pressure-time information, but the data on dynamic pressure is to some extent limited. Loss of some of the dynamic pressure data resulted from high-acceleration effects.

An attempt had been made to apply appropriate correction factors to the q-gage data to obtain free-stream dynamic pressures. The validity of applying these correction factors has not been ascertained. Lack of additional instrumentation precluded the separation of dust flow from air-flow; therefore, the extent of dust influence on the measured data is unknown.

A good comparison was obtained between the predicted blast wave parameters and the measured values, except for dynamic pressure. The predicted dynamic pressures generally overestimated the measured values. However, a good correlation exists between the BRL data of the as-measured differential pressure from past shots with the values measured during Shot Priscilla. The predicted curve was based on past data obtained by SRI using an SC q-gage. The higher values of differential pressure from past tests by SC q-gage implies that the dust registry coefficient n is higher for this gage than for the BRL q-gage. The calculated or corrected dynamic pressures are greater than the ideal by about 50 to 100 percent.

Upon final evaluation the new BRL q-gage does not agree too well with the old BRL q-gage.

The results during Shot Priscilla indicate that the state of knowledge concerning overpressure, time of arrival, and positive duration as a function of distance is good. The information obtained also leads to a better understanding of the flow phenomena associated with precursor formation and dust-laden shock waves.

1.6 RECOMMENDATION

From results of past operations and this test, it is shown that the self-recording gages will yield reasonably accurate information. Two of the shortcomings of these type gages are (1) the effects of acceleration, which can completely distort the waveform and in some cases result in a complete loss of record, and (2) the lack of timing technique to give more accurate time parameter measurements. A development program is recommended to eliminate the above two shortcomings of the gage.

TABLE 1.1 ASSUMED PARAMETERS AND SCALING FACTORS, SHOT PRISCILLA

Location	Frenchman Flat	A-scaled factors	
Elevation of ground zero, ft	3,078		
Height of burst, ft	700	S_p	= 1.150
Atmospheric pressure, ground zero, mb	905	S_d	= 0.2791
Atmospheric pressure, height of burst, mb	881	S_t	= 0.2765
Atmospheric temperature, ground zero, C	17	$S_p \cdot S_t$	= 0.3179
Atmospheric temperature, height of burst, C	14.5	$1/S_p$	= 0.8697
A-scaled height of burst, ft	209	$1/S_d$	= 3.583
		$1/S_t$	= 3.617
		$1/(S_p \cdot S_t$	= 3.146

*Scaling factors

Pressure: $S_p = 14.7/P_o$

Distance: $S_d = (P_o/14.7)^{1/3} (1/W)^{1/3}$

Time: $S_t = (T_o + 273/288)^{1/2} (P_o/14.7)^{1/3} (1/W)^{1/3}$

TABLE 1.2 COMPARISON SHOTS AND SHOT PARAMETERS

Shot	Yield	A-Scaled HOB	Shot Name
Greenhouse 2	46.7	82.9	Easy
Tumbler 4	19.2	363.1	—
Ivy 2	540.0	180.0	King
Upshot-Knothole 1	16.5	112.5	Annie
Upshot-Knothole 10	15.2 ± 0.5	203.4	Grable
Upshot-Knothole 11	60 ± 2	316.8	Climax
Teapot 2	2.39	213.4	Moth
Teapot 3	6.8 ± 0.3	150.0	Tesla
Teapot 4	43.2 ± 2	135.5	Turk
Teapot 5	3.6 ± 0.1	186.1	Hornet
Teapot 6	8.1 ± 0.2	240.1	Bee
Teapot 8	14.2 ± 0.7	195.1	Apple I
Teapot 10	3.2	13,195.7	HA
Teapot 12	22.6	133.7	Met
Teapot 13	28 ± 1.5	154.7	Apple II
Teapot 14	28 ± 1.5	155.0	Zucchini
Plumbbob 2	0.138 ± 0.006	561.8	Franklin
Plumbbob 4	10.3 ± 0.5	218.3	Wilson
Plumbbob 5	36.6 ± 1	201.7	Priscilla
Plumbbob 6	71 ± 2	333.3	Hood
Plumbbob 8	1.73 ± 0.1	11,708.0	John
Plumbbob 9	10.3 ± 0.5	217.0	Kepler
Plumbbob 10	9.7 ± 0.5	222.4	Owens
Plumbbob 11	19 ± 1	—	Stokes
Plumbbob 12	16.5 ± 1.0	184.5	Shasta
Plumbbob 15	44 ± 1	187.6	Smoky
Plumbbob 16	11.1 ± 1	210.5	Gallileo
Plumbbob 22	18.5 ± 0.9	—	Whitney
Plumbbob 23	11.5 ± 0.5	633.0	Charleston
Plumbbob 24	8.0 ± 0.04	237.5	Morgan

TABLE 1.3 SYMBOLS FOR SUBSONIC AND SUPERSONIC FLOWS IN CLEAN AND DIRTY BLAST WAVES

q = dynamic air pressure = $\frac{1}{2}\rho u^2$

q_c = $(P_p - P_s)$

M = u/c = local free-stream Mach number of flow behind blast front = $\frac{\text{particle velocity}}{\text{sound velocity}}$

P_t = free stream total pressure (absolute)

P_p = total head pitot pressure (absolute) $\begin{matrix} M<1\ P_p = P_t \\ M>1\ P_p \neq P_t \end{matrix}$

P_s = free stream static pressure (absolute)

P_o = ambient preshock static pressure (absolute)

ΔP = free stream static overpressure = $P_s - P_o$

ΔP_p = total head overpressure = $P_p - P_o$

ρ = air density (local)

u = particle speed of air (local)

c = speed of sound in air (local)

t = ratio of specific heats

Primes are used to denote uncorrected, "as read" gage values, thus

q_c' = $(P_p - P_s)'$

Additional Symbols in Dirty Airblast Flows (*)

q^* = dynamic air-plus-dust pressure in free stream = $q + \phi_d$

q_c^* = $q_c + \phi_d$

$q_c^{*\prime}$ = $(q_c + n\phi_d)'$

ϕ_d = momentum flux of dust = $\rho_d u_d^2$

n = dust registry coefficient of gage, $o \leq 1$. .1

ρ_d = mass of suspended dust per unit volume of mixture (local)

u_d = particle speed of dust (local)

δ = specific gravity of dust particles = 2.5

TABLE 1.4 SUMMARY OF GAGE INSTALLATIONS ON MAIN BLAST LINE, SHOT PRISCILLA

Station Number	Ground Range	Number and Type of Gages*	
		P_t	q
	ft		
F1.1-9039.01	350	2	
F1.1-9039.02	450	2	
F1.1-9039.03	650	2	
F1.1-9040.01	850	2	1
F1.1-9040.02	1,050	2	1
F1.1-9041.00	1,350	2	2
F1.1-9042.01	1,650	1	1
F1.1-9042.02	2,000	1	1
F1.1-9042.05	2,250	1	2
F1.1-9042.06	2,500	1	2
F1.1-9042.07	3,000	1	2
F1.1-9042.03	3,500	1	1
F1.1-9042.08	4,000	1	2
F1.1-9042.04	4,500	1	1
F1.1-9043.01	5,000	1	
F1.1-9043.02	6,000	1	

* Where two q-gages are noted, a new design q-gage was located for proof testing.

TABLE 1.5 GAGE INSTALLATIONS FOR VARIOUS PROJECTS, SHOT PRISCILLA

Project No.	Station No.	Distance	No. and Type of Gages
		feet	
1.7	F1.7-9031.01	760	3 P_t
	F1.7-9031.02	1,040	4 P_t
	F1.7-9031.03	1,360	2 P_t
3.1	F3.1-9014.01	860	2 P_t
	F3.1-9014.02	1,040	2 P_t
	F3.1-9014.03	1,360	2 P_t
3.2	F3.2-9016.01	970	1 P_t
	F3.2-9016.04	1,040	1 P_t
	F3.2-9016.05	1,150	1 P_t
3.3	F3.3-9019.01	1,150	1 P_t
	F3.3-9019.02	1,360	1 P_t
	F3.3-9019.03	1,360	1 P_t
3.4	F3.4-9021	900	2 P_t, 1 q
	F3.4-9022.01	3,600	1 q
	F3.4-9022.02	5,000	1 q
	F3.4-9024.01	4,200	2 P_t, 1 q
	F3.4-9023.02	4,200	2 P_t
4.3/33.2	F33.2-8015.01	2,030	1 P_t, 1 q
	F33.2-8015.02	2,280	1 P_t, 1 q
	F33.2-8015.03	2,730	1 P_t, 1 q
	F33.2-8015.04	3,930	1 P_t, 1 q
	F33.2-8015.05	4,770	1 P_t, 1 q
	F33.2-8015.06	5,320	1 P_t, 1 q
	F33.2-8015.07	6,120	1 P_t, 1 q
6.1	F6.1-9036	Minefield Area	52 P_t

TABLE 1.6 GAGE PERFORMANCE

Project	Pressure-Time Gages				Dynamic Pressure Gages	
	Total No. P_t-Gages	Pressure-Time Records	Peak Pressure	No Record	Total No. of Gages	Pressure-Time Records
1.1	22	14	6	2	15	12
1.7	9	7	2	—		
3.1	6	6	—	—		
3.2/3.3	6	4	2	—		
3.4	6	3	3	—	4	3
4.3/33.2	7	5	1	1	7	7
C.1	15	11	3	1		
Totals	71	50	17	4	26	22

TABLE 1.7 P_t-GAGE RESULTS, MAIN BLAST LINE

Station	Ground Range	Maximum Overpressure	Arrival Time	Positive Duration
	ft	psi	sec	sec
F1.1-9039.01A	350	No record		
F1.1-9039.01B	350	1030	--	--
F1.1-9039-02A	450	760	--	--
F1.1-9039.02B	450	750	--	0.175
F1.1-9039.03A	650	480	0.364	0.95
F1.1-9039.03B	650	400	0.676	0,162
F1.1-9040.01A	850	225	--	0.236
F1.1-9040,01B	850	206	--	--
F1.1-9040.02A	1050	125	--	0.233
F1.1-9040.02B	1050	138	--	0.195
F1.1-9041.00A	1350	60.0	--	0.343
F1.1-9041.00B	1350	62.0	0.512	0.280
F1.1-9042.01	1650	31.0	--	0.467
F1.1-9042.02	2000	16.3	--	--
F1.1-9042.05	2250	12.4	0.570	0.687
F1.1-9042.06	2500	9.2	0.523	0.852
F1.1-9042.07	3000	9.1	--	0.727
F1.1-9042.03	3500	9.9	--	--
F1.1-9042.08	4000	8.8	1.729	0.818
F1.1-9042.04	4500	7.4	--	--
F1.1-9043.01	5000	5.9	--	0.916
F1.19043.02	6000	No record		--

TABLE 1.8 q-GAGE RESULTS, MAIN BLAST LINE, MAXIMUM VALUES

Station	Ground Range	Total Pressure	Static Overpressure	Pressure Difference $(P_p - P_o)$*'	Dynamic Pressure q*	Mach Number
	ft	psi	psi	psi	psi	(u/a)
F1.1-9040.01	850	--	--	--	--	--
F1.1-9040.02	1050	470.0	125.0	445.0	240.0	3.3
F1.1-9041.00	1350	275.0	60.0	255.0	150.0	3.6
F1.1-9041.00N[x]	1350	--	--	--	--	--
F1.1-9042.01	1650	143.5	31.0	150.0	80.0	2.3
F1.1-9042.02	2000	58.5	23.0x	44.0	32.0	1.3
F1.1-9042.05N	2250	48,0	12.4	36.0	27.0	1.4
F1.1-9042.06	2500	47.0	9.2	38.0	25,0	1.3
F1.1-9042.06Nx	2500	35.0	9.2	28.0	19.0	1.2
F1.1-9042.07	3000	29.0	9.1	20.0	15.1	1.0
F1.1-9042.07Nx	3000	26.5	9.1	20.5	17.0	1.04
F1.1-9042.03	3500	11.2	8.6x	3.4	2.8	0.45
F1.1-9042.08	4000	10.0	9.0	1.3	1.3	0.29
F1.1-9042.08N	4000	--	--	--	--	--
F1.1-9042.04	4500	7.8	6.5x	1.7	1.2	0.29

N, refers to new q-gage
x, values from q-gage

TABLE 1.9 P_t-GAGE RESULTS, PROJECT 1.7

Station	Ground Range	Maximum Overpressure	Arrival Time	Positive Duration
	ft	psi	sec	sec
F1.7-9031.01a	760	235	0.186	--
F1.7-9031.01b	760	225	0.316	0.178
F1.7-9031.01c	760	210	0.186	0.126
F1.7-9031.02a	1040	112	0.250	0.307
F1.7-9031.02b	1040	115	0.241	0.253
F1.7-9031.02c	1040	110	0.306	0.256
F1.7-9031.02d	1040	105	0.210	0.285
F1.7-9031.03a	1360	600	0.305	0.404
F1.7-9031.03b	1360	400	--	--

[redacted]

TABLE 1.10 P_t-GAGE RESULTS, PROJECT 3.1

Station	Ground Range	Maximum Overpressure	Arrival Time	Positive Duration
	ft	psi	sec	sec
F3.1-9014.01a	860	175	0.282	0.260
F3.1-9014.01b	860	No pressure recorded		
F3.1-9014.02a	1040	118	0.087	0.254
F3.1-9014.02b	1040	No pressure recorded		
F3.1-9014.03a	1360	56.1	--	--
F3.1-9014.03b	1360	No pressure recorded		

TABLE 1.11 P_t-GAGE RESULTS, PROJECTS 3.2 and 3.3

Station	Ground Range	Maximum Overpressure	Arrival Time	Positive Duration
	ft	psi	sec	sec
F3.2-9016.01	970	145	--	0.254
F3.2-9016.04	1040	122	0.255	0.206
F3.2-9016.05	1150	98.0	0.241	0.332
F3.3-9019.01	1150	100	--	--
F3.3-9019.02	1360	70.0	--	--
F3.3-9019.03	13( )	56.0	--	0.361

TABLE 1.12 P_t-GAGE RESULTS, PROJECT 3.4

Station	Ground Range	Maximum Overpressure	Arrival Time	Positive Duration
	ft	psi	sec	sec
F3.4-9021 Rear	900	65.2	---	--
F3.4-9021 Door	900	75.4	---	0.336
F3.4-9024.01 Center	4200	7.9	1.956	0.782
F3.4-9024.01 Back	4200	9.0	--	--
F3.4-9023.02 North	4200	8.8	1.887	0.357
F3.4-9023.02 South	4200	14.1	--	--

TABLE 1.13 q-GAGE RESULTS, PROJECT 3.4

Station	Ground Range	Total Pressure	Static Overpressure	Pressure Difference $(P_p - P_s)^{*'}$	Dynamic Pressure q^*	Mach Number
	ft	psi	psi	psi	psi	(u/a)
F3.4-9021	900	--	--	--	--	--
F3.4-9024.01	4200	8.2	6.7 x	1.5	1.2	0.28
F3.4-9022.01*	3600	13.0	10.2 x	3.8	3.7	0.47
F3.4-9022.02*	5000	6.7	6.0 x	1.9	1.8	0.38

*10-foot q gage mounts

xObtained from q-gage as opposed to ground baffle gages.

TABLE 1.14 P_t-GAGE RESULTS, PROJECT 4.3/33.2

Station	Ground Range	Maximum Overpressure	Arrival Time	Positive Duration
	ft	psi	sec	sec
F33.2-8015.01	2030	13.0	0.416	0.010
F33.2-8015.02	2280	13.8	0.503	0.661
F33.2-8015.03	2730	9.0	0.903	0.737
F33.2-8015.04	3930	8.8	1.858	0.825
F33.2-8015.05	4770	6.3	2.386	0.920
F33.2-8015.06	5320	No Record	--	--
F33.2-8015.07	6120	4.9	--	--

TABLE 1.15 q-GAGE RESULTS, PROJECT 4.3/33.2, MAXIMUM VALUES

Station	Ground Range	Total Pressure	Static Overpressure	Pressure Difference $(P_p - P_s)^{**}$	Dynamic Pressure q*	Mach Number
	ft	psi	psi	psi	psi	(u/a)
F33.2-8015.01	2030	61.0	13.0	51.0	37.0	1.6
F33.2-8015.02	2280	50.0	13.8	41.0	28.0	1.3
F33.2-8015.03	2730	23.7	9.0	14.5	11.5	0.89
F33.2-8015.04	3930	11.0	8.8	2.4	2.3	0.39
F33.2-8015.05	4770	6.8	6.3	0.9	0.9	0.23
F33.2-8015.06	5320	6.4	5.1 x	1.2	1.2	0.31
F33.2-8015.07	6120	4.9	4.7 x	0.3	0.35	0.16

x, obtained from q-gage as opposed to ground baffle gage.

TABLE 1.16 P_t-GAGE RESULTS, PROJECT 6.1

Station	Ground Range	Maximum Overpressure	Arrival Time	Positive Duration
	ft	psi	sec	sec
F-6.1-1A	1250	67.0	--	0.422
F-6.1-2A	1370	57.0	--	0.374
F-6.1-3A	1500	40.0	--	0.510
F-6.1-4A	1600	34.0	--	--
F-6.1-5A	1720	28.0	0.353	0.492
F-6.1-6A	1850	21.6	0.429	0.575
F-6.1-7A	1900	15.5	0.415	0.629
F-6.1-8A	2120	11.5	0.472	0.679
F-6.1-9A	2290	11.0	0.535	0.751
F-6.1-10A	2520	10.5	0.609	0.830
F-6.1-11A	2730	8.5	0.772	0.808
F-6.1-12A	2870	10.0	--	--
F-6.1-13A	3250	8.0	--	0.781
F-6.1-14A	4530	--	--	--
F-6.1-15A	5320	5.4	--	--

[redacted]

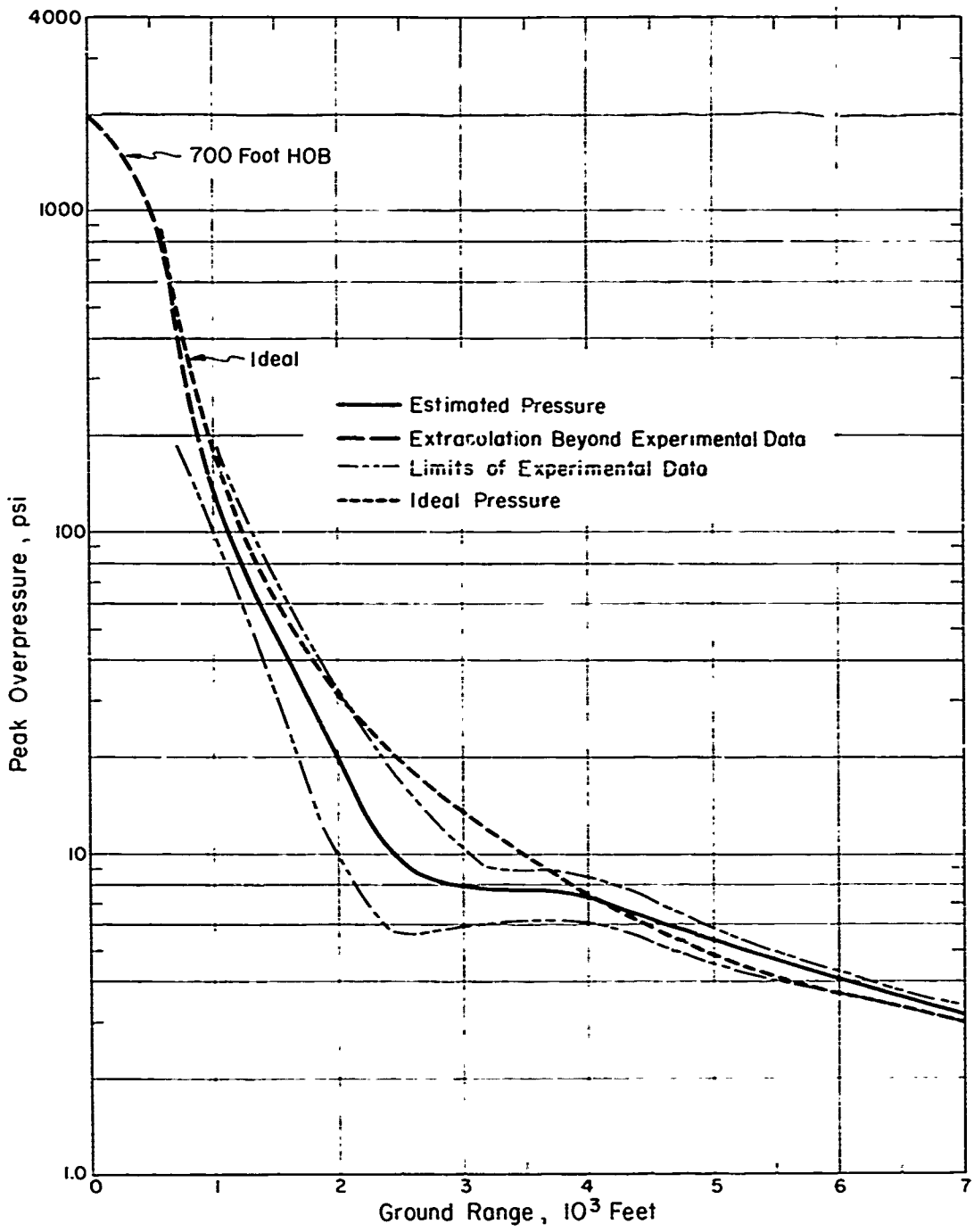

Figure 1.1 Estimated peak overpressure versus distance, Shot Priscilla.

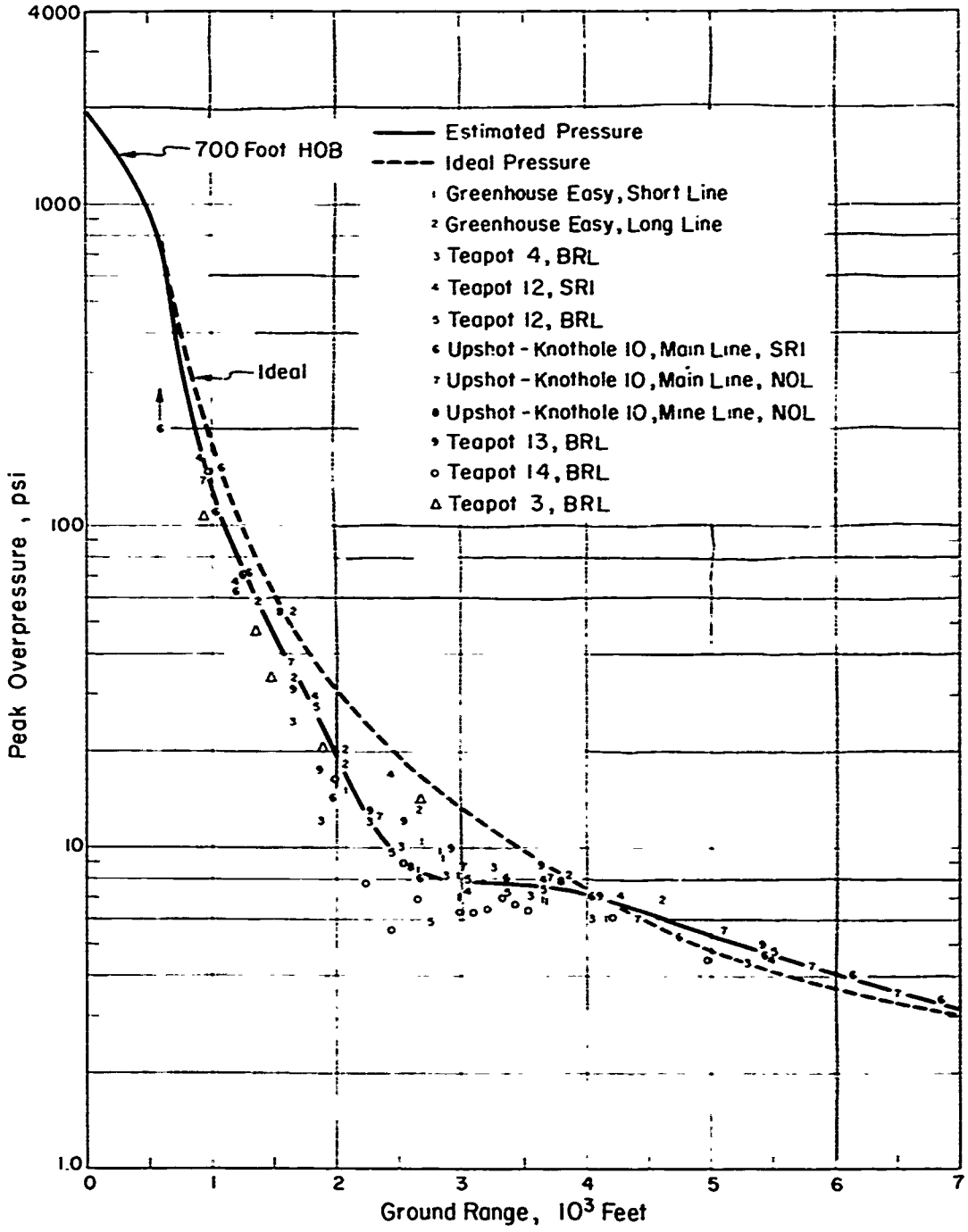

Figure 1.2 Data used in estimating overpressure-distance curve.

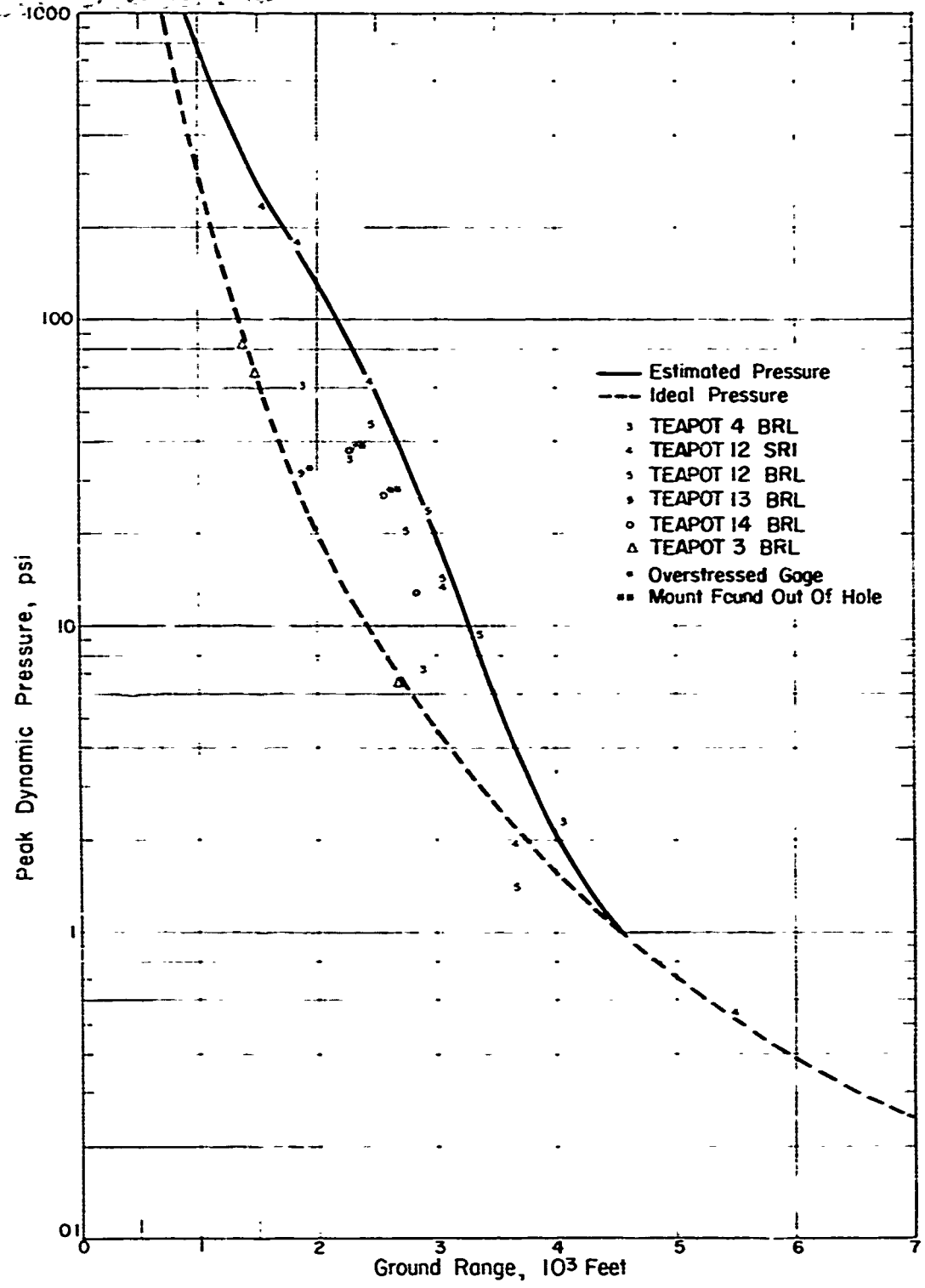

Figure 1.3 Estimated peak dynamic pressure versus distance.

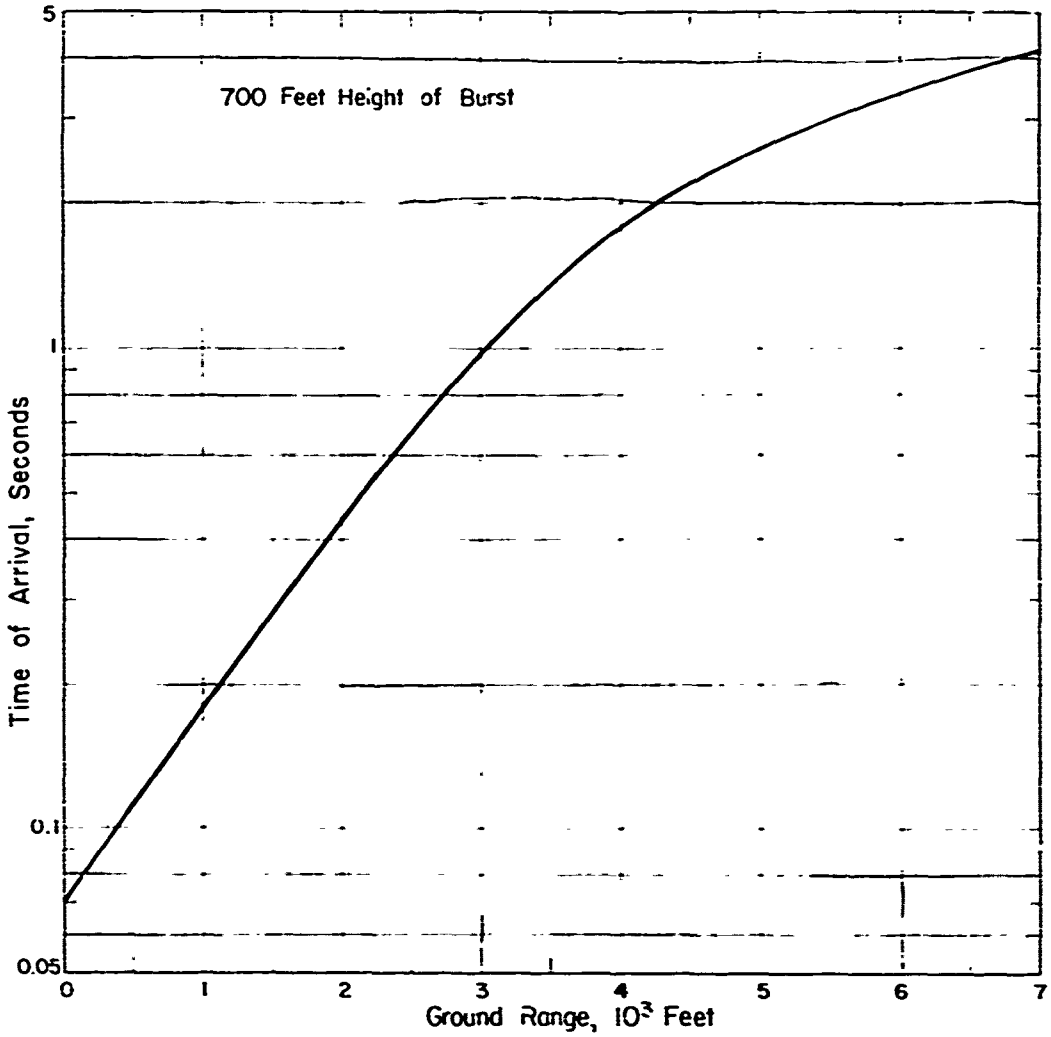

Figure 1.4 Estimated time of arrival of initial disturbance.

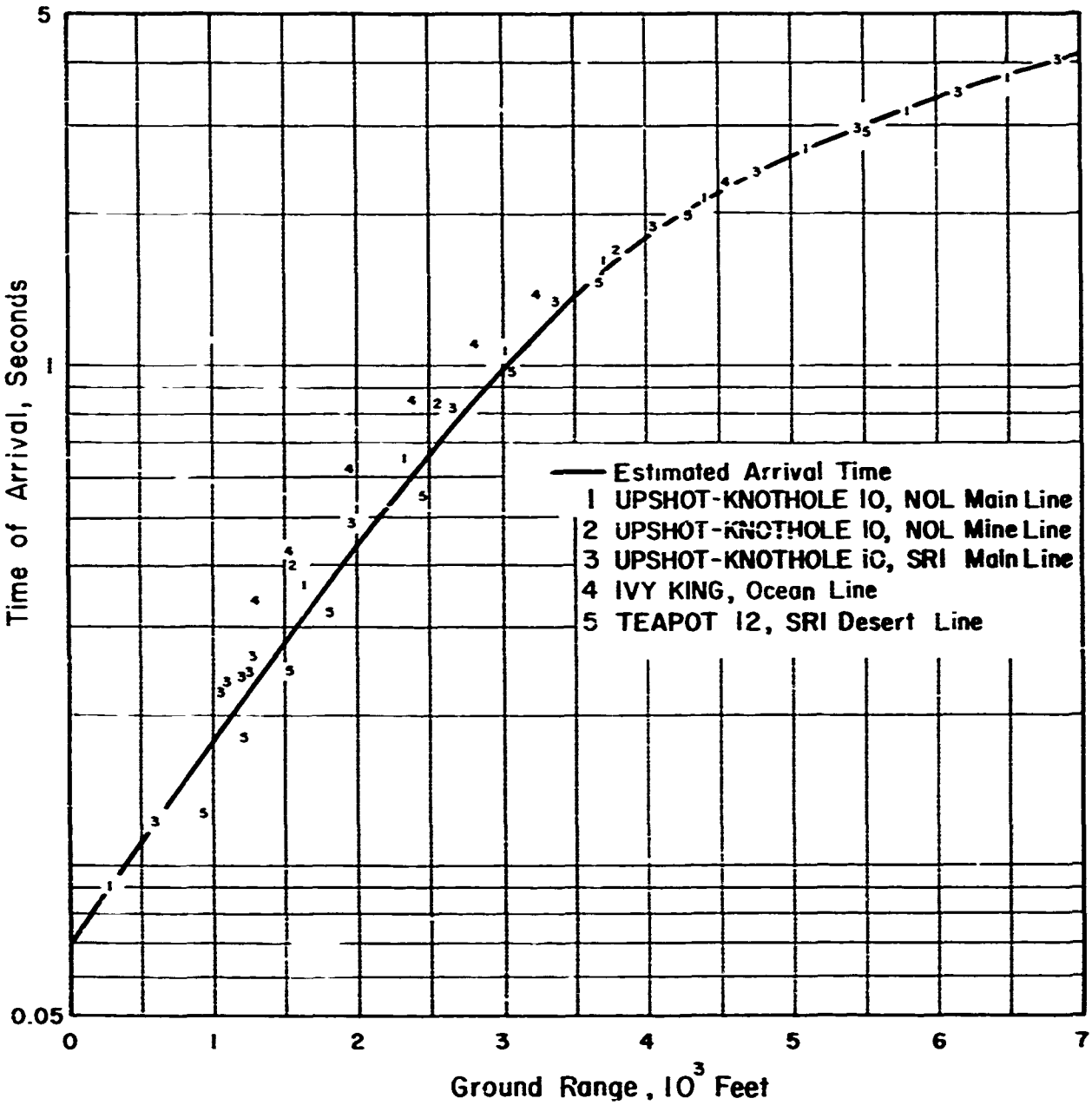

Figure 1.5 Estimated time of arrival curve, computed curves, and experimental data.

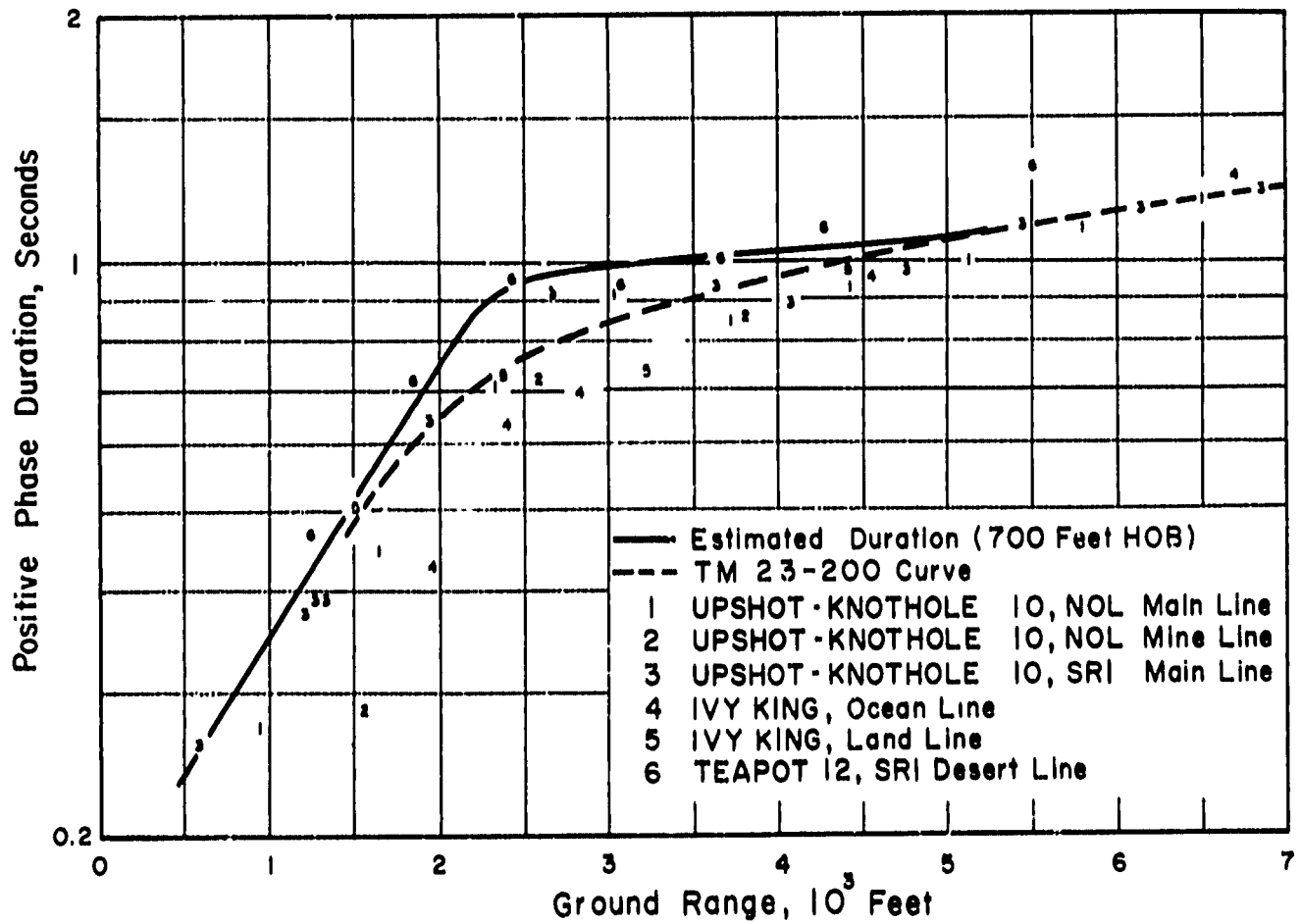

Figure 1.6 Estimated positive-phase duration.

SANDIA PITOT-STATIC DIFFERENTIAL GAGE

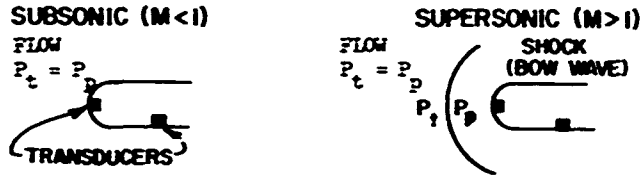

Direct Measurements: -

Clean Blast: $(\Delta p_p - \Delta p)'$ and $\Delta p'$. First Term = q_c'.

Dusty Blast: $(q_c + n\phi_d)'$ and $\Delta p'$. n and ϕ_d unknown.

SANDIA SNOB GAGE

Clean Blast: $(\Delta p_p - \Delta p)'$ and $\Delta p'$. First term = q_c'.

Dusty Blast: $(q_c + n\phi_d)'$ and $\Delta p'$. n = 0.15, ϕ_d unknown.

SANDIA GREG GAGE

Clean Blast: $\Delta p_p'$ and $\Delta p'$. Difference = q_c'.

Dusty Blast: $\Delta p_p^{*'}$ and $\Delta p'$. Difference = $q_c^{*'} = (q_c + n\phi_d)'$.

n = 0.9, ϕ_d unknown.

BRL "q" GAGE

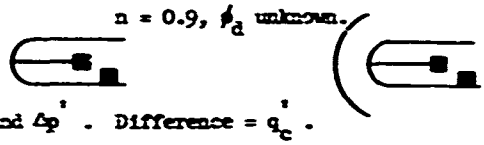

Clean Blast: $\Delta p_p'$ and $\Delta p'$. Difference = q_c'.

Dusty Blast: $\Delta p_p^{*'}$ and $\Delta p'$. Difference = $q_c^{*'} = (q_c + n\phi_d)'$.

n, ϕ_d unknown.

SRI TOTAL HEAD GAGE

Clean Blast: $\Delta p_p'$ and $\Delta p'$. Difference = q_c'.

Dusty Blast: $\Delta p_p^{*'}$ and $\Delta p'$. Difference = $q_c^{*'} = (q_c + n\phi_d)'$.

n, ϕ_d unknown.

Figure 1.7 Gage responses.

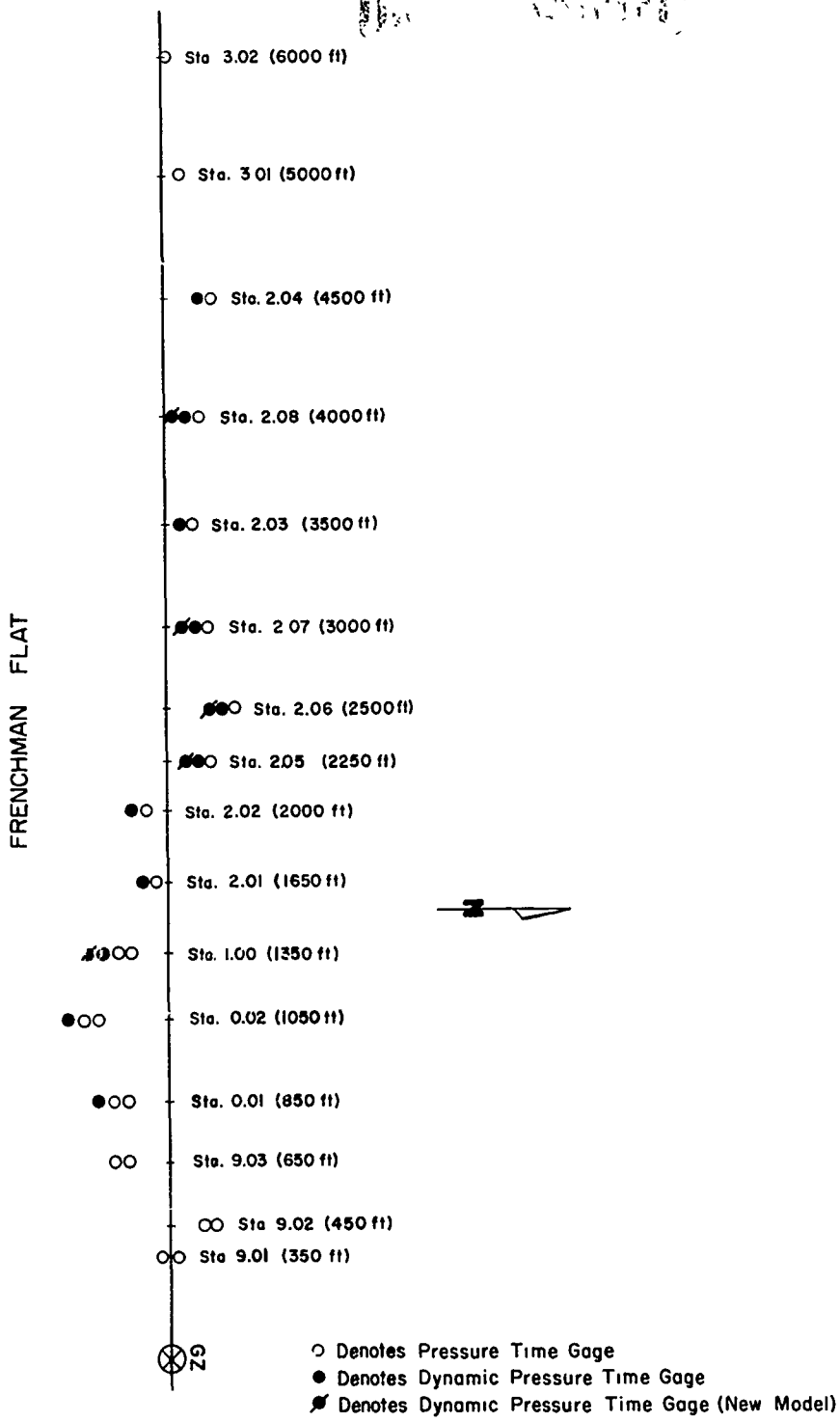

Figure 1.8 Station layout, blast line, Shot Priscilla.

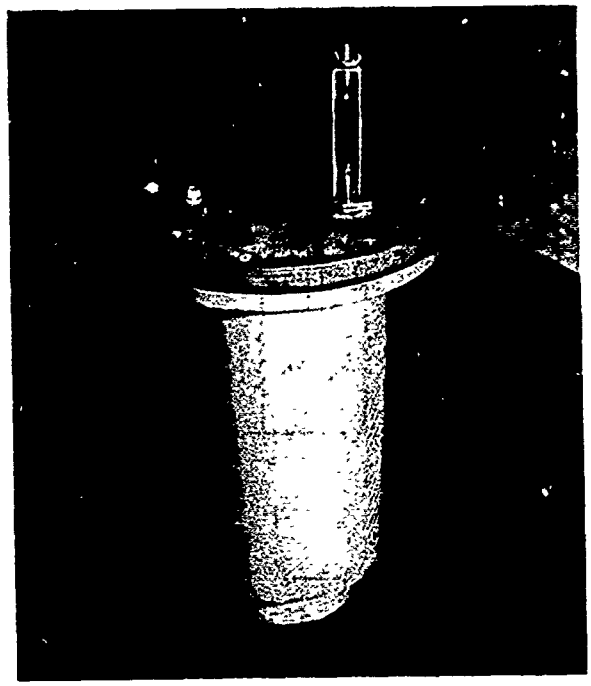

Figure 1.9 Self-recording P_t-gage.

Figure 1.10 Self-recording q-gage.

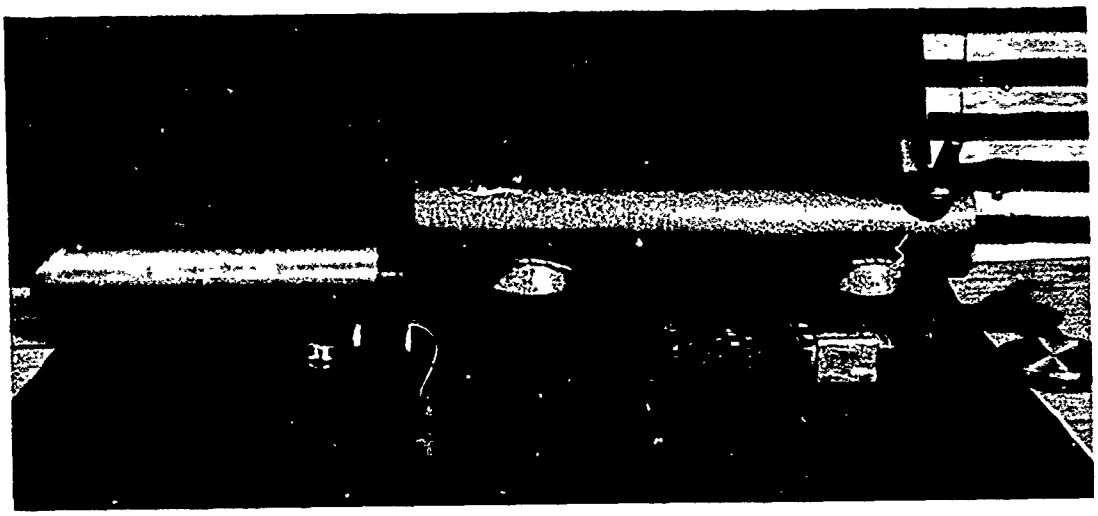

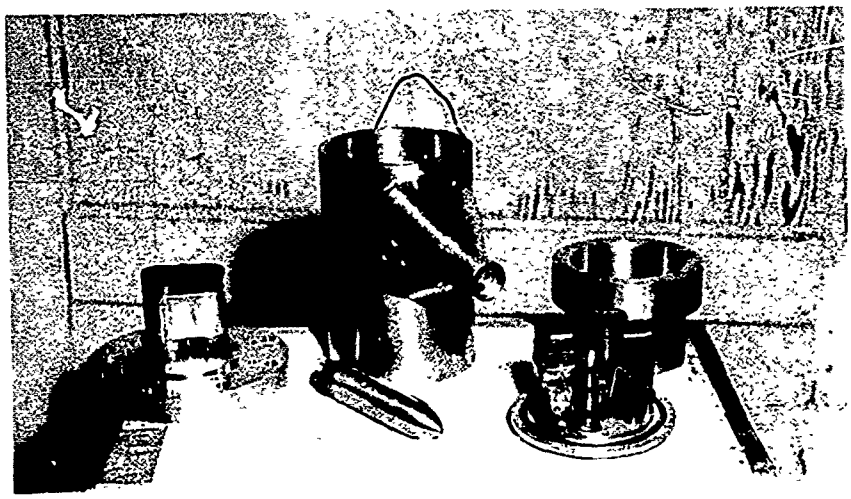

Figure 1.11 Self-recording q-gage, new model.

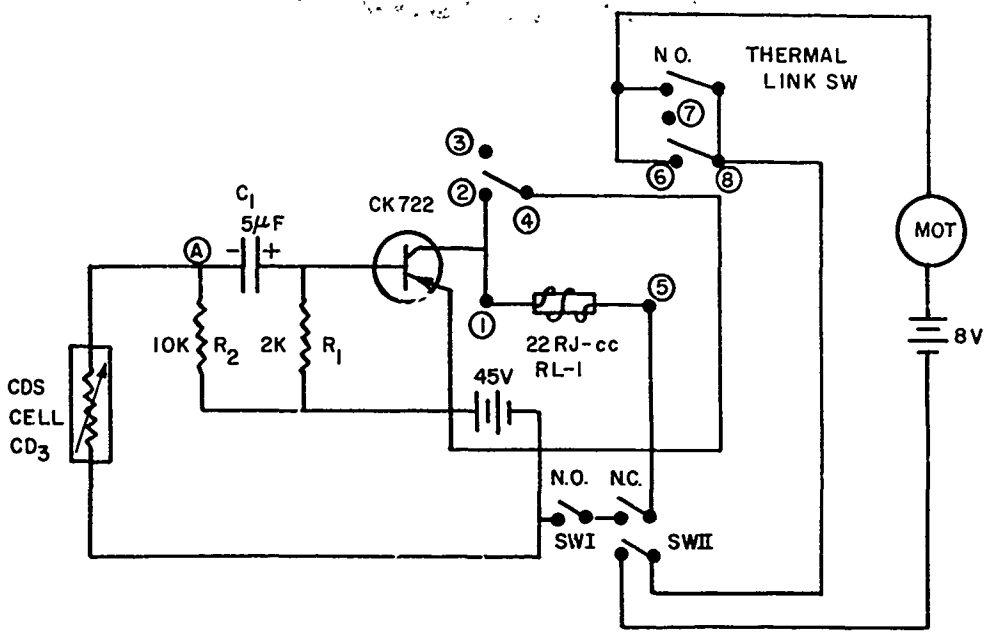

SWI- SAFETY SWITCH NORMALLY OPEN, CLOSED MANUALLY.

SWII- ROTATION LIMIT SWITCHES. TWO IN PARALLEL NORMALLY CLOSED.

Figure 1.12 Schematic diagram, photo-initiation circuit.

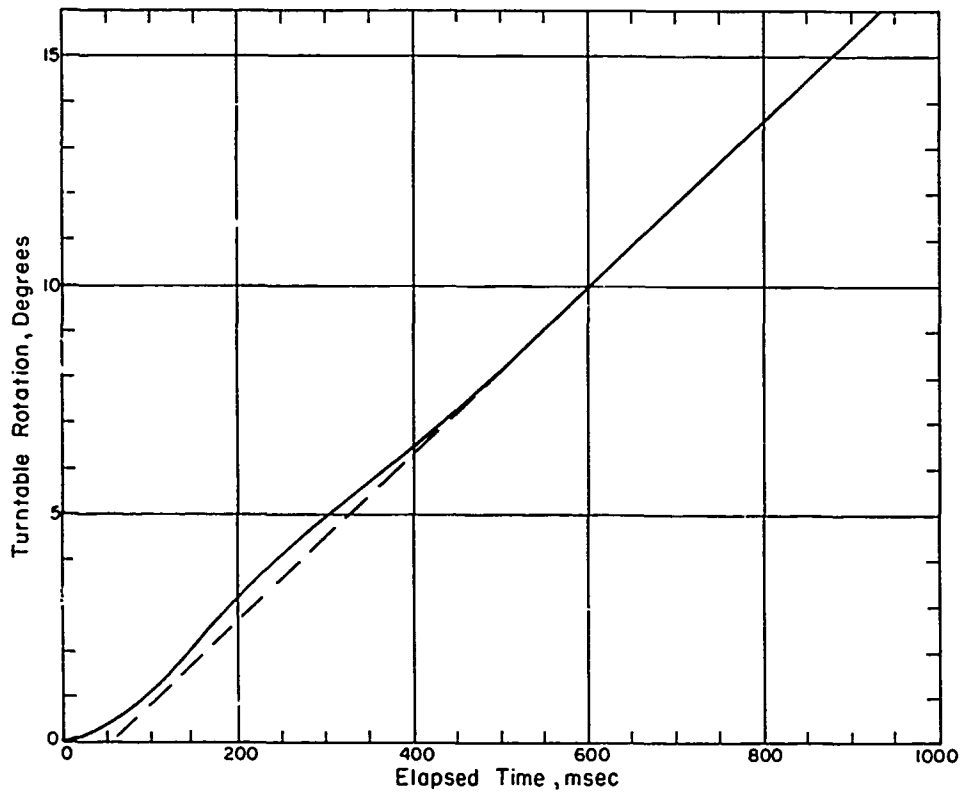

Figure 1.13 Turntable rotation versus elapsed time, 3-rpm motor.

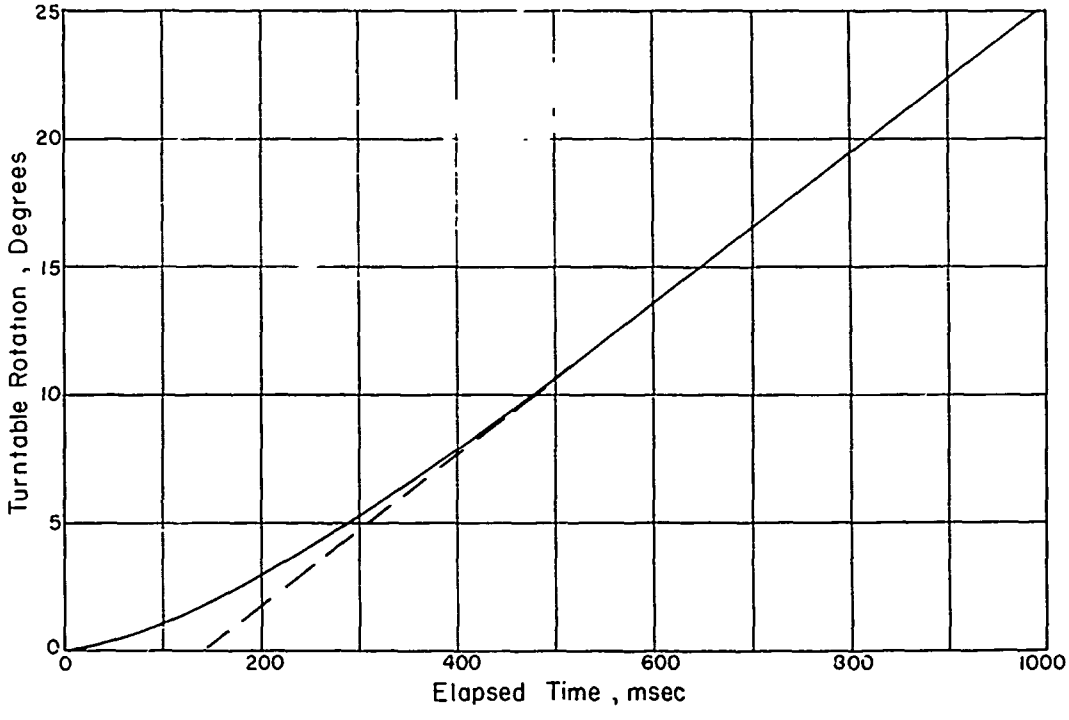

Figure 1.14 Turntable rotation versus elapsed time, 10-rpm motor.

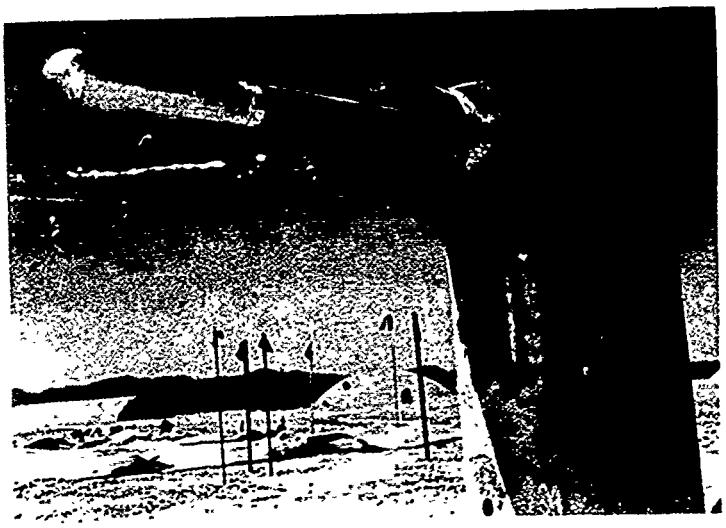

Figure 1.15 Contractor-installed q-gage tower with new midbody for standard q-gage.

Figure 1.16 Contractor-installed towers for old and new model q-gages.

Figure 1.17 BRL-installed q-gage mount, new model.

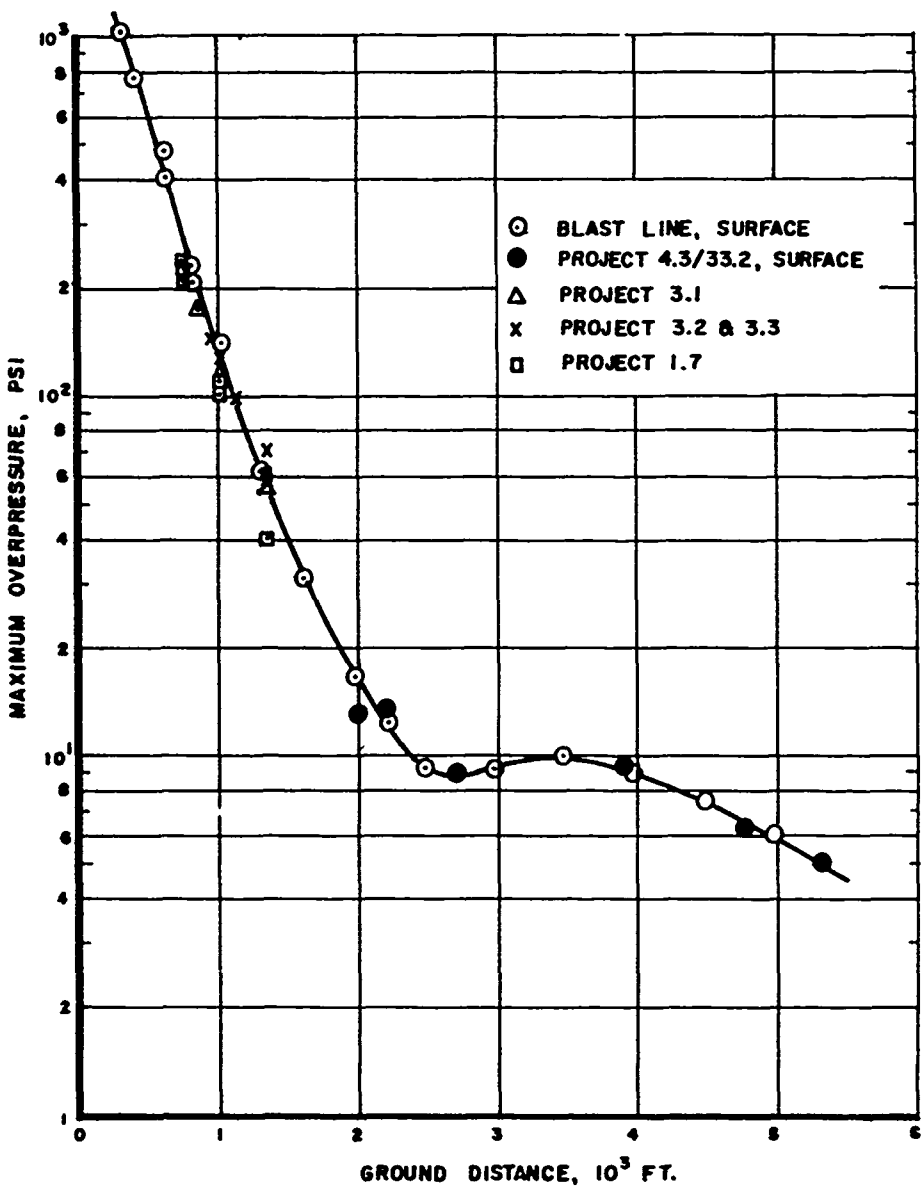

Figure 1.18 Maximum overpressure versus distance, main blast line.

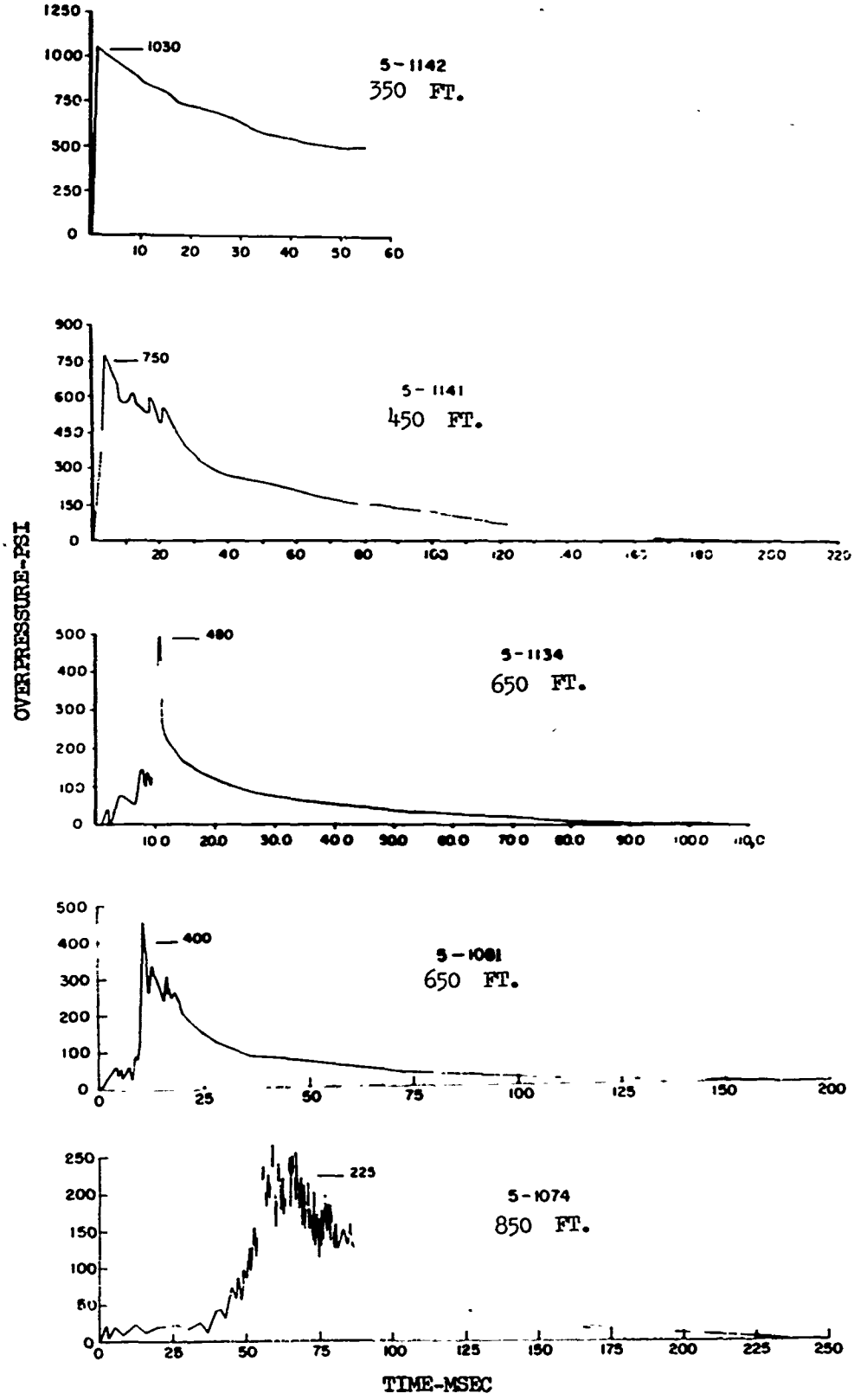

Figure 1.19 Overpressure-time histories, main blast line at distances of 350, 450, 650, and 850 feet.

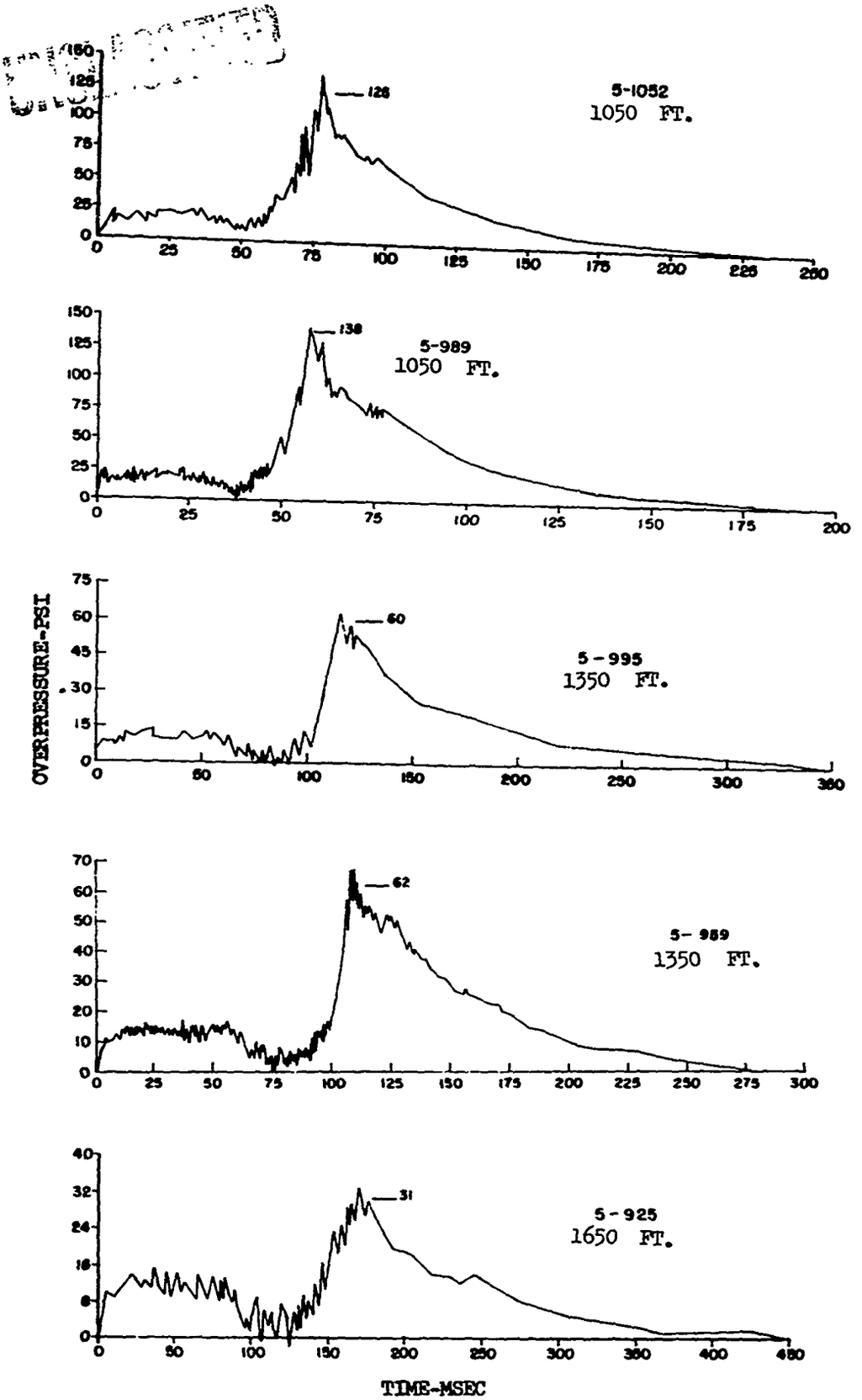

Figure 1.20 Overpressure-time histories, main blast line at distances of 1,050, 1,350, and 1,650 feet.

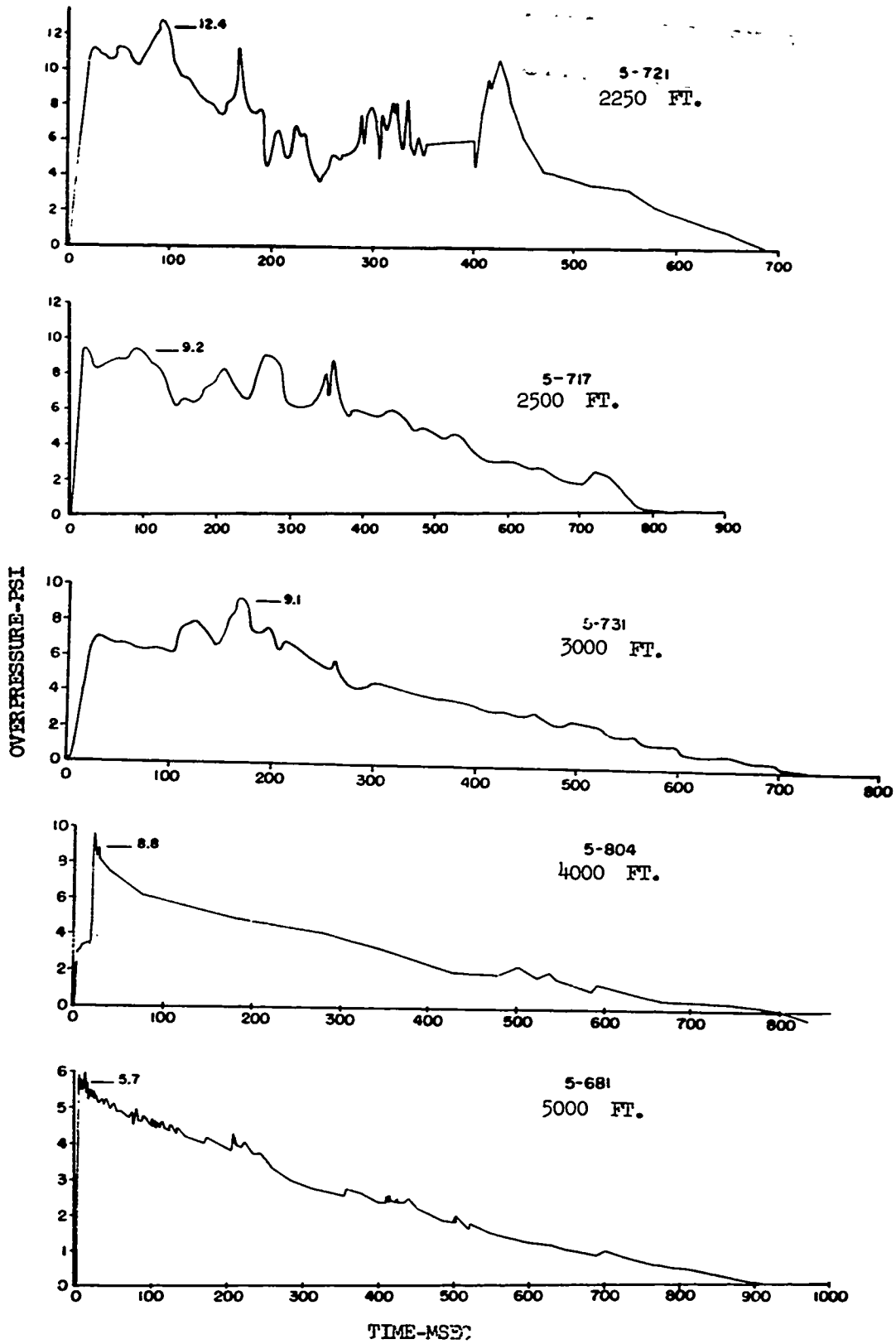

Figure 1.21 Overpressure-time histories, main blast line at distances of 2,250, 2,500, 3,000, 4,000 and 5,000 feet.

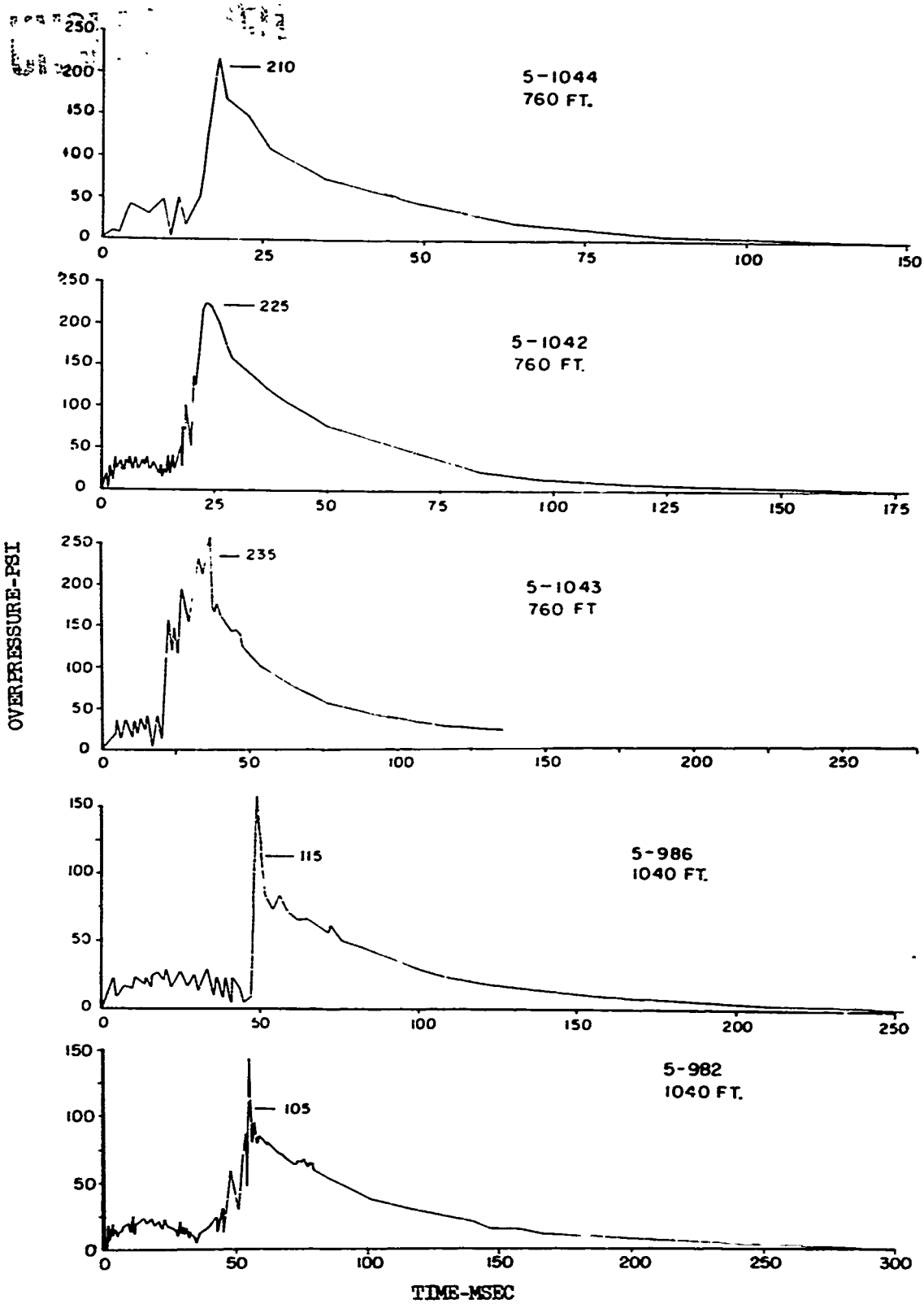

Figure 1.22 Overpressure-time histories, Project 1.7 at distances of 760 and 1,040 feet.

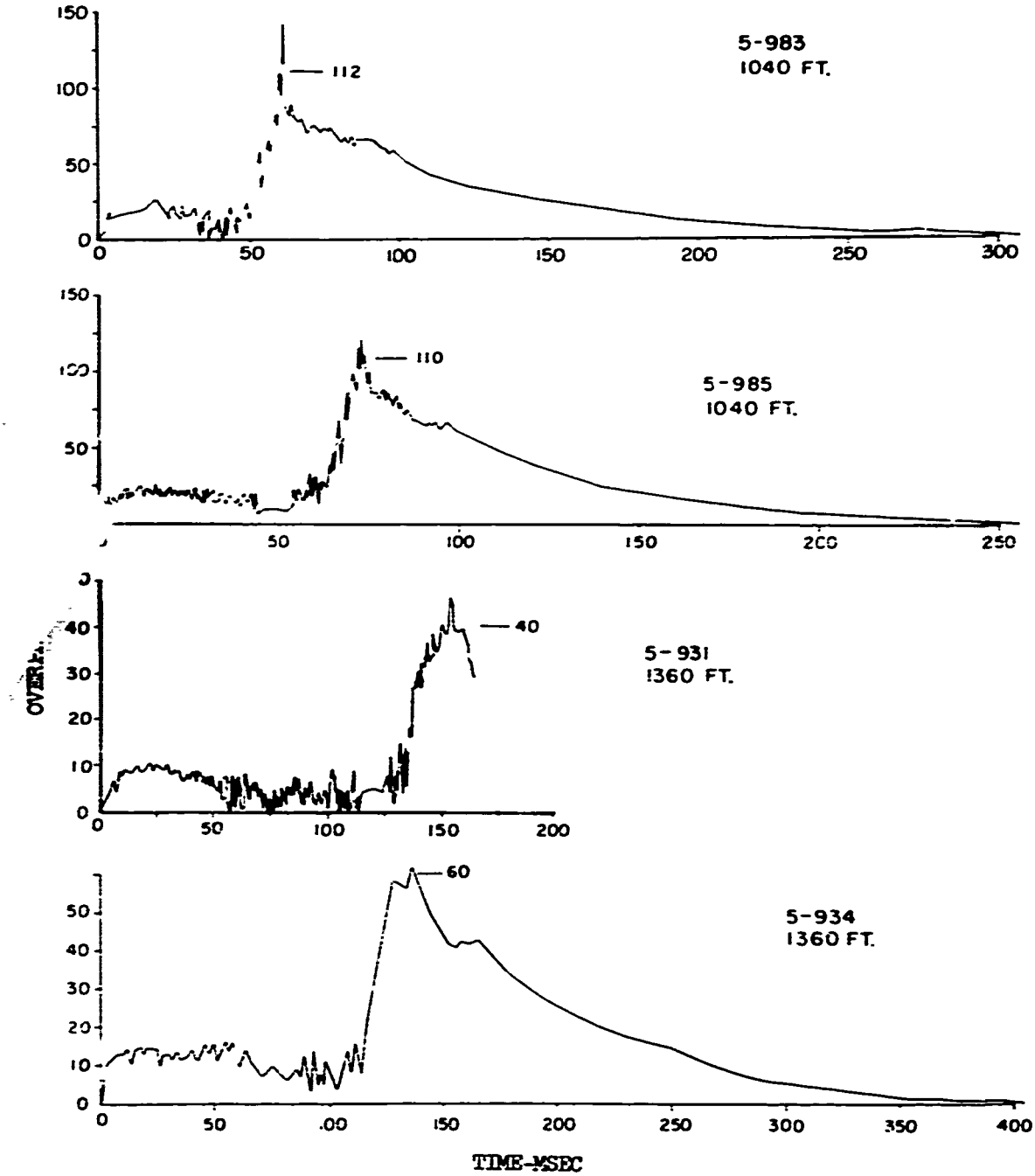

Figure 1.23 Overpressure-time histories, Project 1.7 at distances of 1,040 and 1,360 feet.

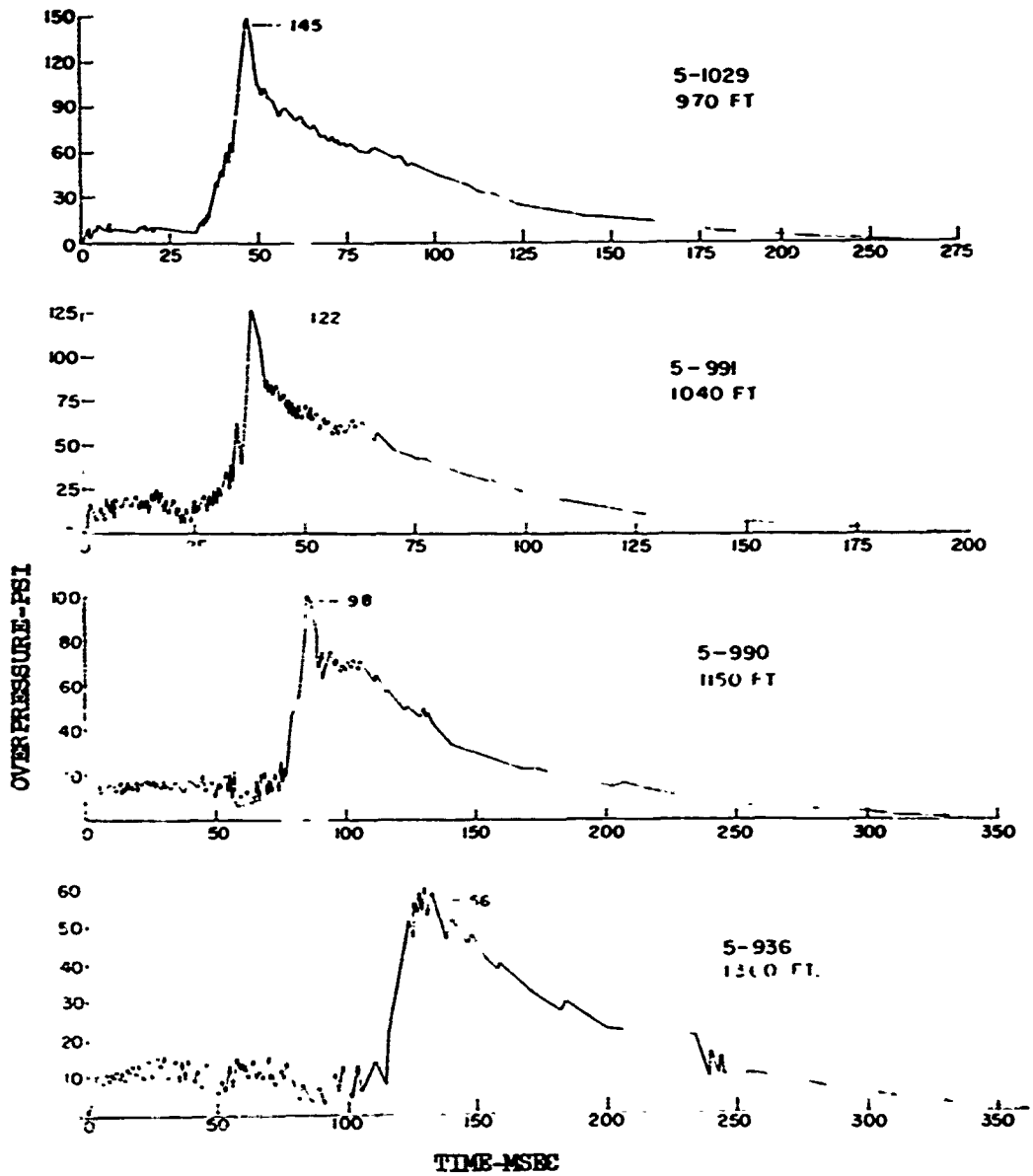

Figure 1.24 Overpressure-time histories, Projects 3.2 and 3.3 at distances of 970, 1,040, 1,150 and 1,360 feet.

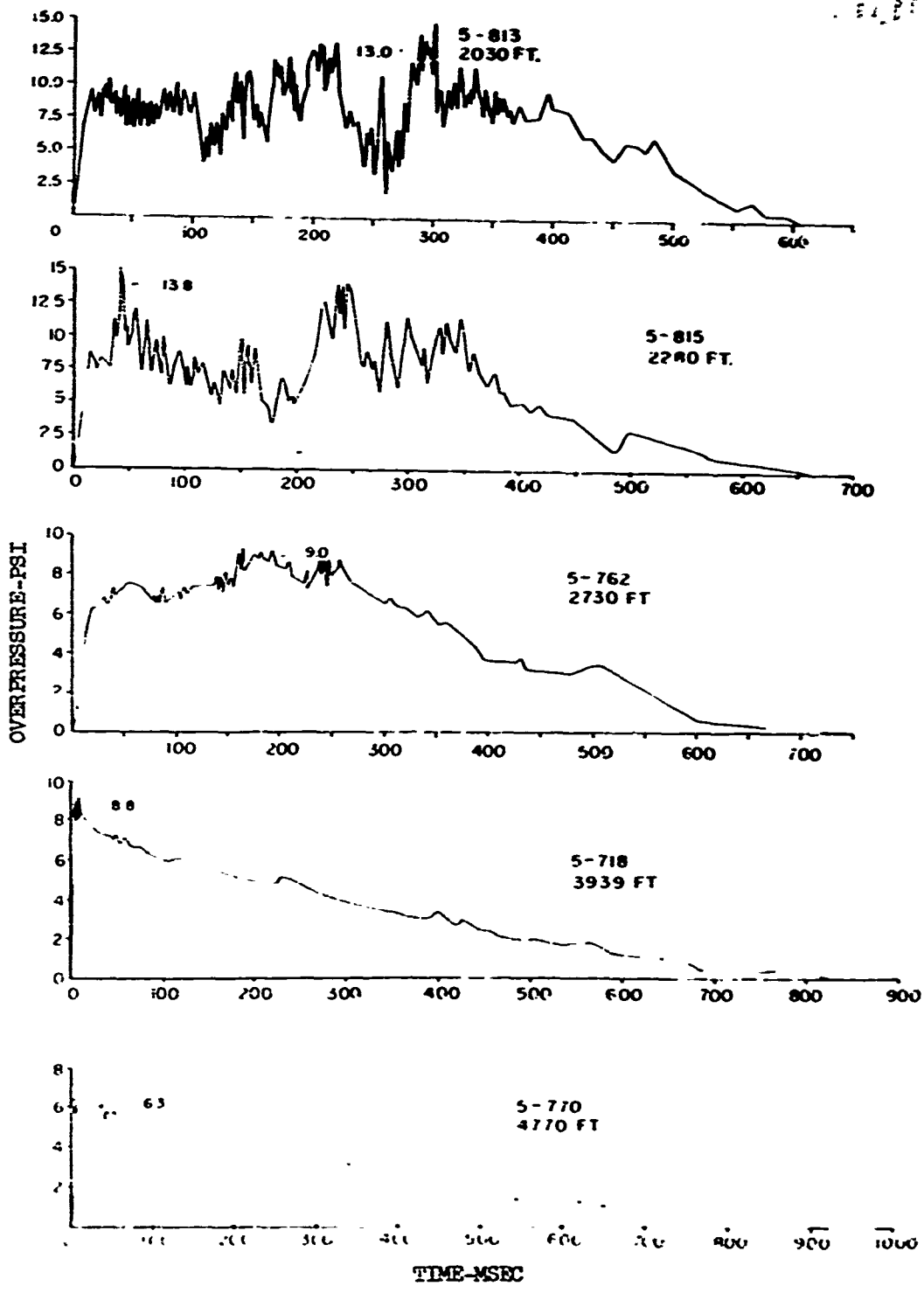

Figure 1.25 Overpressure-time histories, Project 4.3/33.2 at distances of 2,030, 2,280, 2,730, 3,939, and 4,770 feet.

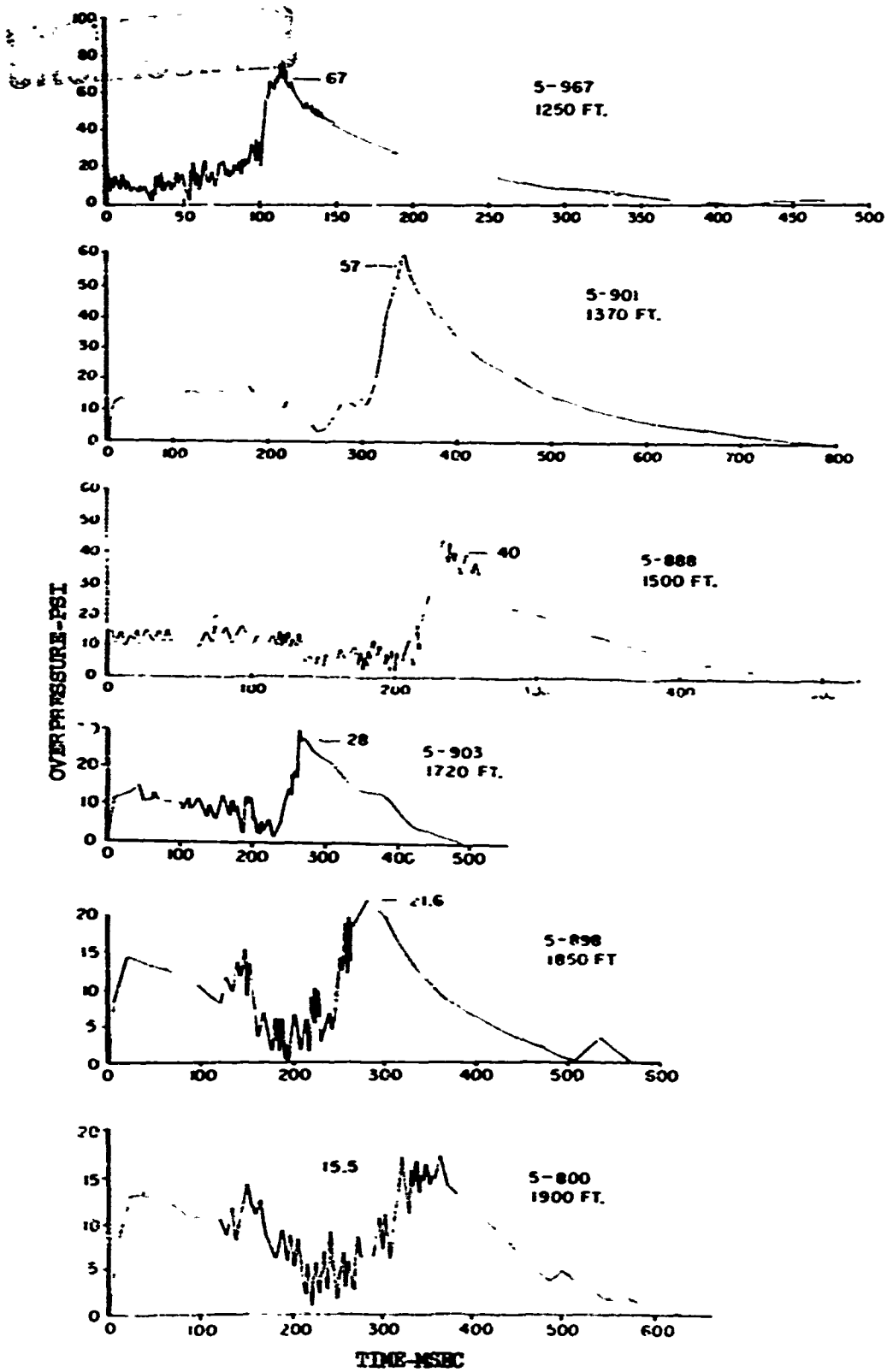

Figure 1.26 Overpressure-time histories, Project 6.1 at distances of 1,250, 1,370, 1,500, 1,720, 1,850 and 1,900 feet.

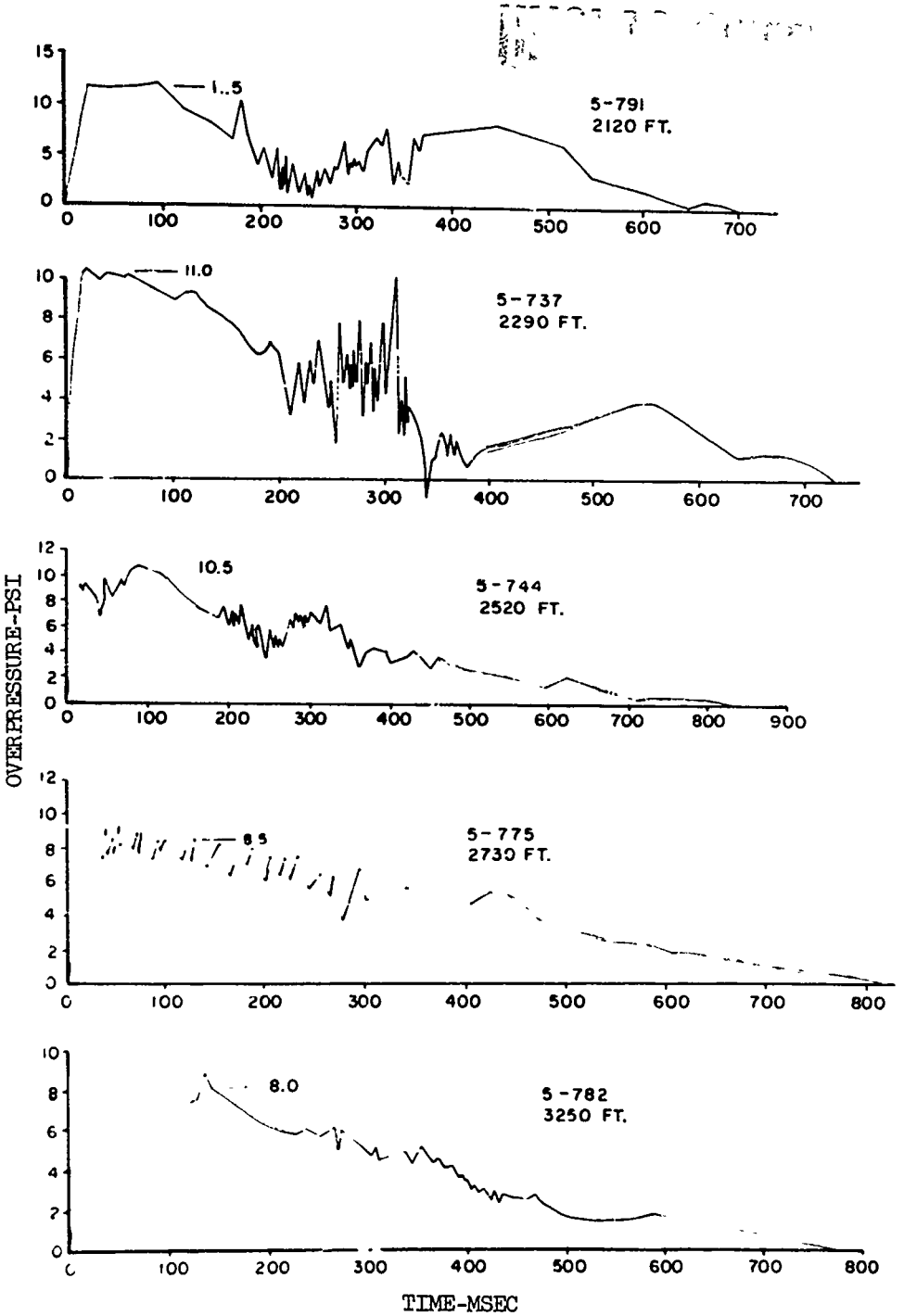

Figure 1.27 Overpressure-time histories, Project 6.1 at distances of 2,120, 2,290, 2,520, 2,730 and 3,250 feet.

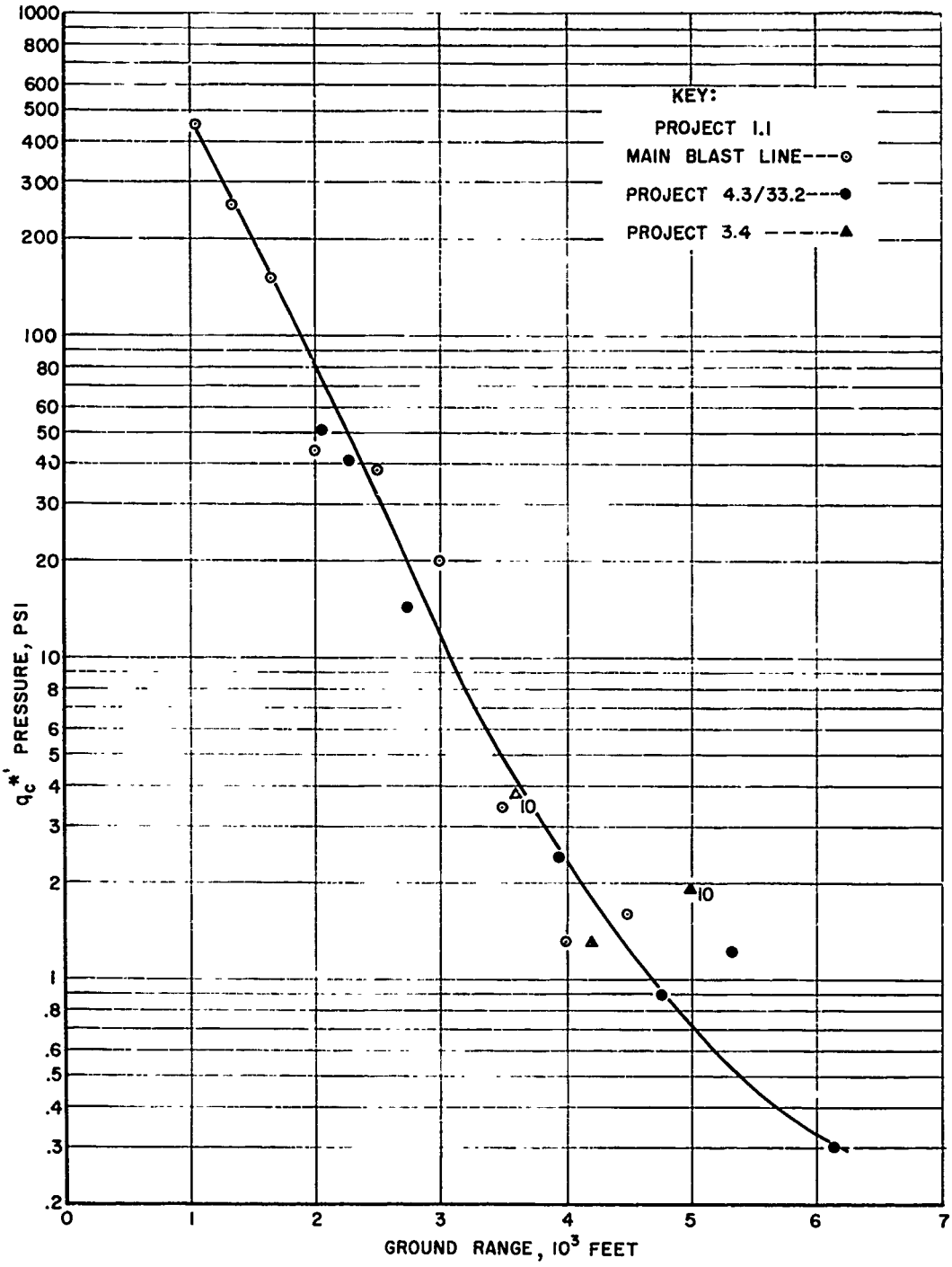

Figure 1.28 Pressure difference $(P_p - P_s)^{*'}$ (maximum) versus distance.

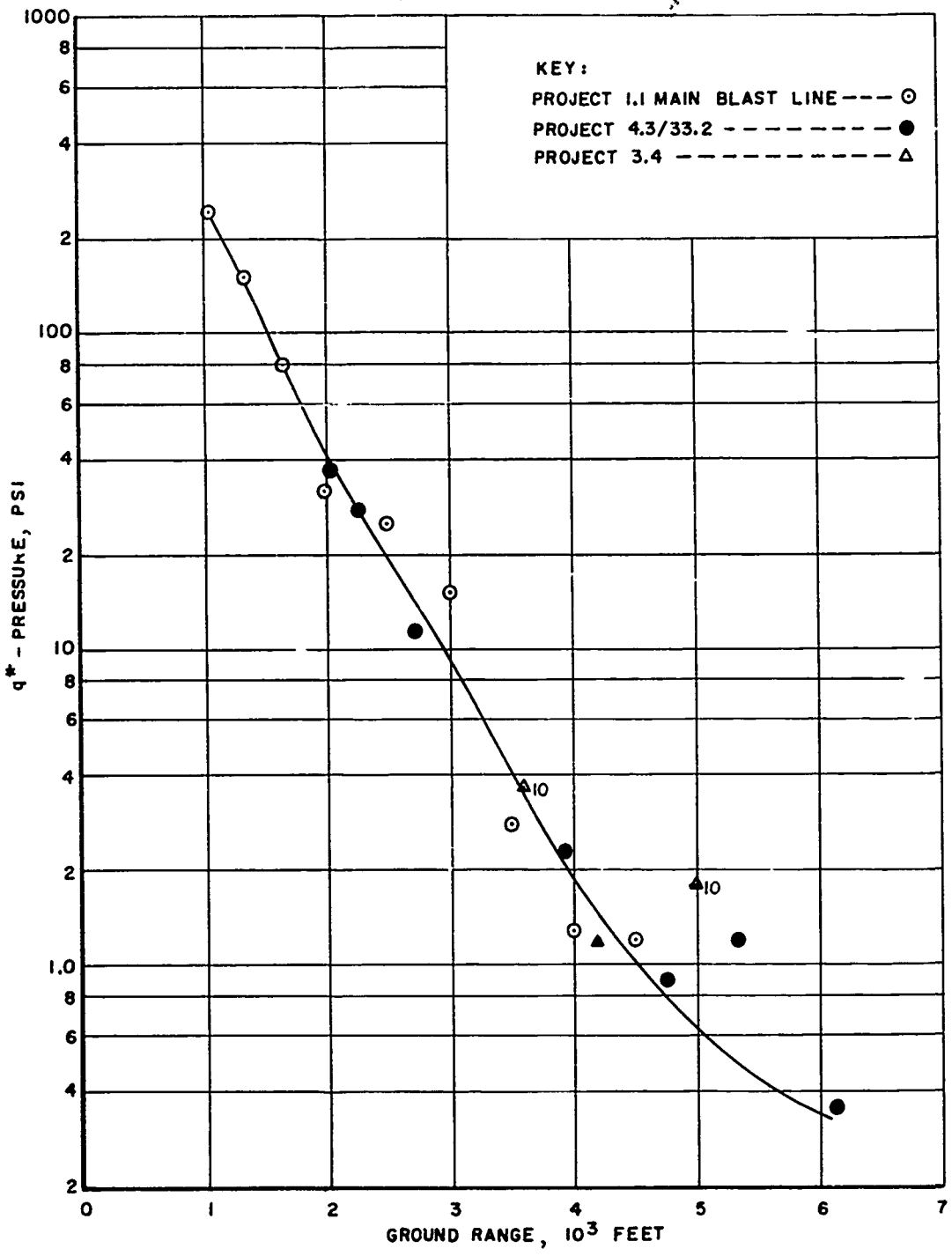

Figure 1.29 Maximum dynamic pressure q*versus distance.

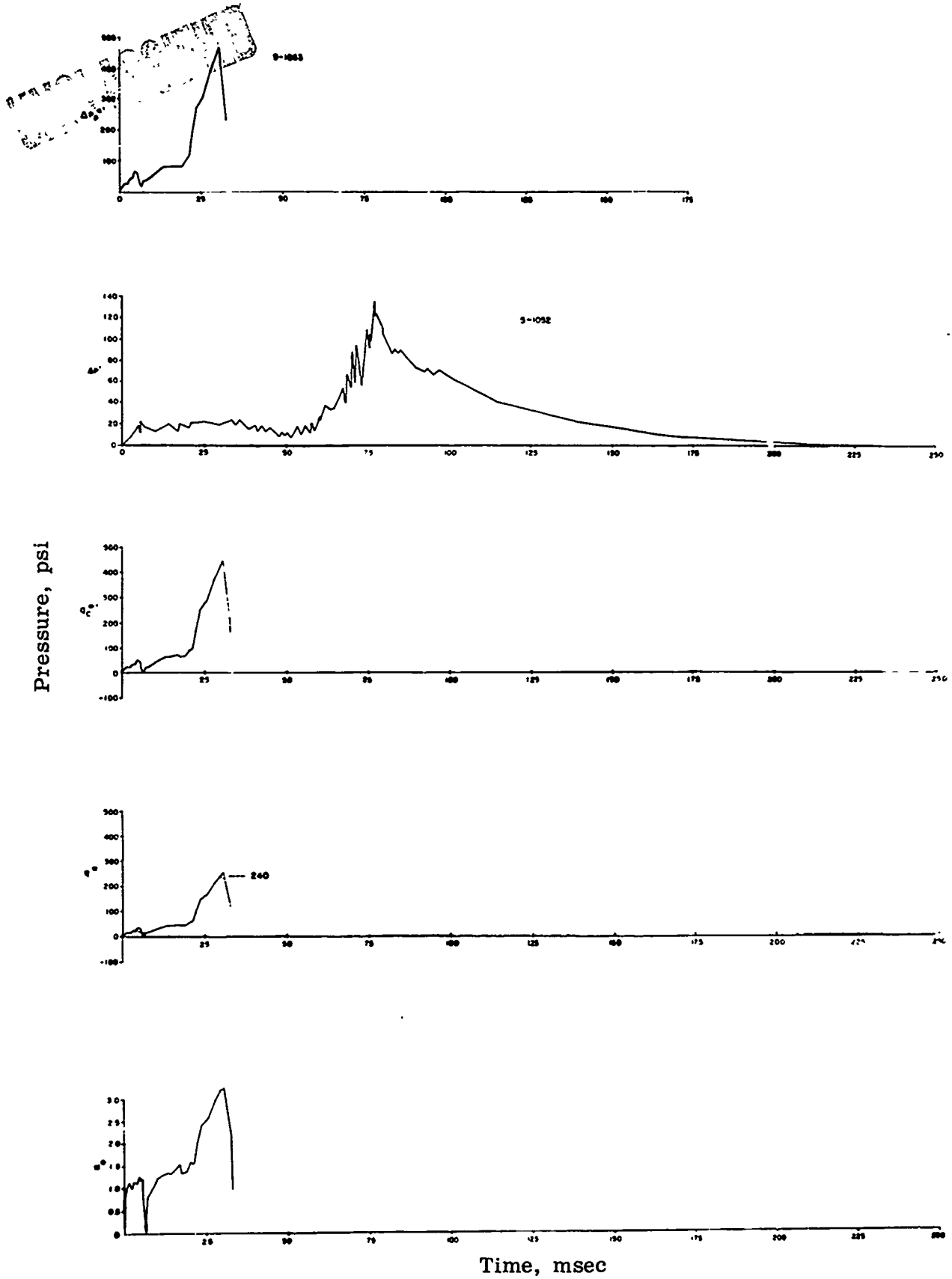

Figure 1.30 Pressure and Mach number versus time, main blast line at 1,050 feet.

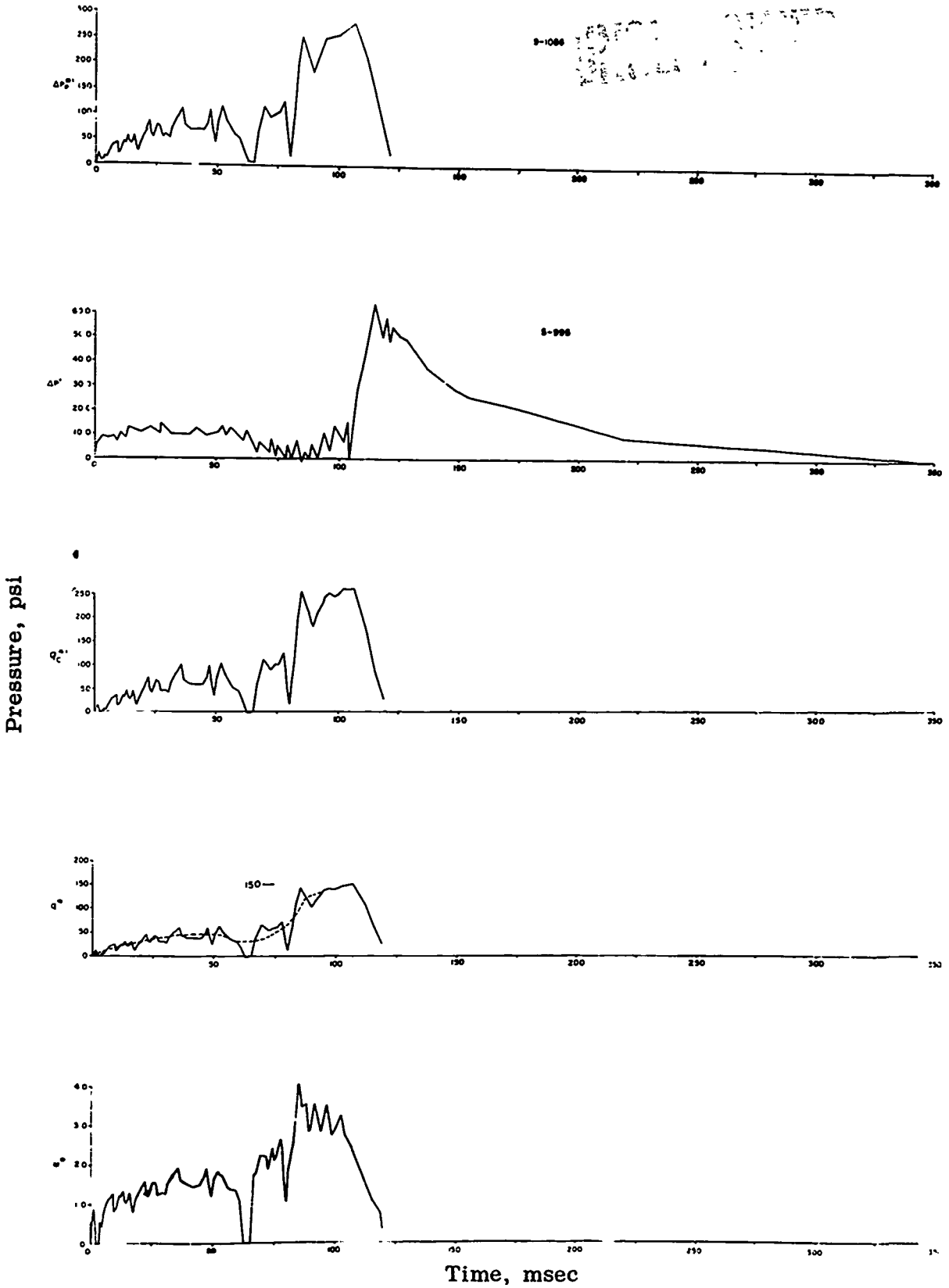

Figure 1.31 Pressure and Mach number versus time, main blast line at 1,350 feet.

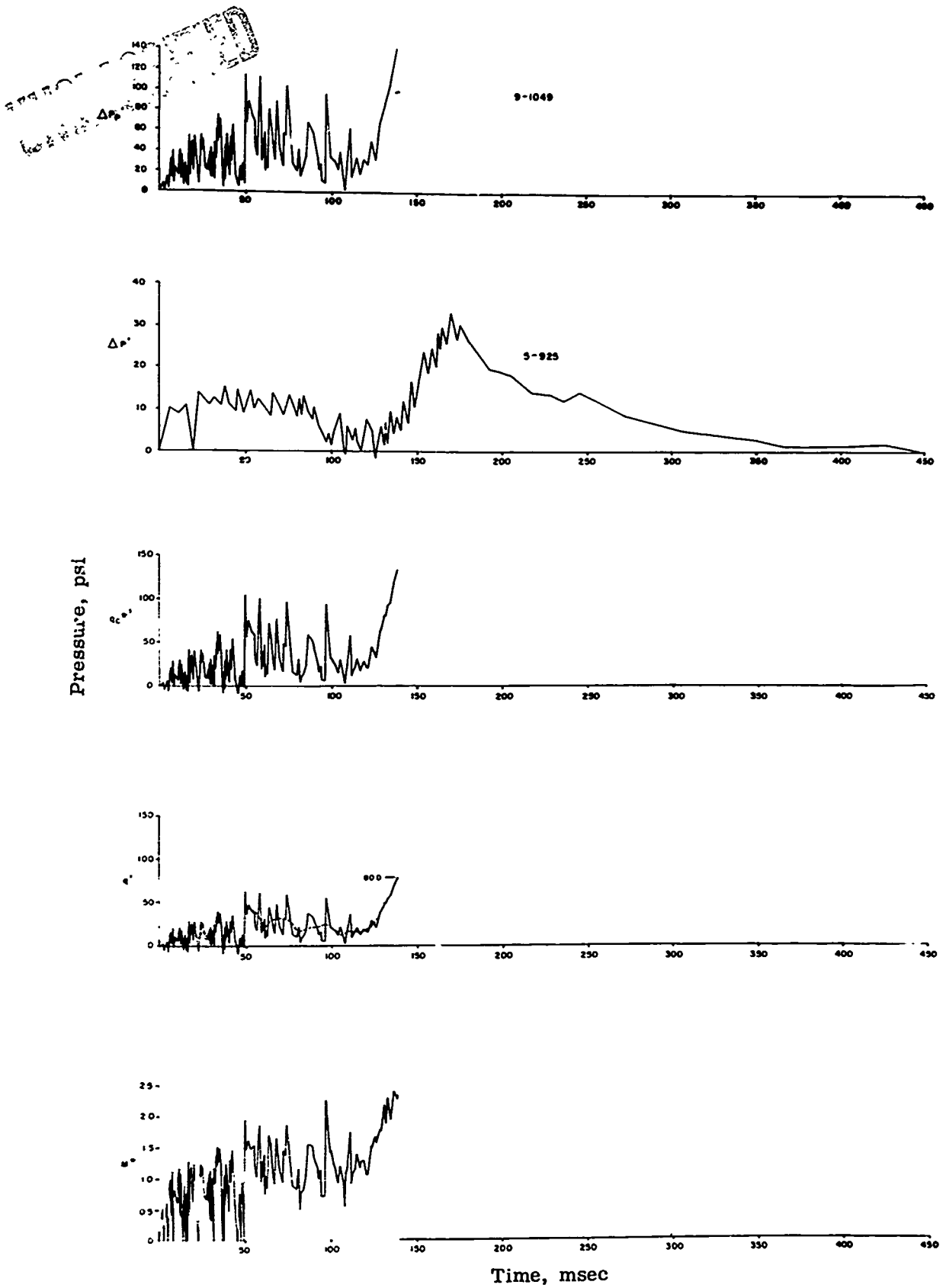

Figure 1.32 Pressure and Mach number versus time, main blast line at 1,650 feet.

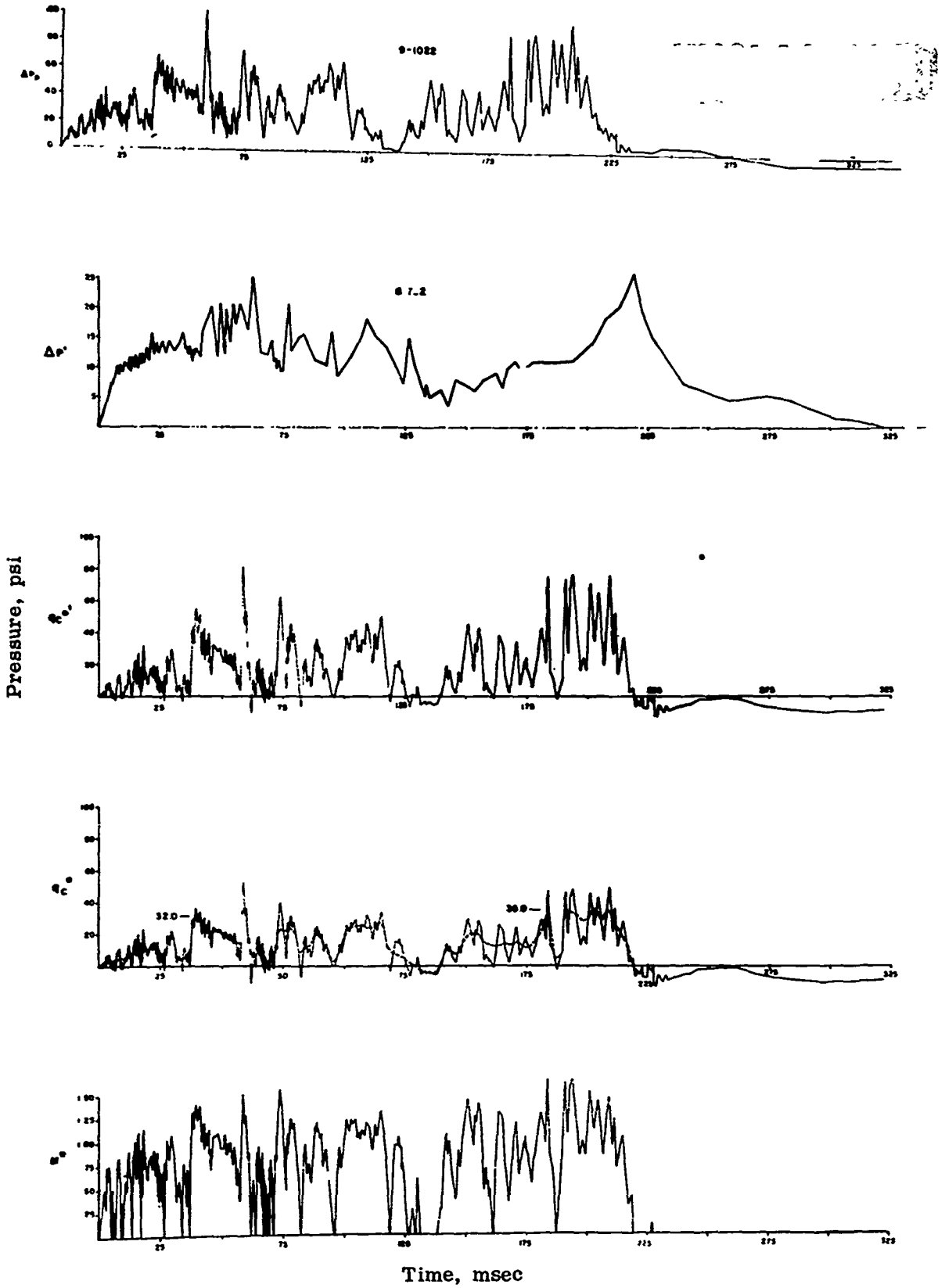

Figure 1.33 Pressure and Mach number versus time, main blast line at 2,000 feet.

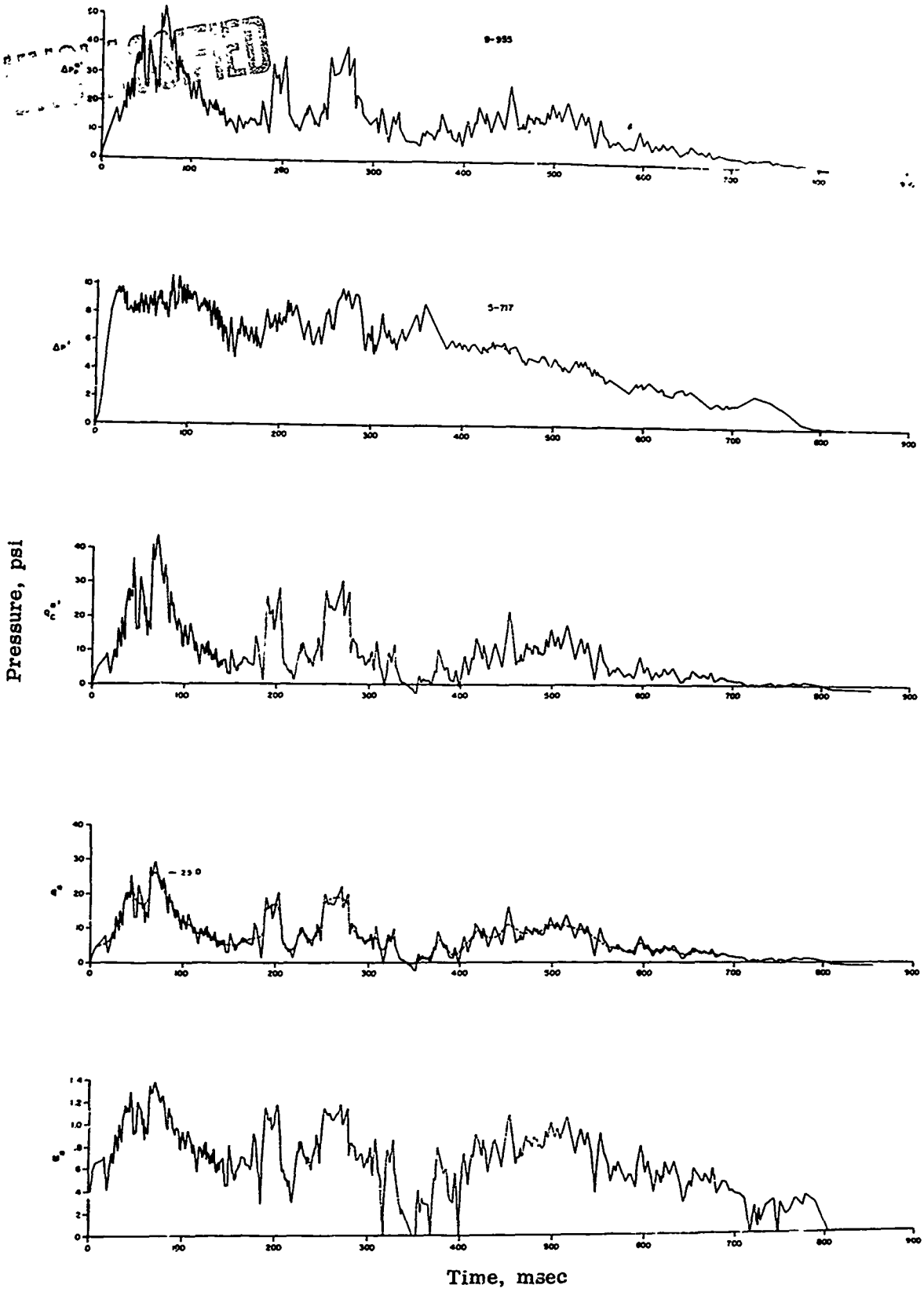

Figure 1.34 Pressure and Mach number versus time, main blast line at 2,500 feet.

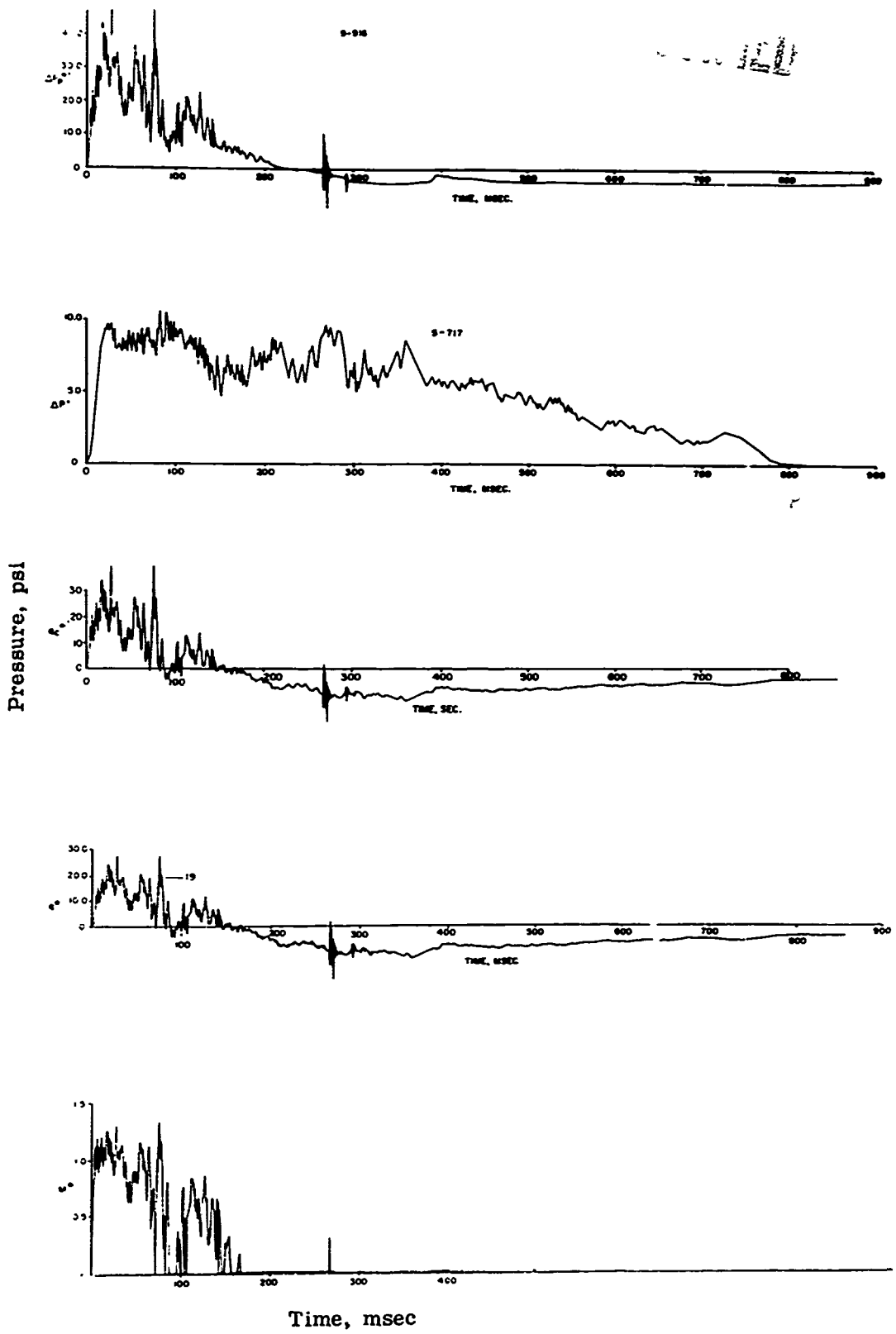

Figure 1.35 Pressure and Mach number versus time, main blast line at 2,500 feet.

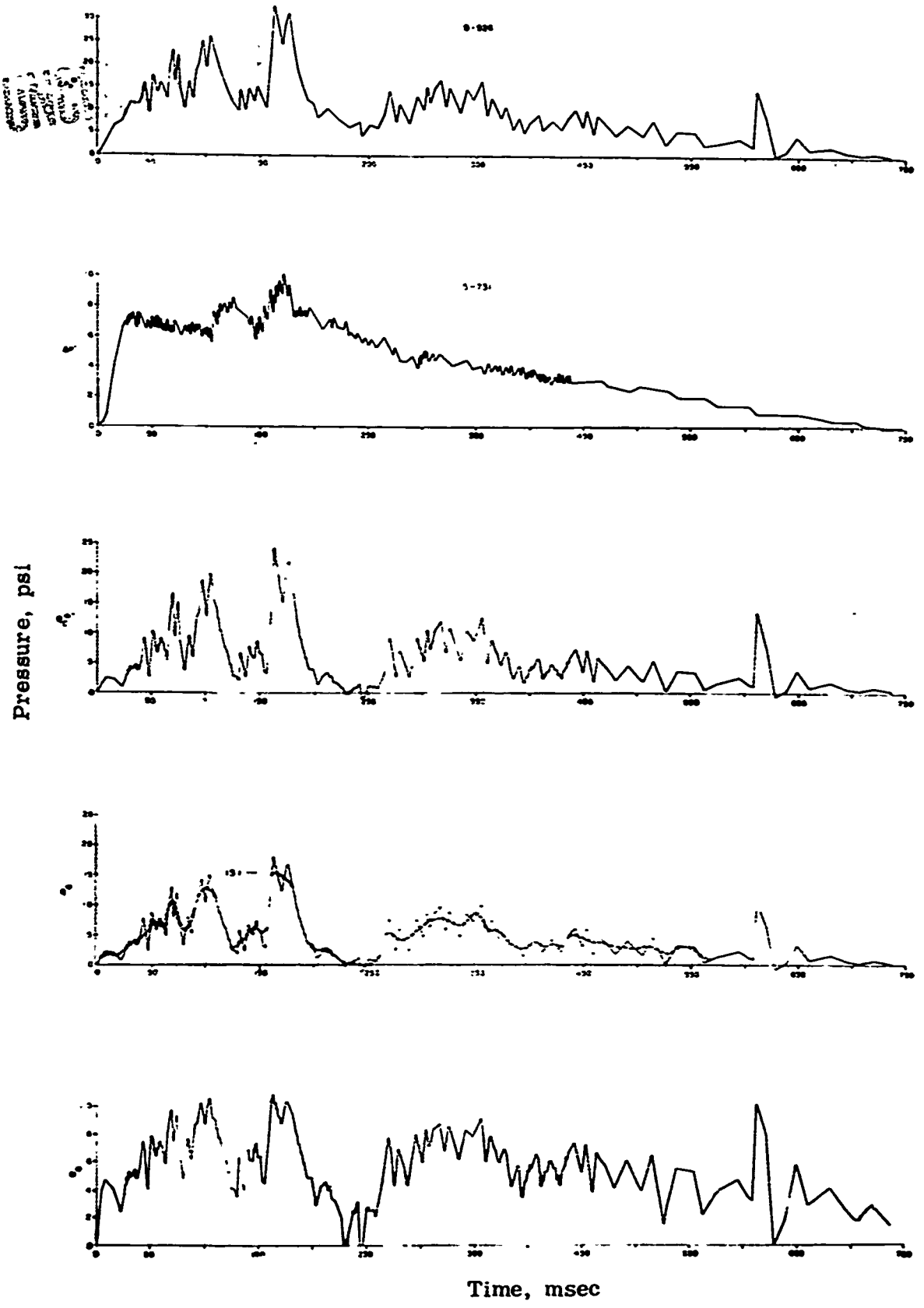

Figure 1.36 Pressure and Mach number versus time, main blast line at 3,000 feet.

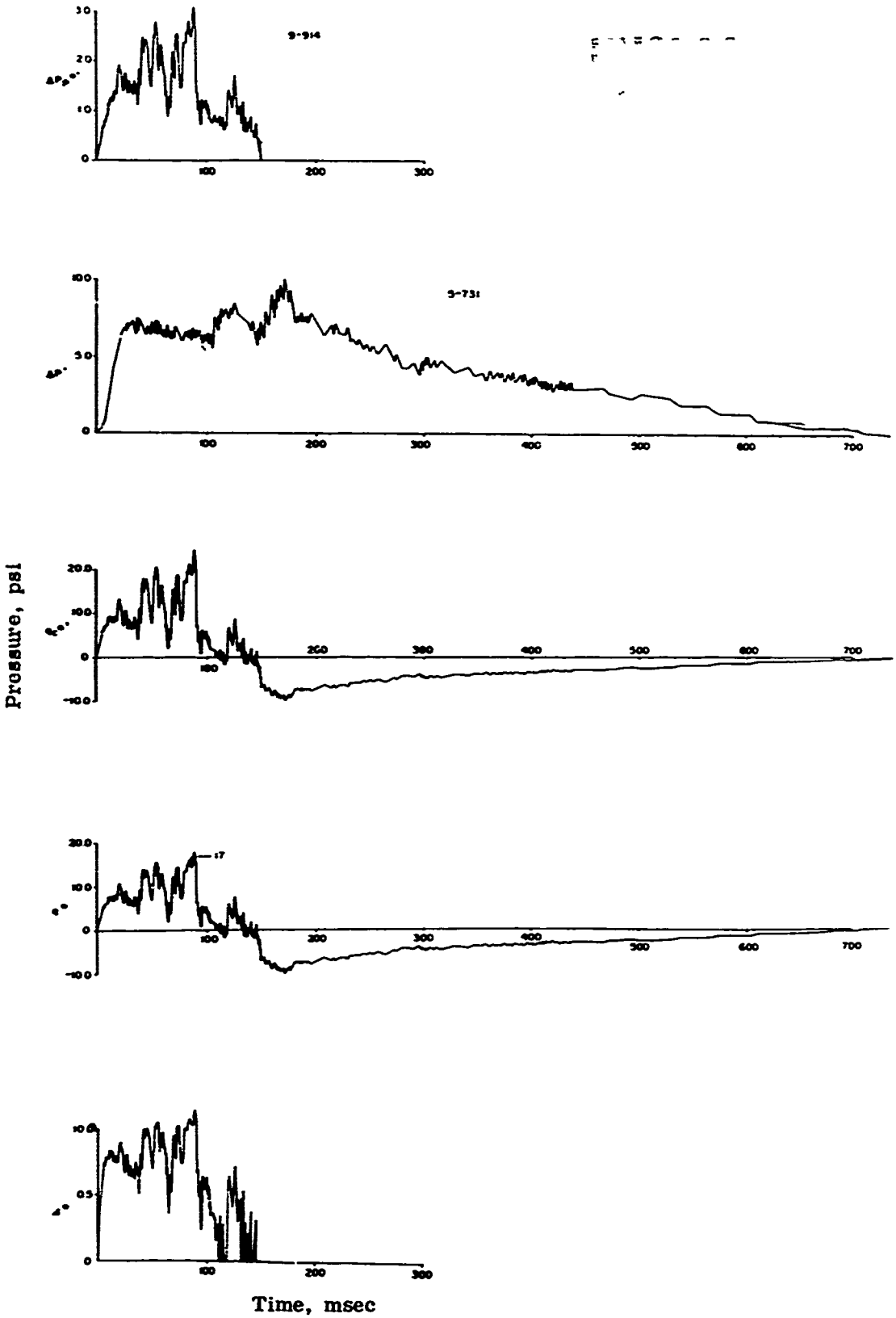

Figure 1.37 Pressure and Mach number versus time, main blast line at 3,000 feet.

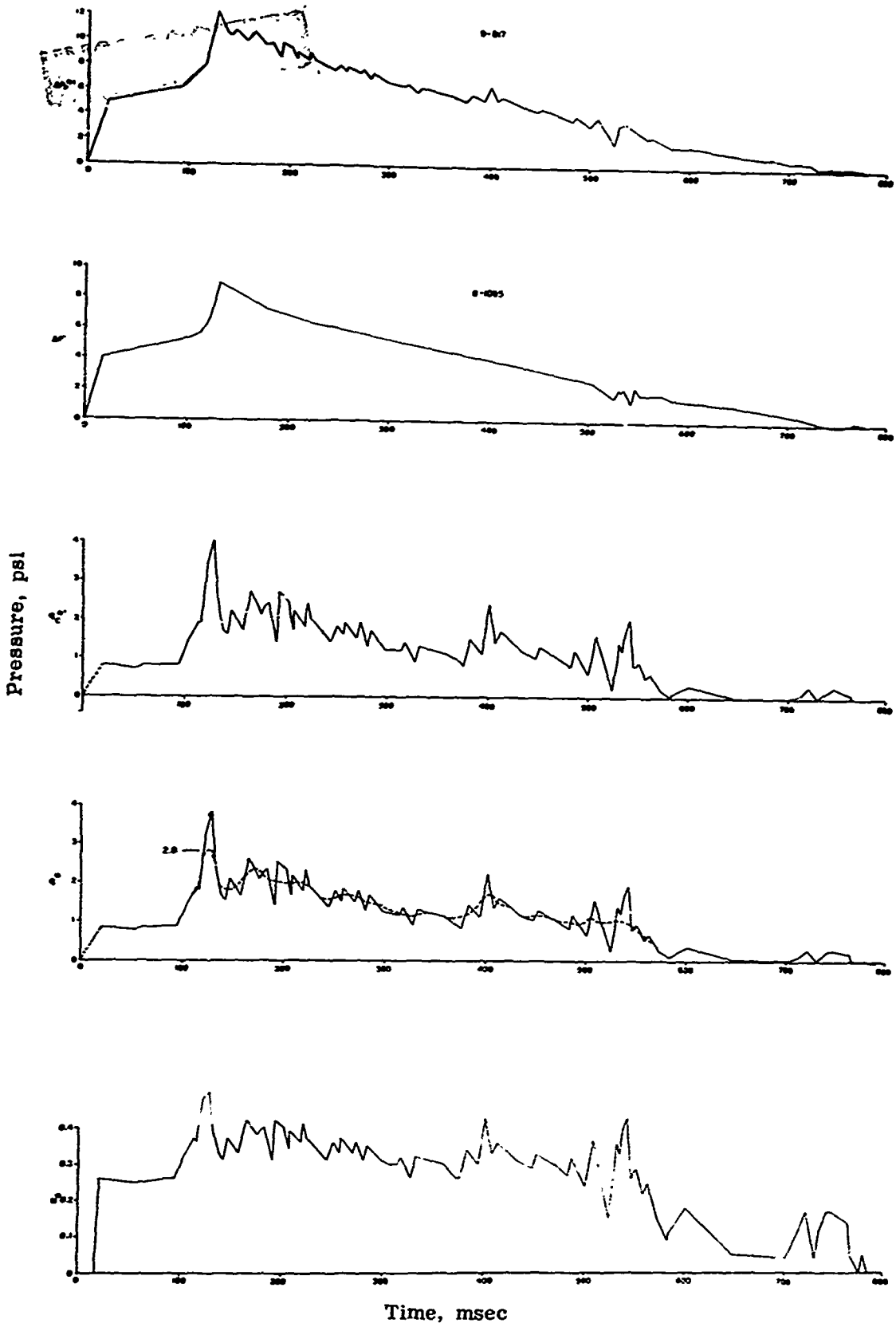

Figure 1.38 Pressure and Mach number versus time, main blast line at 3,500 feet.

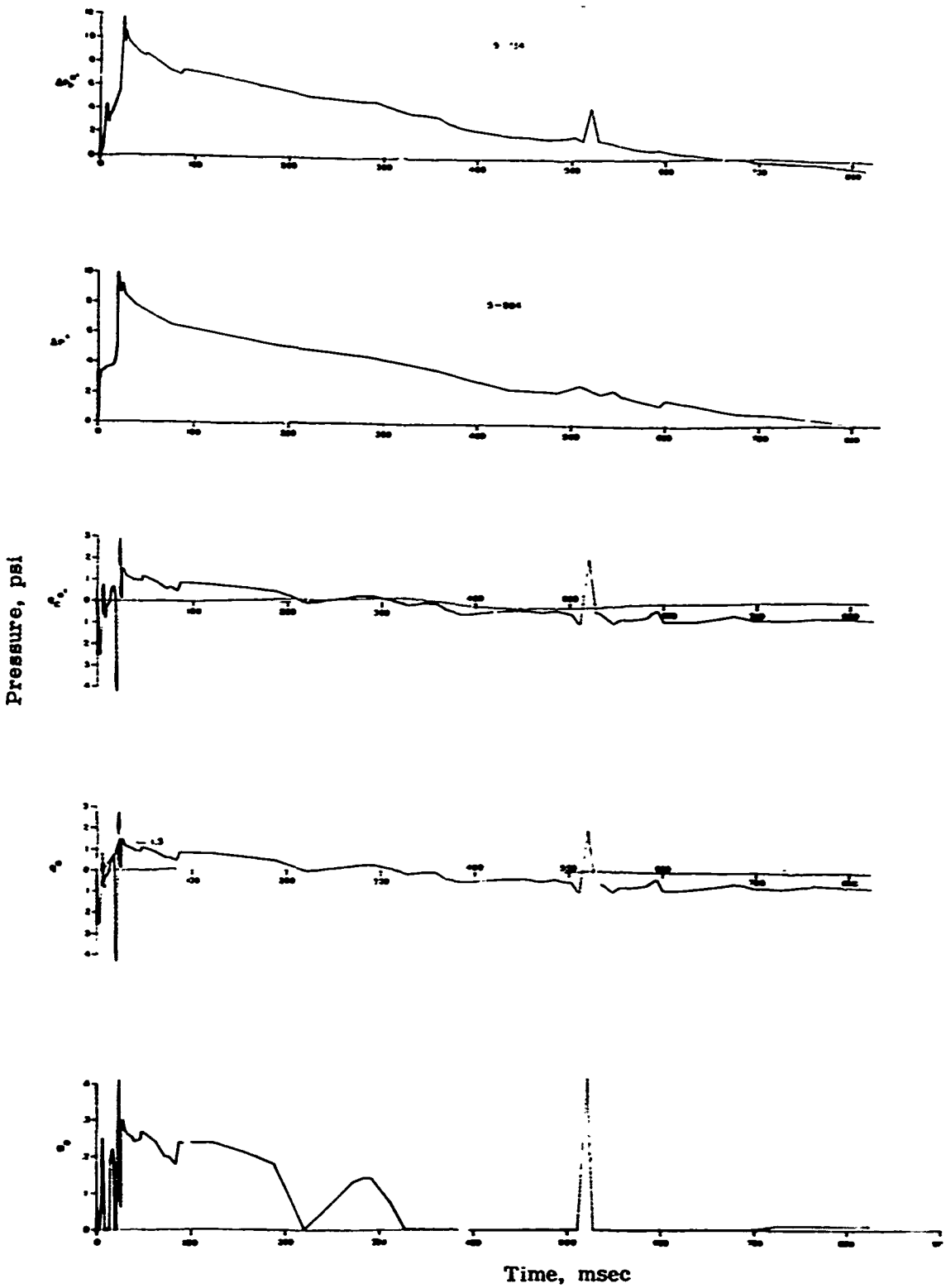

Figure 1.39 Pressure and Mach number versus time, main blast line at 4,000 feet.

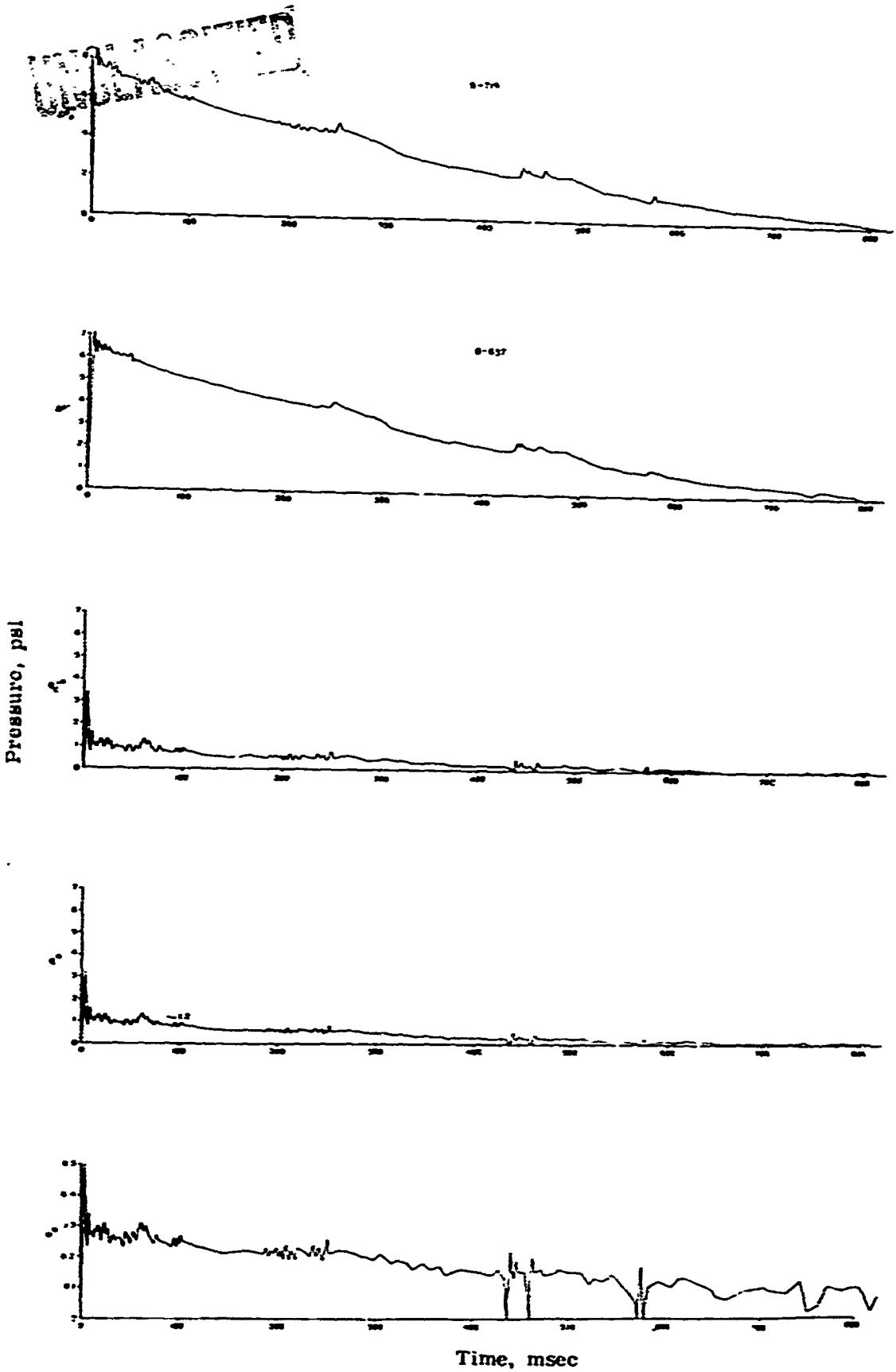

Figure 1.40 Pressure and Mach number versus time, main blast line at 4,500 feet.

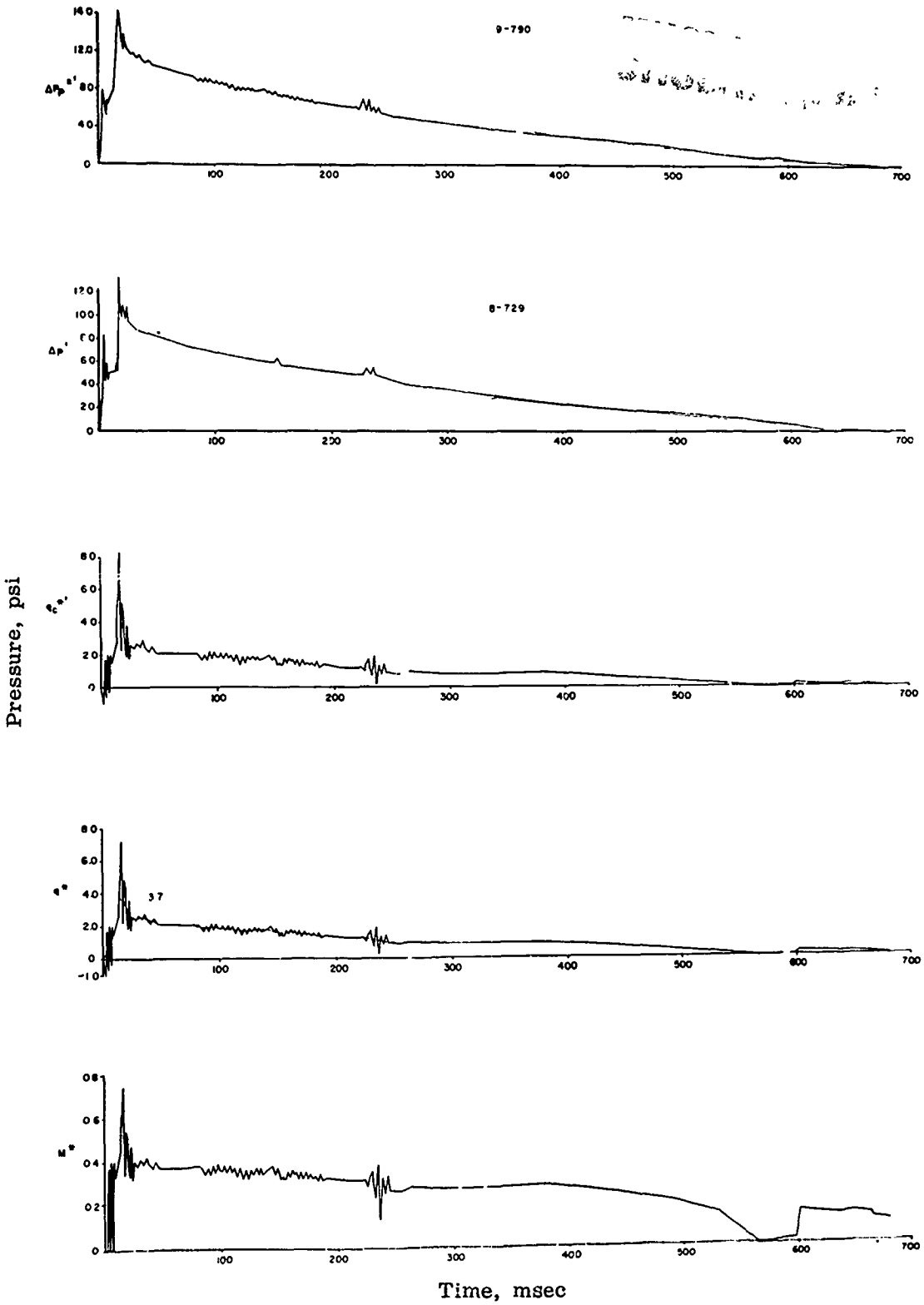

Figure 1.41 Pressure and Mach number versus time, Project 3.4 at 3,600 f...

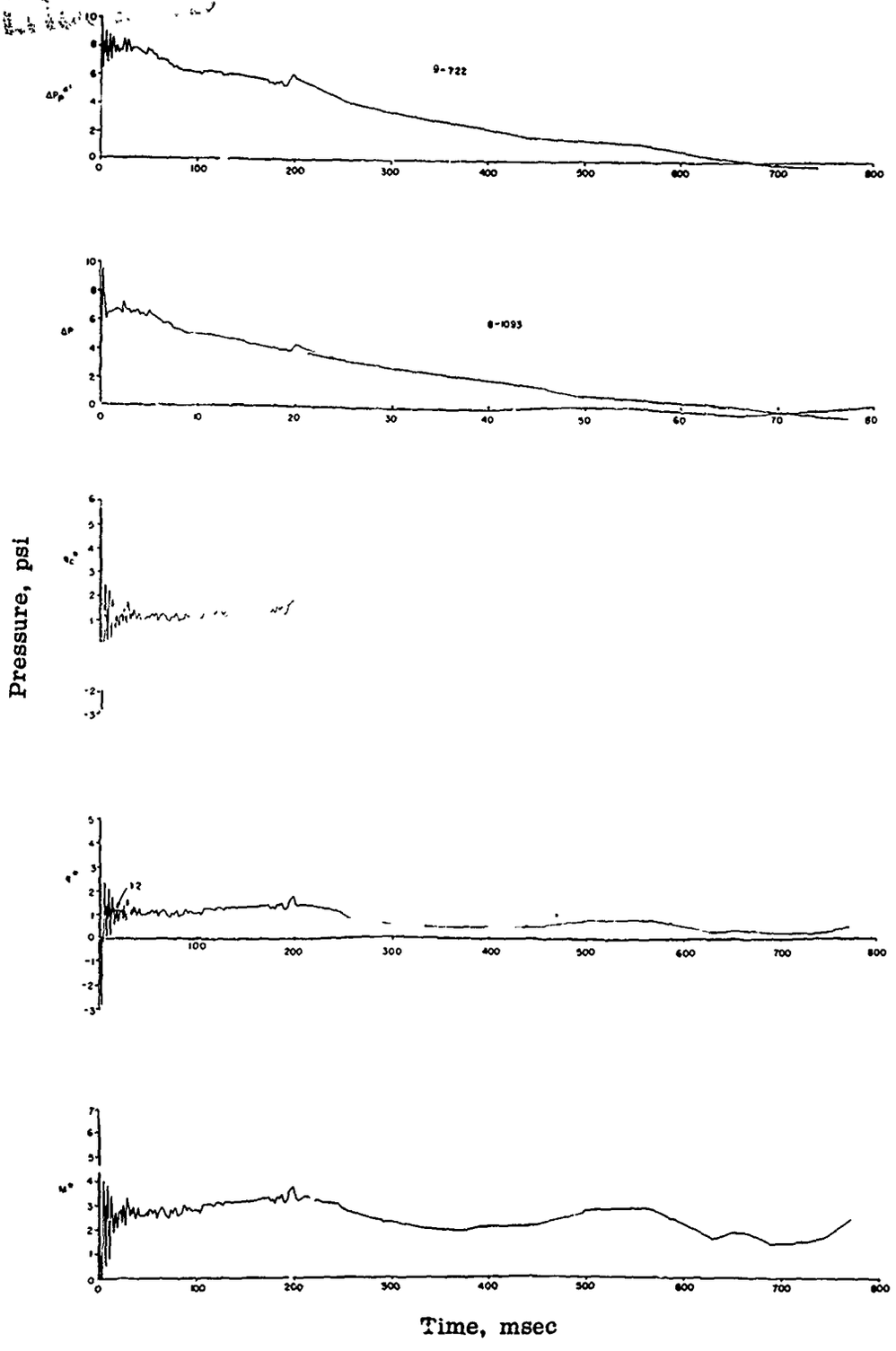

Figure 1.42 Pressure and Mach number versus time, Project 3.4 at 4,200 feet.

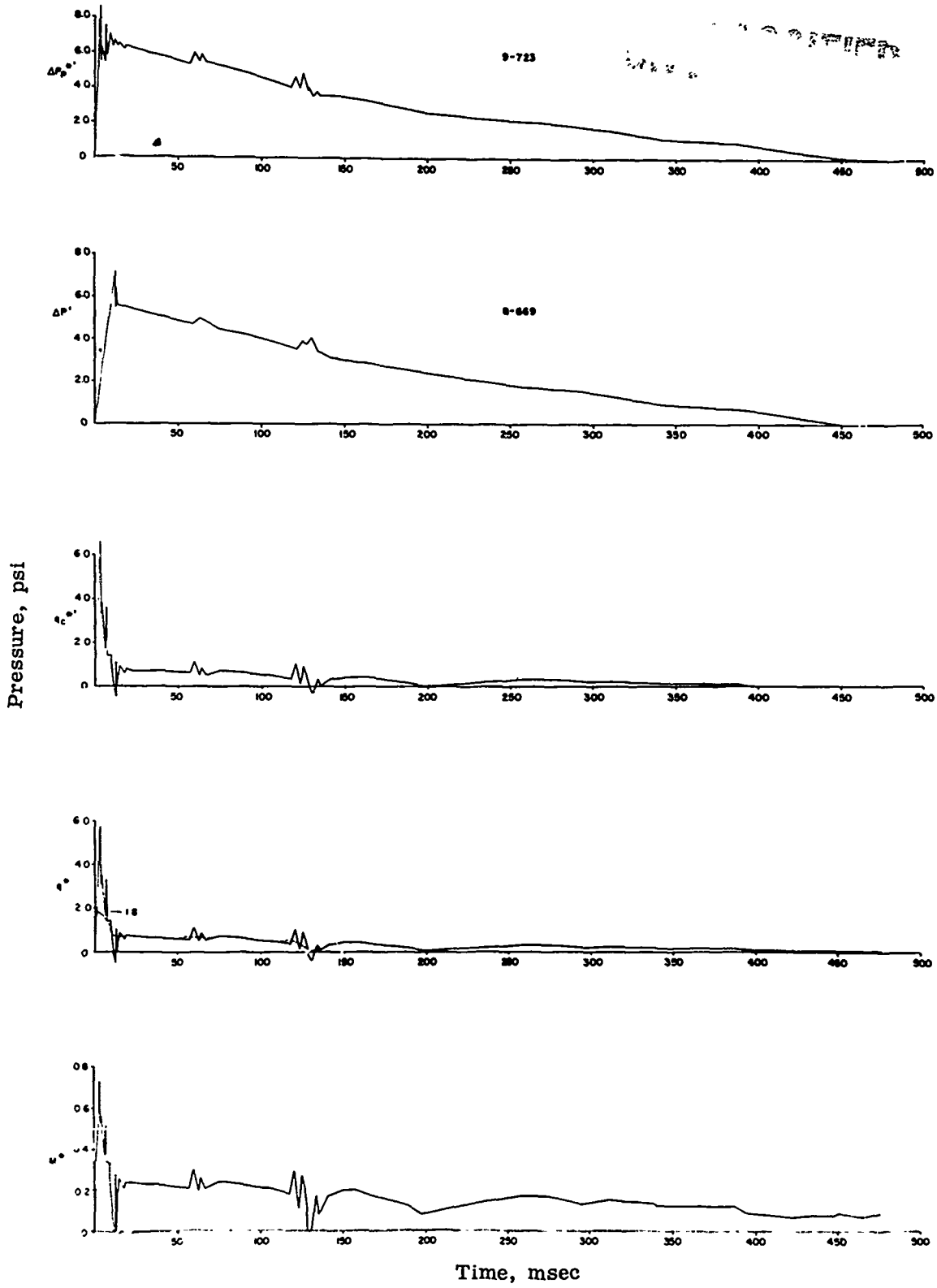

Figure 1.43 Pressure and Mach number versus time, Project 3.4 at 5,000 feet.

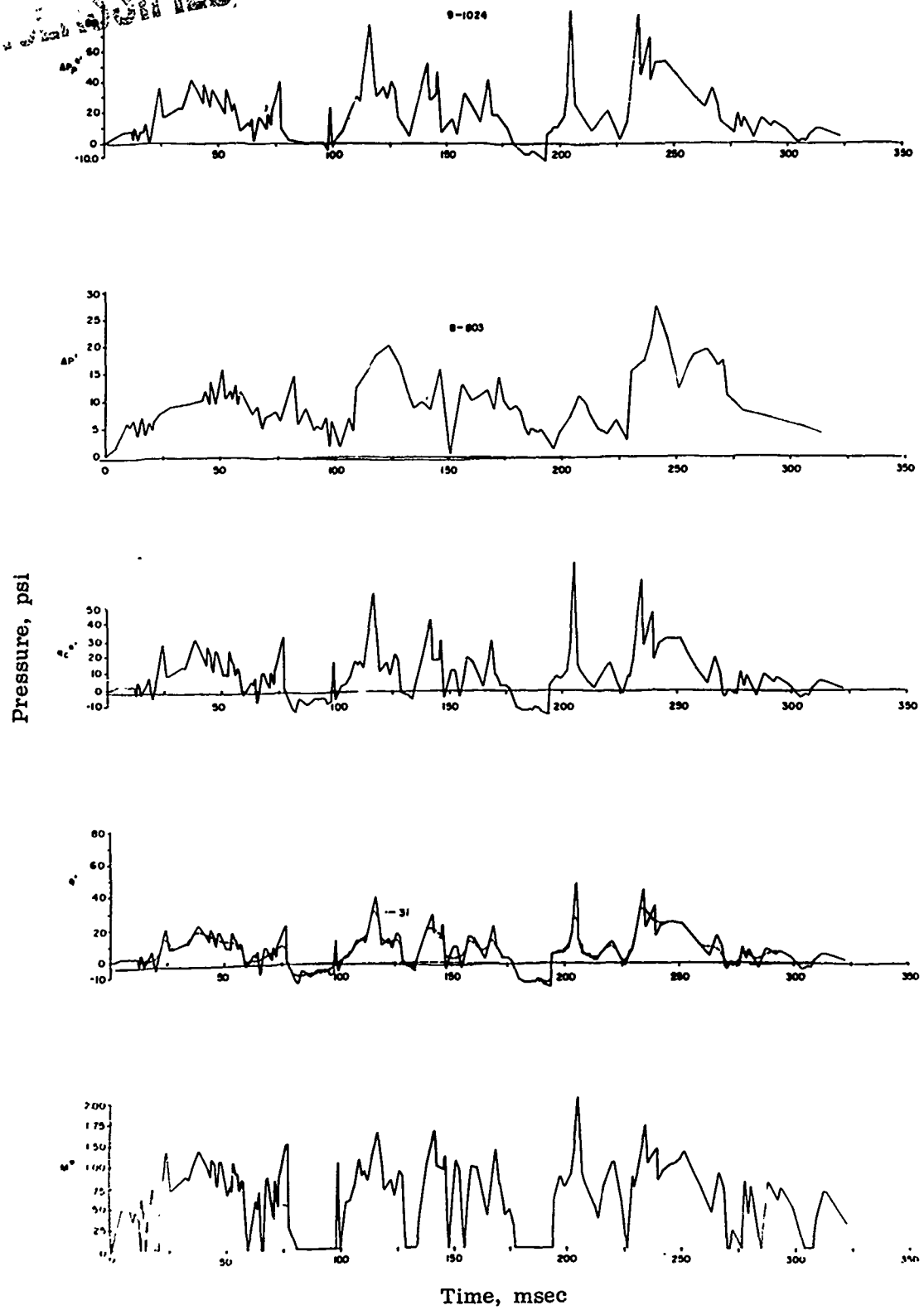

Figure 1.44 Pressure and Mach number versus time, Project 4.3/33.2 at 2,030 feet.

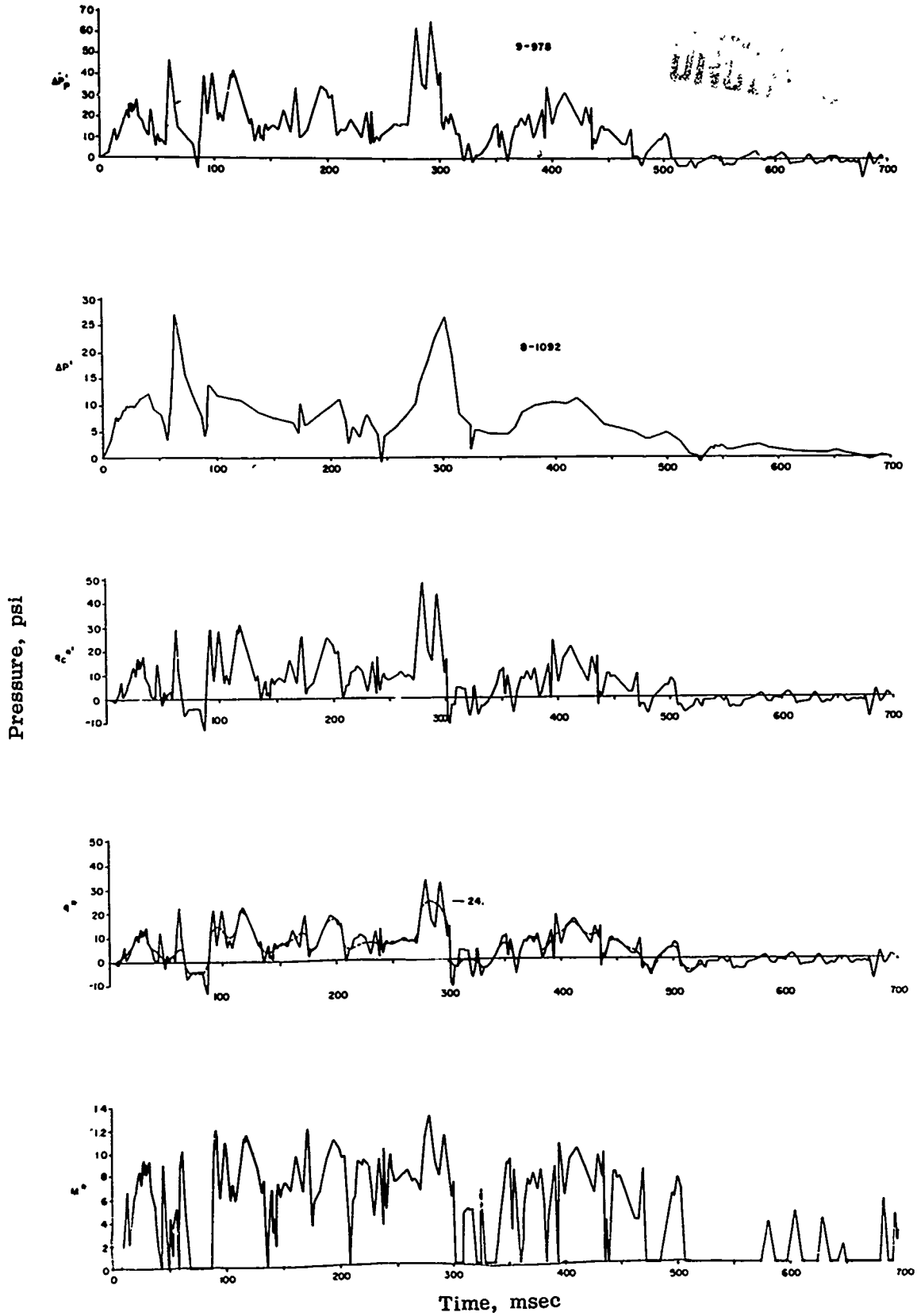

Figure 1.45 Pressure and Mach number versus time, Project 4.3/33.2 at 2,280 feet.

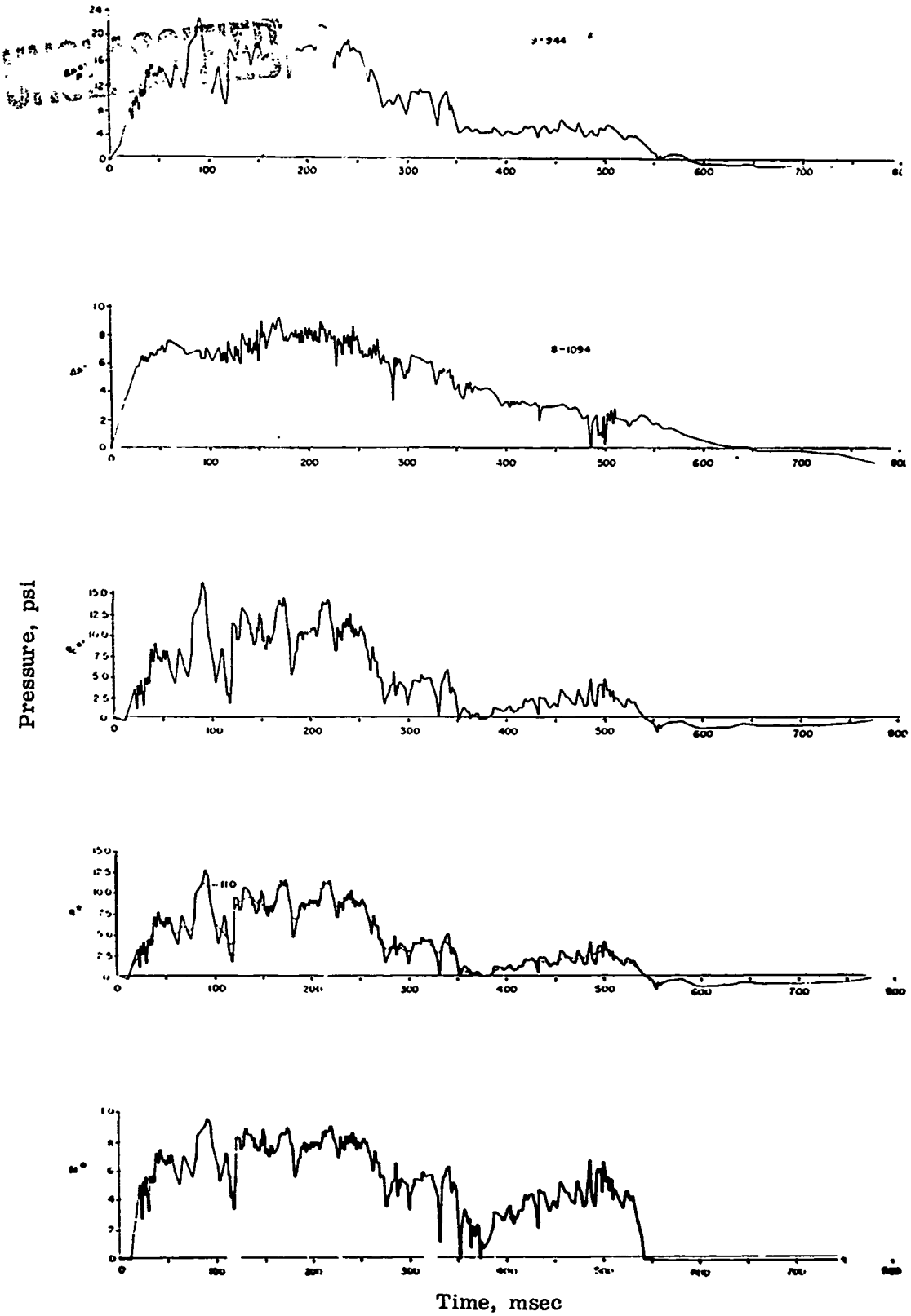

Figure 1.46 Pressure and Mach number versus time, Project 4.3/33.2 at 2,730 feet.

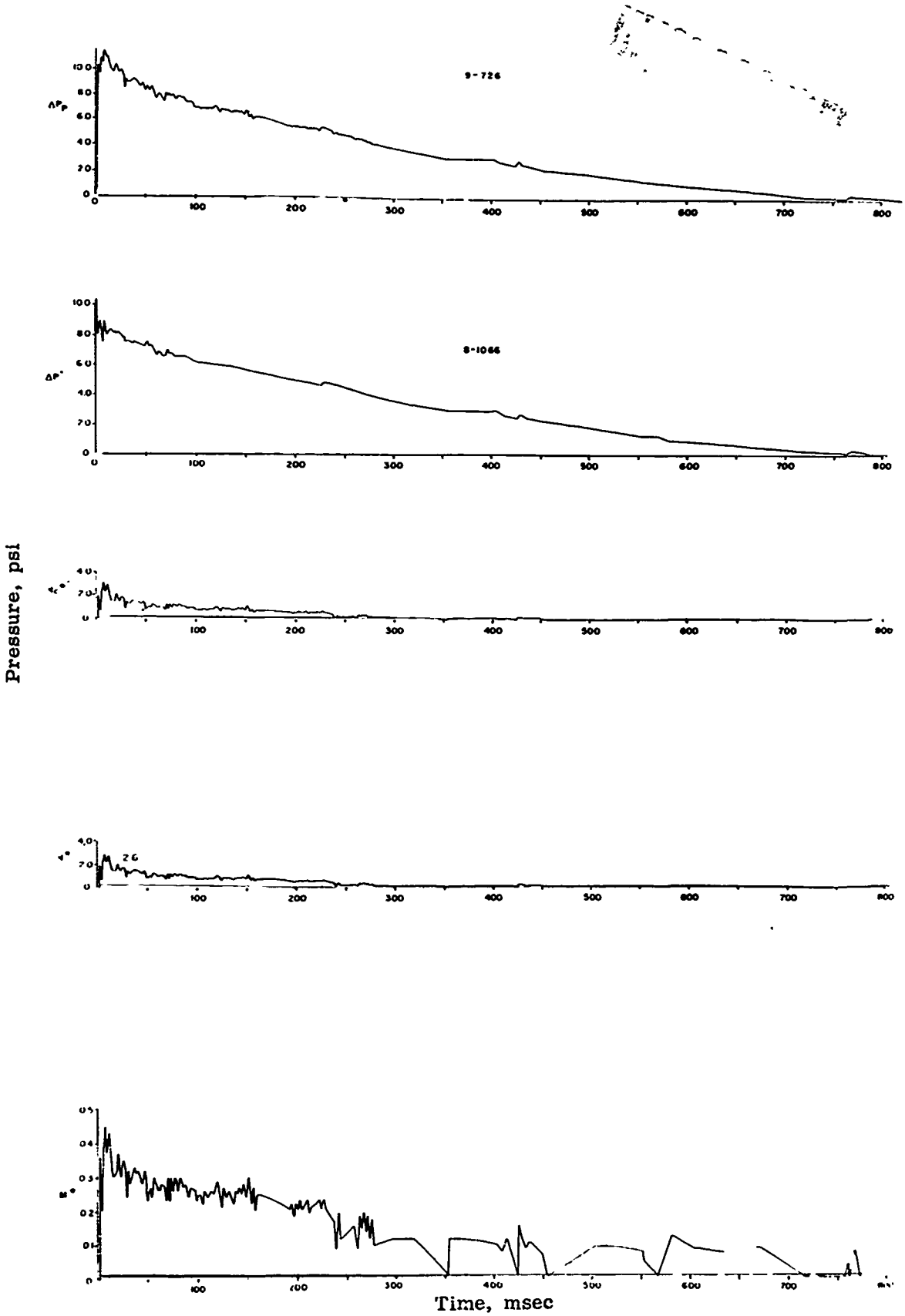

Figure 1.47 Pressure and Mach number versus time, Project 4.3/33.2 at 3,930 feet.

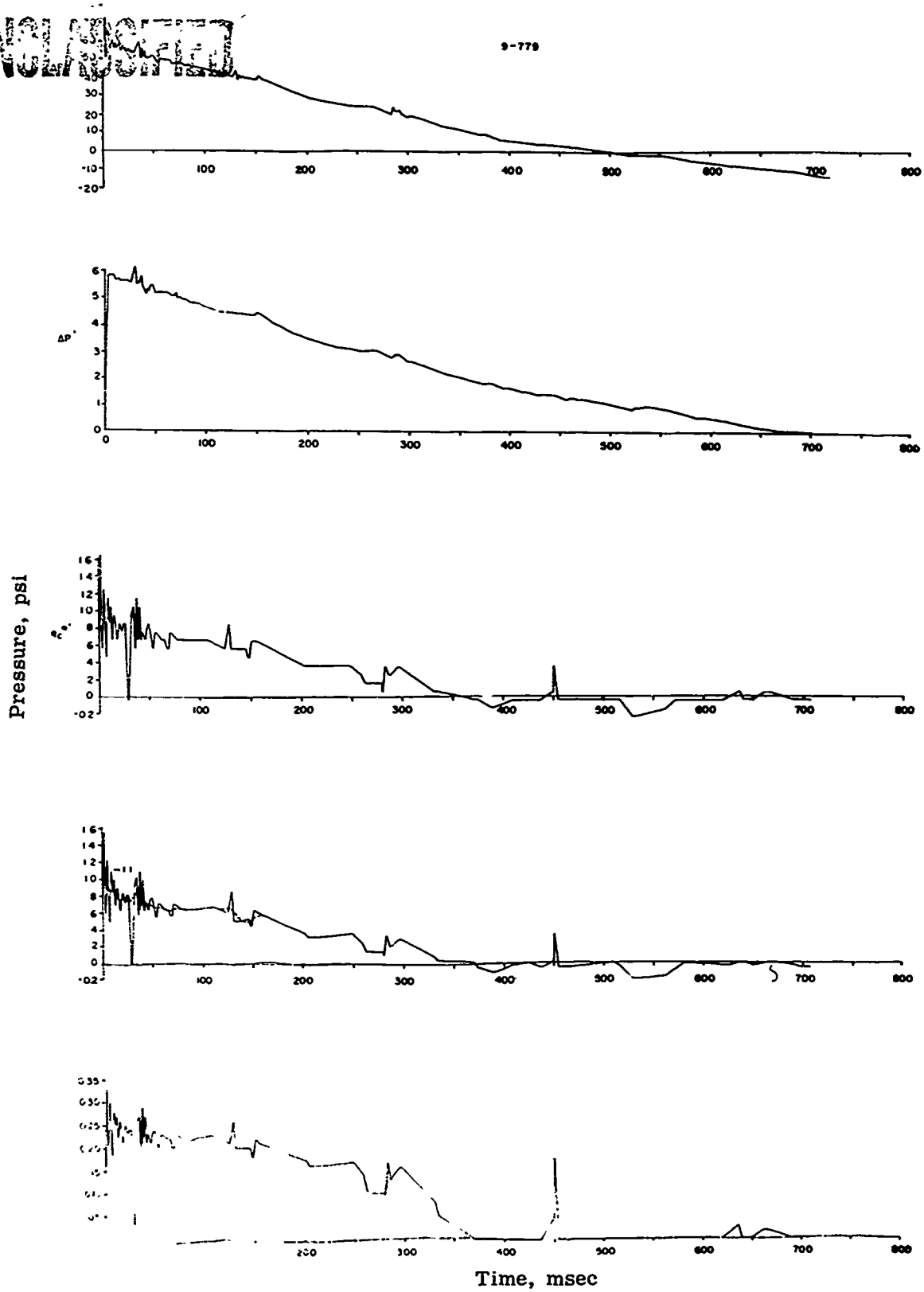

Figure 1.48 Pressure and Mach number versus time, Project 4.3/33.2 at 4,770 feet.

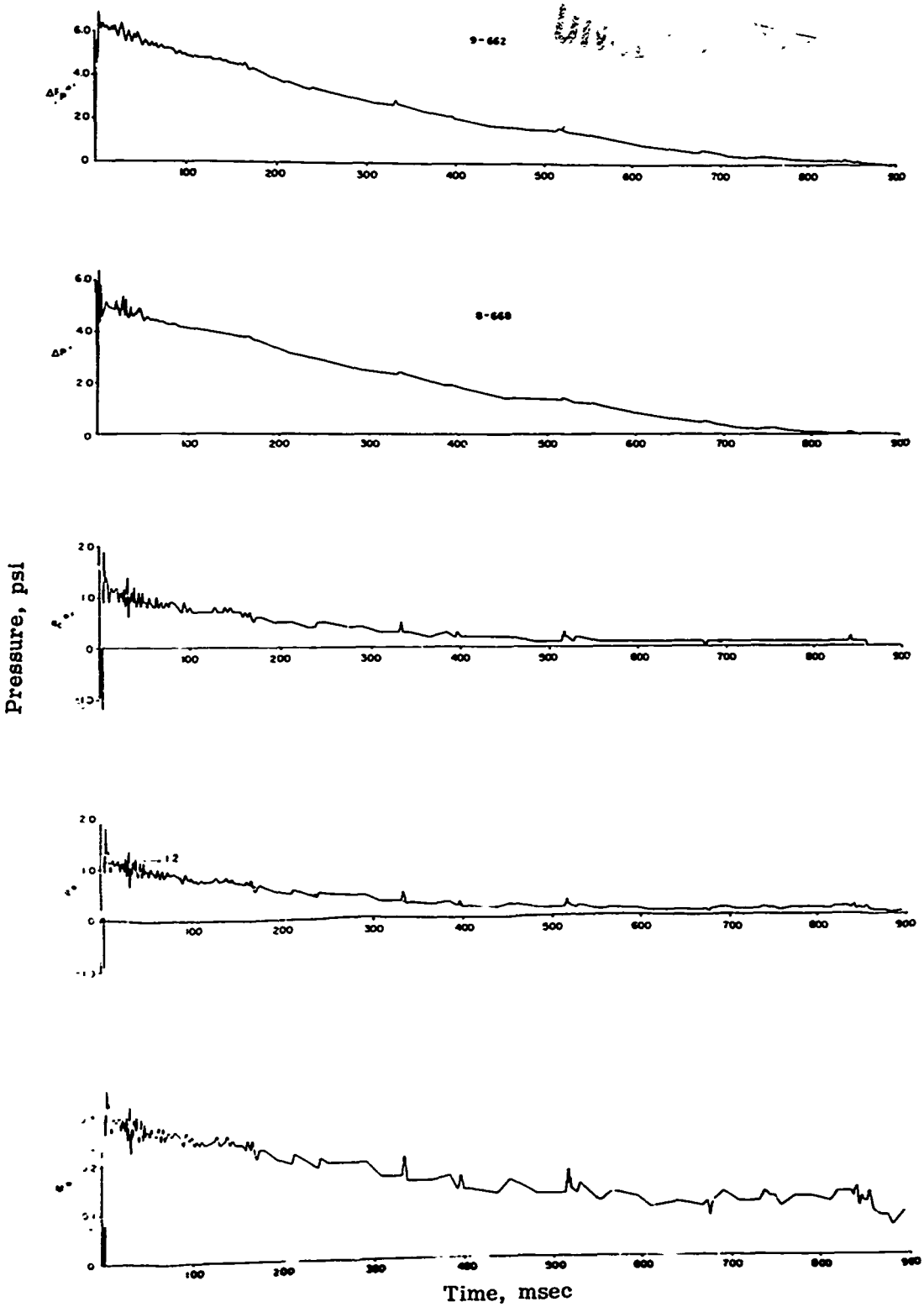

Figure 1.49 Pressure and Mach number versus time, Project 4.3/33.2 at 5,320 feet.

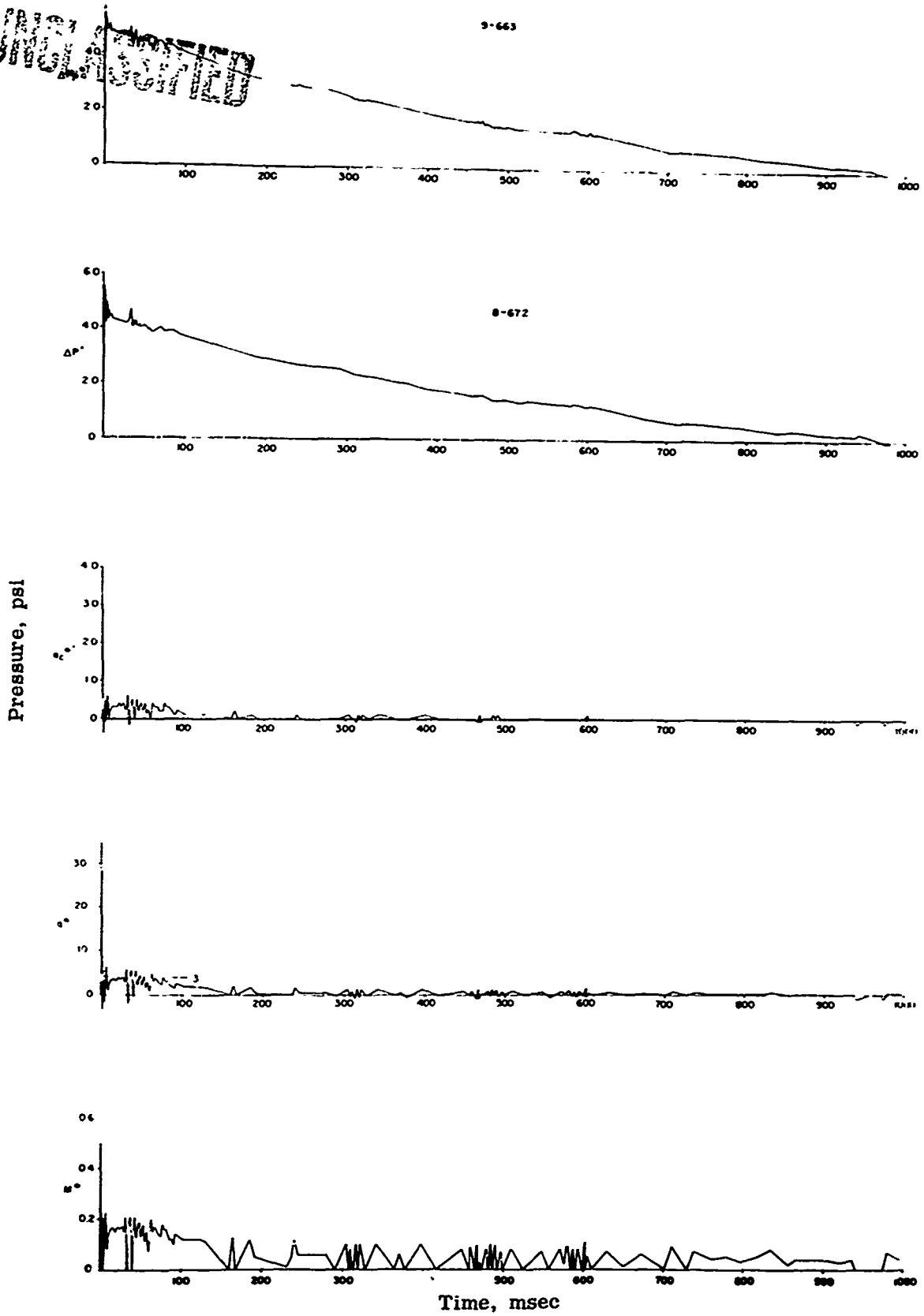

Figure 1.50 Pressure and Mach number versus time, Project 4.3/33.2 at 6,120 feet.

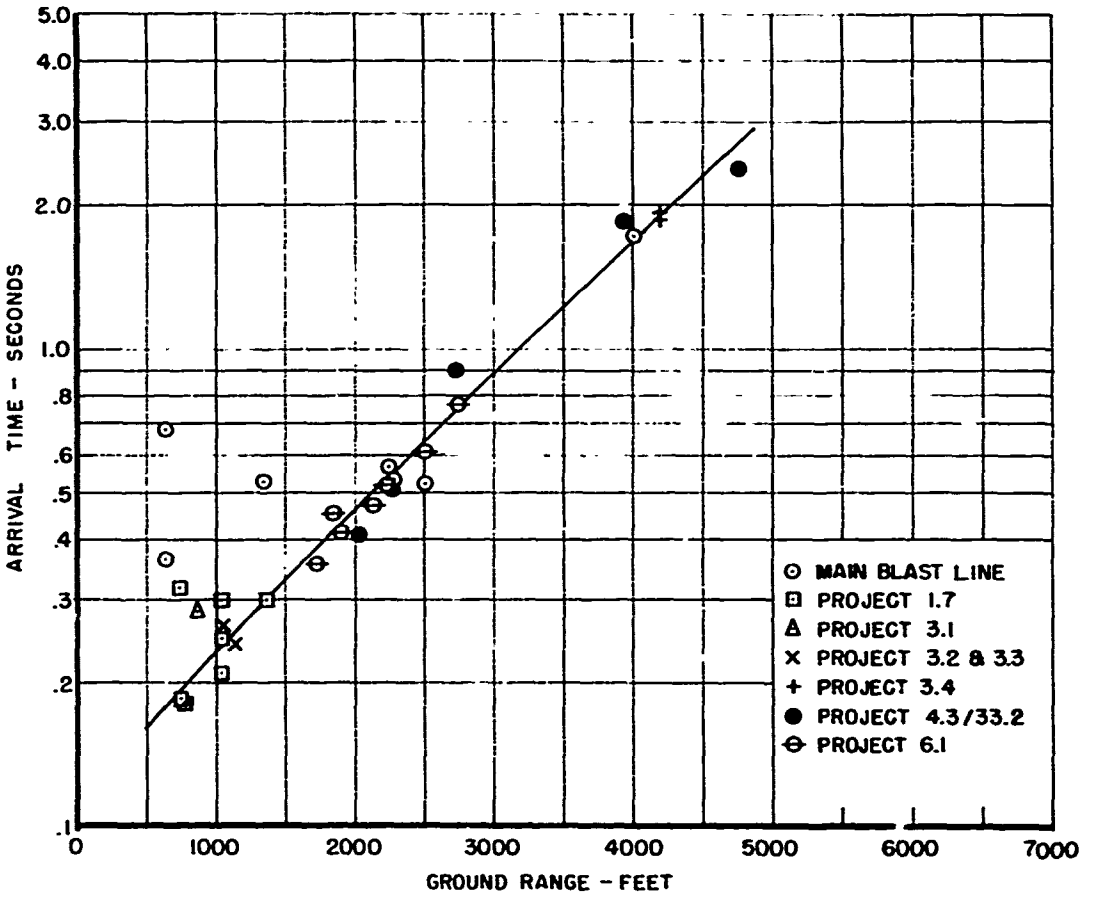

Figure 1.51 Time of arrival versus distance.

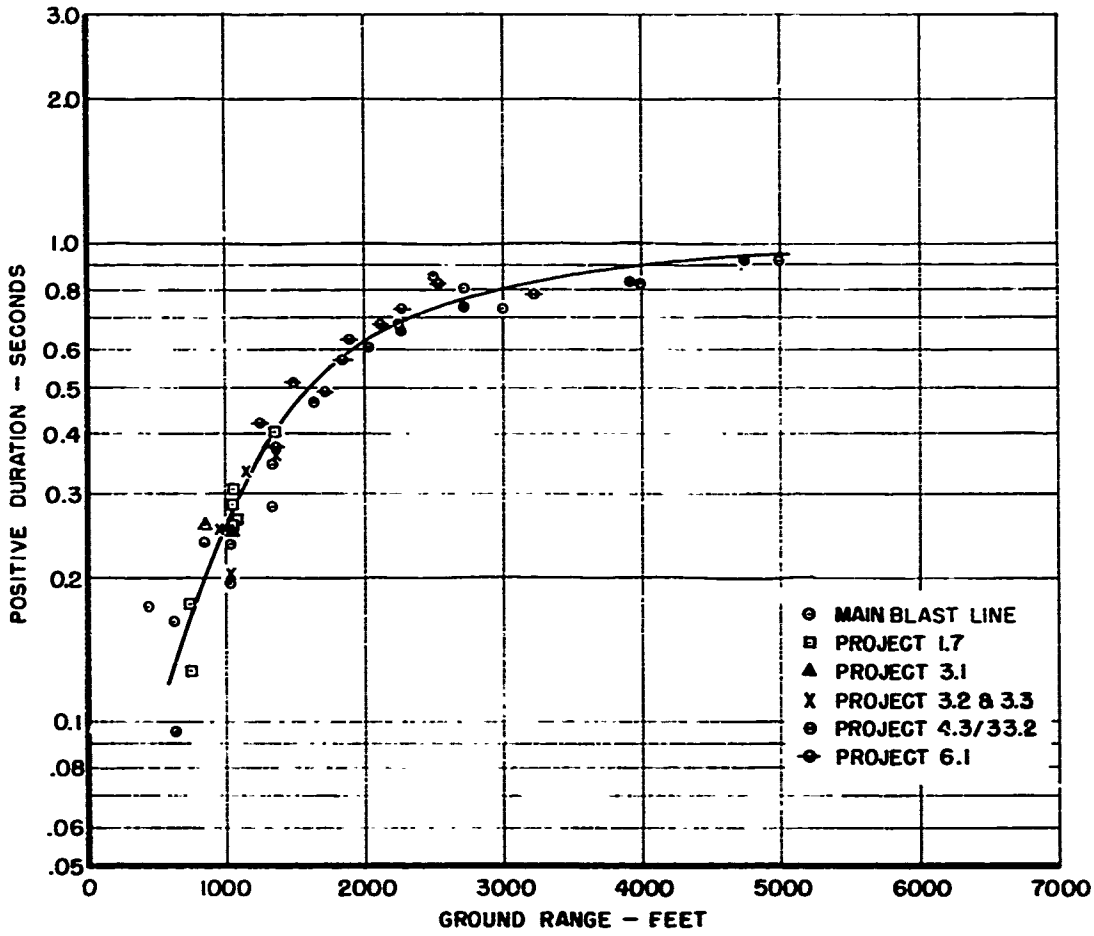

Figure 1.52 Positive duration versus distance.

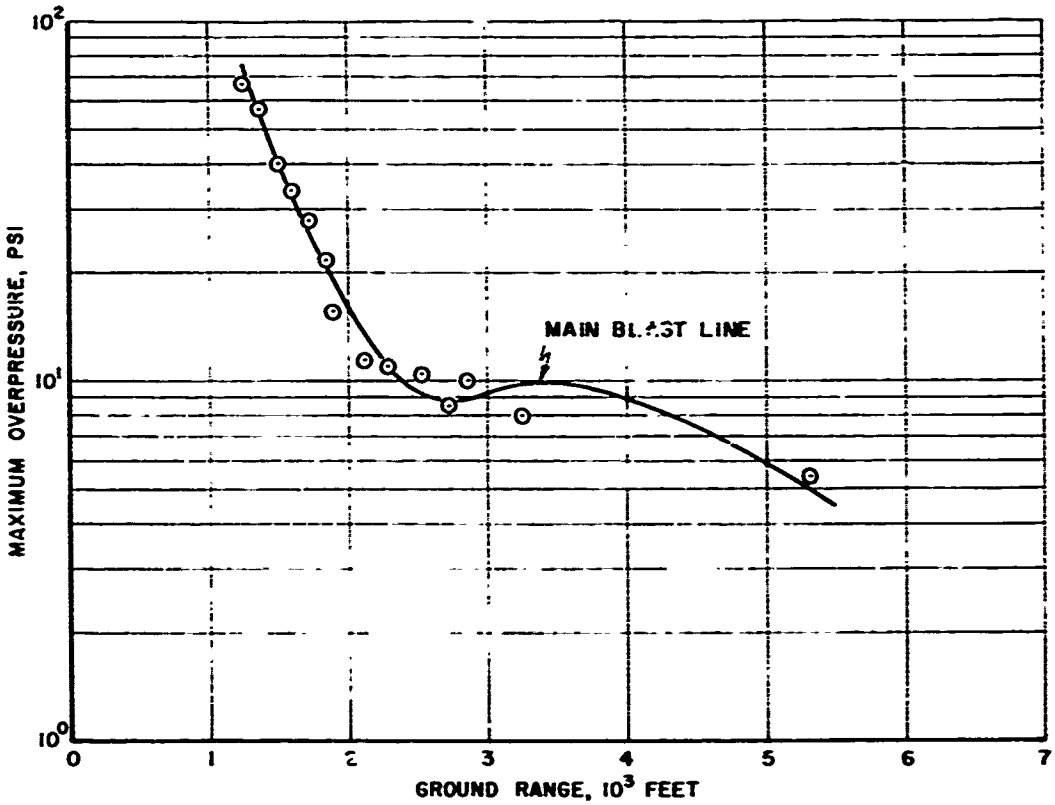

Figure 1.53 Maximum overpressure versus distance, Project 6.1.

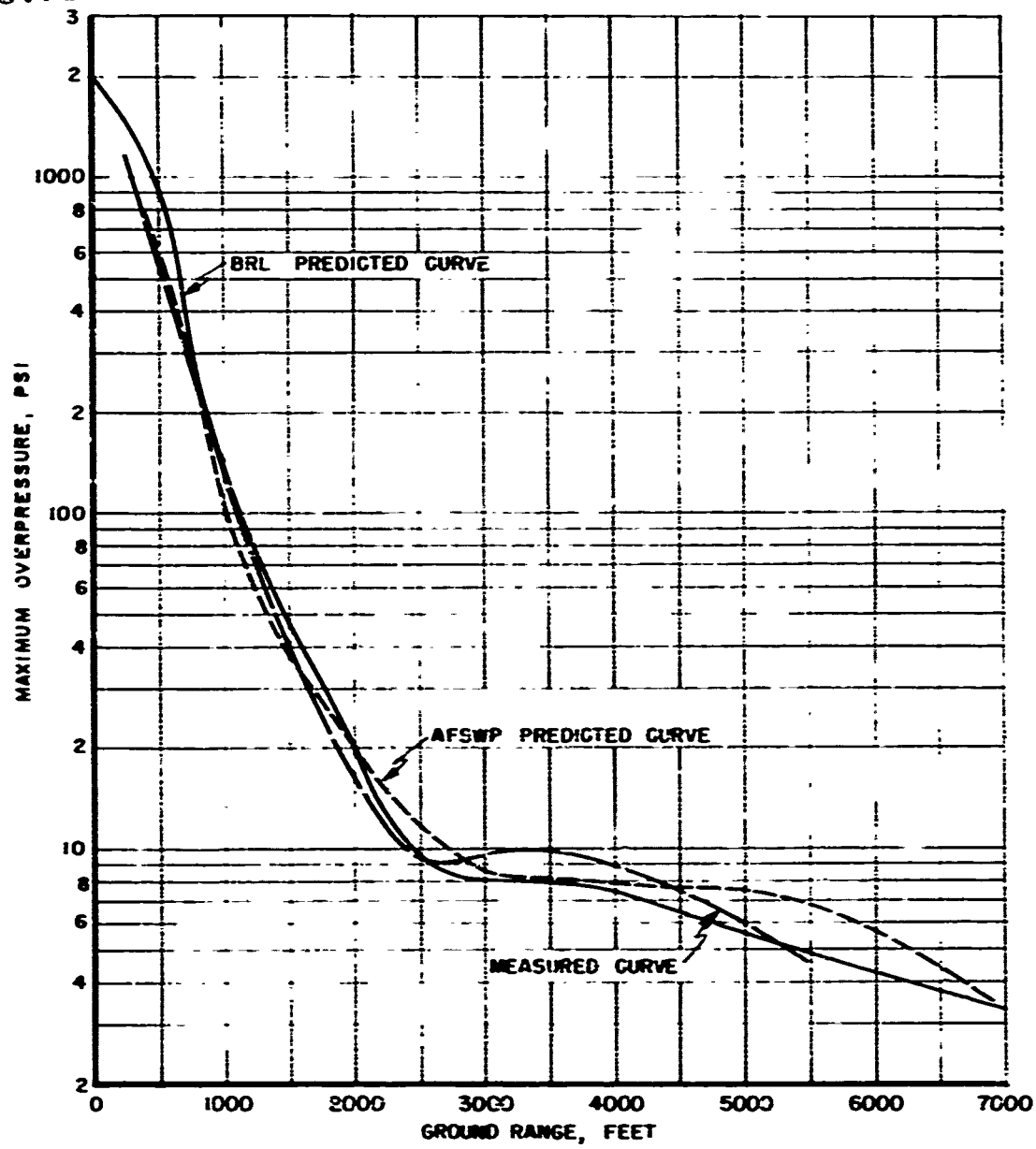

Figure 1.54 Comparison of predicted maximum overpressure with measured values as a function of distance.

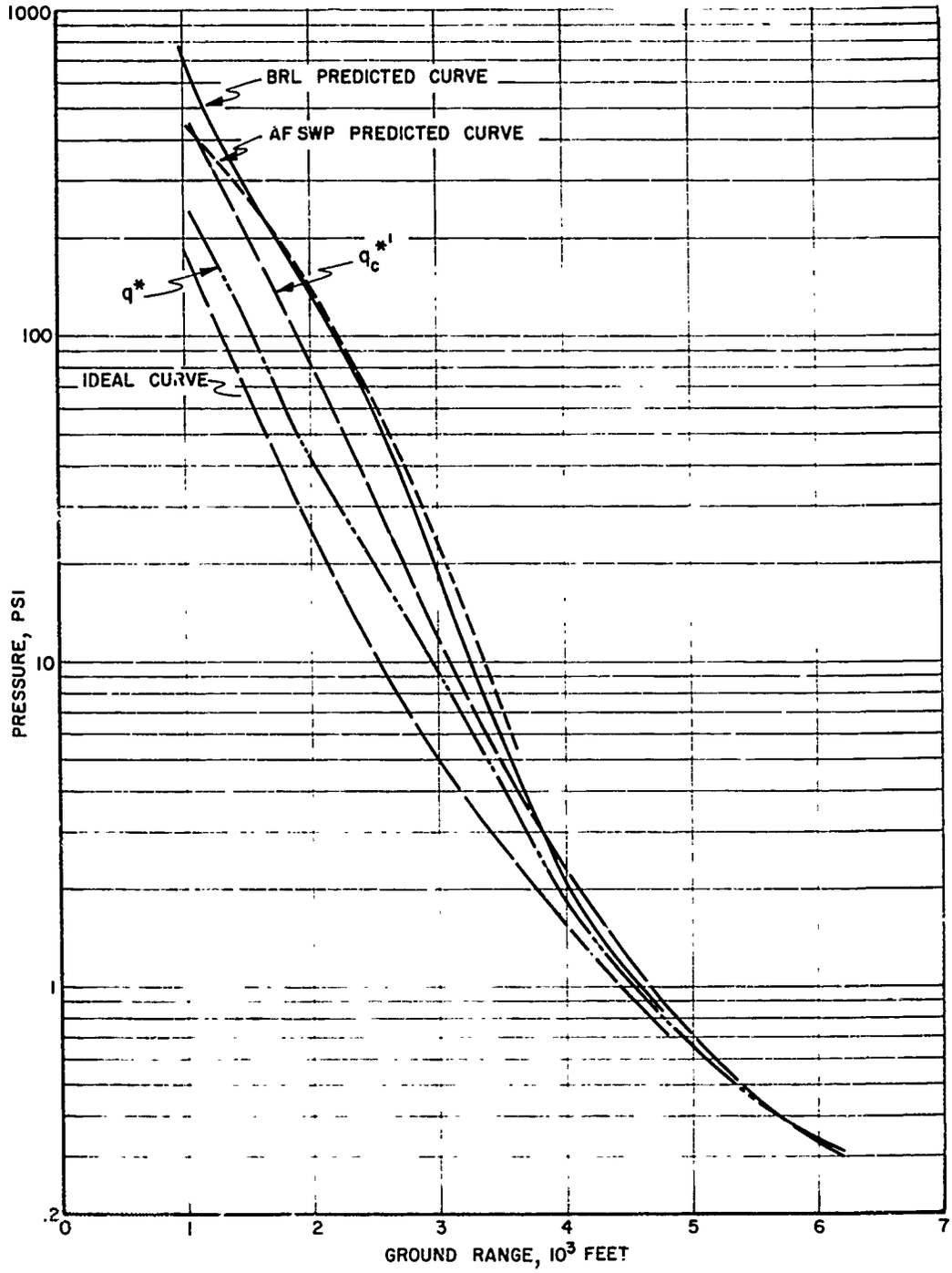

Figure 1.55 Comparison of predicted maximum dynamic pressure with measured values as a function of distance.

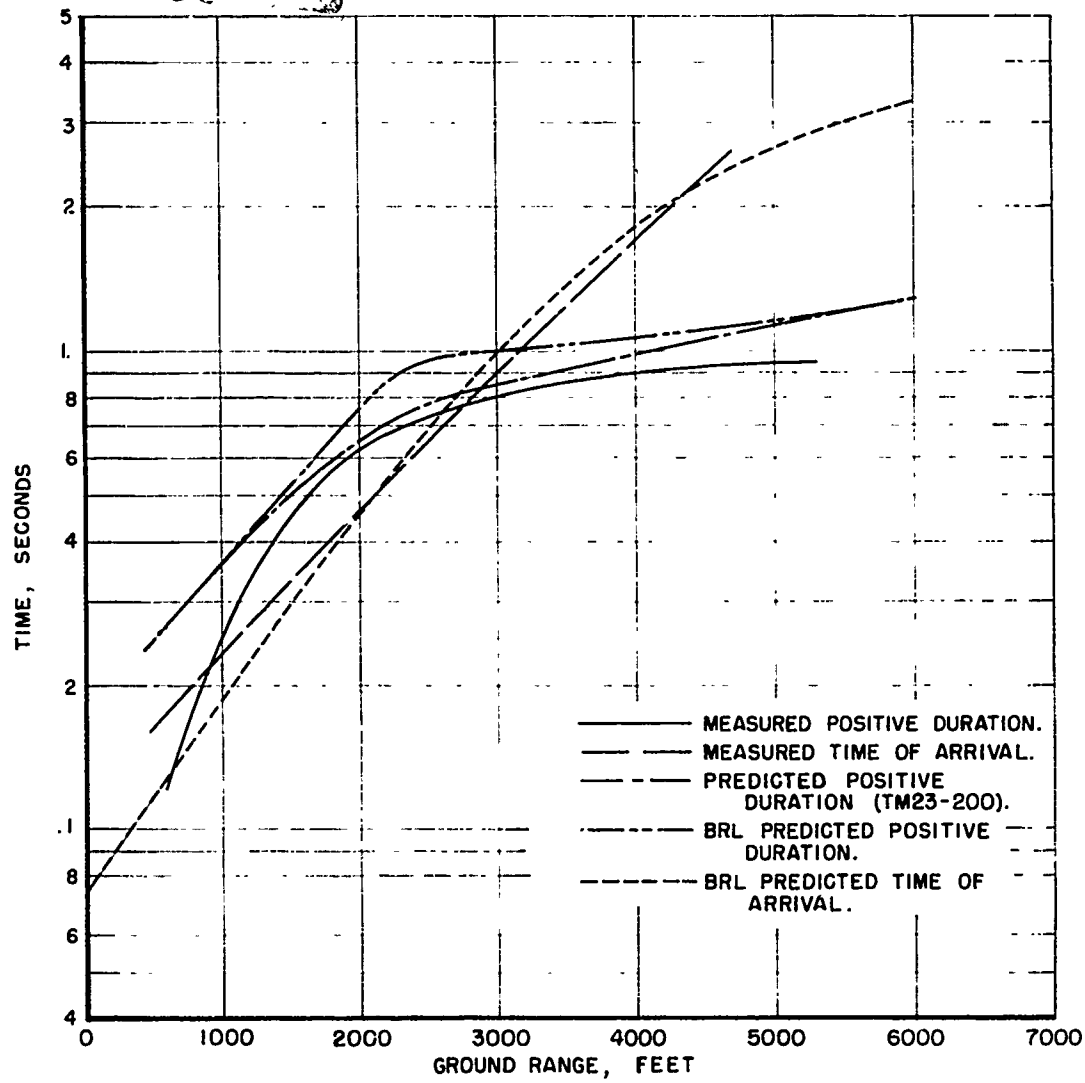

Figure 1.56 Comparison of predicted time of arrival and positive duration with measured values as a function of distance.

Chapter 2

PRECURSOR WAVEFORMS

In predicting damage to equipment or structures, peak pressures are frequently not as important a parameter as is the whole pressure-time waveform. Much information has been accumulated on overpressure-time waveforms. These have been classified into types, and a method has been developed for predicting what form will occur.

Additional information was necessary to extend the prediction method to waveforms in the precursor region above 50 psi and to yields that have scaled heights of burst higher than 300 feet. Practically no information was available on dynamic pressure waveforms. It was the objective of this project, therefore, to collect data on both dynamic and overpressure waveforms; overpressure waveform data was to be integrated into the existing prediction system; and dynamic pressure waveform data was to be used to develop a prediction system. The prediction systems were to be evolved as a separate BRL report and not as a part of the final WT report.

BRL participated in nine shots during Operation Plumbbob. Self-recording gages were installed at various distances from ground zero, and data was accumulated on overpressure and dynamic pressure versus time.

The remainder of this chapter is concerned with presenting the blast wave data accumulated during the operation and showing, where applicable, how this data fits the existing prediction system for waveforms of the pressure-time histories.

2.1 PRECURSOR WAVEFORM CLASSIFICATION

Pressure waveform data accumulated from previous operations has been analyzed, and the BRL classification system evolved is presented in this section.

The waveforms of the pressure versus time records obtained in precursor regions are quite different from those obtained at similar pressure levels where there is no precursor. In the precursor zone, there are many different wave shapes; the variations in wave shape are a function of ground distance. The BRL classification system divides the waveforms into four main types, which represent pertinent stages of the precursor cycle (Figure 2.1). Type A represents the initial stages of precursor; Type B represents the fully developed precursor; Type C represents the final stages of the precursor cycle; and Type D is the classical waveform that completes the precursor cycle.

Specific criteria for classification into type are based upon measurements of pertinent parameters concerning the waveform. These parameters are shown in Figure 2.2. Specifically, the wave types are divided in accordance with the following criteria:

Type A $P_{p_i}/P_m < 1$, t_m increasing with increasing ground distance

Type B $P_{p_i}/P_m \geq 1$, t_m undefined

Type C $P_{p_i}/P_m < 1$, t_m decreasing with increasing ground distance

Type D Classical wave shape (Figure 2.1)

Possible wave shapes that would fit Type A criteria are shown in Figure 2.1; all in the early stages of precursor development. In this stage, as the precursor moves out from ground zero,

the separation between the two peaks shown in Figure 2.1 increases. In addition, the rise time for the main shock front also increases with distance. (The shape of the dynamic pressure wave need not follow that of the overpressure wave.) The wave is classified as Type A so long as the second peak is greater than the first peak pressure and so long as the time interval between arrival of the two maximums increases with distance from ground zero.

2.2 PREDICTION OF WAVEFORMS

The procedure for predicting wave type and pressure-time parameters is described below. The method amounts essentially to obtaining predicted values of type and of pertinent parameters of the pressure-time pulse from best-fit curves derived from data available from 12 precursor-forming blasts (Figures 2.3 through 2.12). These 12 shots were over several different desert-type surfaces; accordingly, the prediction technique is probably applicable only for shots over desert surfaces.

2.2.1 Prediction of Wave Type. Pressure-time data from the 12 shots has been (1) classified as to type according to the criteria established in Section 2.1 and (2) plotted on a scaled yield versus distance chart (Figure 2.3). With best-fit curves separating the four wave types completely, the chart shows that generally an accurate prediction of wave type can be made (for the distances and yield for which data is plotted).

2.2.2 Prediction of Type A Waveforms. Once the wave type is known, the prediction procedure is concerned with providing specific information about the wave, such as the ratio of first peak to second peak pressure. The procedure for predicting the specific data has been evolved only for the Type A waveform (a similar analysis has not yet been carried out for Types B and C waveforms). The Type A method is based on computation of the specific information shown in Figure 2.2 from the pressure-time records of the previously mentioned 12 shots. These computations have been plotted on various types of charts, and best-fit curves have been drawn (Figures 2.4 through 2.12). These curves, then, form the basis for prediction.

If the specifics of the wave shape are desired for a given yield, height of burst, and at a position where a particular peak overpressure exists, the first step in the prediction procedure is to establish the ground range corresponding to this pressure. This ground range can be obtained from charts such as Figures 2.4 or 2.5. Figure 2.4 gives the ground distances of specific overpressures for various heights of burst. Figure 2.5 gives the ground distance for a range of overpressures but for a given height of burst (around 200 feet).

Once the ground range of the desired overpressure has been established, the succeeding steps in waveform prediction involve using curves such as found in Figures 2.6 through 2.11 to obtain the significant wave parameters. There is considerable scatter of plotted points about the best-fit curves in many cases; this gives an estimate of the accuracy of predicted values. The best-fit curves can often be biased to give predictions for a particular shot of interest. For example, in the drawing of a curve all the data points for low shots might be ignored, thus making the curve more applicable to higher heights of burst, which strongly indicates a height of burst dependency. This has been done in Figure 2.10 (TU 4, Upshot-Knothole [illegible] and Teapot 12 were ignored). Finally, Figure 2.11 deserves some explanation, since the reliability of the two drawn curves is not readily apparent. For an individual shot, such as Teapot 5, a trend can be seen for high values of the peak-pressure ratio to exist at great and small ground distances, with minimum values at intermediate distances. Almost all individual shots show this trend, and the curves have been drawn with this in mind.

The waveforms predicted for three pressure ranges for Shot Priscilla using the procedure described above are shown in Figure 2.13.

Tables 2.1 and 2.2 list the values and sources used to plot Figures 2.4 through 2.12. From the plotted figures it should be possible to predict the wave shape for any of the pressures in

the Type A classification occurring beyond a scaled ground range of 200 feet or 716 feet actual ground distance. In Figure 2.12, the slant range was used to plot arrival time, since some of the stations were close to ground zero.

2.3 PROCEDURE

To collect the most significant data for precursor waveform studies, the shots selected for participation were those with yields for which there was a paucity of data. The distances selected for location of gages were such that the complete precursor cycle would be covered. This is true particularly for surface pressure versus time. Because of the limited number of q-gages available, an extensive coverage of dynamic pressure versus time could not be made. On the other hand, it was expected that the selection of distances for placement of the q-gages would yield sufficient data for the study of formation of the dynamic pressure waveform in the precursor zone cycle. Self-recording pressure-time and dynamic-pressure-time gages were used. Most gage stations were installed by BRL personnel.

Tabulations of the shots and the estimated yield on which participation was effected are given in Table 2.3. Included in the table are the distances from ground zero for pressure gage locations. Shots Priscilla and Smoky are included in Table 2.3, but the collection of data for precursor waveform studies was a secondary objective for these events. The data for Shot Smoky is reported in Reference 15. The field layouts of station locations for the shots, except Priscilla and Smoky, are shown in Figures 2.14 through 2.22.

2.4 RESULTS

To achieve the primary objective associated with this portion of the project, a total of 158 P_t- and q-gages were deployed in nine shots. A small number of very-low-pressure (VLP) gages are included in the above total. The VLP data although not pertinent to this chapter is reported herein to extend the blast line information out to farther ranges from ground zero. Summaries of gage performance and shot data are given in Tables 2.4 and 2.5. Of the failures on the nine shots, some were due to the initiation system, and others were caused by high-acceleration effects that broke the glass recording disks.

A large amount of data has been collected that will improve, upon final analysis, the present prediction technique for overpressure waveforms. The coverage of the dynamic pressure data was not as extensive as for the overpressure data. However, it is believed, that the data obtained, together with the data from past operations, will permit the development of a prediction technique for dynamic pressure waveforms.

2.4.1 Pressure-Time Histories. The plots of the pressure-time histories of all records are presented in Figures 2.23 through 2.58. The records are arranged by shot and by distance from ground zero, so the waveforms at discrete points along the blast times can be seen and compared to other shots. The maximum overpressure, arrival time, and positive phase duration associated with each P_t-gage record are listed in Table 2.6. The q-gage records are shown in Table 2.7. This table presents the maximum values for total and static pressure, pressure difference, and calculated dynamic pressure. Dynamic pressure records above 50 psi show excessive hash and high-frequency oscillation, whereas, in general, the static overpressure-time records were good.

For stations where two P_t gages were located, a reasonably good agreement was obtained for the maximum overpressure value and for the positive phase duration of the blast wave. The time of arrival records for some shots have considerable scatter; for other shots where no arrival time is given in the tables, the data was erratic and therefore meaningless. For the latter case, it was difficult to ascertain the start-up time because of a series of markings on the glass disk. The cause for the markings is unknown.

The records for the q-gages were reported only for those values that gave pressure-time histories. The reduction of the data was similar to that described in Chapter 1. It should be noted that no value for the corrected dynamic pressure is presented for Shot Franklin. The selection of gage ranges and locations for Shot Franklin was based on a yield higher than actually realized. Hence, the deflections on the glass disks of the pressure-time record were small and possibly subject to large error in reading. For the low value of pressure difference obtained, the correction for Mach compressibility would be negligible, and for this reason as the existence of a possible large error, the application of a Mach correction factor did not seem to be justified.

2.4.2 Waveforms. Precursor waveforms were observed on six of the nine shots. Of the six shots, Shot Galileo and Kepler showed only the early stages of the precursor; the remaining three shots showed only the ideal Type D waveform. Between Shots Galileo and Kepler, the precursor waveform of Shot Kepler formed into an ideal waveform sooner than during Shot Galileo.

The nonprecursor shots were Franklin, Shasta, and Charleston. For Franklin, as mentioned previously, gage ranges and locations were selected based on a higher yield. If a gage had been located at a range closer to ground zero, it is possible that a precursor would be evident. On the other hand, the height of burst for Shot Franklin is near the region where a precursor would not form, based on the criteria of Figure 2.17 of Reference 7. Similarly, the burst height of Shot Charleston is in the same category as Shot Franklin. Hence, the lack of precursor for these two events could be predicted. Based on the same criteria of Reference 7, a precursor should have been evident during Shot Shasta.

The classification of waveform for each event is presented in Table 2.6. All the precursor-producing shots provided waveform data in the desired region above 50 psi. Shot Hood also fulfills the requirement for more waveform data at scaled heights of burst greater than 300 feet and for larger yields than previously considered.

2.4.3 Maximum Pressure versus Distance. Curves showing the maximum pressure values as a function of distance are given in Figures 2.59 through 2.73. Along with the dynamic pressure q* plots, the values of the difference between total and static pressure are also plotted. The maximum overpressure versus distance curves generally confirm the absence or presence of precursor formation and also indicate the degree of precursor action. For Shots Wilson and Hood (Figures 2.61 and 2.63), a typical precursor depression of the curve is observed. The depression of the curve for Shot Hood extends out to farther ranges and to lower pressure values than the curve of Shot Wilson, indicating a stronger precursor action during Shot Hood. The curves for Shots Franklin and Kepler (Figures 2.59 and 2.67) show the steady decrease of pressure with distance, which is the usual pattern for nonprecursor conditions.

A trend is apparent in the dynamic pressure-distance curve in the presence of a precursor. Following a steady decrease of pressure with distance, the pressure decreases gradually, then drops steeply when the precursor no longer exists. This is shown in Figure 2.62 for Shot Wilson and Figure 2.66 for Shot Owens. The above characteristics are also found in the curve for Shot Hood (Figure 2.64) except for the later portion of the curve. The steep decrease of pressure with distance for Shot Hood is not as pronounced as it is for Wilson and Owens.

2.4.4 Arrival Time and Positive Duration. The arrival time and positive duration measurements are plotted in Figures 2.74 through 2.82. The curves drawn through the data points were fitted by eye. The arrival time curves are less accurate than the positive duration curves. The data is useful to add to the present state of knowledge about nuclear blast waves, particularly the data from Shot Hood (Figure 2.76) where little information is available for this height of burst.

2.5 DISCUSSION

2.5.1 Nonprecursor Shots. The shot that did not yield precursor waveforms (although expected) was Shasta. In the early stages of Shots Kepler and Galileo, precursor waveforms were obtained, but they very quickly formed into ideal waveforms. For Kepler and Galileo, the usual precursor cycle was not observed in the same pattern as for Shots Wilson or Hood. It is of interest to note that Kepler, Shasta, and Galileo were tower shots with the devices heavily shielded, and Wilson and Hood were balloon shots with no appreciable shielding. It is felt that these heavy shields minimized the factors for precursor formation.

The general layouts of shield configurations for Shots Kepler, Galileo, and Shasta are shown in Figures 2.83 through 2.85. The long axis of the shield for Kepler and Galileo was approximately parallel to the blast line. The growth of the fireball for the heavily shielded shots would reveal whether the shields affected the thermal output of the detonation, and any affect of the thermal output would, in turn, reflect in the formation of precursors. This premise is based on the fact that an experimental thermal pulse can be calculated from the fireball radii as a function of time.

Motion photography of the fireball growth indicates that, during Shots Kepler and Galileo, the radius along the blast line as a function of time is less than in the direction perpendicular to the blast line (Reference 16). For Shot Kepler, the difference in fireball radius, from photography, expressed in terms of the ratio of weapon yield gives:

$$\frac{W_1}{W_2} = \left[\frac{\phi_1}{\phi_2}\right]^5 = 1.22 \qquad (2.1)$$

Where: W_1 = weapon yield, kt, perpendicular to the blast line
W_2 = weapon yield, kt, along blast line
$\phi_1 = (d_1/t^{2/5})$
$\phi_2 = (d_2/t^{2/5})$
and d = radius of fireball, meters
t = time, msec

The yield of weapon W_2 along the blast line is less by about 22 percent. The fireball growth as a function of time of Shot Newton, a nonshielded device and similar in yield to Shot Kepler, compares reasonably well with Shot Kepler. A small variation in radius will indicate a large variation in yield because of raising the value d to the fifth power. The variation in yield by itself is not sufficient to show any affect on precursor formation.

The irradiation rate dq/dt from the fireball is given by:

$$\frac{dq}{dt} = f \sigma T^4 4\pi R^2 \qquad (2.2)$$

Where: f = fraction of radiation spectrum transmitted
σ = Stefan-Boltzmann constant
T = temperature of fireball
R = radius of fireball

For Shot Kepler, then, assuming all values to be constant except R, the radiation rate difference along the blast line is 8 percent less than it is perpendicular to the blast line. This small decrease of the thermal pulse along the blast line would not minimize the thermal action for precursor formation. Evidently, for Kepler, the fireball growth was approximately normal, and the effect of minor variation of the fireball on precursor formation, from the above discussion, does not appear to be justified. On the other hand, consideration was not given to two parameters for the irradiation rate from the fireball radius; one is the value f and the other is the temperature T.

The shield consisted of large masses of steel, concrete, paraffin, and lead. This, upon decomposition by the intense heating, would result in a considerable amount of debris in the surrounding vicinity other than air. This debris would then decrease the amount of thermal energy transmitted and also decrease the temperature of the fireball. Evidence of this decrease is indicated to some degree by the measurements of thermal radiation phenomena by Project 5.3 (Reference 17). Reference 17 contains a comparison between the measured and calculated quantities of thermal radiation. The measured thermal energy output was 100 to 400 percent less than the calculated values for the shielded shots and about 30 percent less for the nonshielded shots. Furthermore, between the calculated and measured values of time to maximum temperature rise, the measured values were larger by greater percentages for the shielded shots than for the nonshielded shots. The decrease of thermal radiation and the increase of time for the maximum temperature rise would decrease the heating of the surface prior to shock arrival and, in turn, minimize the conditions for precursor formation. Qualitatively then, it can be inferred that the shielding of the device will minimize the thermal action for precursor formation. From a military standpoint the above discussion has no real significance, since it is unlikely that any weapon will be fired with a large mass of shielding about the device. Therefore, it can be implied that for the shot conditions of Kepler, Galileo, and Shasta, a precursor would be formed without the existence of the shield around the device.

2.5.2 Scaled Pressure-Distance Curves. The scaled maximum overpressure-distance curves are shown in Figures 2.86 through 2.94. Points have been selected from these scaled curves (including precursor and nonprecursor shots) and plotted on height-of-burst curves versus ground range (Figure 2.95). Not many of the points lie near the isopressure contours given in this set of height-of-burst curves. For those shots at lower burst height and higher pressures, a reasonable fit is obtained. However, for the higher burst heights and lower pressures, a large difference exists. In view of the additional data obtained and the variations noted, the height-of-burst curve as presently constructed should be revised. The dynamic pressure versus distance curves have not been scaled or compared to any height-of-burst curves. In view of the data accumulated in this operation and the new technique used for data processing and analysis, new height-of-burst curves versus ground range are needed for dynamic pressure as well.

Of interest is the comparison of the basic blast parameters between precursor and nonprecursor shots. Wilson, a precursor shot, was selected for comparison with Kepler, since the scaled height of burst and weapon yield are similar for both events. Figure 2.96 compares the overpressure for Shots Kepler and Wilson. The difference in pressure at the close-in stations is not as great as at the farther ranges. For the precursor shot, the usual depression in the pressure-distance curve is observed, whereas there is a steady decrease of pressure with distance for the nonprecursor shot. Lack of data at closer stations for Shot Wilson precludes any comparison of dynamic pressure as a function of distance (Figure 2.97). A later time of arrival is noted for Shot Kepler than for Shot Wilson (Figure 2.98). For strong precursor action, as during Shot Wilson, this would be expected. Also, another distinction between precursor and nonprecursor shots, is the longer duration for precursor shots (Figure 2.99); the positive duration is longer for Shot Wilson than for Shot Kepler.

The overpressure values obtained on the nonprecursor shots are compared with a predicted curve for the good surface height-of-burst curve of TM 23-200 (Reference 7). In general, a reasonable comparison is obtained particularly at the lower pressure values (Figure 2.100).

2.5.3 Wave-Type Prediction Chart. Wave types from precursor-forming shots have been plotted on the BRL wave-type-prediction chart (Figure 2.101). It can be seen from the plotted data that there is general agreement with data from previous shots, except in the case of Shot Hood. The Hood data is particularly interesting, as it is at a scaled height of burst for which data was needed, and because it is apparent that the current prediction chart will have to be modified for yields and heights of burst of the order of those of Shot Hood.

2.5.4 Waveform Prediction. It can be seen from Figure 2.101 that the Priscilla waveform data in the high-pressure region, Type A, falls in an area where little previous data was available. It was, therefore, of interest to see whether the waveform prediction technique outlined in Section 2.2.2 would be valid for this region. Predictions were made for Shot Priscilla for the two peak overpressures, 70 and 40 psi. Good overpressure-time records were obtained from Priscilla for these pressure levels. The actual waveforms have been drawn in Figure 2.102 and are compared to the predicted waveforms. The comparison shows good agreement throughout.

2.6 CONCLUSIONS

Overpressure wave data was collected from six precursor-forming shots (not including Priscilla and Smoky), extending the capability for predicting waveforms. In particular, waveform data in pressure regions above 50 psi was furnished by Shots Hood, Wilson, and Owens. Also, Shot Hood provided data for scaled heights of burst greater than 300 feet.

Considerable dynamic-pressure waveform data was collected from the three precursor-forming shots. This data was of good quality for prediction-development purposes in overpressure regions below 50 psi, but its quality in regions above 50 psi is questionable.

The current BRL wave-type-prediction method appears to be applicable to yields lower than 60 kt and to heights of burst ranging from 136 to 300 feet. At higher yields or scaled heights of burst, a revision in the prediction chart is necessary.

The current BRL waveform-prediction method for Type A appears to be valid for overpressure ranges up to 70 psi, at least for heights of burst less than 300 feet, and yields less than 60 kt.

Two of four tower shots (not including Smoky) gave evidence of precursor waveforms that were short lived. All balloon shots produced strong precursor zones except Shot Charleston. The two shots, one tower and one balloon, were of such a nature that precursors were not expected to form according to the chart given in Reference 7. It is felt that heavy shielding of the nuclear device decreased the thermal action for precursor formation.

Comparison of measured overpressures with the isopressure contours on a height of burst versus ground range indicate large variations at the lower pressure values.

2.7 RECOMMENDATION

The recommendation made in Chapter 1 is applicable to this portion as well. Although mention has been made for the need of new height-of-burst curves for overpressure and dynamic pressure, such work is already under progress or has been completed at the time of writing of this report.

TABLE 2.1 TYPE A PRECURSOR DATA, AS READ

Slant Range	Horizontal Distance	t_p	t_+	t_r	t_{ps}	t_m	P_{p_1}	P_{p_2}	P_m
feet	feet	sec	sec	sec	sec	sec	psi	psi	psi
Upshot-Knothole Shot 10, Yield 14.9 kt*, Height of Burst 524 feet									
854	675	0.134	0.195	0.005	0.023	0.053	23.6	20.0	139.0
926	765	0.161	—	0.015	0.029	0.038	23.2	22.1	112.0
1,011	865	0.173	0.270	0.025	0.048	0.062	19.7	0.7	63.8
1,035	893	0.177	0.280	0.020	0.061	0.072	11.6	4.2	69.7
1,060	921	0.192	0.280	0.025	0.060	0.071	14.4	13.7	71.5
1,282	1,170	0.266	0.320	0.025	0.105	0.239	17.9	8.0	37.6
1,513	1,419	0.351	0.457	0.017	0.180	0.200	10.3	4.2	14.3
Upshot-Knothole Shot 11, Yield 60.8 kt, Height of Burst 1,334 feet									
2,046	1,552	0.472	0.582	0.005	0.100	0.146	9.9	3.3	39.6
2,413	2,011	0.621	0.685	0.008	0.176	0.244	8.4	6.1	24.3
Upshot-Knothole Shot 1, Yield 16.2 kt, Height of Burst 500 feet									
762	700	0.087	—	0.010	0.0[illegible]	0.034	60.0	25.0	112.0
949	900	0.121	—	0.014	0.050	0.085	28.7	15.0	48.4
1,092	1,050	0.153	0.397	0.025	0.080	0.133	23.0	14.0	33.0
1,188	1,150	0.180	0.384	0.013	0.120	0.161	17.7	5.0	19.5
Shot TU 4, Yield 19.6 kt, Height of Burst 1,040 feet									
1,205	608	0.284	0.300	0.001	0.018	0.035	27.5	25.0	82.7
1,425	974	0.368	0.414	0.023	0.052	0.075	10.6	10.0	43.6
1,701	1,345	0.486	0.539	0.021	0.122	0.162	8.7	9.0	24.5
Shot TP 2, Yield 2.4 kt, Height of Burst 300 feet									
734	670	0.147	0.190	0.017	0.037	0.047	23.0	7.0	48.4
850	795	0.163	0.220	0.009	0.063	0.082	18.0	10.0	23.0
Shot TP 4, Yield 43 kt, Height of Burst 500 feet									
1,839	1,770	—	0.640	0.020	0.215	0.230	15.4	9.0	27.0
Shot TP 5, Yield 3.6 [illegible], Height of Burst 300 feet									
698	630	0.122	0.150	0.004	0.035	0.038	26.1	6.0	76.0
771	710	0.121	0.160	0.007	0.058	0.068	27.8	5.0	44.0
892	840	0.137	0.250	0.013	0.080	0.097	25.0	4.0	30.0
987	940	0.163	0.280	0.005	0.118	0.125	16.5	5.5	17.0
Shot TP 6, Yield 7.76 kt, Height of Burst 500 feet									
1,190	1,080	0.265	0.270	0.022	0.108	0.145	14.0	8.0	19.2
Shot TP 8, Yield 14.2 kt, Height of Burst 500 feet									
1,145	1,030	0.195	0.280	0.012	0.055	0.060	35.0	20.0	64.0
Shot TP 12, Yield 22 kt, Height of Burst 400 feet									
850	750	0.104	—	0.011	0.016	0.029	81.0	48.0	164.0
1,077	1,000	0.149	0.361	0.006	0.046	0.085	38.3	7.9	68.6
1,552	1,500	0.265	0.553	0.008	0.183	0.253	19.5	5.1	29.6
1,552	1,500	0.225	0.420	0.020	0.215	0.230	15.4	9.0	27.0
PREDICTION FOR PLUMBBOB									
DOD Shot Priscilla, Yield 40 kt, Height of Burst 700 feet									
1,563	1,397	0.266	0.432	0.014	0.094	0.150	23.8	4.2	70.0
1,724	1,576	0.324	0.490	0.022	0.126	0.176	23.0	3.5	50.0
1,889	1,755	0.378	0.558	0.029	0.158	0.216	20.3	5.2	35.0
2,158	2,041	0.475	0.662	0.047	0.259	0.324	18.0	15.4	20.0

* Yields listed are those used in these calculations and are not necessarily the latest refinement of yield data.

TABLE 2.2 TYPE A PRECURSOR DATA, A-SCALED

Slant Range	Horizontal Distance	t_p	t_+	t_r	t_{ps}	t_m	P_{p_1}/P_m	P_{p_2}/P_m	P_{p_2}/P_{p_1}	P_m
feet	feet	sec	sec	sec	sec	sec				psi
Upshot-Knothole Shot 10, Yield 14.9 kt*, Scaled Height of Burst 203 feet, S_d 0.3885, S_t = 0.3839, S_p = 1.146										
328	262	0.052	0.073	0.002	0.009	0.020	0.17	0.14	0.8.	159.0
360	297	0.062	—	0.006	0.011	0.015	0.21	0.20	0.95	128.3
393	336	0.066	0.104	0.010	0.018	0.024	0.17	0.01	0.07	73.1
402	347	0.068	0.108	0.008	0.023	0.028	0.17	0.06	0.36	80.0
412	358	0.074	0.108	0.010	0.023	0.027	0.20	0.19	0.95	81.9
498	454	0.102	0.123	0.011	0.040	0.092	0.48	0.21	0.45	43.1
588	551	0.135	0.175	0.007	0.069	0.077	0.072	0.29	0.41	16.4
Upshot-Knothole Shot 11, Yield 60.8 kt, Scaled Height of Burst 316 feet, S_d 0.2370, S_t 0.2340, S_p = 1.229										
485	368	0.111	0.136	0.001	0.023	0.034	0.25	0.08	0.33	48.7
572	477	0.145	0.160	0.002	0.041	0.057	0.35	0.25	0.73	29.8
Upshot-Knothole Shot 1, Yield 16.2 kt, Scaled Height of Burst 112 feet, S_d = 0.3750 S_t = 0.3670, S_p = 1.1704										
286	262	0.032	—	0.004	0.007	0.013	0.54	0.22	0.41	131.1
356	338	0.044	—	0.005	0.018	0.031	0.59	0. .	0.53	56.6
410	394	0.056	0.146	0.009	0.029	0.049	0.70	0.42	0.60	38.6
446	431	0.066	0.141	0.005	0.044	0.060	0.91	0.26	0.29	22.8
Shot TU 4, Yield 19.6 kt, Scaled Height of Burst 363 feet, S_d = 0.349, S_t = 0.346, S_p = 1.199										
421	212	0.098	0.104	0.001	0.006	0.012	0.33	0.30	0.91	99.2
497	340	0.127	0.143	0.008	0.018	0.026	0.24	0.23	0.95	52.3
594	469	0.168	0.186	0.007	0.042	0.056	0.36	0.37	1.02	29.4
Shot TP 2, Yield 2.4 kt, Scaled Height of Burst 213 feet, S_d = 0.7112, S_t = 0.6812, S_p = 1.163										
521	475	0.100	0.129	0.011	0.025	0.03.	0.48	0.14	0.21	56.3
603	564	0.111	0.150	0.007	0.043	0.056	0.78	0.43	0.55	26.7
Shot TP 4, Yield 43 kt, Scaled Height of Burst 136 feet, S_d = 0.2696, S_t = 0.2630, S_p = 1.186										
498	480	—	0.169	0.007	0.072	0.077	0.57	0.33	0.58	32.0
Shot TP 5, Yield 3.6 kt, Scaled Height of Burst 186 feet, S_d = 0.6203, S_t = 0.6064, S_p = 1.161										
433	391	0.068	0.090	0.002	0.021	0.023	0.35	0.08	0.23	88.2
479	441	0.073	0.097	0.004	0.035	0.041	0.60	0.11	0.18	51.1
554	522	0.083	0.152	0.008	0.048	0.059	0.80	0.13	0.16	34.8
613	584	0.099	0.170	0.003	0.072	0.076	0.97	0.32	0.33	19.7
Shot TP 6, Yield 7.76 kt, Scaled Height of Burst 240 feet, S_d = 0.4893, S_t = 0.4679, S_p = 1.163										
572	519	0.124	0.126	0.010	0.050	0.068	0.73	0.42	0.58	22.3
Shot TP 8, Yield 14.2 kt, Scaled Height of Burst 195.1 feet, S_d = 0.3901, S_t = 0.3842, S_p 1.186										
447	402	0.075	0.108	0.005	0.021	0.023	0.54	0.31	0.57	75.9
Shot TP 12, Yield 22 kt, Scaled Height of Burst 137 feet S_d = 0.3425, S_t = 0.3418, S_p 1.132										
291	257	0.036	—	0.004	0.005	0.010	0.49	0.29	0.59	185.6
369	343	0.051	0.123	0.002	0.016	0.029	0.56	0.12	0.21	77.6
532	514	0.091	0.189	0.003	0.062	0.085	0.66	0.17	0.26	33.5
532	514	0.077	0.144	0.007	0.073	0.079	0.57	0.33	0.58	30.6
PREDICTION FOR PLUMBBOB										
Shot Priscilla, Yield 40 kt, Scaled Height of Burst 195 feet, S_d 0.2792, S_t 0.2778, S_p 1.15										
436	390	0.074	0.120	0.004	0.026	0.036	0.34	0.06	0.18	80.5
481	440	0.090	0.136	0.005	0.035	0.049	0.46	0.07	0.15	57.5
527	490	0.105	0.155	0.008	0.044	0.060	0.58	0.15	0.26	40.2
602	570	0.132	0.184	0.013	0.072	0.090	0.90	0.77	0.86	23.0

* See footnote, Table 2.1.

[redacted]

TABLE 2.3 GAGE LOCATIONS FOR PRECURSOR WAVEFORM STUDIES

Gage locations are given as distances from ground zero in feet.

Shot	Franklin	Wilson	Priscilla	Hood	Kepler	Owens	Shasta	Smoky	Galileo	Charleston	Morgan
Estimated yield, kt	0.138 ± 0.006	10.3 ± 5%	36.6 ± 1	74.1 ± 5%	10.3 ± 0.5	9.6 ± 5%	16.8 ± 5%	43.71 ± 5%	11.3 ± 1	11.5 ± 5%	7.8 ± 5%
Height of burst, ft	300T	500B	700B	1,500B	500T	500B	500T	700T	500T	1,500B	500B
	400	600 q	350	1,000	550	500	1,000	840	600	1,100	—
	700	1,000 q	450	1,511	900	600 q	1,500	900	1,050	1,300	600
	800 q	1,150	650	1,700 q	1,050	800	2,000	1,005	1,200 q	1,500	1,000
	900 q	1,250 q	850 q	2,200 q	1,200 q	1,000 q	2,500	1,176	1,400	2,300	1,250
	1,000	1,420	1,050 q	2,400	1,400	1,150	3,000	1,500 q	1,700 q	3,000	2,200
	1,200 q	1,511	1,350 q	3,000 q	1,700 q	1,420	18,000	2,018	1,950	5,500	3,000
	1,500 q	1,575	1,650 q	4,000 q	1,950	1,511 q		2,589 q	2,100 q	8,000	5,000
	1,800	1,650	2,000 q	4,590	2,100 q	1,575		2,943 q	2,200	16,000	6,600
		1,700 q	2,250 q	5,000 q	2,200	1,650		3,406 q	2,350	21,120	8,000
		1,800	2,500 q	5,500	2,350	1,700 q		3,875 q	2,500	25,872	15,000
		1,950 q	3,000 q	6,000	2,500 q	1,800		4,155	2,600	51,216	21,120
		2,100	3,500 q	6,600 q	2,600	3,000		4,320	2,765 q	73,000	25,872
		2,200 q	4,000 q	7,000	2,800	6,600		5,680 q	4,700		35,000
		2,400	4,500	8,000	22,616			6,000			
		2,800	5,000					8,000			
		3,000	6,000								

TABLE 2.4 GAGE PERFORMANCE

Shot	Pressure-Time Gages				Dynamic Pressure Gages	
	Total Number P_t-Gages	Pressure-Time Record	Peak Pressure Only	No Record	Total Number q-Gages	Pressure-Time Record
Franklin	11	9	2	–	4	4
Wilson	18	17	1	–	8	5
Hood	18	14	4	–	6	5
Owens	16	12	4	–	4	4
Kepler	15	14	1	–	5	3
Shasta	6	5	1	–	—	—
Galileo	13	12	1	–	4	4
Charleston	18	10	6	2	—	—
Morgan	12	9	3	–	—	—
TOTAL	127	102	23	2	31	25

TABLE 2.5 SUMMARY OF SHOT DATA

Shot	Franklin	Wilson	Priscilla	Reed	Kepler	Owens	Shasta	Smoky	Galileo	Charleston	Morgan
Date	2 June	16 June	24 June	5 July	24 July	25 July	18 August	31 August	2 September	28 September	7 October
Area	3	9a	FF	9a	4	9a	2a	2c	1	9a	9a
Time	0455	0445	0630	0440	0450	0630	0500	0530	0540	0559	0500
Coordinates	N 837,020.05 E 698,416.41	N 808,033.00 E 687,118.00	N 746,249.98 E 716,000.20	N 808,033.00 E 632,418.00	N 854,233.66 E 664,463.68	N 808,033.00 E 682,418.00	N 866,030.33 E 663,322.51	N 887,090.00 E 674,450.00	N 838,780.81 E 559,790.83	N 838,780.81 E 559,790.83	N 838,780.81 E 559,790.83
Height of ground zero (MSL), ft	4,024.70	4,214.46	3,070.00	4,216.46	4,307.50	4,214.46	4,382.35	4,479.12	4,235.00	4,216.46	4,214.46
Height of burst, ft	300T	500B	700B	1,500B	500T	500B	500T	700T	500T	1,500B	500B
Yield, kt *	0.135 ± 0.006	10.3 ± 5%	36.6 ± 1	74.1 ± 5%	10.3 ± 0.5	9.6 ± 5%	16.8 ± 5%	43.7 ± 5%	11.3 ± 1	11.5 ± 5%	7.8 ± 5%
Ambient pressure, psi											
Burst height	12.73	12.54	12.86	11.89	12.33	12.39	12.36	12.24	12.35	12.02	12.39
Surface	12.62	12.79	13.19	12.70	12.54	12.63	12.56	12.42	12.73	12.70	12.60
Air temperature, °C											
Burst height	14.0	20.3	24.0 ± 2	21.0	21.0	23.1	26.5	14.0	21.0	18.5	11.9
Surface	21.0	17.0	17.5 ± 1	21.0	21.0	20.0	26.4	15.2	15.8	18.1	7.3
S_p	1.154	1.149	1.114	1.156	1.171	1.163	1.170	1.183	1.154	1.157	1.167
S_d	1.945	0.439	0.291	0.227	0.436	0.448	0.370	0.269	0.423	0.422	0.478
S_t	1.365	0.436	0.289	0.228	0.438	0.446	0.377	0.269	0.421	0.424	0.472
$1/S_p$	0.866	0.870	0.898	0.865	0.854	0.860	0.855	0.845	0.866	0.864	0.857
$1/S_d$	0.542	2.278	3.436	4.405	2.294	2.232	2.703	3.717	2.364	2.370	2.092
$1/S_t$	0.547	2.294	3.460	4.386	2.283	2.232	2.653	3.717	2.375	2.356	2.119
Height of burst to 1 kt at sea level, ft	554	220	204	341	218	224	185	188	212	633	239

* See footnote Table 2.1.

TABLE 2.6 SURFACE PRESSURE-TIME RESULTS

Station	Ground Range	Maximum Overpressure	Arrival Time	Positive Duration	Type Waveform
	feet	psi	sec	sec	
Shot Franklin					
3-1.1-9004.00	400	25.0	0.555	0.086	D
3-1.1-9004.00	400	26.0	-	-	-
3-1.1-9004.01	700	11.8	0.269	0.098	D
3-1.1-9004.01	700	11.2	-	0.095	D
3-1.1-9003.01	800	7.7	0.328	0.091	D
3-1.1-9003.01	800	8.6	0.359	0.165	D
3-1.1-9003.02	900	7.2	0.202	0.080	D
3-1.1-9004.02	1000	6.4	0.521	0.153	D
3-1.1-9003.03	1200	4.8	0.328	0.155	D
3-1.1-9003.04	1500	3.5	0.568	0.121	D
3-1.1-9004-03	1800	2.5	-	-	-
Shot Wilson					
9-1.1-9021.01	600	140.0	0.405	0.144	A
9-1.1-9021.01	600	140.0	0.076	0.170	A
9-1.1-9021.02	1000	38.0	0.119	0.276	A
9-1.1-9021.02	1000	42.0	0.194	0.308	A
9-1.1-9022.01	1150	31.0	-	-	-
9-1.1-9021.03	1250	24.0	0.131	0.302	A
9-1.1-9021.03A	1420	12.0	0.200	0.329	B
9-1.1-9022.02	1511	10.6	0.280	0.496	B
9-1.1-9022.02A	1575	12.6	-	0.476	B
9-1.1-9022.02B	1650	9.0	0.438	0.436	B
9-1.1-9021.04	1700	9.3	0.488	0.428	B
9-1.1-9022.03	1800	9.0	0.499	0.494	B
9-1.1-9021.05	1950	9.7	0.659	0.482	C
9-1.1-9021.06	2100	10.1	0.67[illegible]	0.482	C
9-1.1-9021.07	2200	9.3	0.846	[illegible]	C
9-1.1-9022.05	2400	7.8	1.013	0.533	D
9-1.1-9021.06	2800	6.6	1.063	0.551	D
9-1.1-9021.08	3000	6.2	1.417	0.613	D
Shot Hood					
9-1.1-9021.02	1000	86.0	-	0.406	A
9-1.1-9021.02	1000	92.0	-	0.465	A
9-1.1-9022.02	1511	52.0	0.394	0.543	A
9-1.1-9021.04	1700	47.5	0.421	0.708	A
9-1.1-9021.07	2200	18.4	0.546	0.839	A
9-1.1-9022.05	2400	17.0	0.675	0.808	A
9-1.1-9021.08	3000	8.5	0.865	1.045.3	B
9-1.1-9021.09	4000	6.7	-	-	-
9-1.1-9021.09	4000	6.8	-	-	-
9-1.1-9022.07	4590	6.8	1.749	1.153	C
9-1.1-9021.10	5000	6.2	2.266	1.173	C
9-1.1-9022.08	5500	6.0	2.670	1.185	D
9-1.1-9022.09	6000	5.4	2.838	1.229	D
9-1.1-9022.09	6000	5.5	2.904	1.272	D
9-1.1-9021.11	6600	4.7	3.341	1.334	D
9-1.1-9022.10	7000	4.1	-	-	-
9-1.1-9022.10	8000	3.3	4.118	1.426	D
9-1.1-9022.11	8000	3.3	-	-	-
Shot Kepler					
4-1.1-9022.00	550	195.0	-	0.141	A
4-1.1-9021.00	900	58.0	-	0.181	A
4-1.1-9021.01	1050	39.0	0.196	0.220	B
4-1.1-9021.01	1050	48.0	0.140	0.235	D
4-1.1-9022.01	1200	30.0	0.236	0.263	D
4-1.1-9021.02	1400	26.0	0.216	0.345	D
4-1.1-9022.02	1700	20.0	0.474	0.381	D
4-1.1-9021.03	1950	14.6	0.573	0.441	D
4-1.1-9022.03	2100	14.0	0.733	0.455	D
4-1.1-9021.04	2200	11.5	0.784	0.498	D
4-1.1-9021.05	2350	10.8	0.981	0.482	D
4-1.1-9022.04	2500	10.2	-	-	-
4-1.1-9021.06	2600	9.5	1.045	0.560	D
4-1.1-9022.05	2800	8.7	1.031	0.580	D
4-1.1-9021.11	22,616	0.30	15.08	0.492	-

TABLE 2.6 SURFACE PRESSURE-TIME RESULTS (Continued)

Station	Ground Range	Maximum Overpressure	Arrival Time	Positive Duration	Type Waveform
	feet	psi	sec	sec	
Shot Owens					
9-1.1-9021.01A	500	225.0	-	0.255	A
9-1.1-9021.01B	600	115.-	-	-	-
9-1.1-9021.01B	600	102.5	-	0.148	A
9-1.1-9021.01C	800	62.0	-	0.228	A
9-1.1-9021.02	1000	37.0	-	-	-
9-1.1-9021.02	1000	35.5	-	0.282	A
9-1.1-9022.01	1150	27.0	-	0.354	A
9-1.1-9021.03A	1420	13.3	-	0.270	B
9-1.1-9022.02	1511	11.0	-	0.441	B
9-1.1-9022.02A	1575	11.6	-	0.423	B
9-1.1-9022.02B	1650	8.6	-	0.460	B
9-1.1-9021.04	1700	8.7	-	0.456	B
9-1.1-9022.03	1800	9.1	-	0.450	B
9-1.1-9022.03	1800	9.4	-	-	-
9-1.1-9021.08	3000	5.9	-	-	-
9-1.1-9021.11	6600	2.3	-	0.840	D
Shot Shasta					
2-1.1-9020.01	1000	55.0	-	-	-
2-1.1-9020.02	1500	25.8	0.231	0.407	D
2-1.1-9020.03	2000	14.0	0.578	0.448	D
2-1.1-9020.04	2500	10.0	-	0.559	D
2-1.1-9020.05	3000	8.0	1.165	0.622	D
2-1.1-9020.06	18,000	1.2	13.51	1.218	D
Shot Galileo					
1-1.1-9001.00	600	160.0	-	-	-
1-1.1-9001.01	1050	36.5	-	0.255	A
1-1.1-9002.01	1200	25.0	-	0.315	A
1-1.1-9001.02	1400	23.7	-	0.324	A
1-1.1-9002.02	1700	16.5	-	0.402	A
1-1.1-9001.03	1950	12.2	-	0.436	B
1-1.1-9002.03	2100	10.5	-	0.463	B
1-1.1-9001.04	2200	10.7	-	0.476	B
1-1.1-9001.05	2350	9.8	-	0.510	D
1-1.1-9002.04	2500	10.0	-	0.475	D
1-1.1-9001.06	2600	9.2	-	0.503	D
1-1.1-9002.05	2765	8.3	-	0.581	D
1-1.1-9002.06	4700	4.2	-	0.745	D
Shot Charleston					
9-1.9-9020.01	1100	17.5	-	0.410	D
9-1.9-9020.01	1100	17.2	-	0.331	D
9-1.9-9020.02	1300	-	-	-	-
9-1.9-9020.03	1500	14.5	-	0.433	D
9-1.9-9020.03	1500	15.0	-	-	-
9-1.9-9020.04	2300	12.2	-	0.520	D
9-1.9-9020.04	2300	13.0	-	0.490	D
9-1.1-9021.08	3000	8.5	-	-	-
9-1.1-9021.08	3000	8.4	-	0.577	D
9-1.1-9022.08	5500	3.8	-	-	-
9-1.1-9022.08	5500	3.7	-	0.737	D
9-1.1-9022.11	8000	2.1	-	1.060	D
9-1.1-9022.12	16,000	1.10	-	-	-
9-1.1-9022.13	21,120	-	-	-	-
9-1.1-9022.14	25,873	0.95	-	-	-
9-1.1-9022.14	25,873	0.85	-	1.250	-
9-1.1-9022.16	51,216	0.22	-	-	-
9-1.1-9022.17	73,000	0.07	-	1.580	-
Shot Morgan					
9-1.1-9021.01	600	95.0	-	-	-
9-1.1-9021.02	1000	33.0	-	0.281	A
9-1.1-9021.04	1250	20.0	-	0.397	A
9-1.1-9021.07	2200	7.7	-	0.461	C
9-1.1-9021.08	3000	5.6	-	0.574	D
9-1.1-9021.10	5000	2.8	-	0.684	D
9-1.1-9021.11	6600	2.1	-	0.829	D
9-1.1-9022.11	8000	1.45	-	0.844	D
9-1.1-9021.12	15,000	1.10	-	-	-
9-1.1-9022.13	21,120	0.90	-	-	-
9-1.1-9022.14	25,872	0.70	-	0.987	D
9-1.1-9022.15	25,000	0.32	-	1.004	D

[redacted]

TABLE 2.7 q-GAGE RESULTS, 3-FOOT LEVEL, MAXIMUM VALUES

Station	Ground Range	Total Pressure	Static Overpressure	Pressure Difference $(P_p - P_s)^{\frac{1}{2}}$	Dynamic Pressure q	Mach Number u/a
	feet	psi	psi	psi	psi	
Shot Franklin						
3-1.1-9003.01	800	10.6	8.1	2.5	-	-
3-1.1-9003.02	900	8.8	7.4	1.4	-	-
3-1.1-9003.03	1200	6.0	5.4	0.6	-	-
3-1.1-9003.04	1500	4.0	3.6	0.4	-	-
Shot Wilson						
9-1.1-9021.01	600	-	-	-	-	-
9-1.1-9021.02	1000	205.0	35.5	196.0	120.0	2.5
9-1.1-9021.02M	1000	-	-	-	-	-
9-1.1-9021.03	1250	84.0	24.5	69.0	44.0	1.6
9-1.1-9021.04	1700	27.5	9.6	18.4	14.5	1.0
9-1.1-9021.04M	1700	-	-	-	-	-
9-1.1-9021.05	1950	23.0	9.6	13.4	11.0	0.83
9-1.1-9021.07	2200	12.3	9.4	3.2	3.0	0.44
Shot Hood						
9-1.1-9021.04	1700	129.0	48.0	120.0	72.0	2.0
9-1.1-9021.07	2200	-	-	-	-	-
9-1.1-9021.08	3000	20.0	8.3	12.0	11.0	0.81
9-1.1-9021.09	4000	11.3	6.3	6.2	6.0	0.66
9-1.1-9021.10	5000	8.3	6.2	2.1	1.9	0.40
9-1.1-9021.11	6000	5.4	4.8	0.7	0.6	0.22
Shot Owens						
9-1.1-9021.01	600	620.0	105.0	590.0	340.0	3.5
9-1.1-9021.02	1000	144.0	35.0	116.0	73.0	1.6
9-1.1-9022.02	1500	39.0	11.0	34.5	24.0	1.4
9-1.1-9021.04	1700	15.9	8.8	9.1	7.4	0.87
Shot Kepler						
4-1.1-9022.01	1200	-	-	-	-	-
4-1.1-9022.02	1700	-	-	-	-	-
4-1.1-9022.03	2100	16.8	13.7	4.7	4.3	0.50
4-1.1-9022.04	2500	13.5	11.0	2.6	2.3	0.38
4-1.1-9022.05	2800	10.0	8.7	1.5	1.3	0.30
Shot Galileo						
9002-01	1200	55.0	24.5	32.0	24.0	0.98
9002.02	1700	37.0	16.0	20.5	16.0	0.90
9002.03	2100	22.0	10.3	14.1	11.3	0.86
9002.05	2765	10.2	8.3	2.1	2.1	0.36

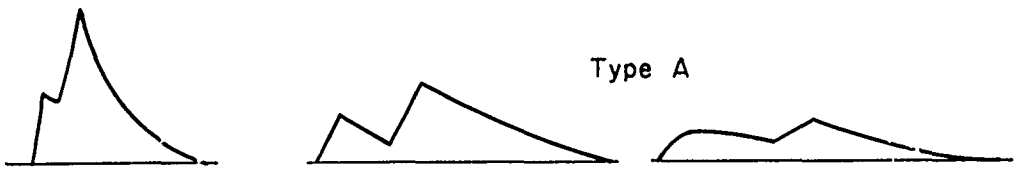

Figure 2.1 Types of waveforms in precursor zone.

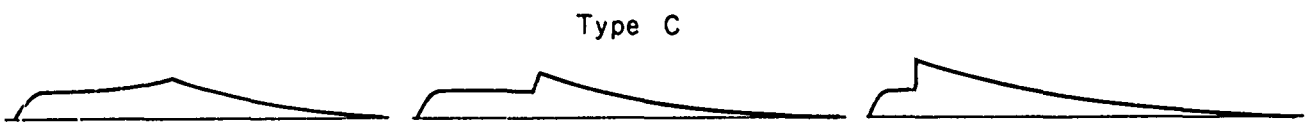

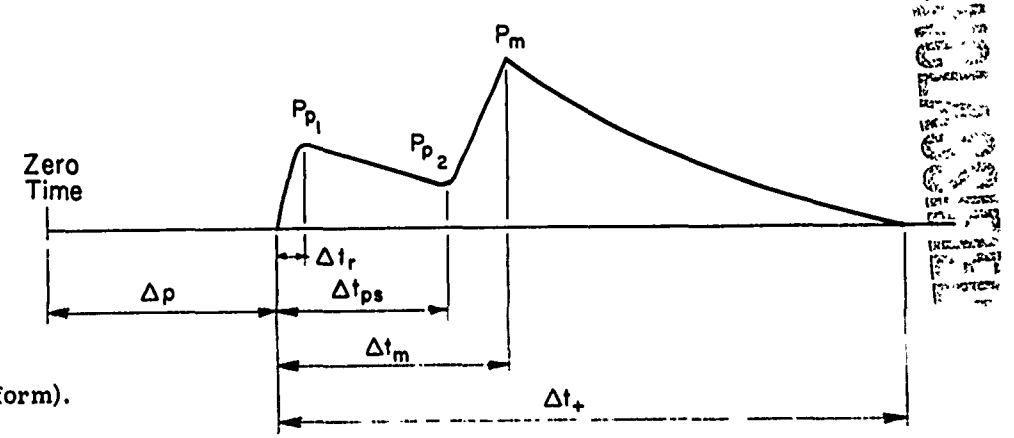

Figure 2.2 Time and pressure notation (Type A waveform).

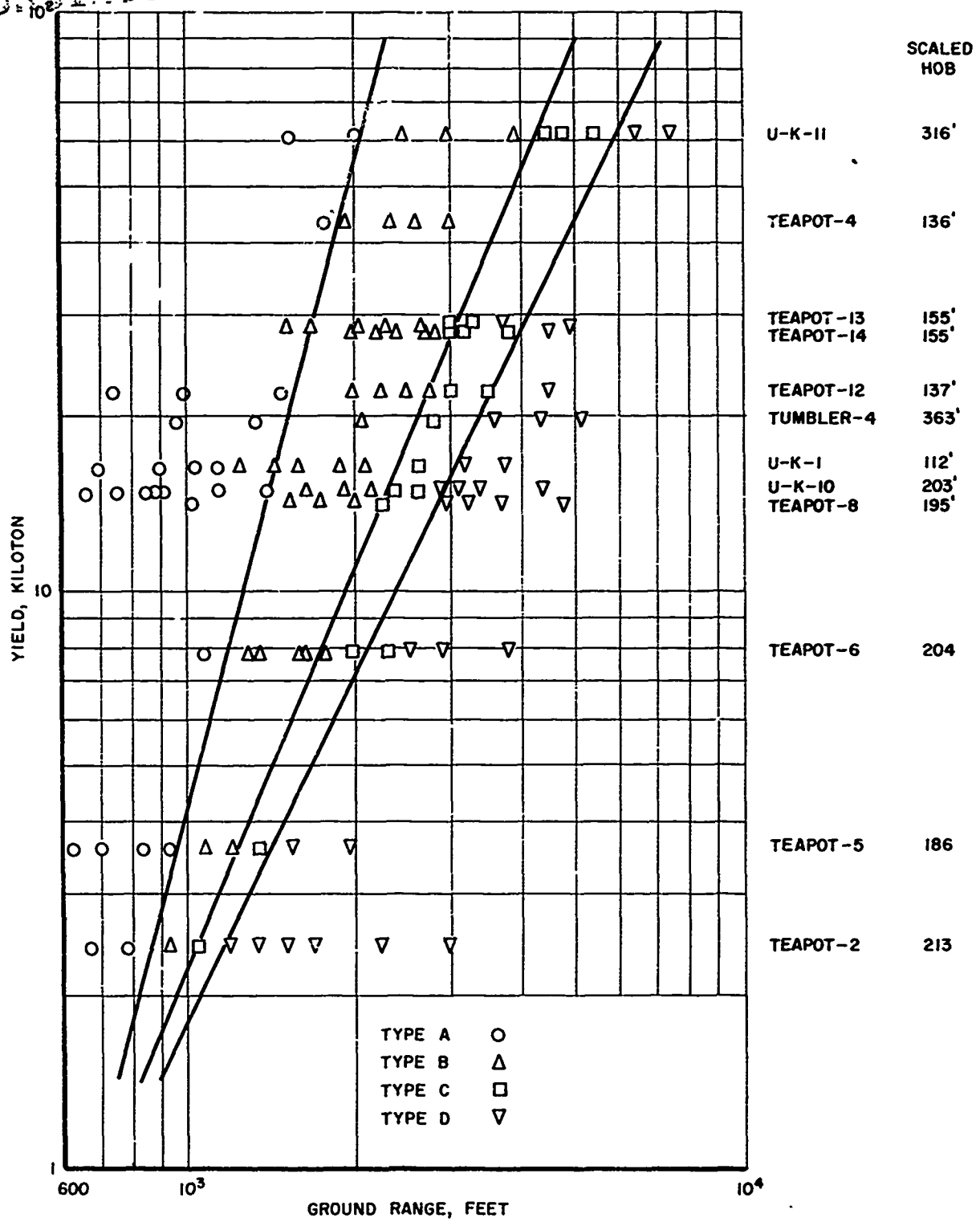

Figure 2.3 Wave shape versus ground distance for various yields.

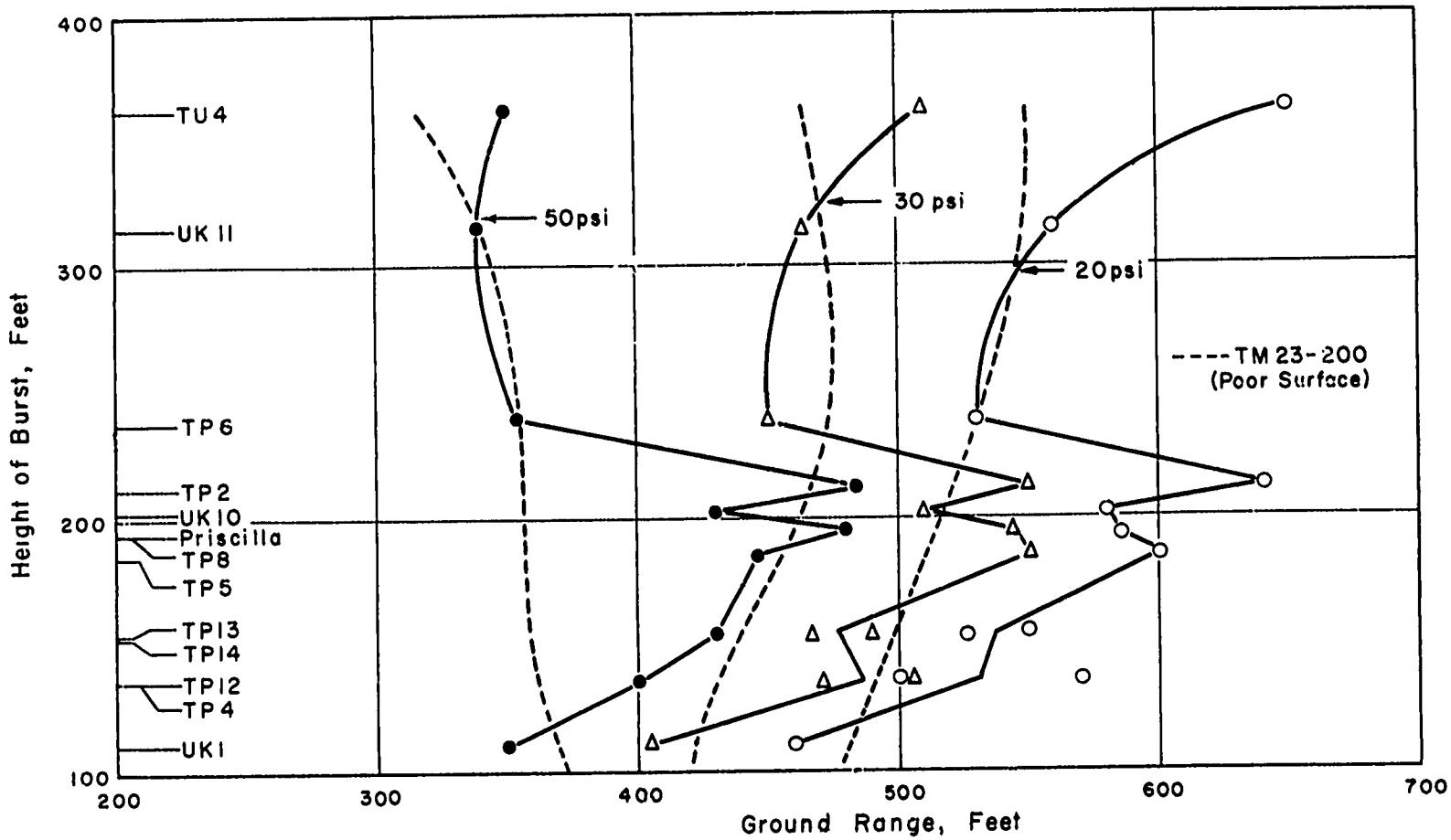

Figure 2.4 Height of burst versus ground distance scaled to 1 kt, sea level.

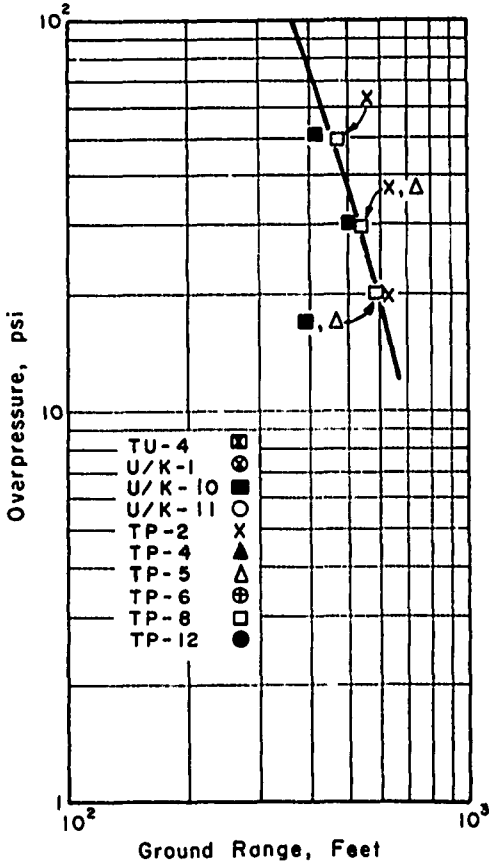

Figure 2.5 Pressure versus distance, scaled to 1 kt. Key defines points for Figures 2.5 through 2.12.

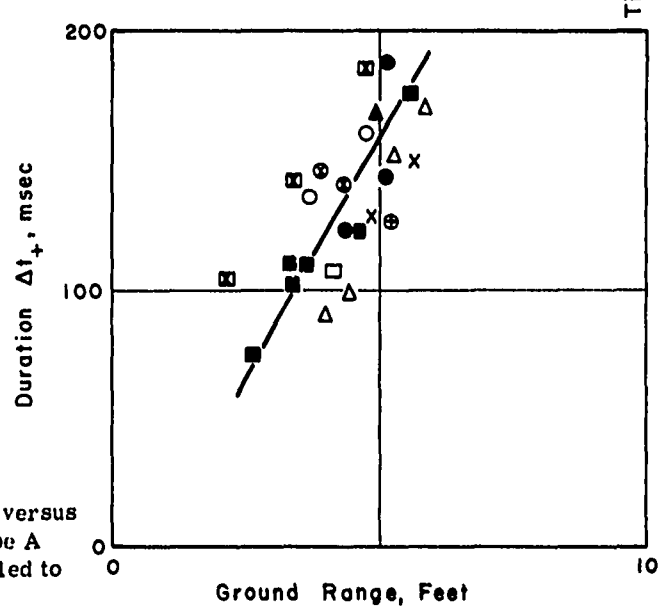

Figure 2.6 Duration versus ground distance, Type A precursor wave, scaled to 1 kt.

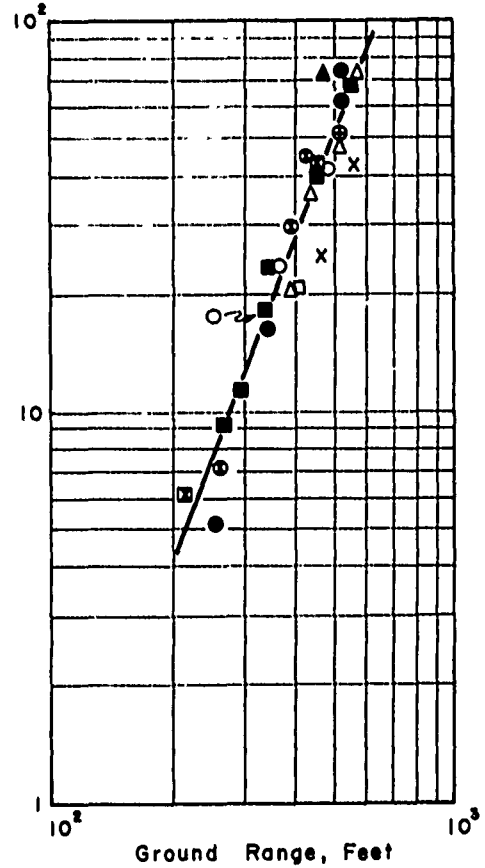

Figure 2.7 Time between arrival of precursor and second rise pressure versus ground distance, scaled to 1 kt.

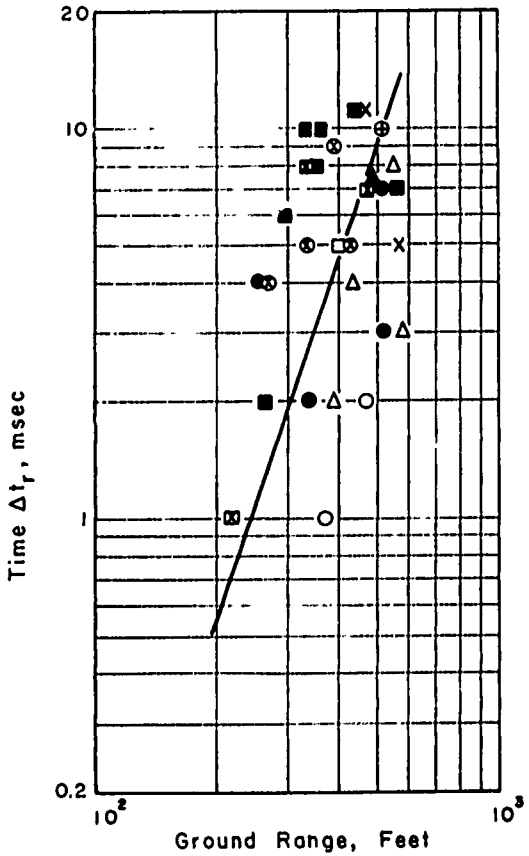

Figure 2.8 Time between arrival of precursor and first peak pressure versus ground distance, scaled to 1 kt.

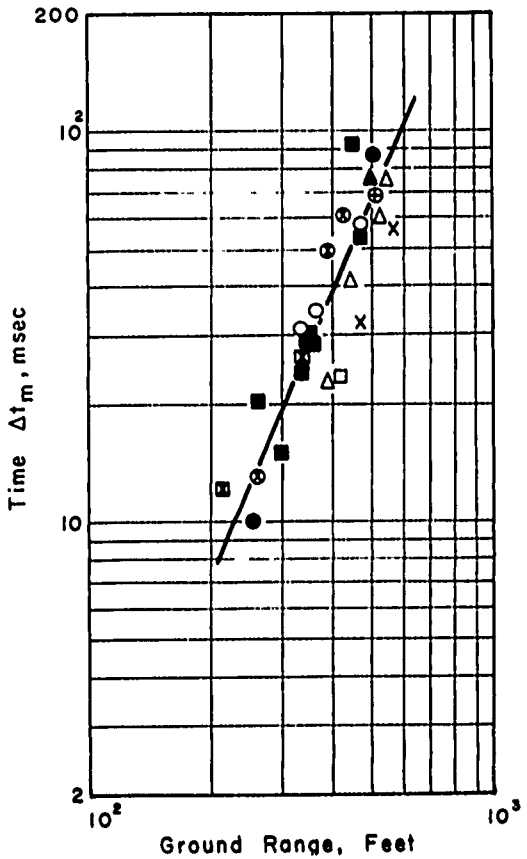

Figure 2.9 Time between arrival of precursor and second peak pressure versus ground distance, scaled to 1 kt.

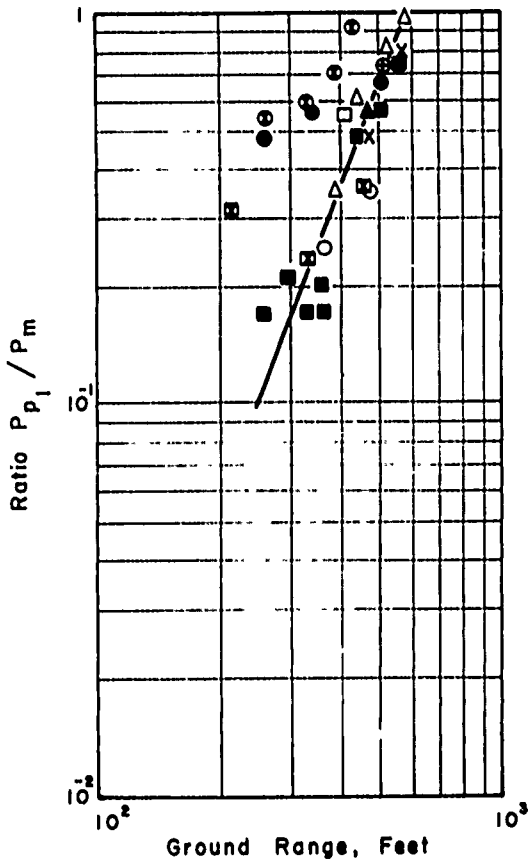

Figure 2.10 Ratio of precursor maximum pressure to main shock peak pressure P_m versus ground distance, scaled to 1 kt.

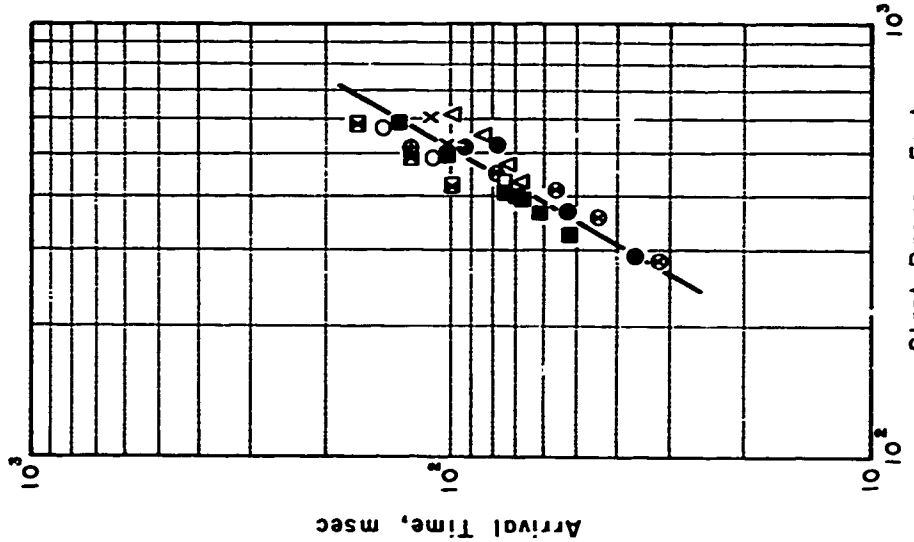

Figure 2.12 Precursor arrival time versus slant range, scaled to 1 kt.

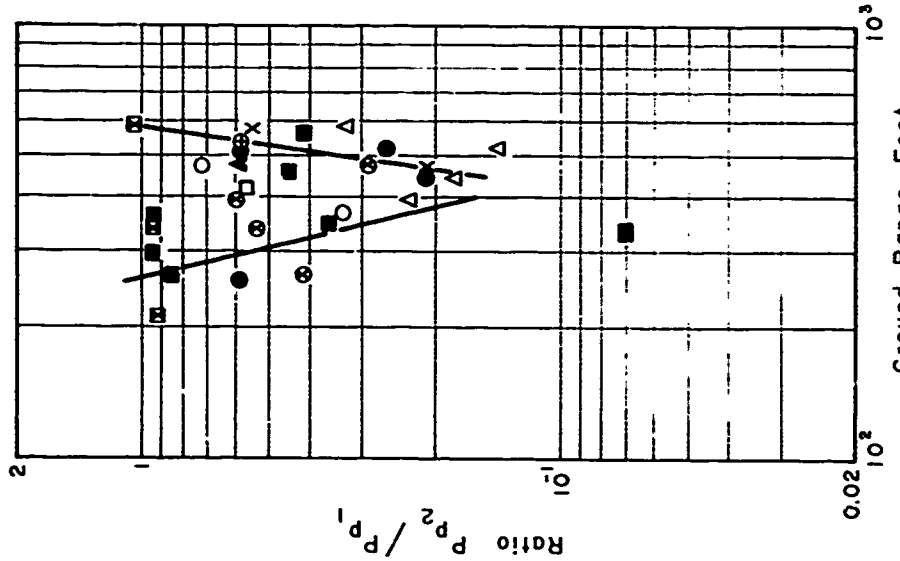

Figure 2.11 Ratio of pressure P_{p_2} to P_{p_1} versus ground distance, scaled to 1 kt.

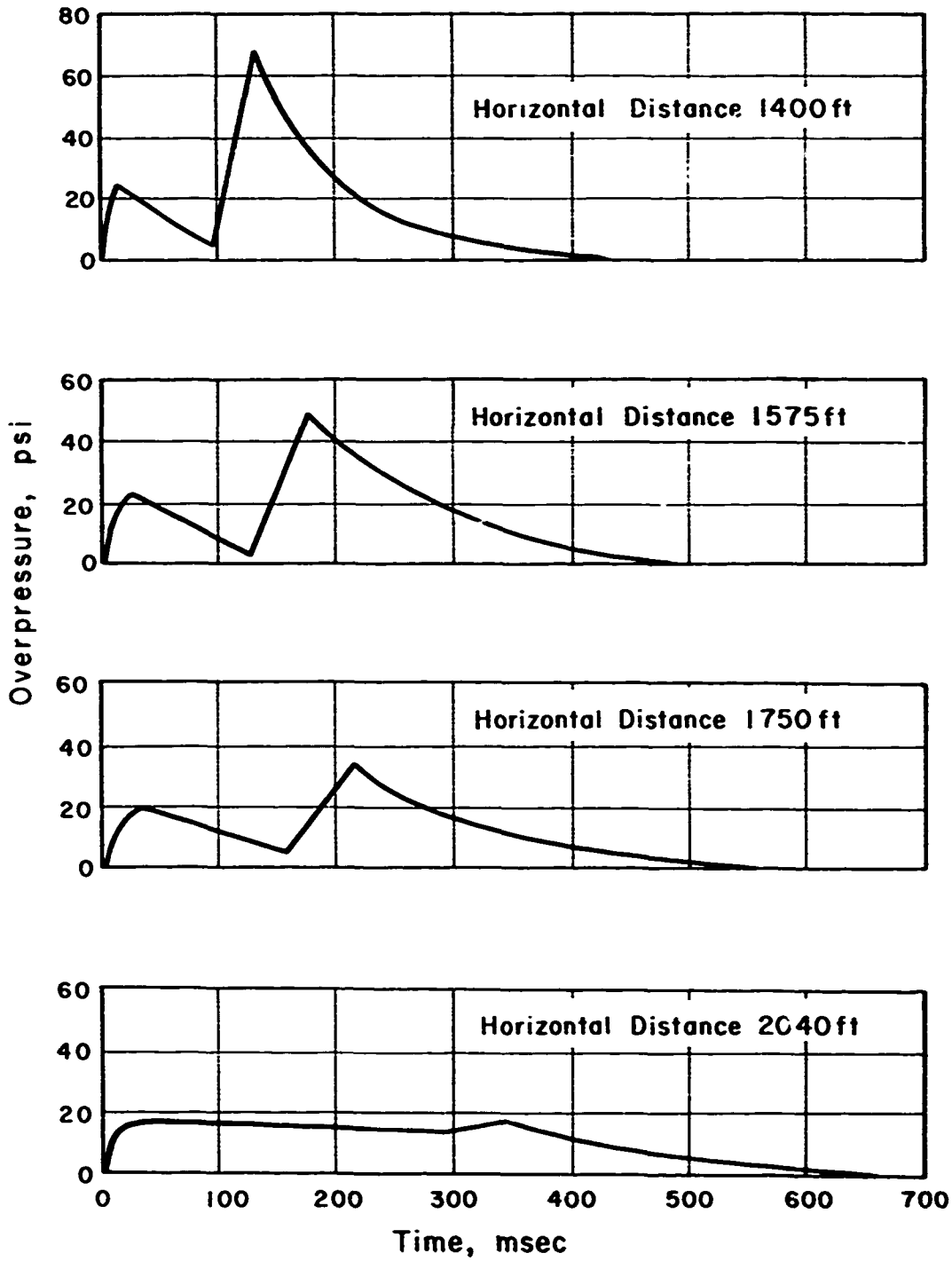

Figure 2.13 Predicted wave shapes, Shot Priscilla.

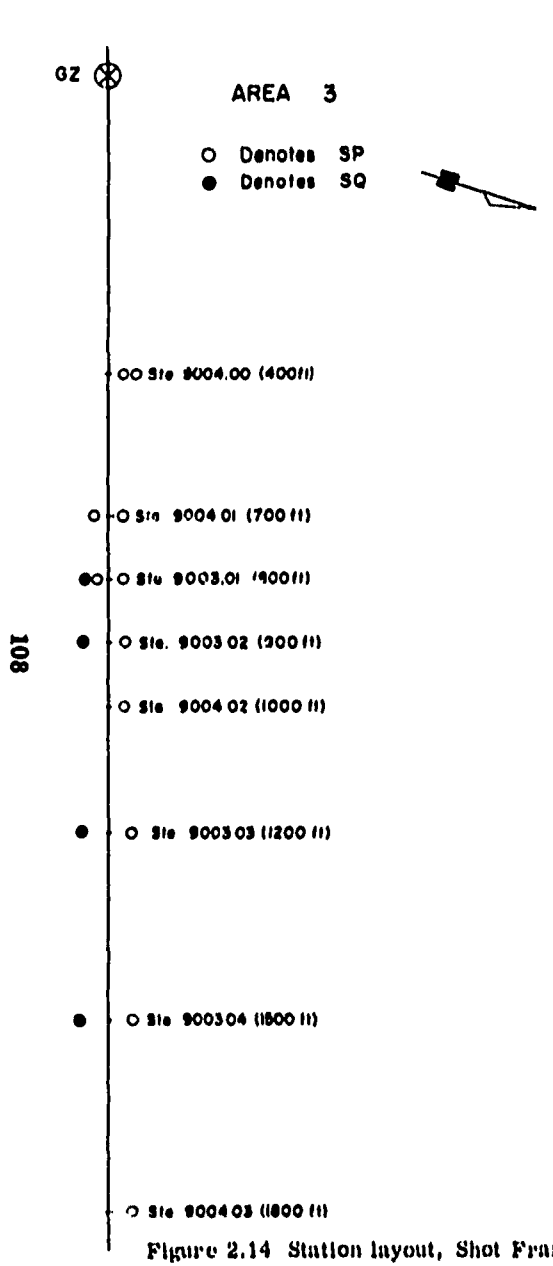

Figure 2.14 Station layout, Shot Franklin.

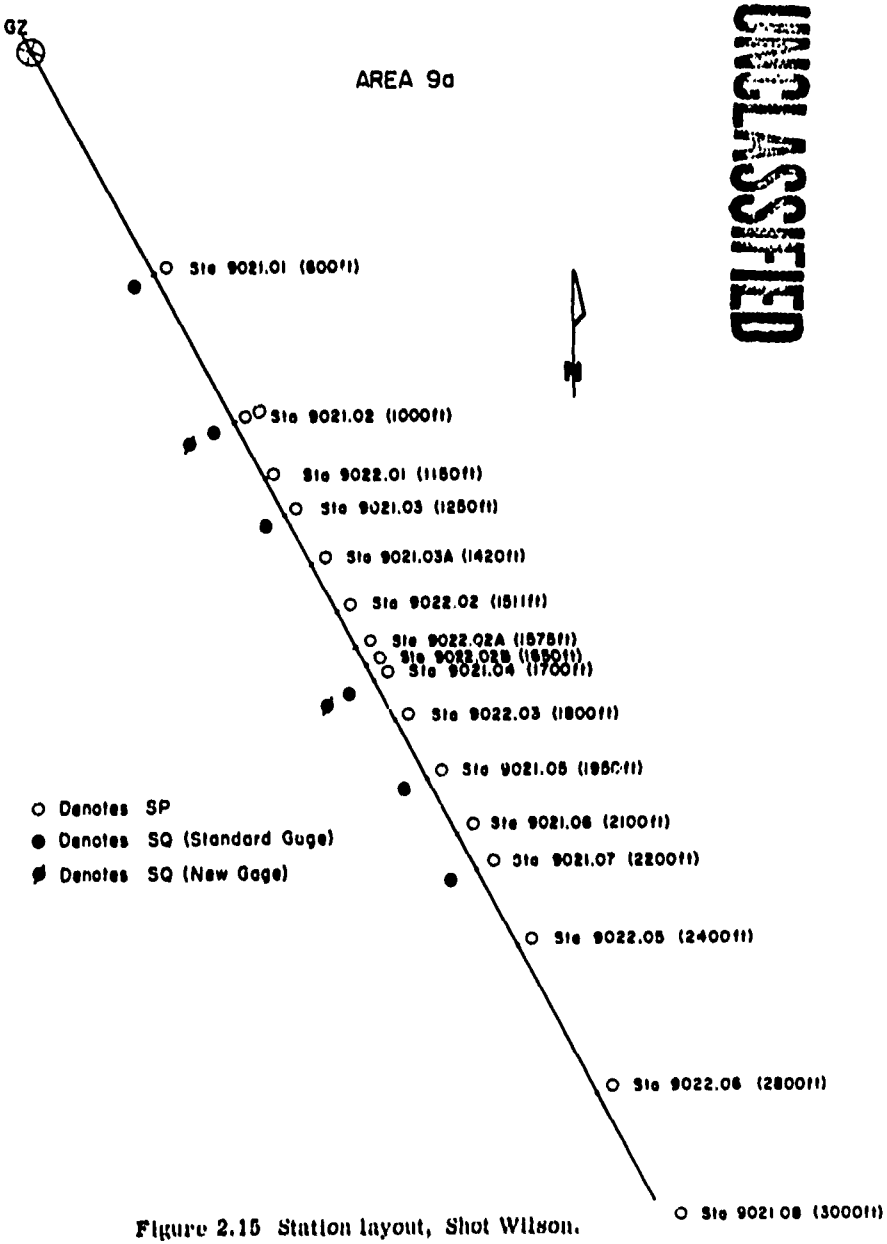

Figure 2.15 Station layout, Shot Wilson.

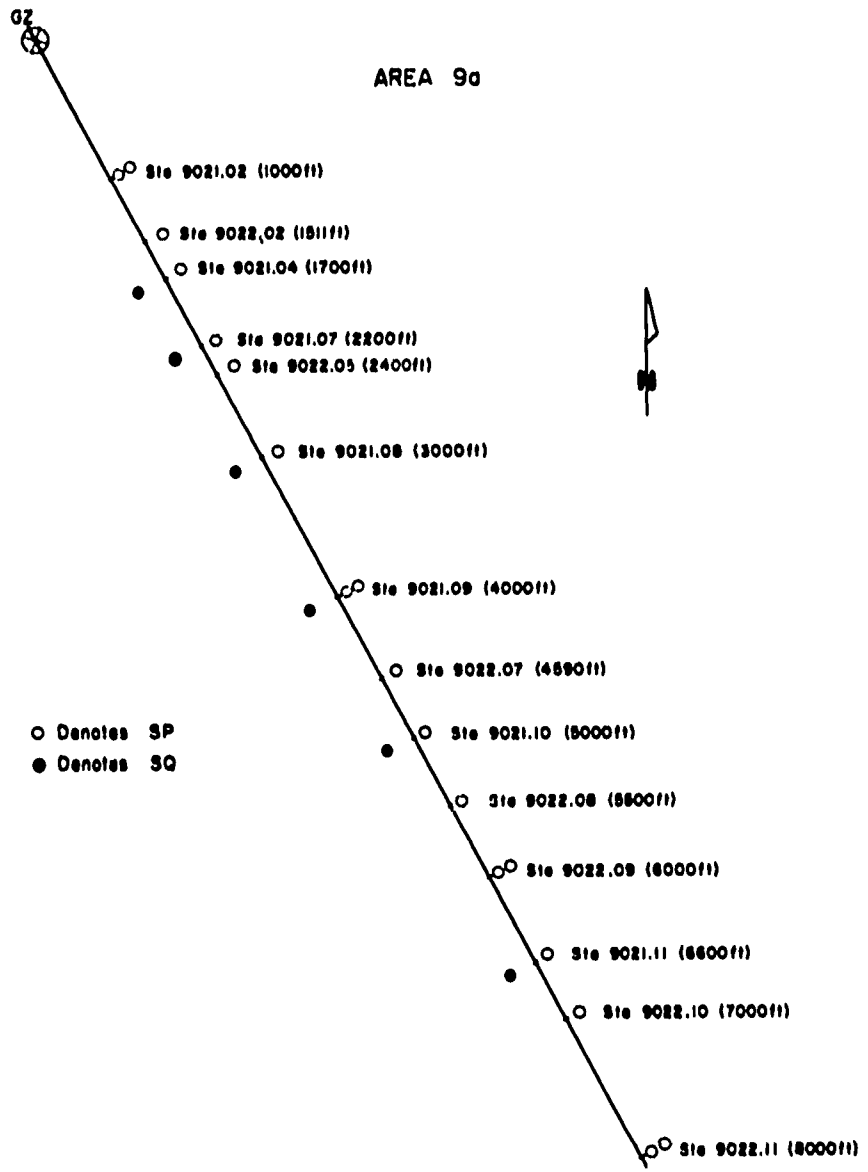

Figure 2.16 Station layout, Shot Hood.

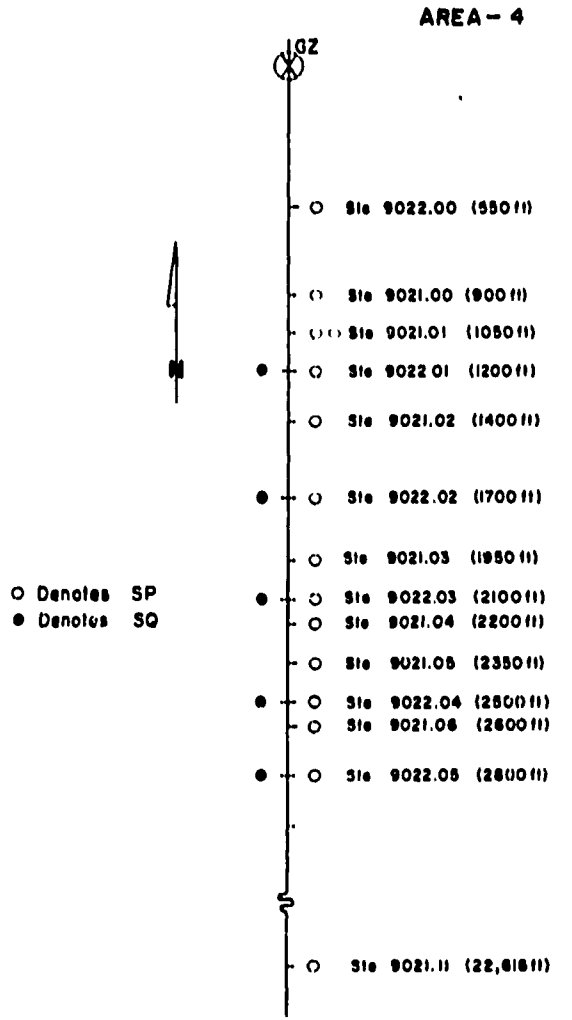

Figure 2.17 Station layout, Shot Kepler.

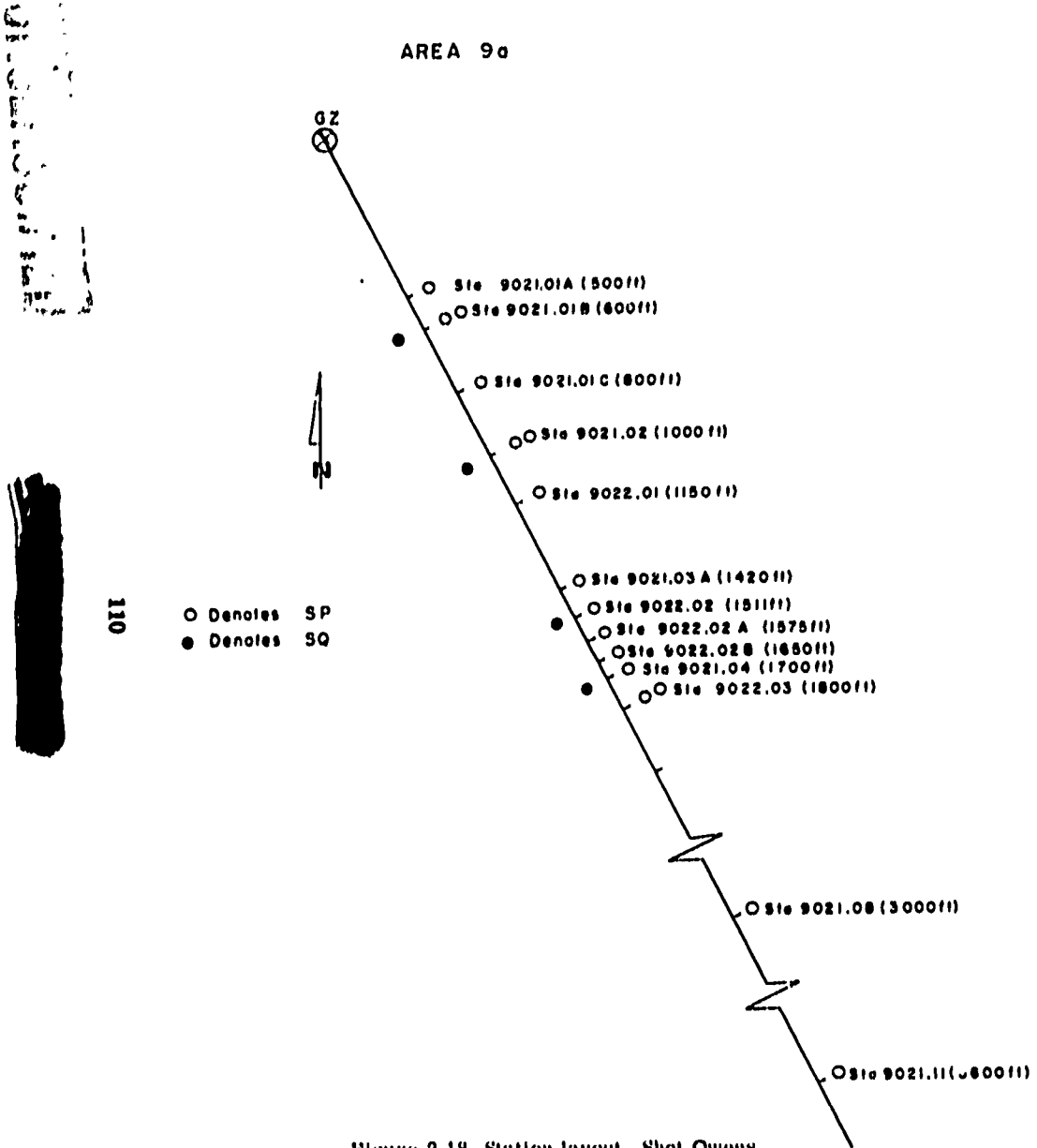

Figure 2.18 Station layout, Shot Owens.

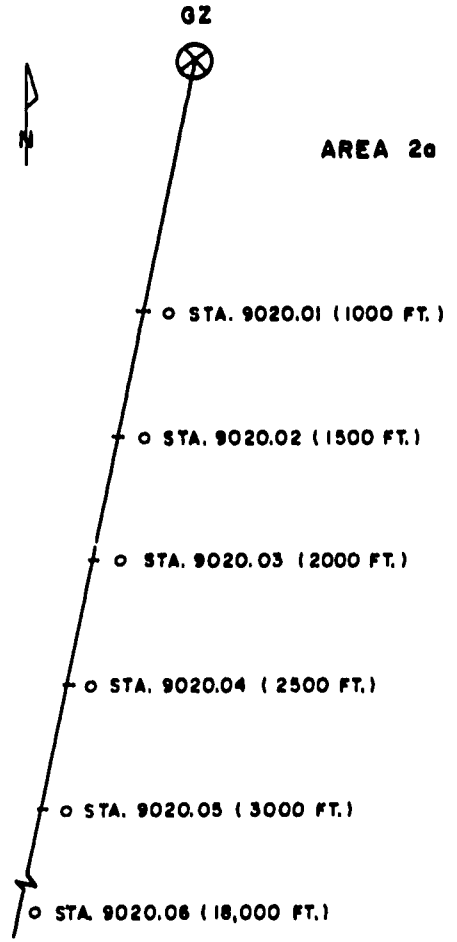

Figure 2.19 Station layout, Shot Shasta.

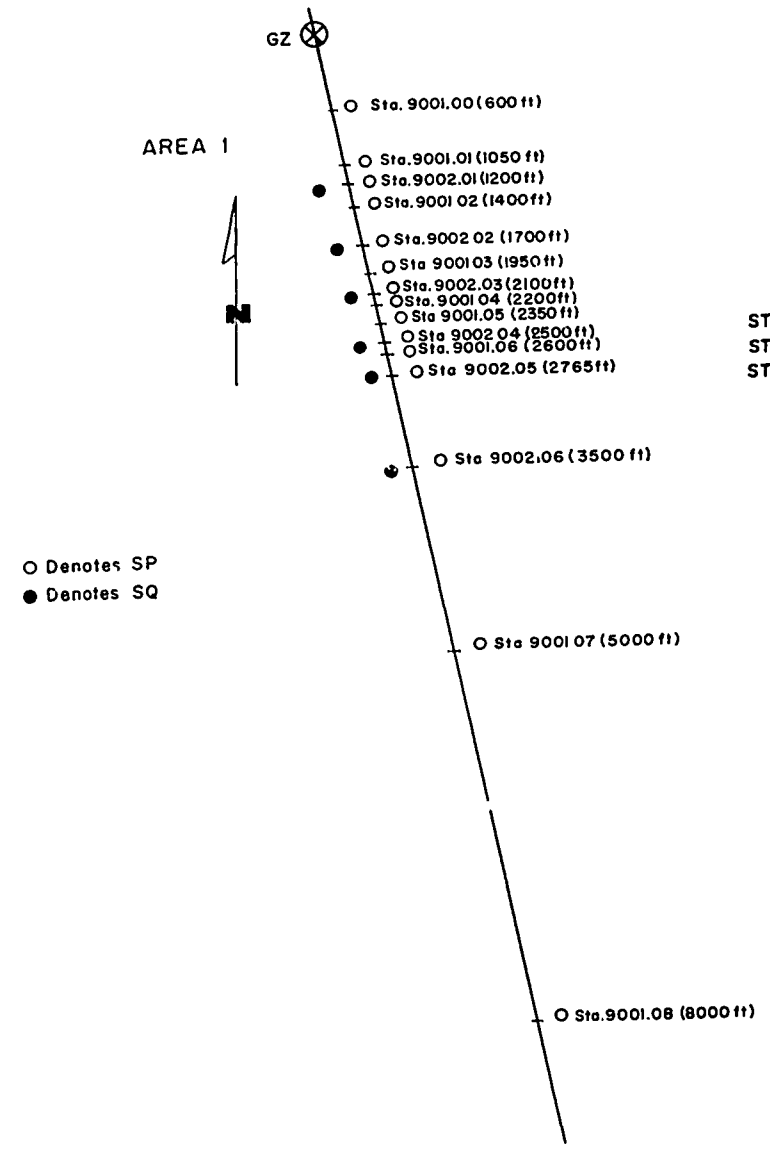

Figure 2.20 Station layout, Shot Galileo.

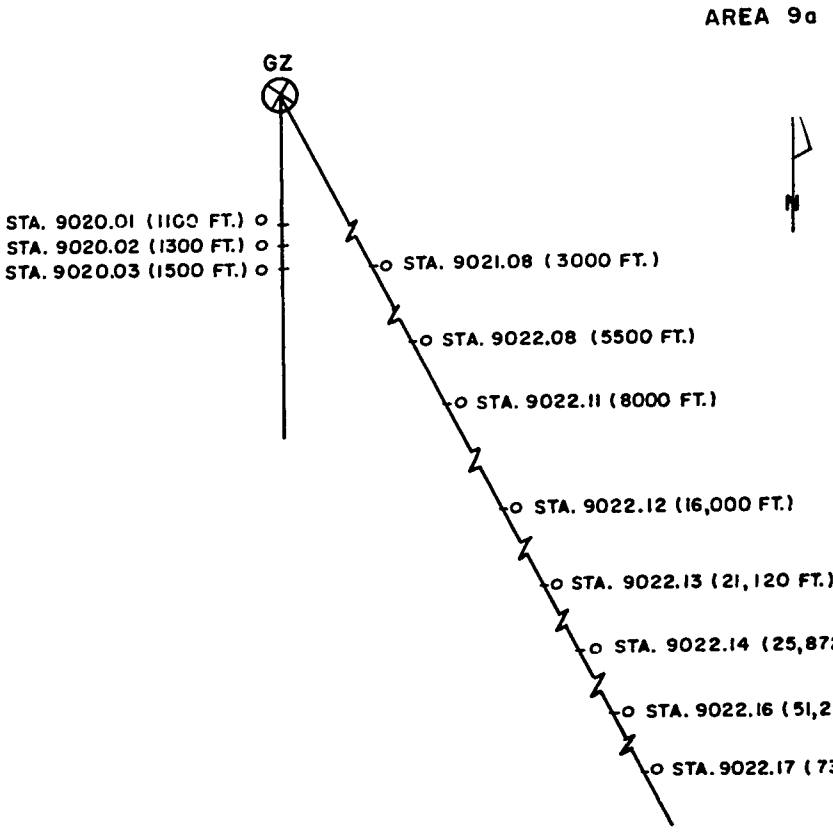

Figure 2.21 Station layout, Shot Charleston.

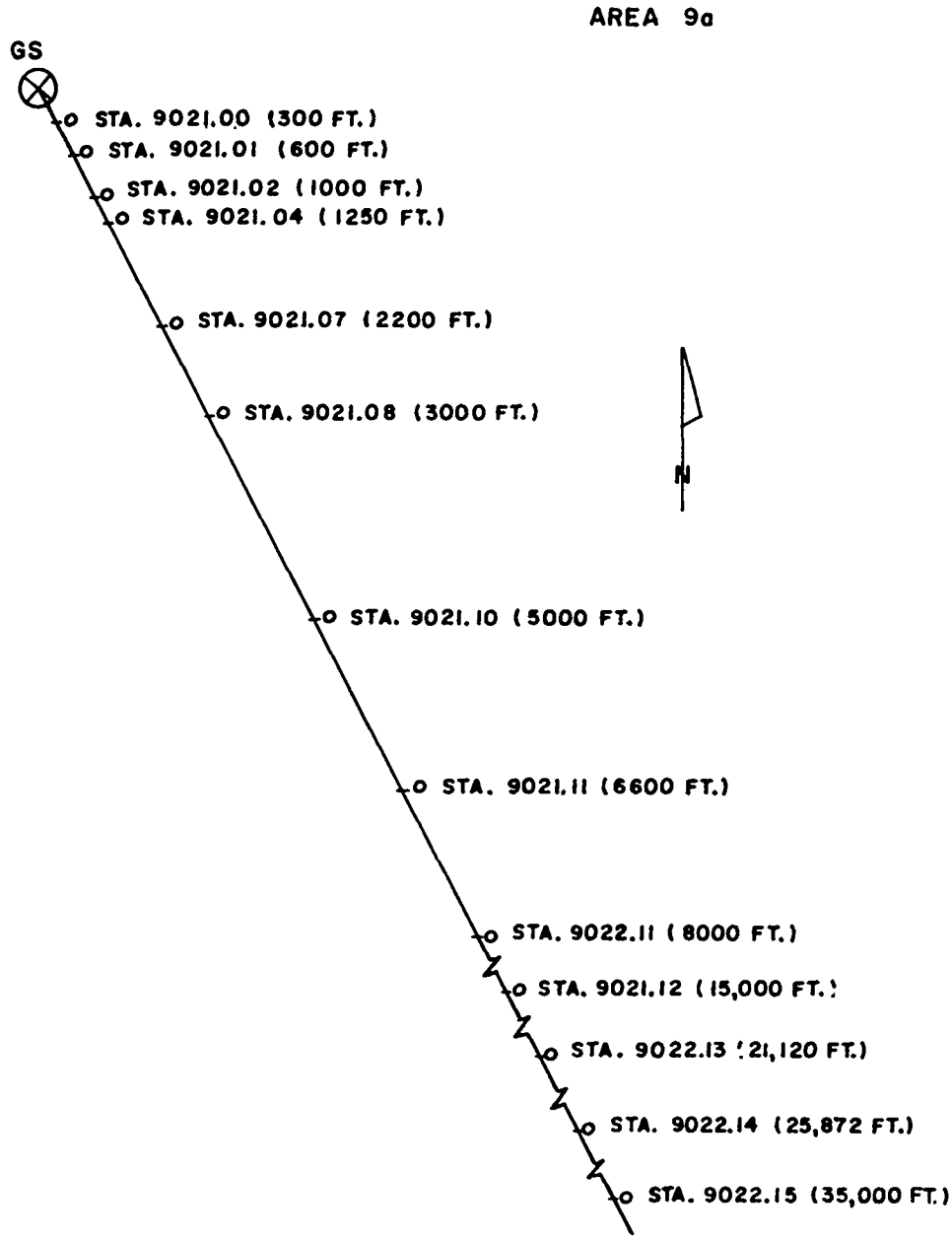

Figure 2.22 Station layout, Shot Morgan.

[redacted]

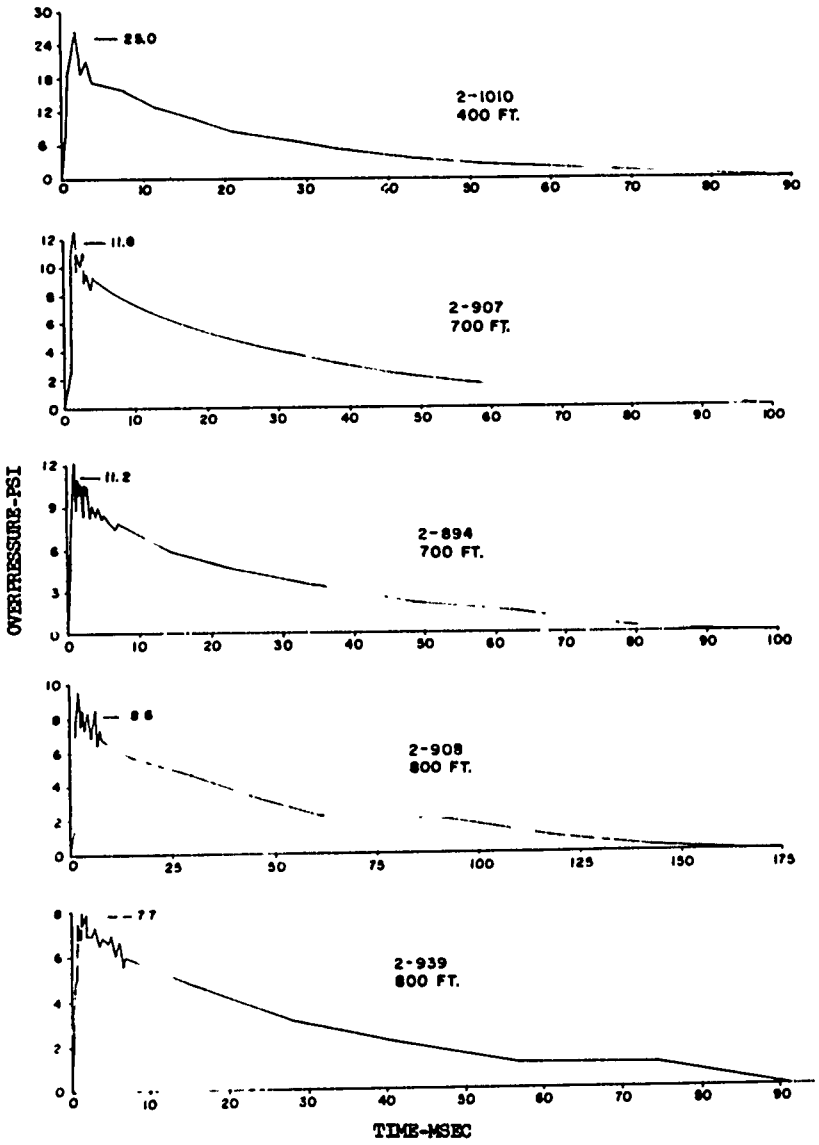

Figure 2.23 Overpressure-time histories, Shot Franklin, at distances of 400, 700, and 800 feet.

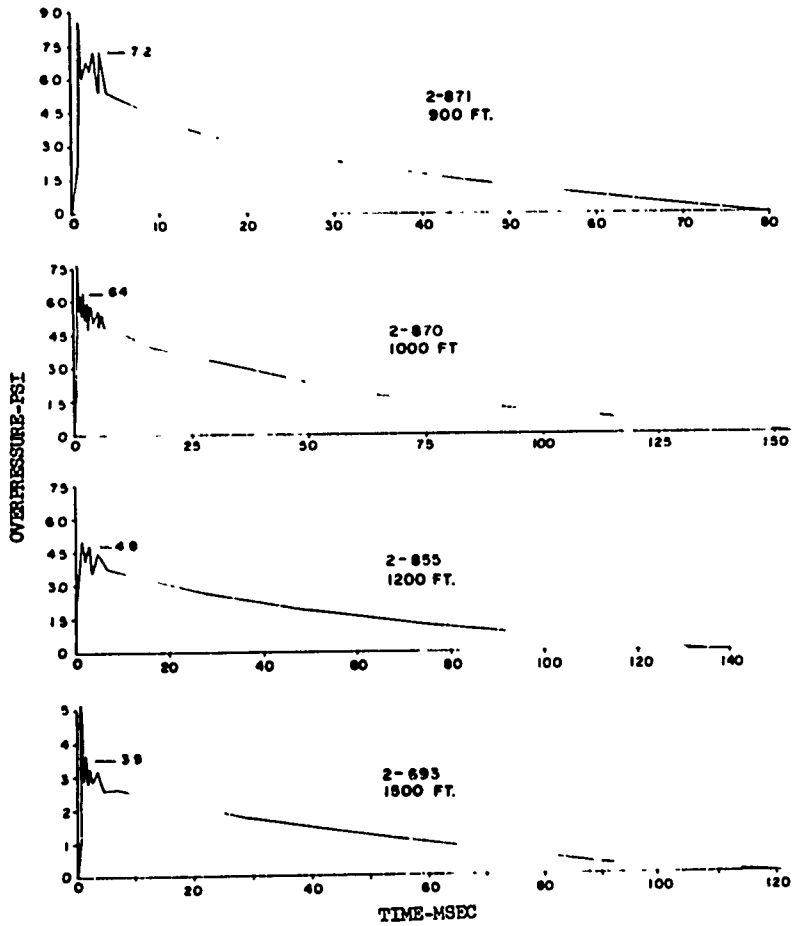

Figure 2.24 Overpressure-time histories, Shot Franklin, at distances of 900, 1,000, 1,200, and 1,500 feet.

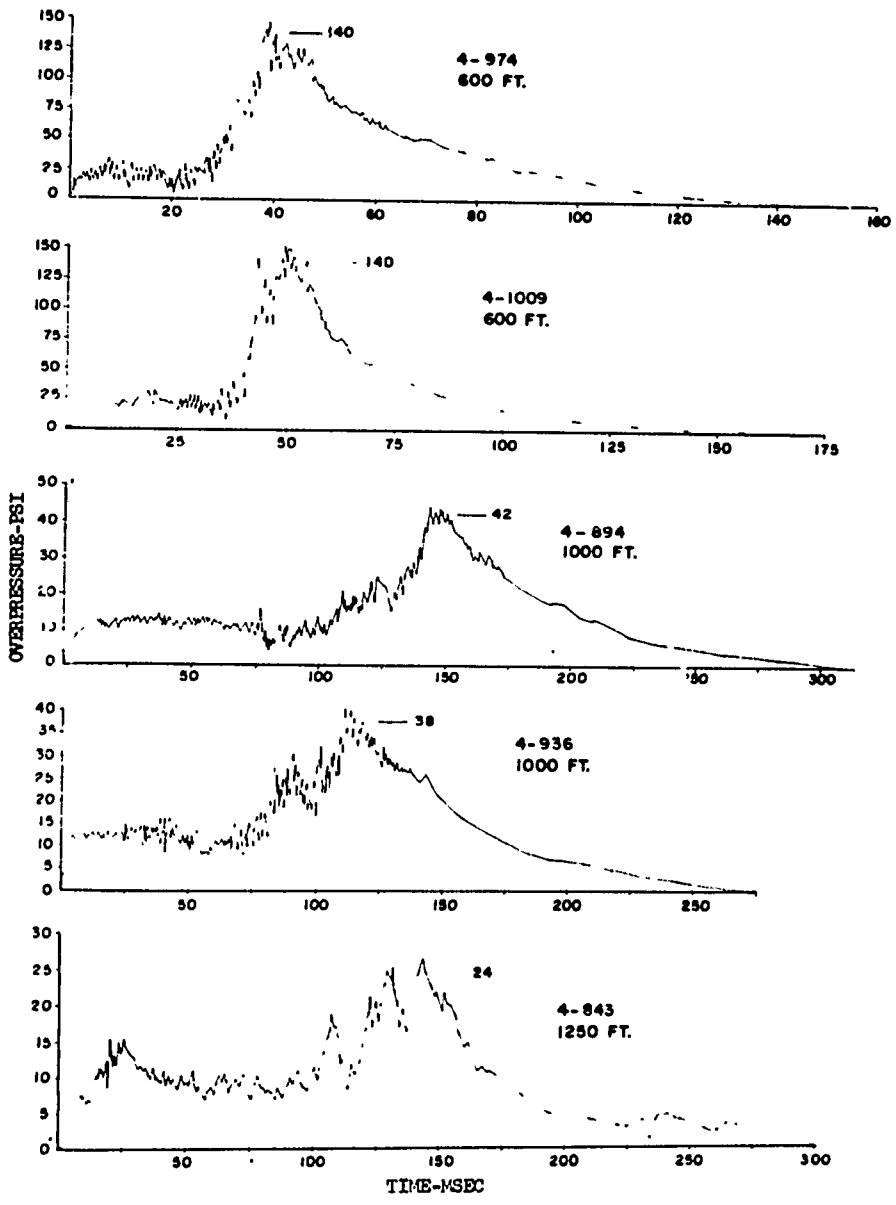

Figure 2.25 Overpressure-time histories, Shot Wilson, at distances of 600, 1,000, and 1,250 feet.

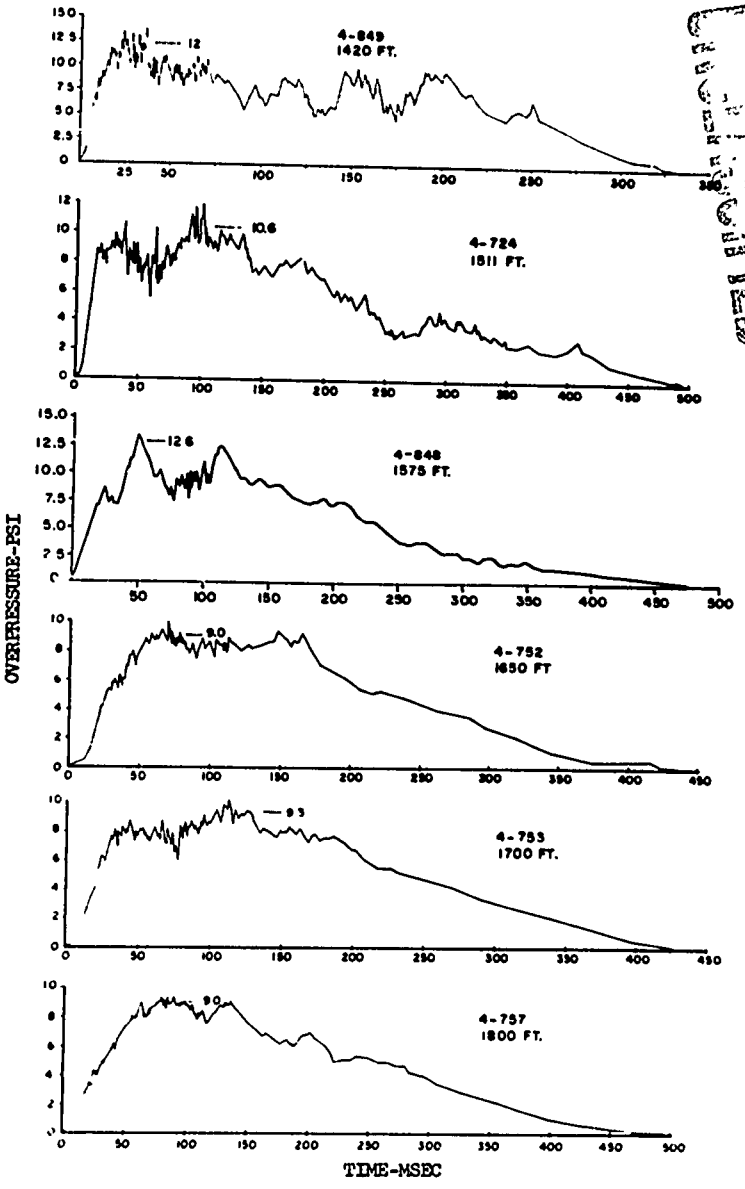

Figure 2.26 Overpressure-time histories, Shot Wilson, at distances of 1,420, 1.511, 1,575, 1,650, 1,700, and 1,800 feet.

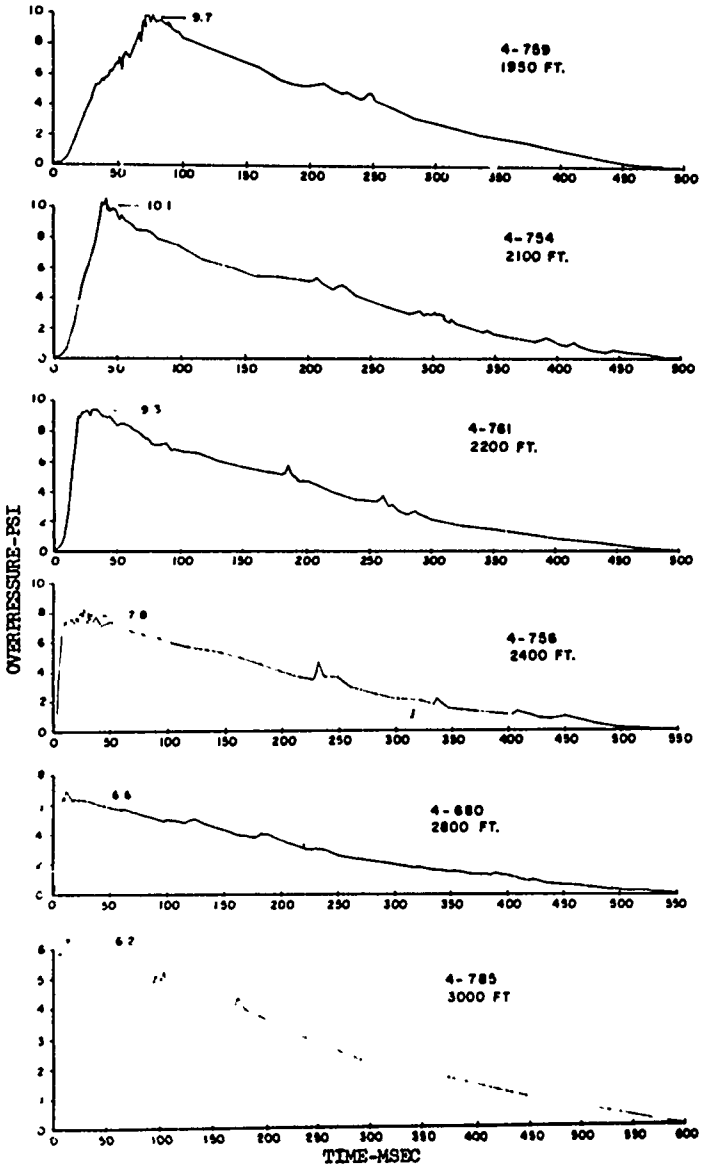

Figure 2.27 Overpressure-time histories, Shot Wilson, at distances of 1,950, 2,100, 2,200, 2,400, 2,800, and 3,000 feet.

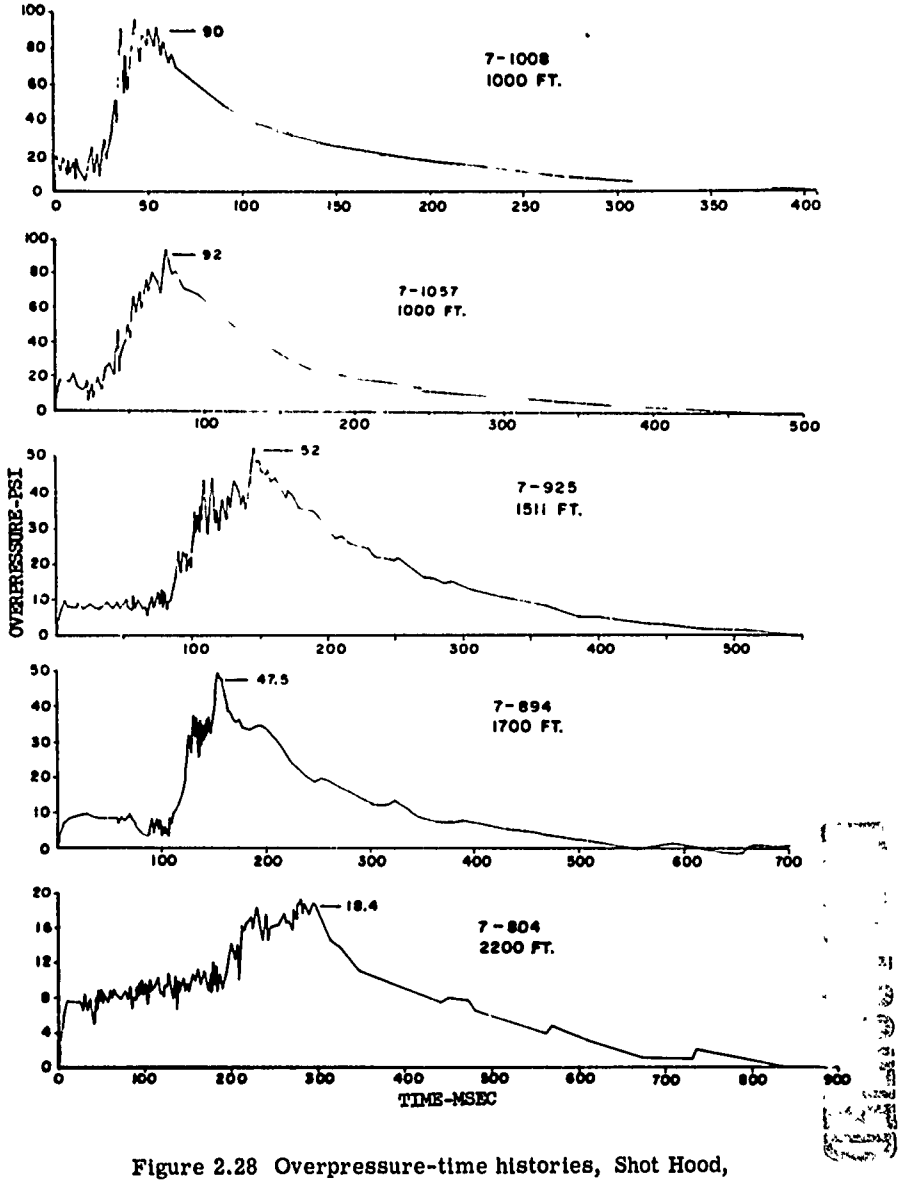

Figure 2.28 Overpressure-time histories, Shot Hood, at distances of 1,000, 1,511, 1,700, and 2,200 feet.

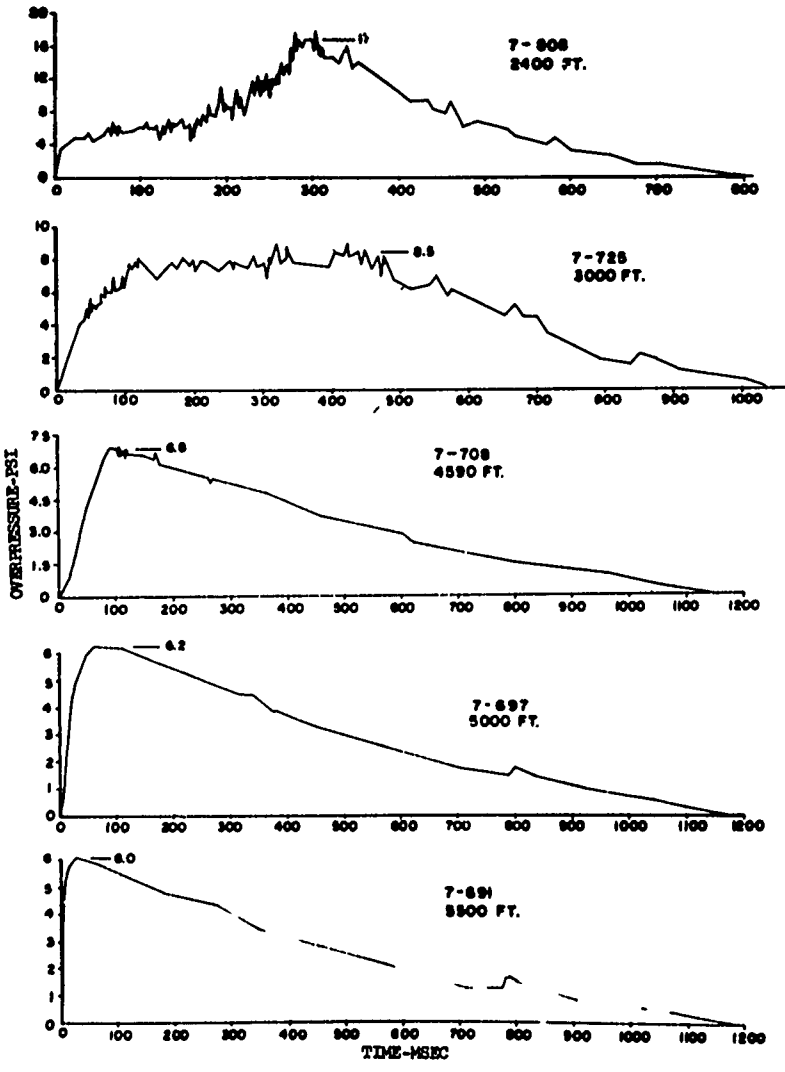

Figure 2.29 Overpressure-time ·ories, Shot Hood, at distances of 2,400, 3,000, 4,590, ɔ,000, and 5,500 feet.

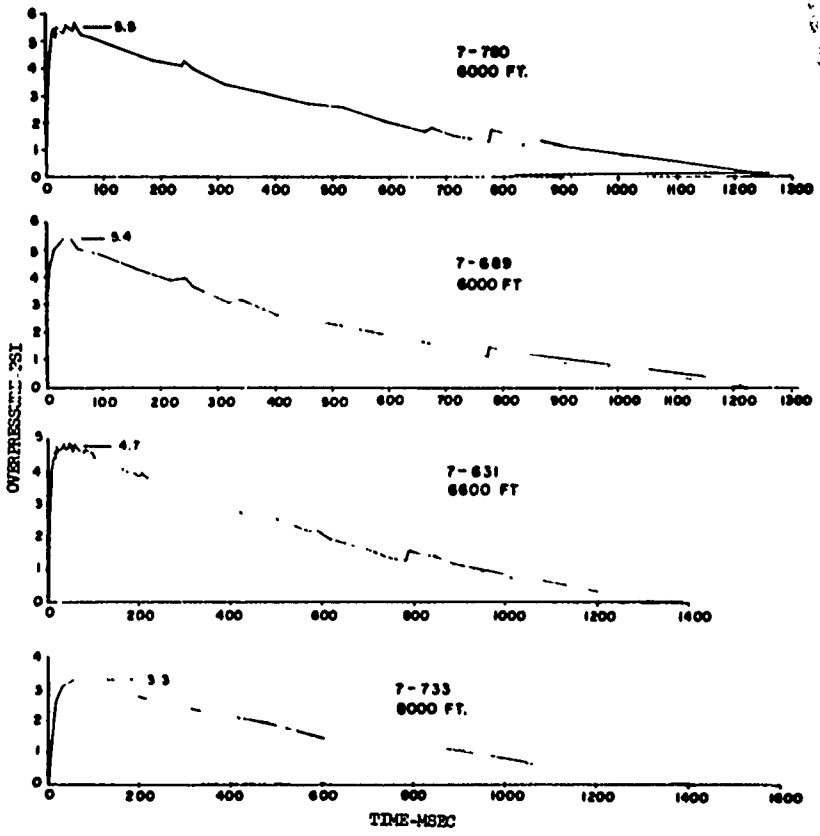

Figure 2.30 Overpressure-time histories, Shot Hood, at distances of 6,000, 6,600, and 8,000 feet.

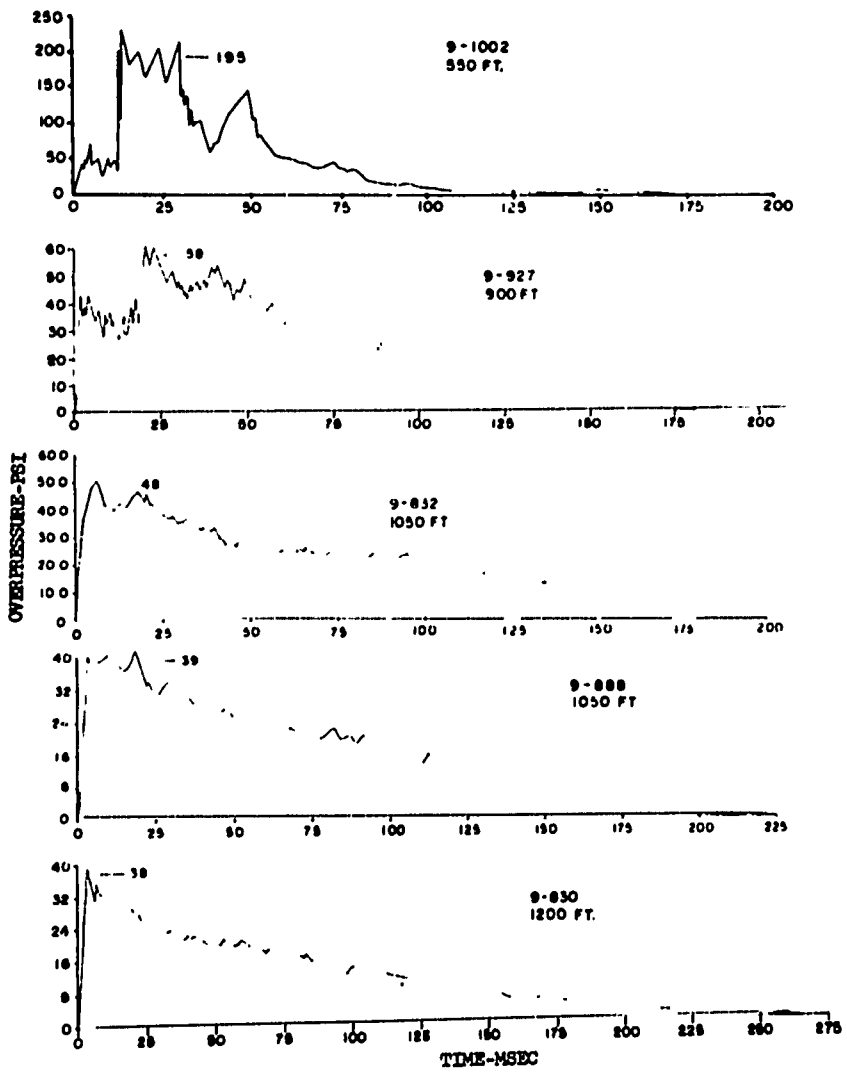

Figure 2.31 Overpressure-time histories, Shot Kepler, at distances of 550, 900, 1,050, and 1,200 feet.

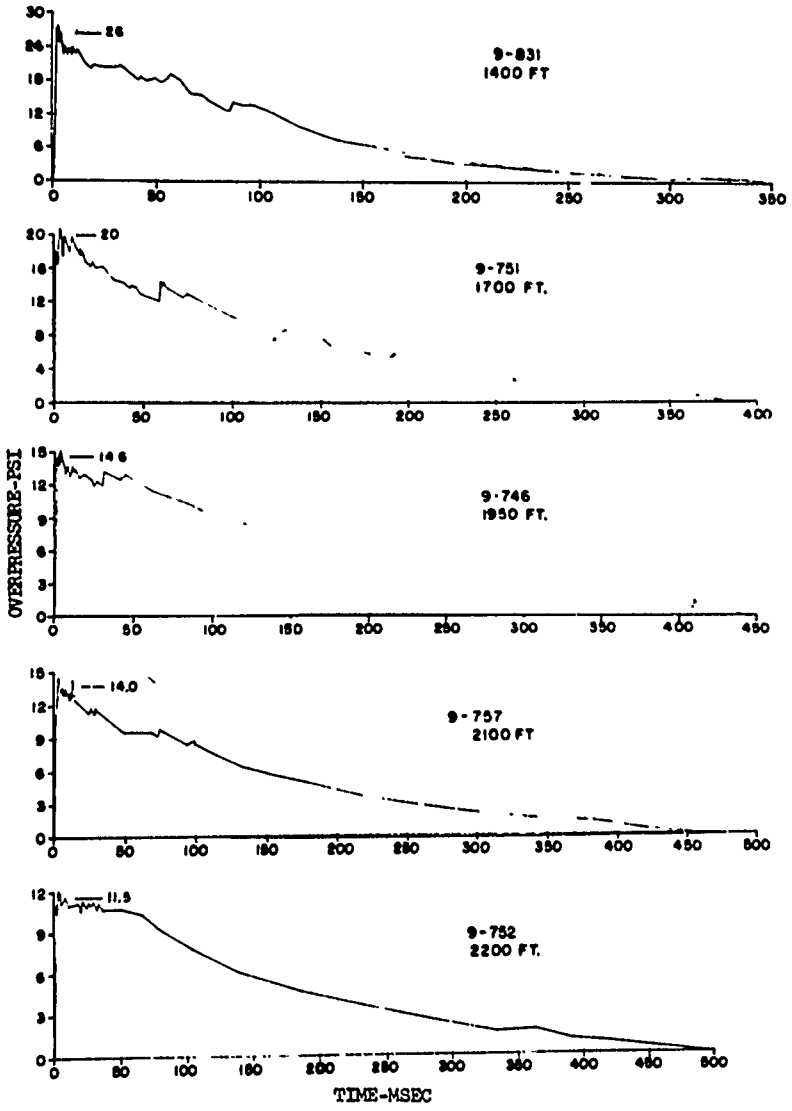

Figure 2.32 Overpressure-time histories, Shot Kepler, at distances of 1,400, 1,700, 1,950, 2,100, and 2,200 feet.

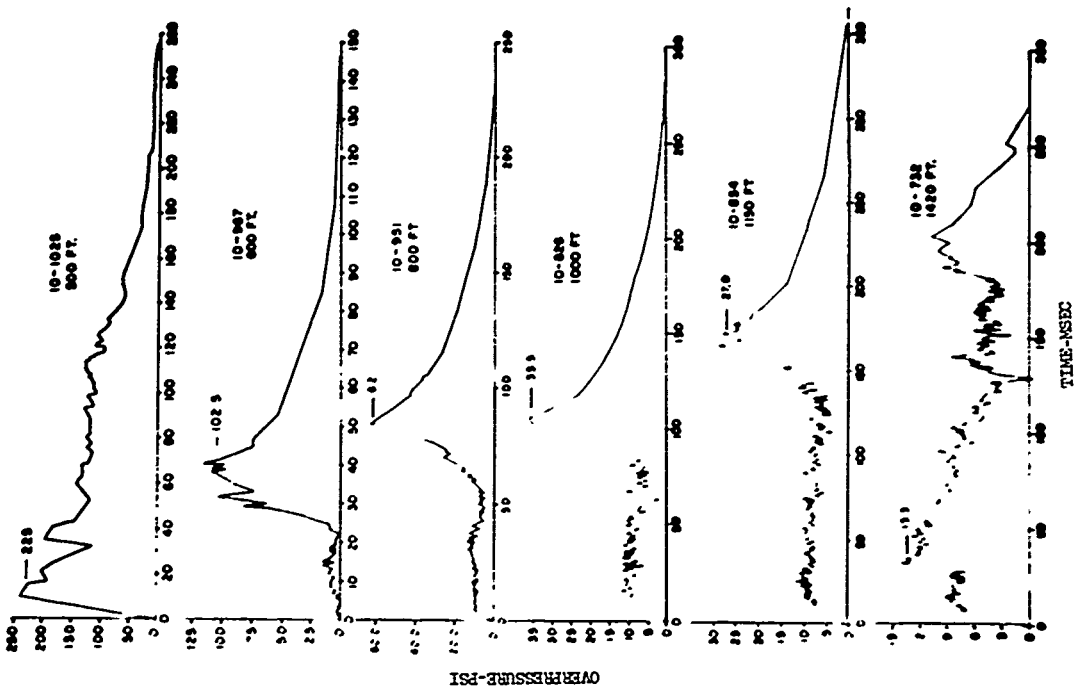

Figure 2.34 Overpressure-time histories, Shot Owens, at distances of 500, 600, 800, 1,000, 1,150, and 1,420 feet.

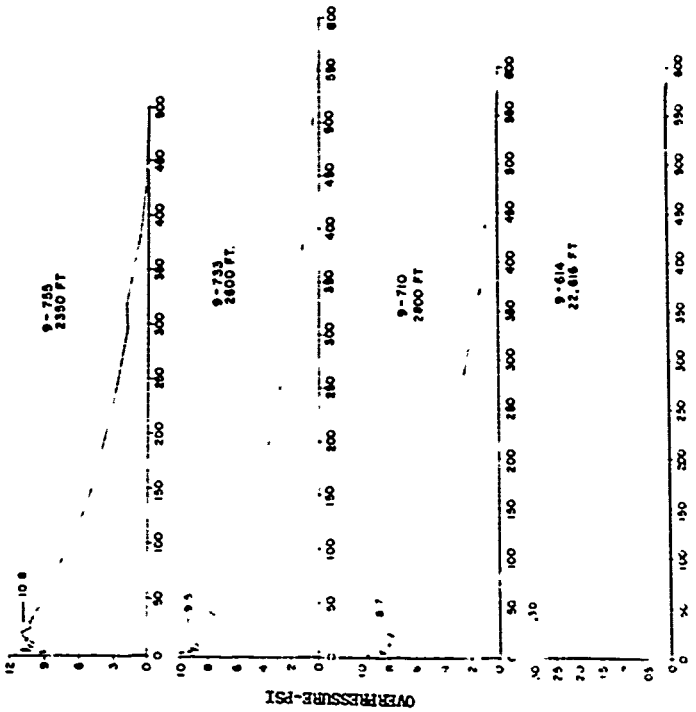

Figure 2.33 Overpressure-time histories, Shot Kepler, at distances of 2,350, 2,600, 2,800, and 22,616 feet.

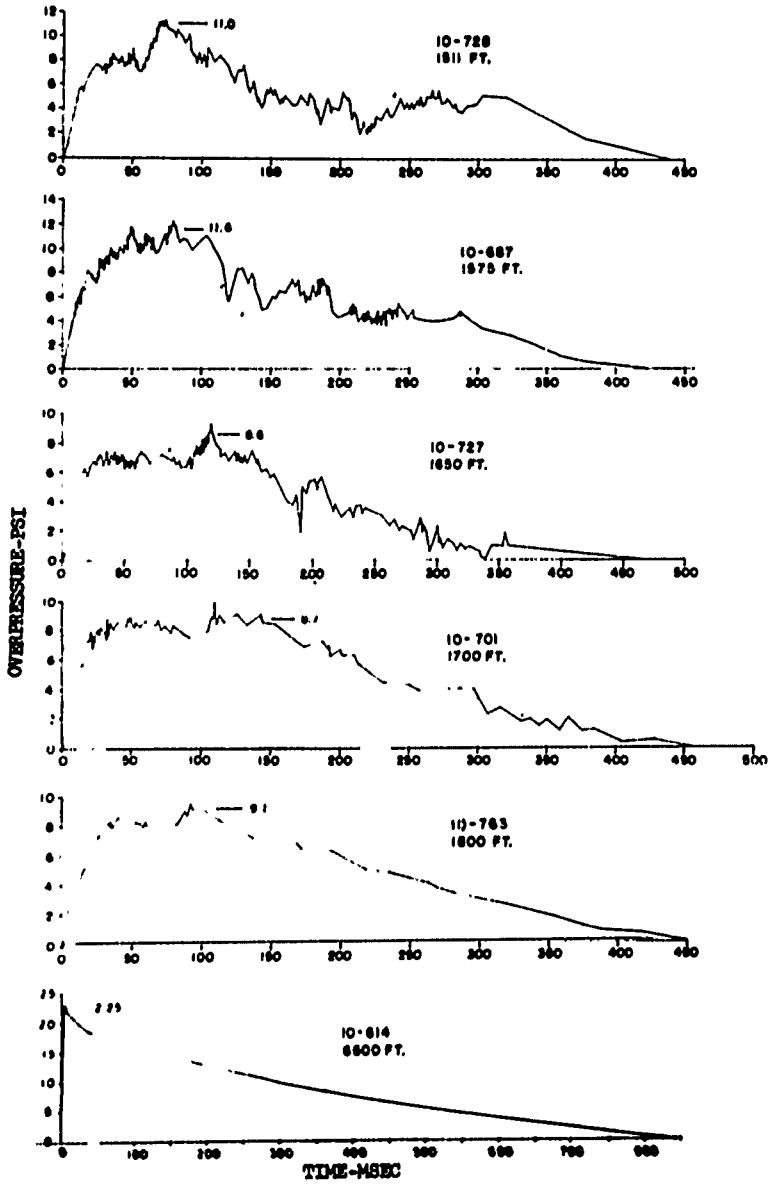

Figure 2.35 Overpressure-time histories, Shot Owens, at distances of 1,511, 1,575, 1,650, 1,700, 1,800, and 6,600 feet.

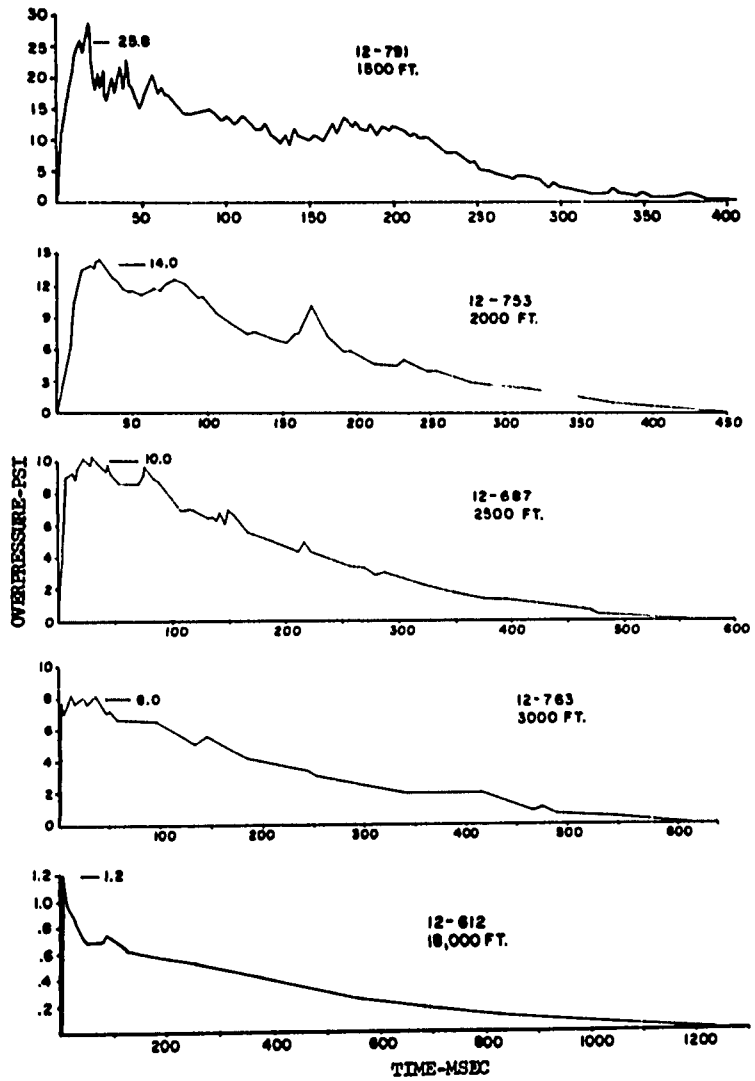

Figure 2.36 Overpressure-time histories, Shot Shasta, at distances of 1,500, 2,000, 2,500, 3,000, and 18,000 feet.

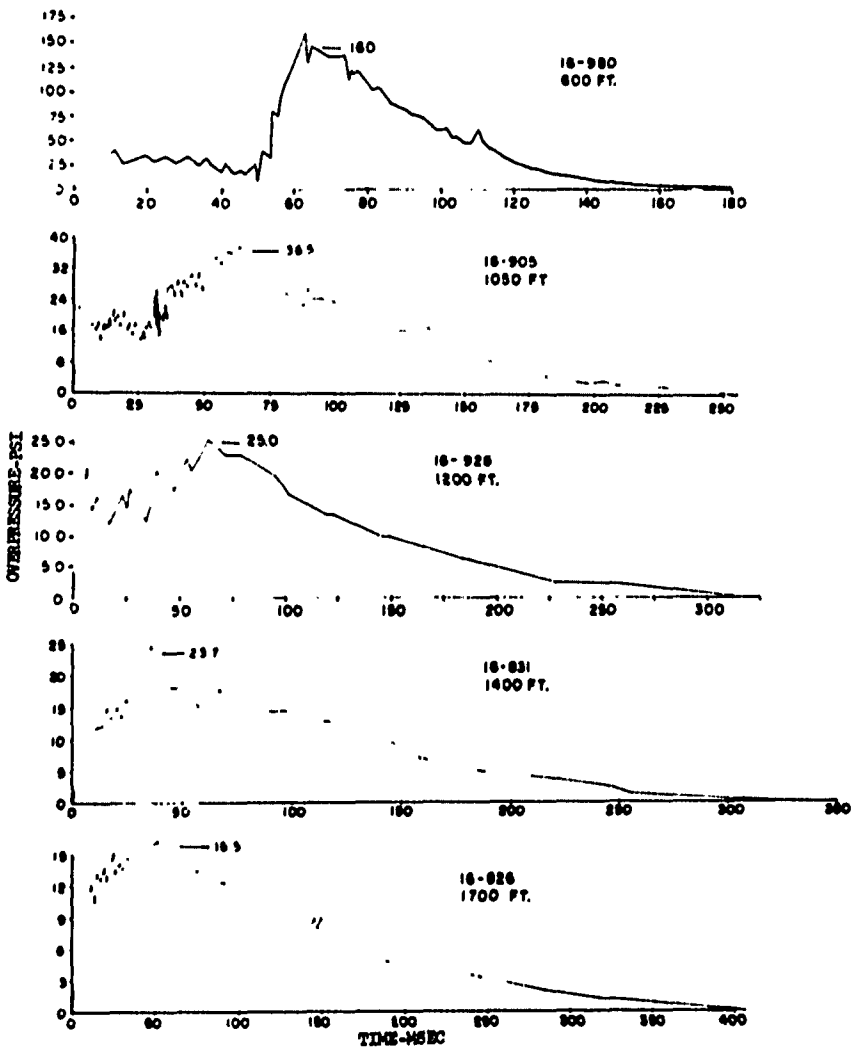

Figure 2.37 Overpressure-time histories, Shot Galileo, at distances of 600, 1,050, 1,200, 1,400, and 1,700 feet.

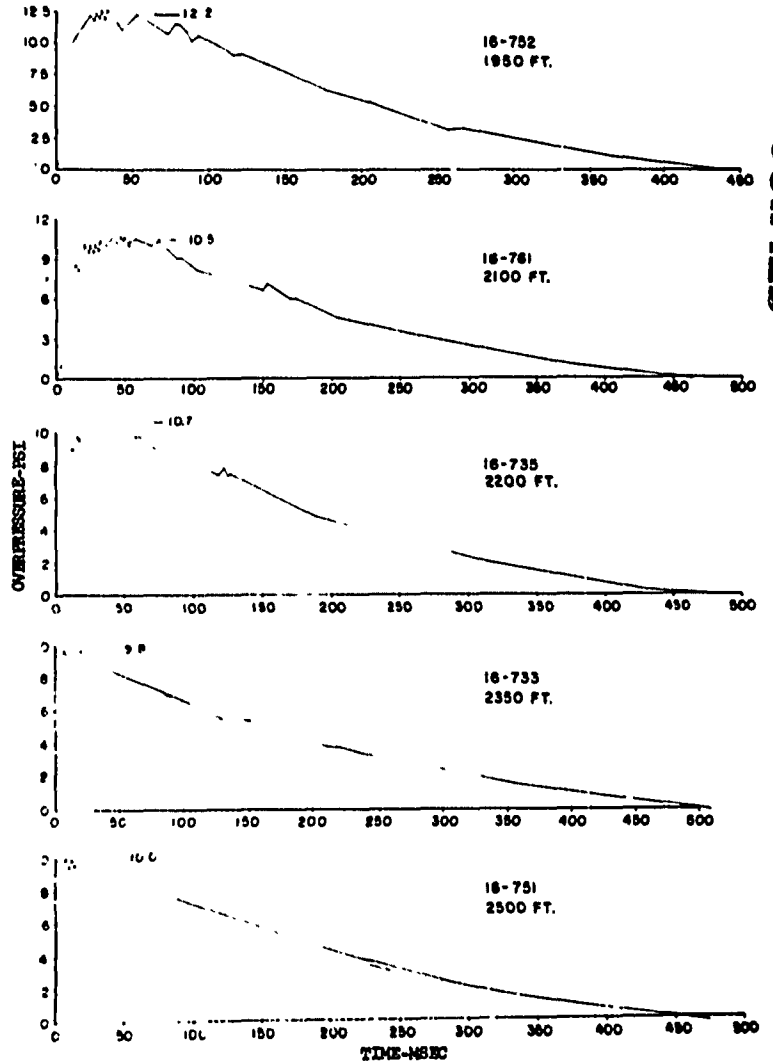

Figure 2.38 Overpressure-time histories, Shot Galileo, at distances of 1,950, 2,100, 2,200, 2,350, and 2,500 feet.

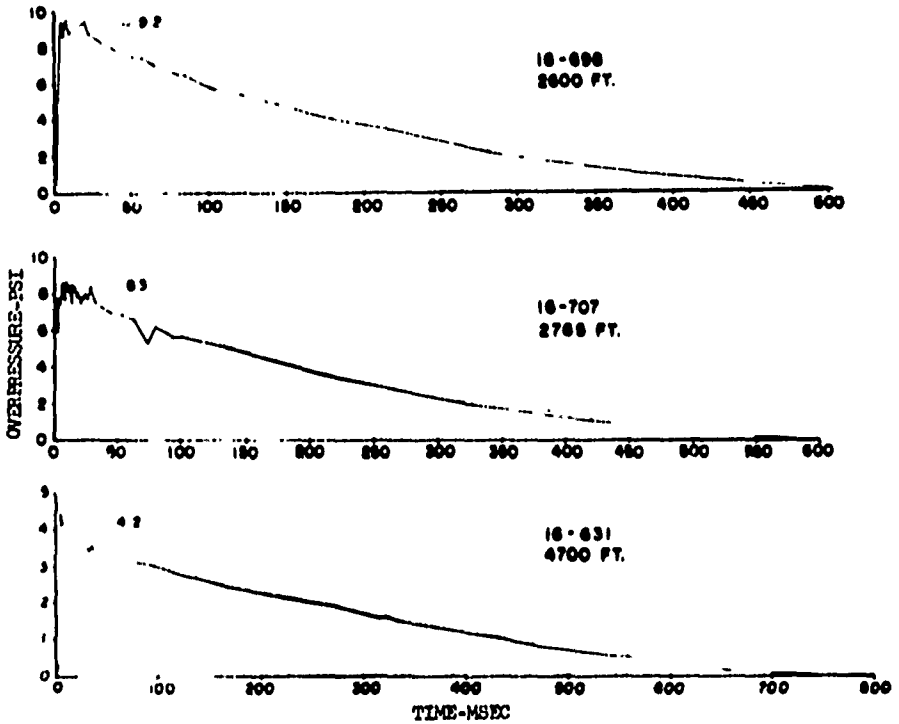

Figure 2.39 Overpressure-time histories, Shot Gallileo, at distances of 2,600, 2,765, and 4,700 feet.

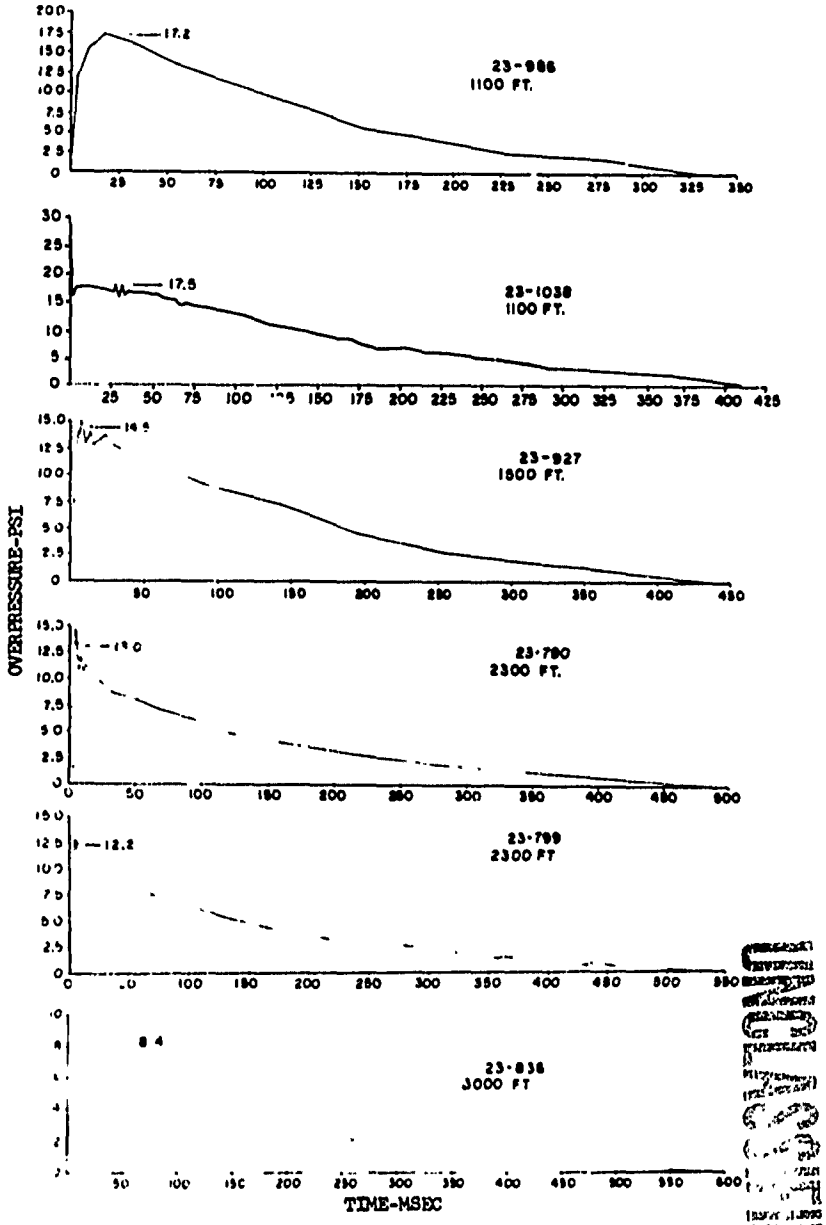

Figure 2.40 Overpressure-time histories, Shot Charleston, at distances of 1,100, 1,500, 2,300, and 3,000 feet.

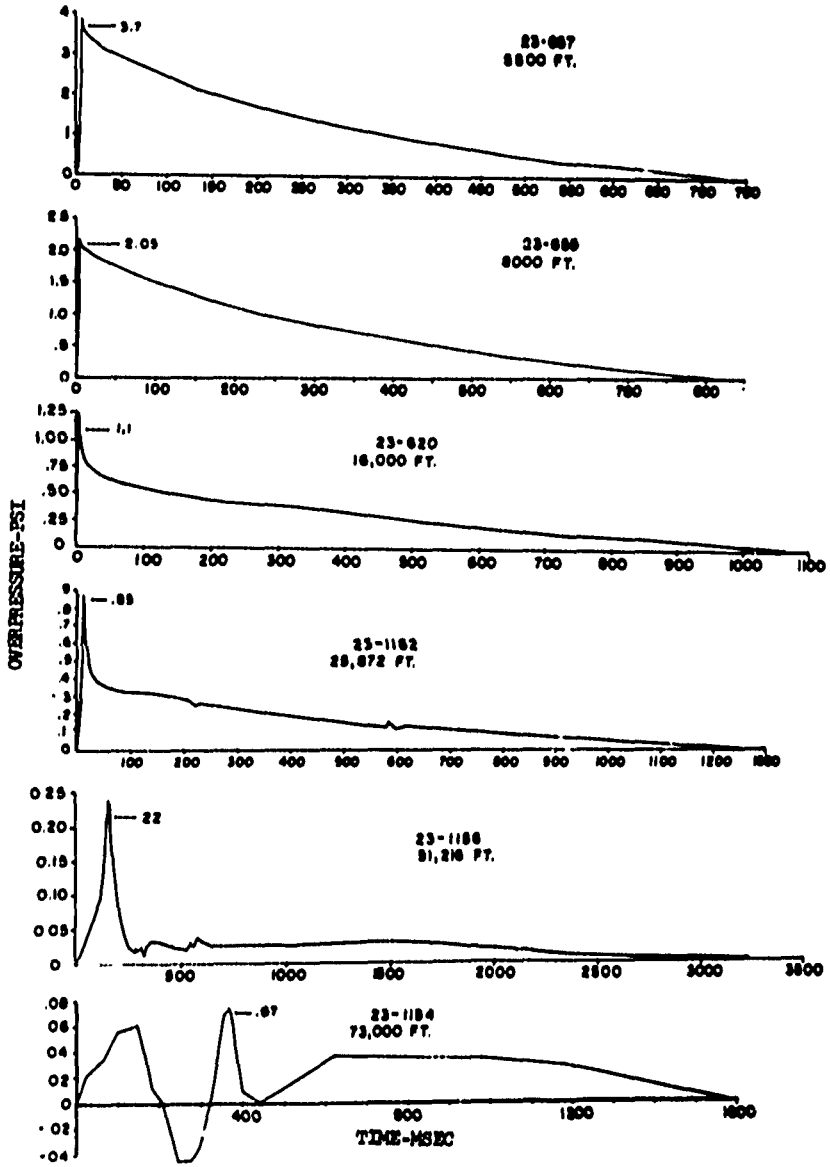

Figure 2.41 Overpressure-time histories, Shot Charleston, at distances of 5,500, 8,000, 16,000, 25,872, 51,216, and 73,000 feet.

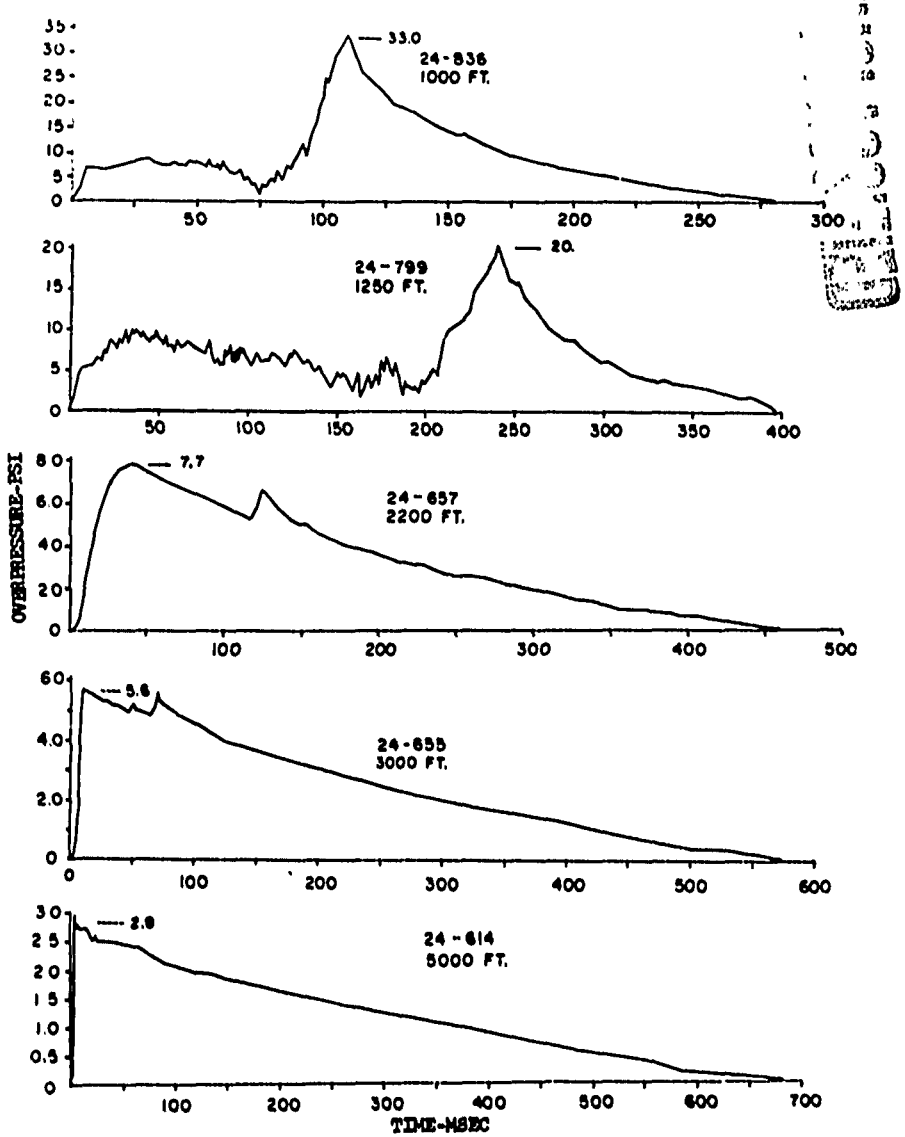

Figure 2.42 Overpressure-time histories, Shot Morgan, at distances of 1,000, 1,250, 2,200, 3,000, and 5,000 feet.

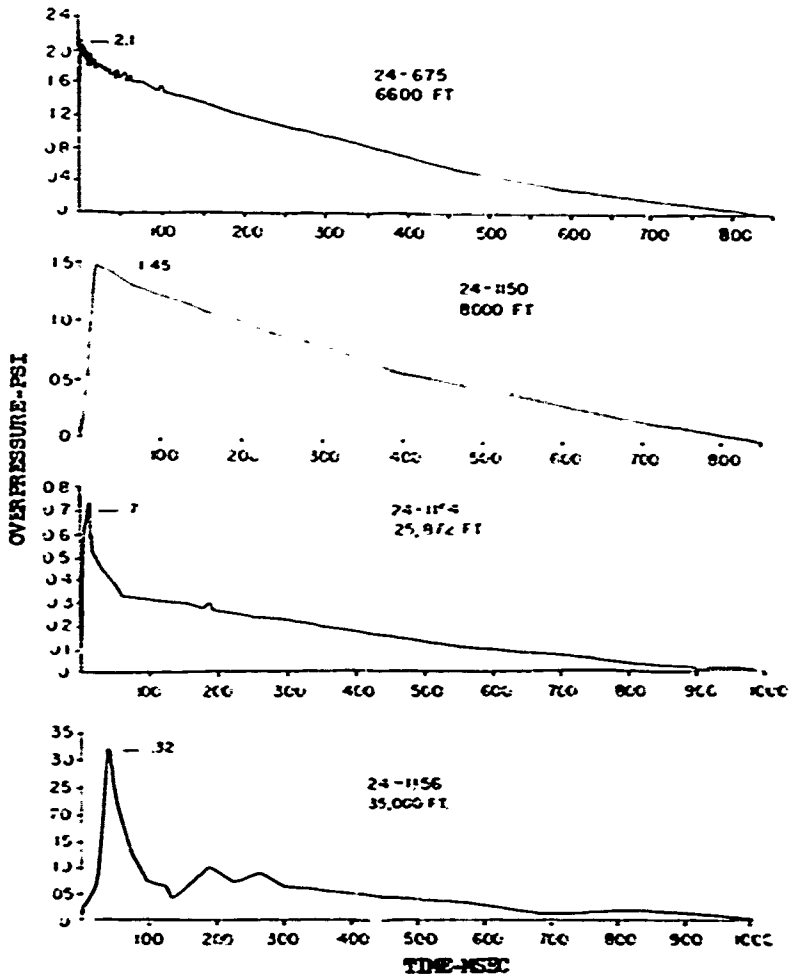

Figure 2.43 Overpressure-time histories, Shot Morgan, at distances of 6,600, 8,000, 25,872, and 35,000 feet.

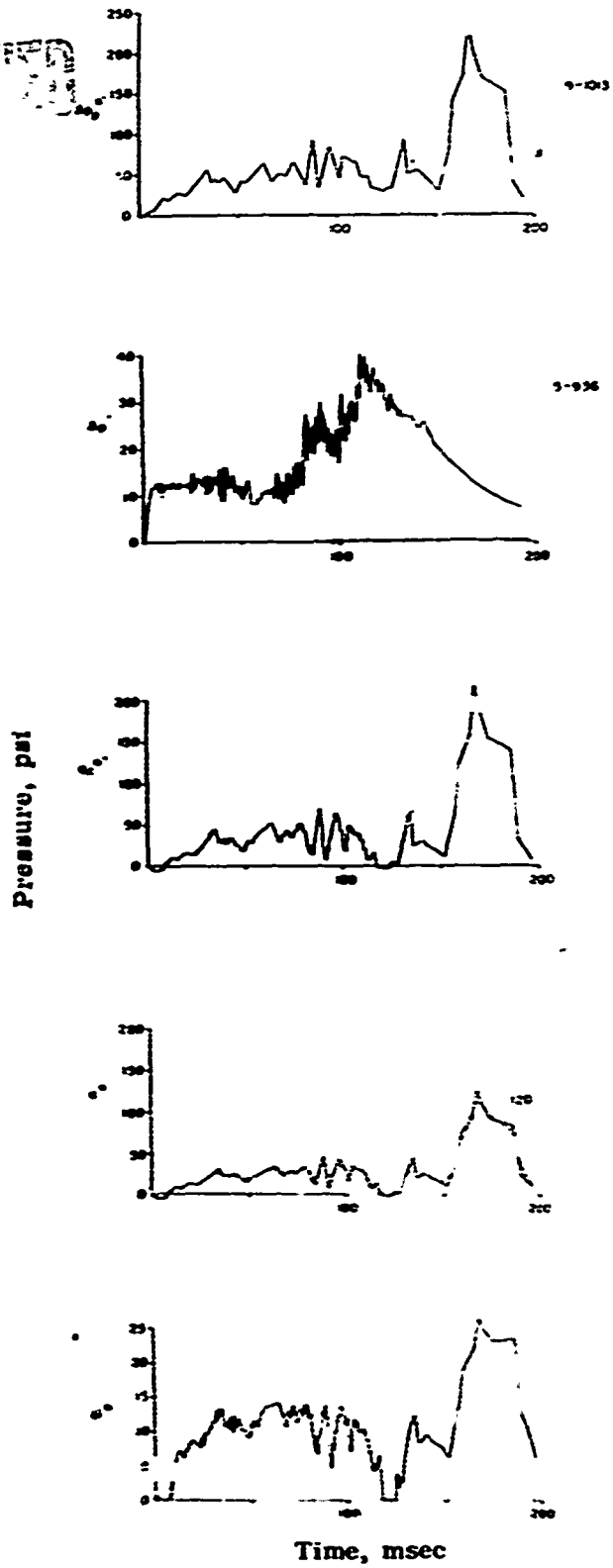

Figure 2.44 Pressure and Mach number versus time, at 1,000 feet, Shot Wilson.

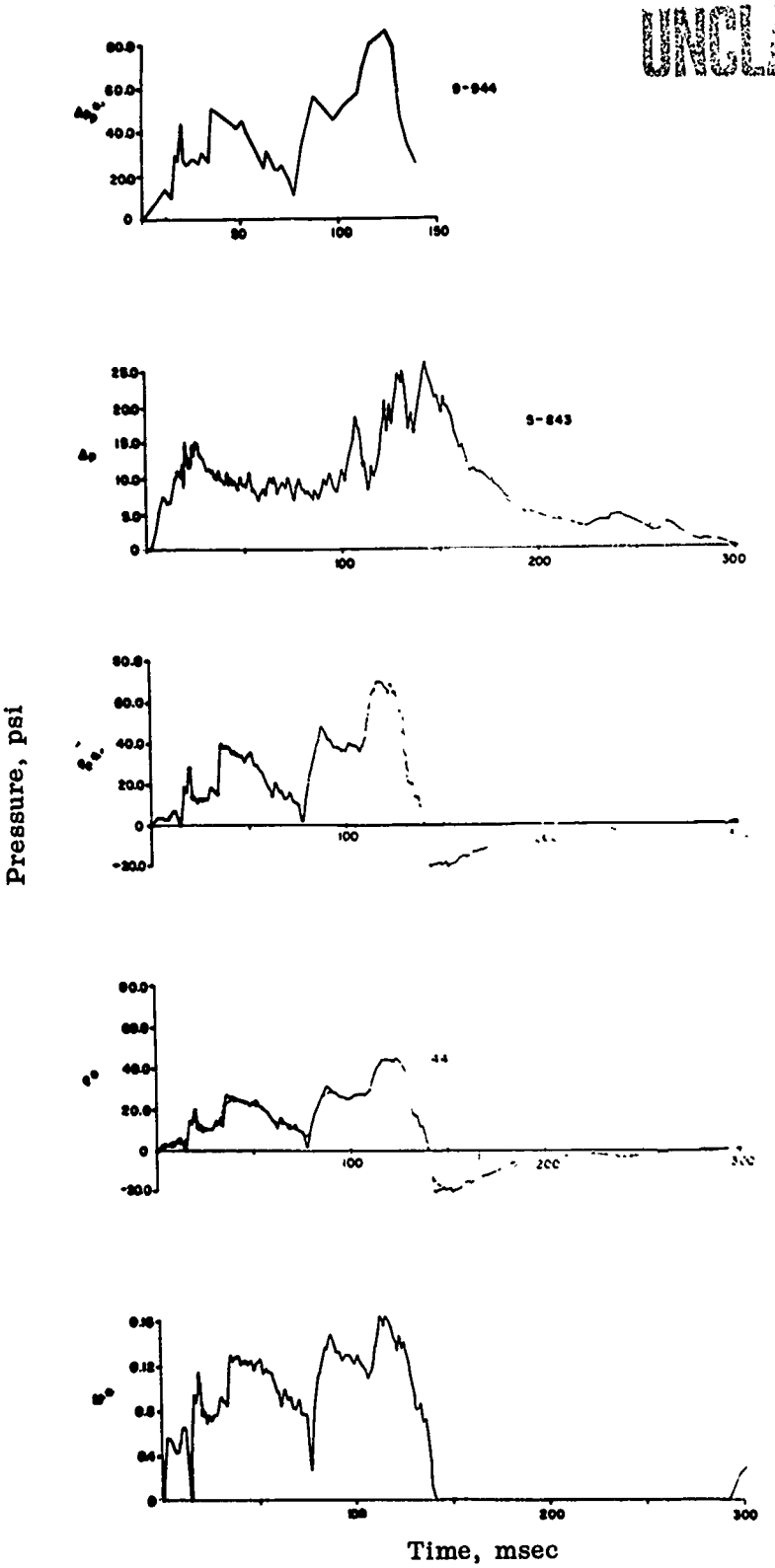

Figure 2.45 Pressure and Mach number versus time, at 1,250 feet, Shot Wilson.

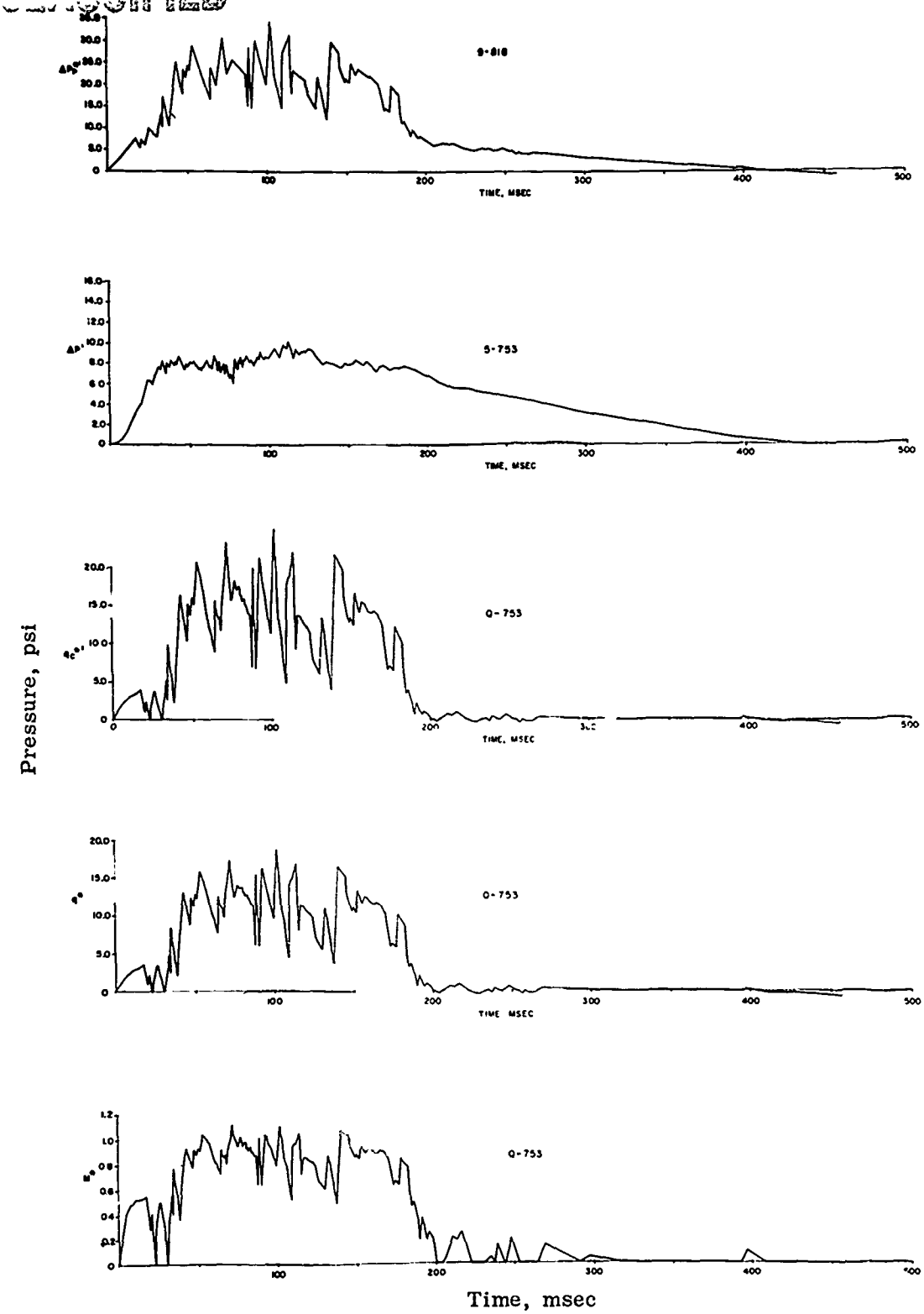

Figure 2.46 Pressure and Mach number versus time, at 1,700 feet, Shot Wilson.

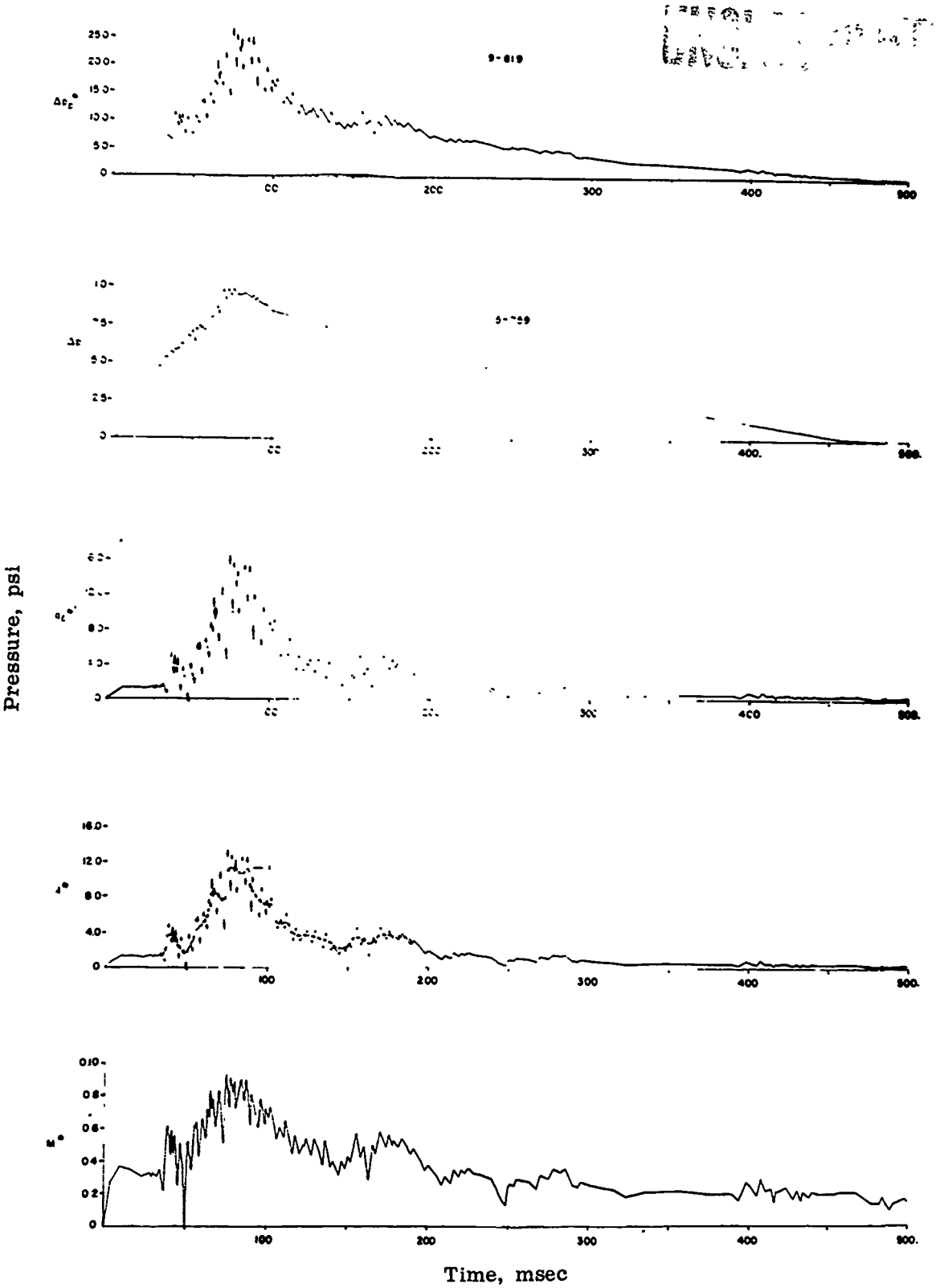

Figure 2.47 Pressure and Mach number versus time, at 1,950 feet, Shot Wilson.

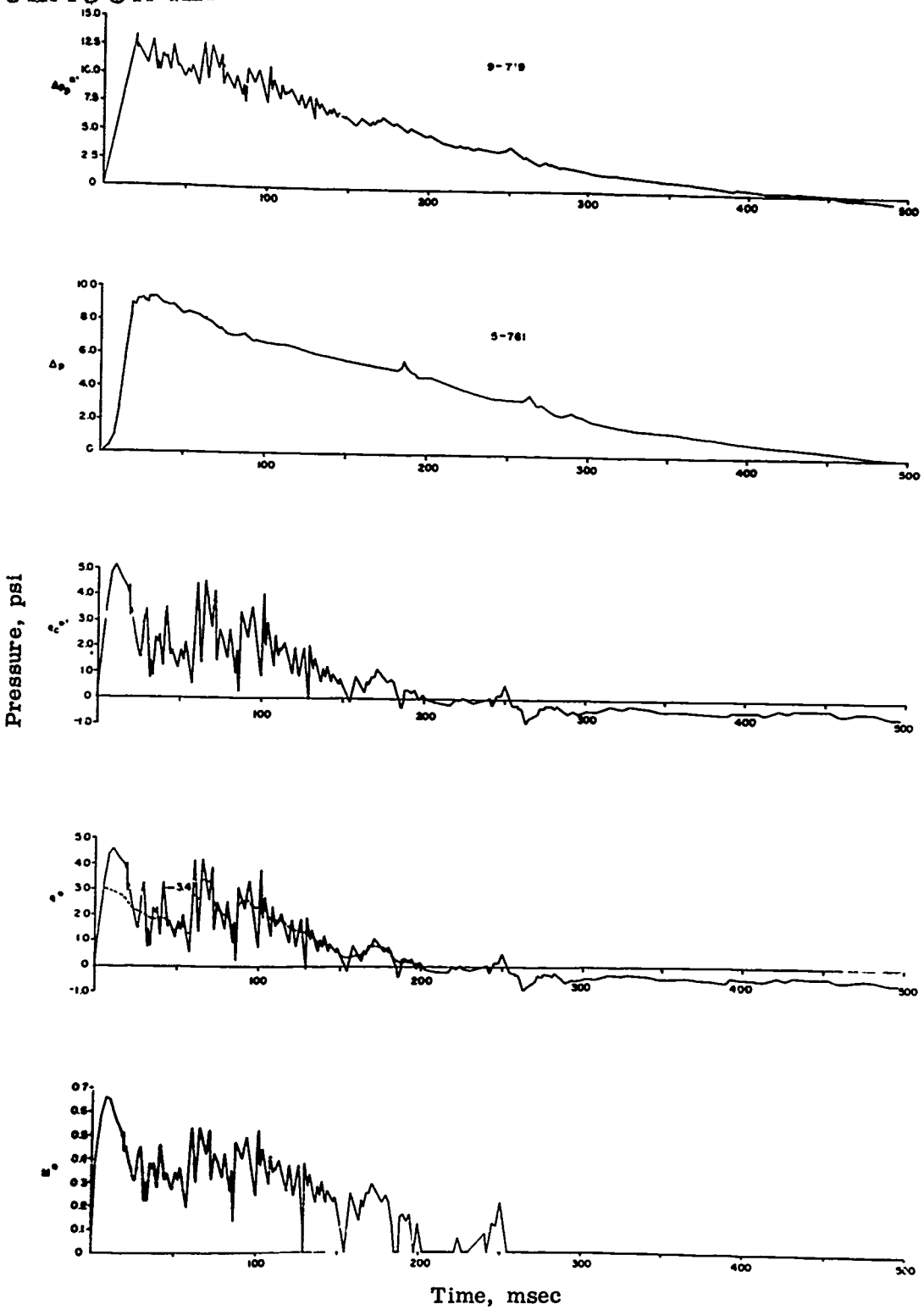

Figure 2.48 Pressure and Mach number versus time, at 2,200 feet, Shot Wilson.

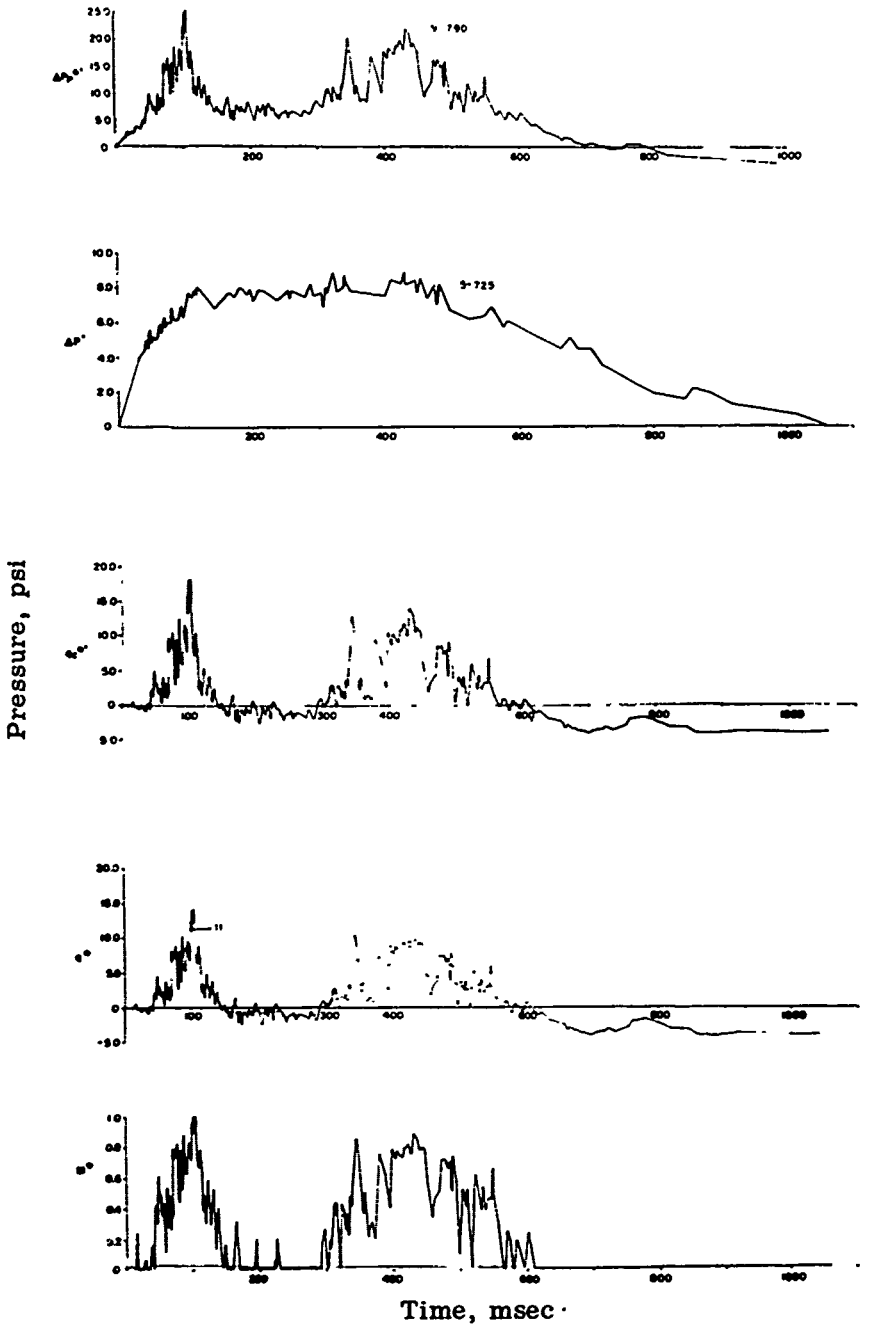

Figure 2.49 Pressure and Mach number versus time, at 3,000 feet, Shot Hood.

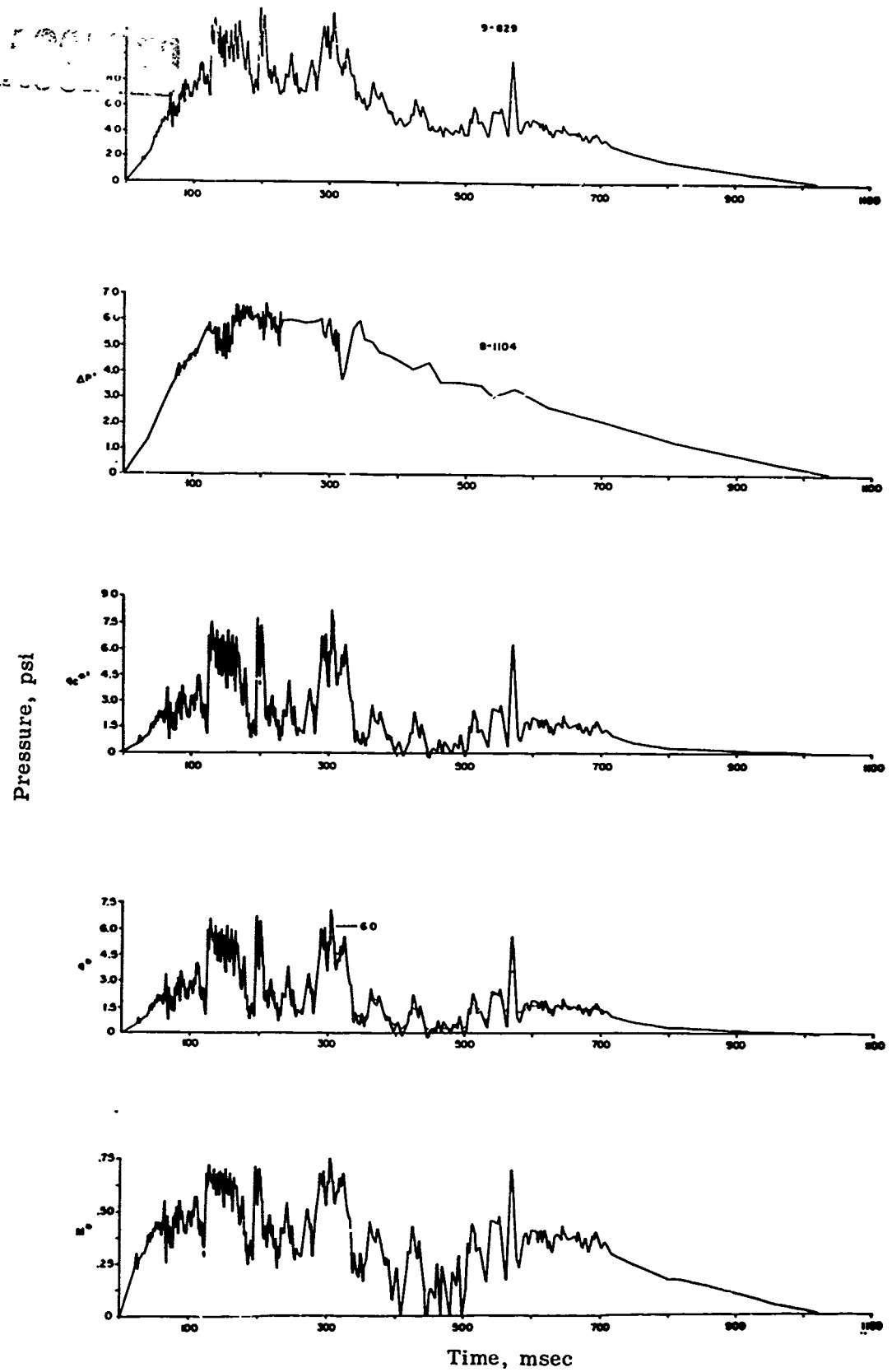

Figure 2.50 Pressure and Mach number versus time, at 4,000 feet, Shot Hood.

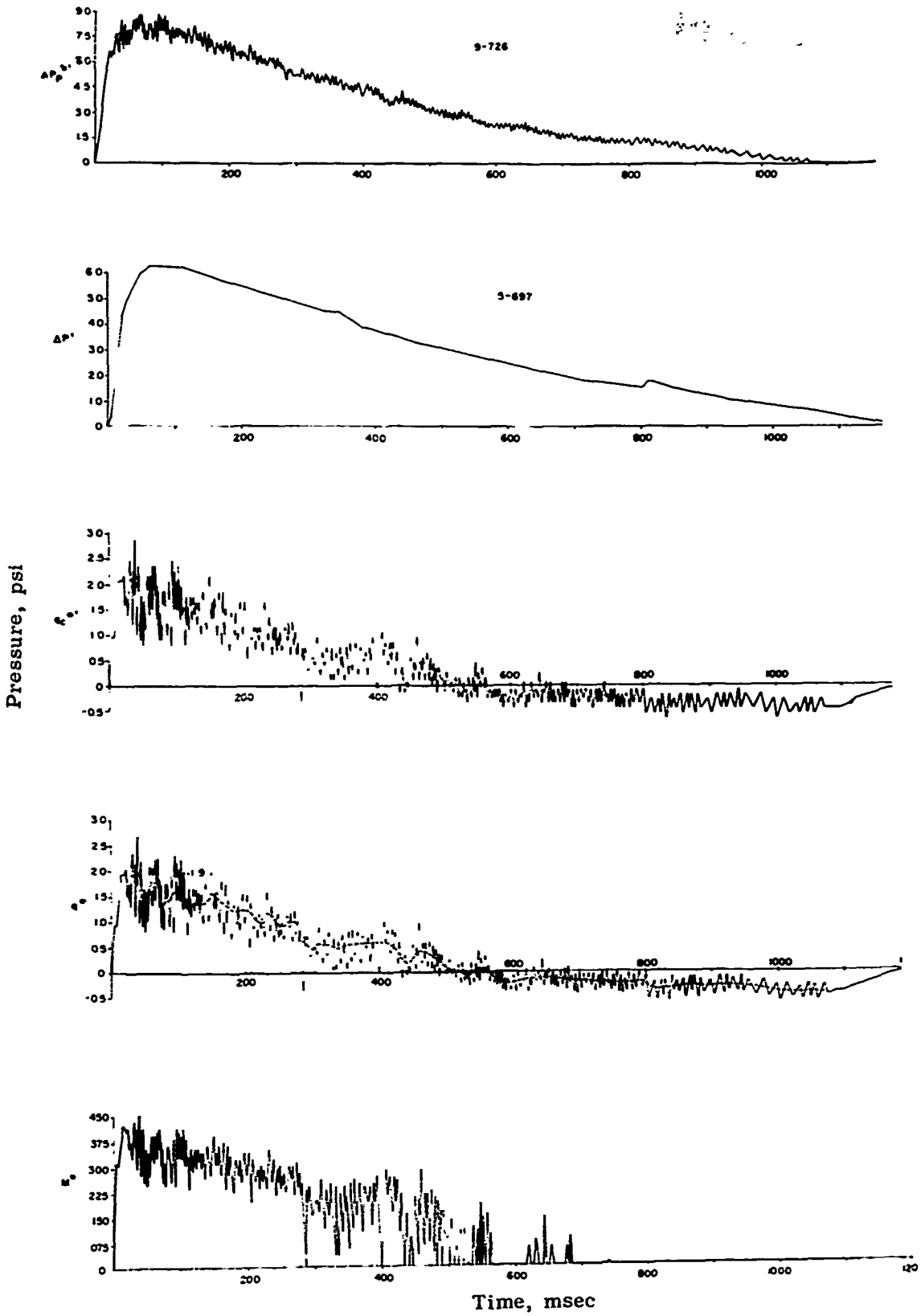

Figure 2.51 Pressure and Mach number versus time, at 5,000 feet, Shot Hood.

[redacted]

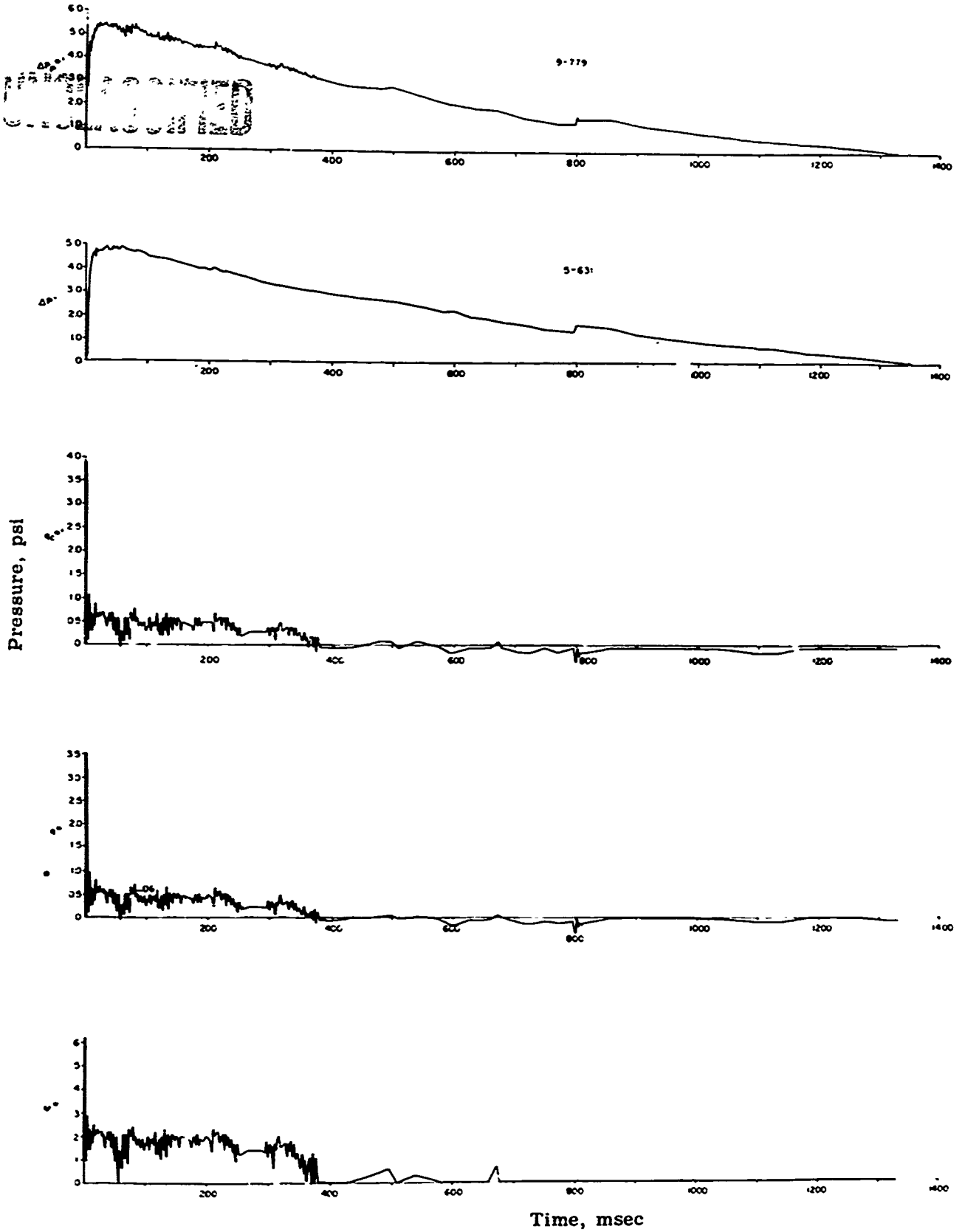

Figure 2.52 Pressure and Mach number versus time, at 6,500 feet, Shot Hood.

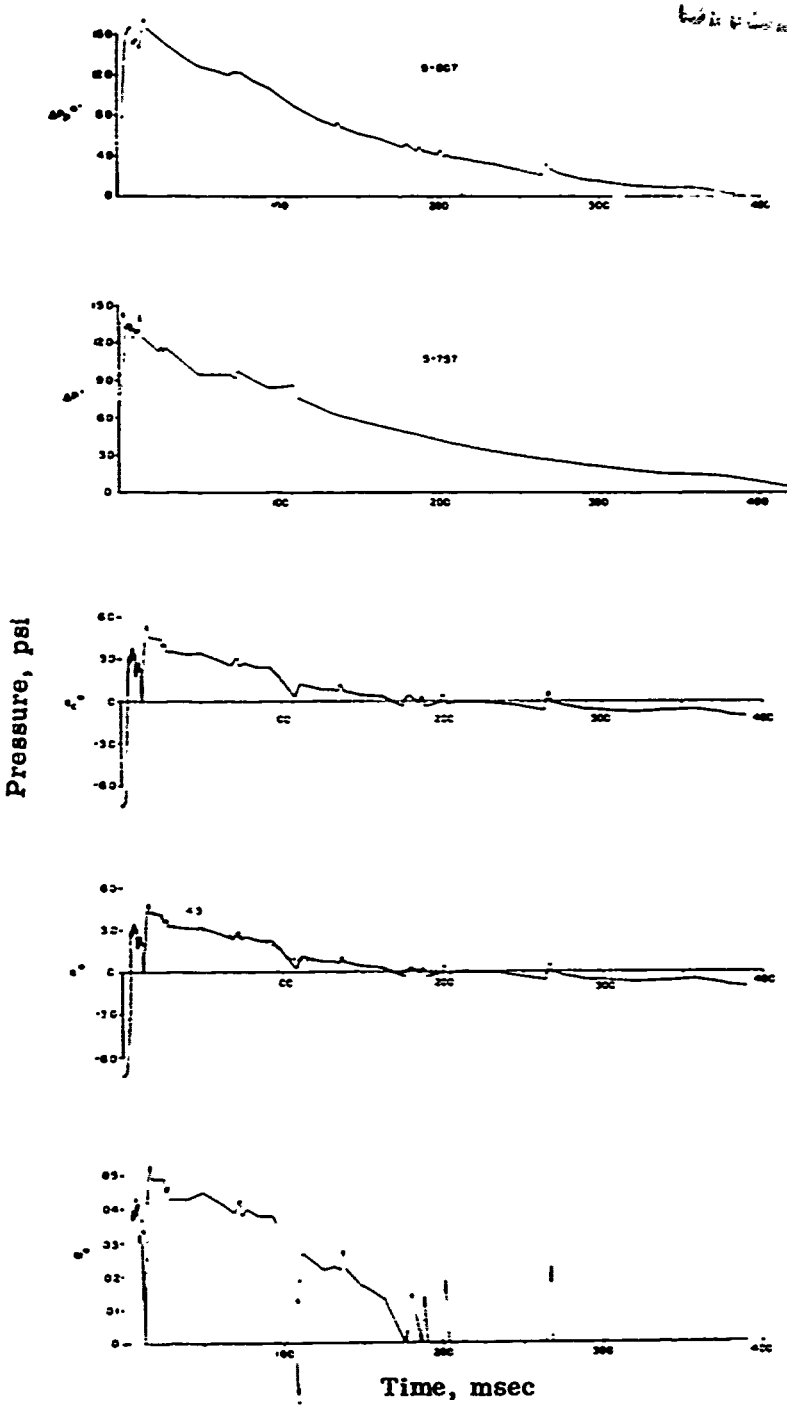

Figure 2.53 Pressure and Mach number versus time, at 2,100 feet, Shot Kepler.

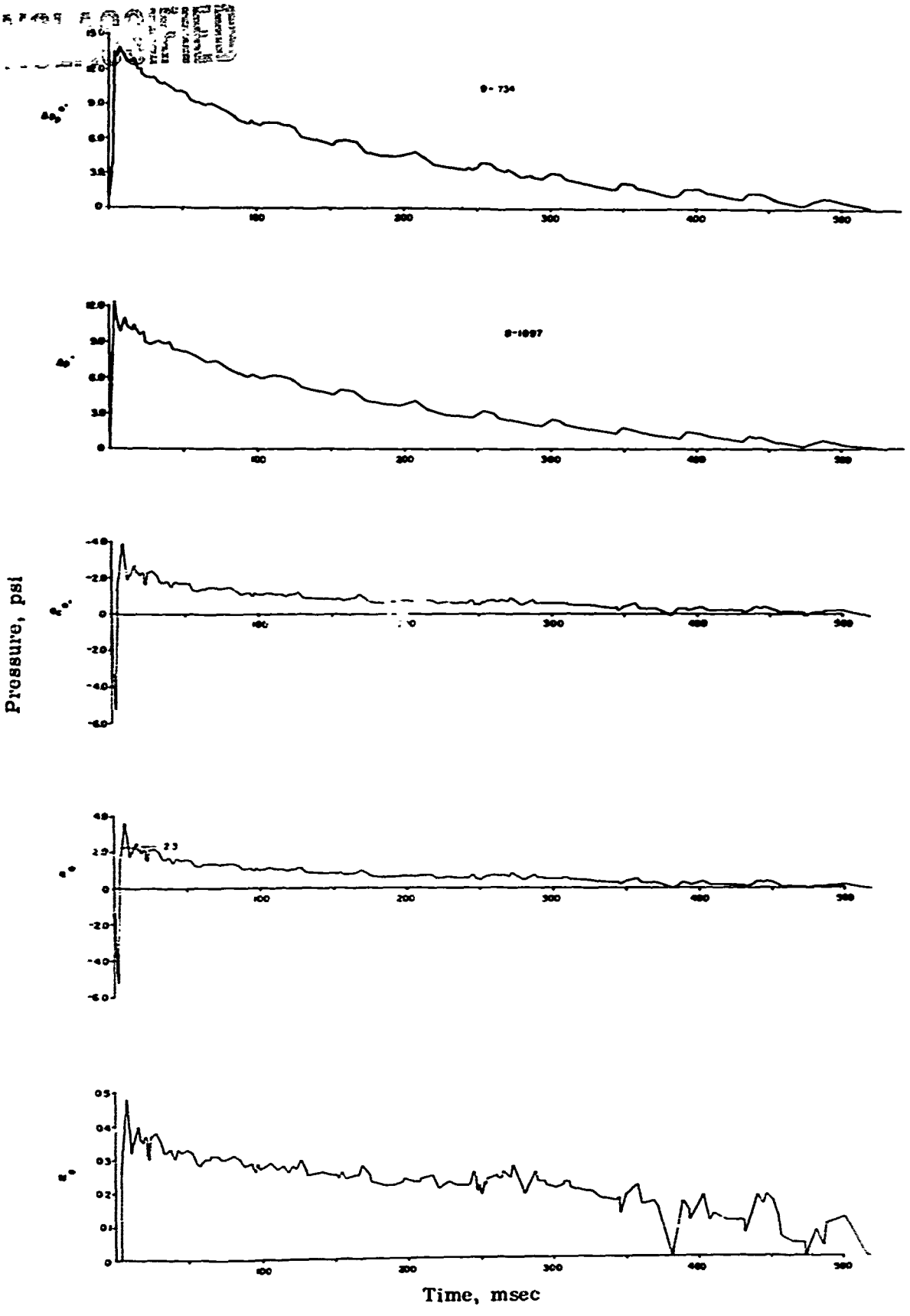

Figure 2.54 Pressure and Mach number versus time, at 2,500 feet, Shot Kepler.

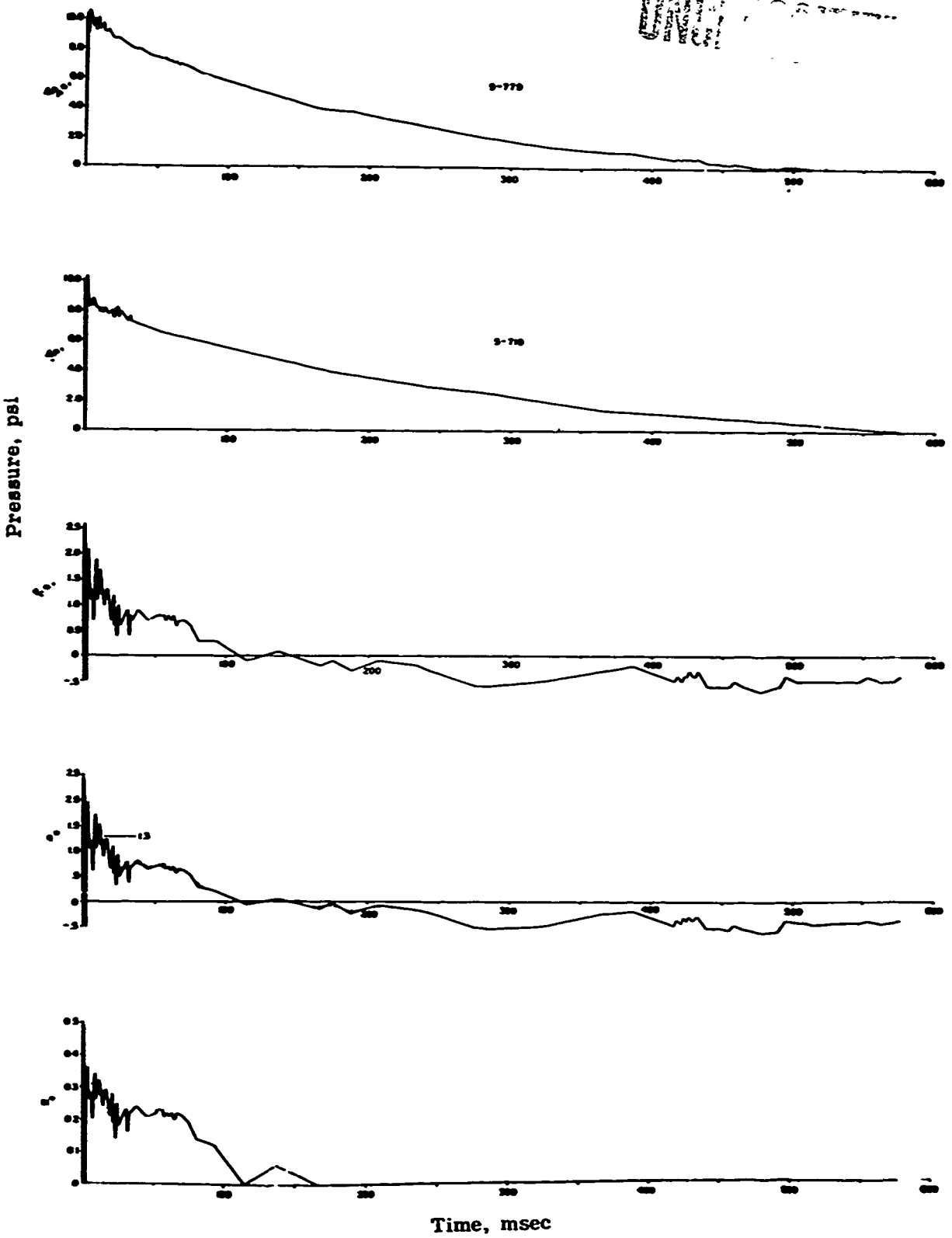

Figure 2.55 Pressure and Mach number versus time, at 2,800 feet, Shot Kepler.

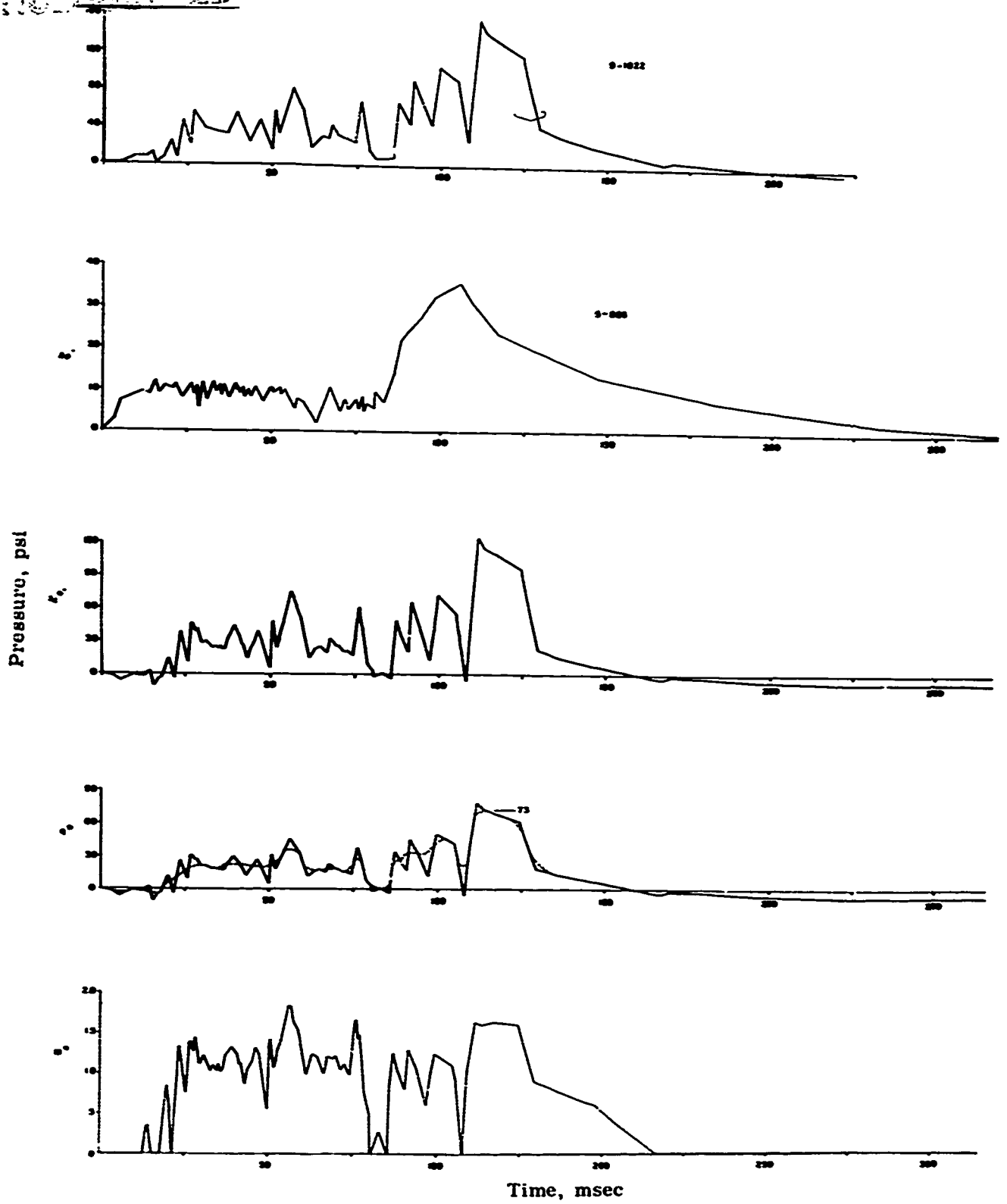

Figure 2.56 Pressure and Mach number versus time, at 1,000 feet, Shot Owens.

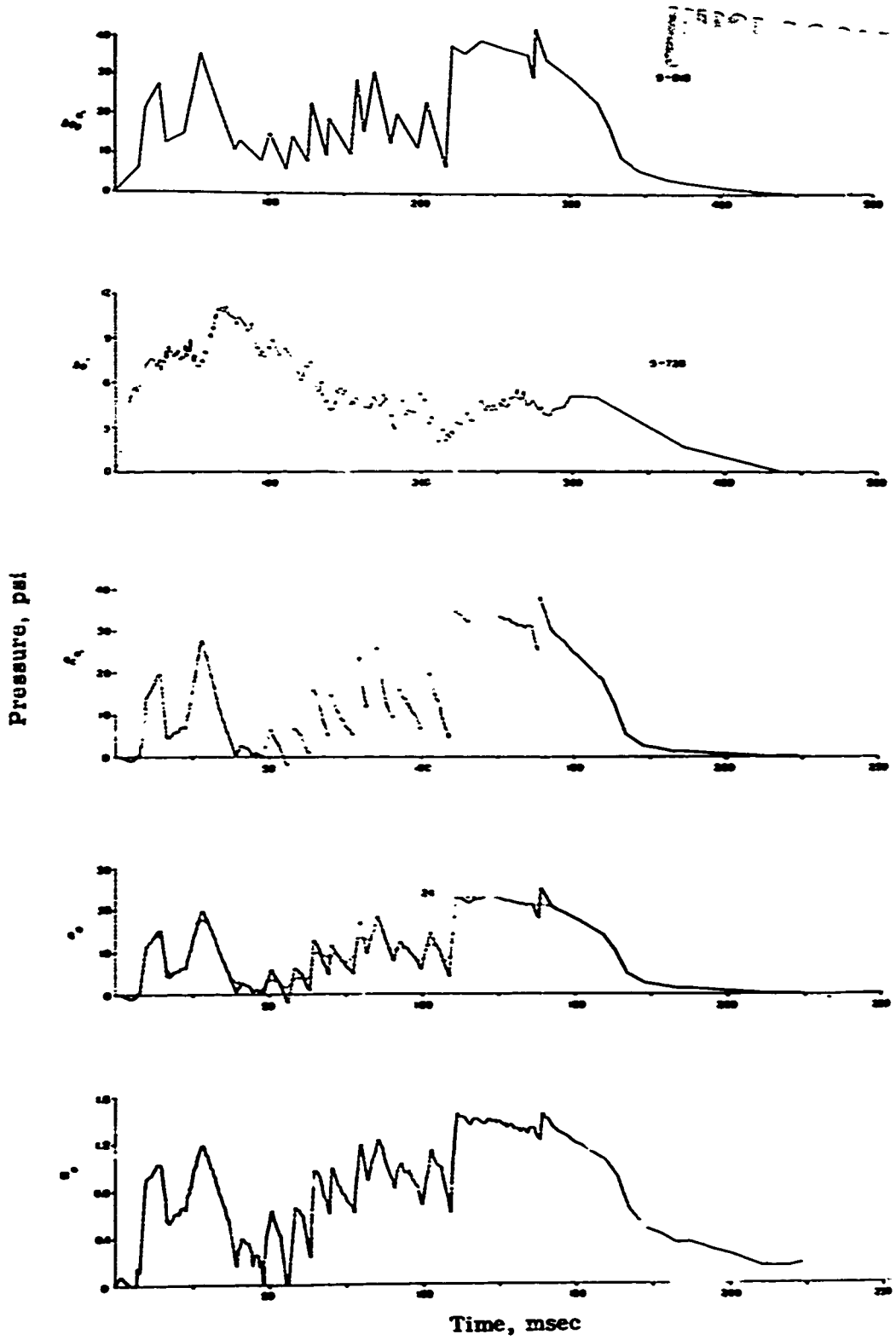

Figure 2.57 Pressure and Mach number versus time, at 1,500 feet, Shot Owens.

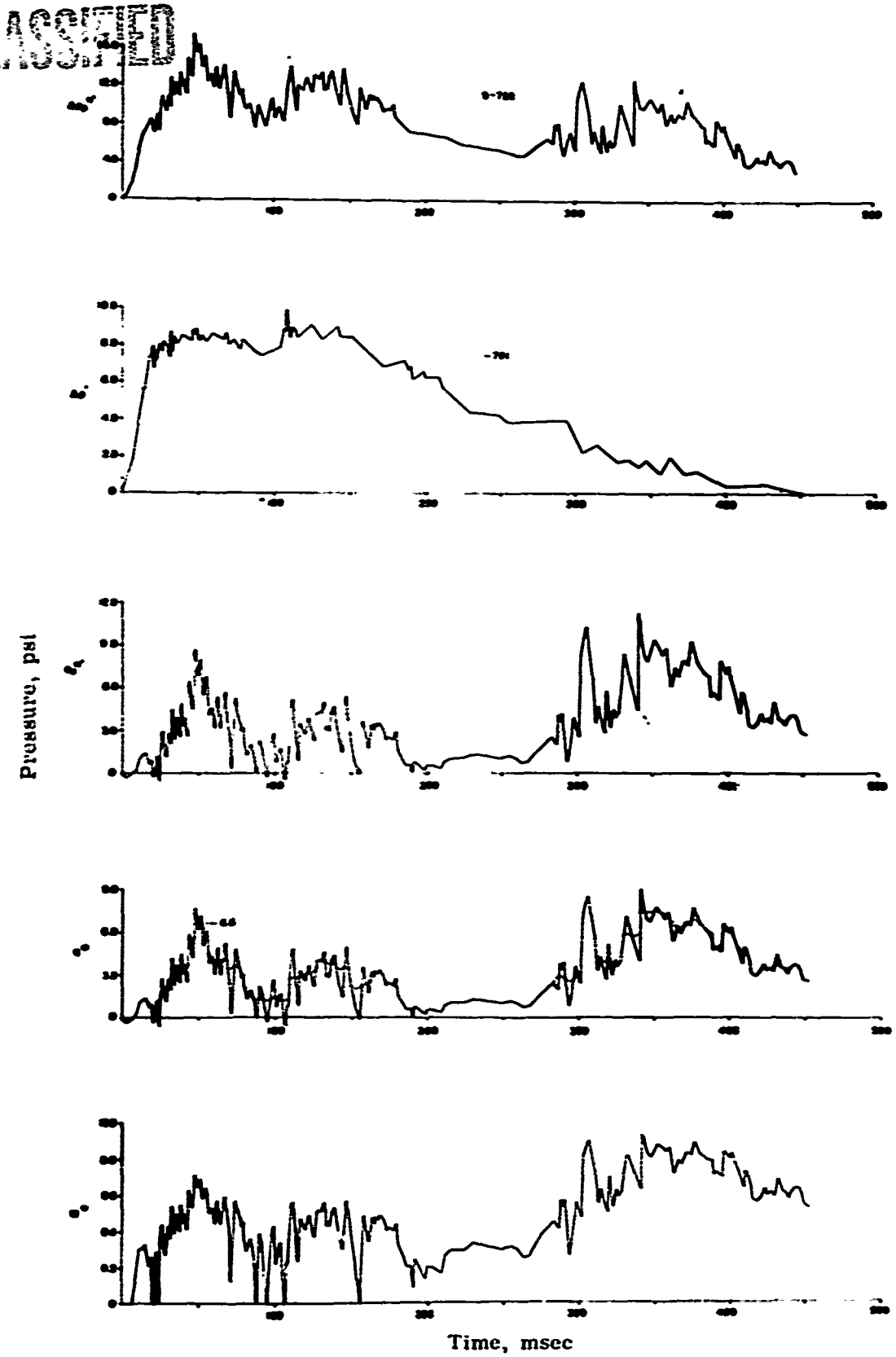

Figure 2.58 Pressure and Mach number versus time, at 1,700 feet, Shot Owens.

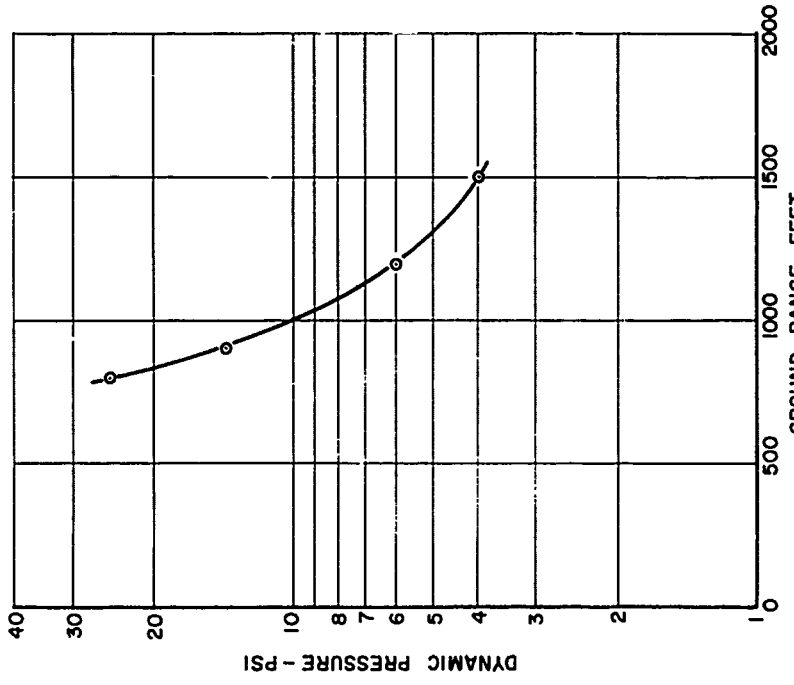

Figure 2.60 Maximum dynamic pressure versus ground range, Shot Franklin.

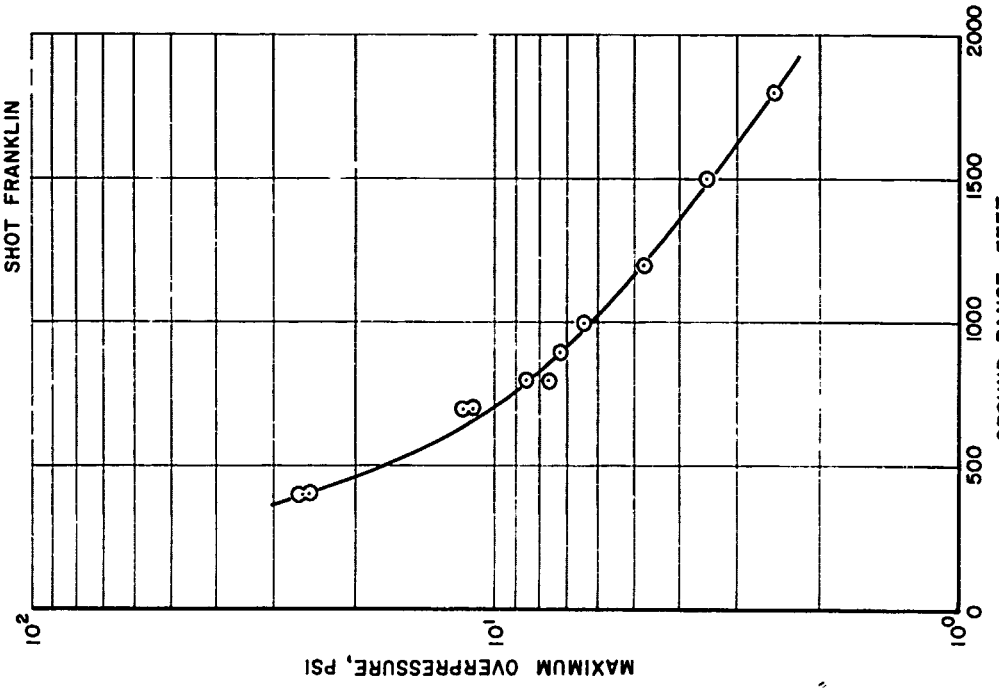

Figure 2.59 Maximum overpressure versus ground range, Shot Franklin.

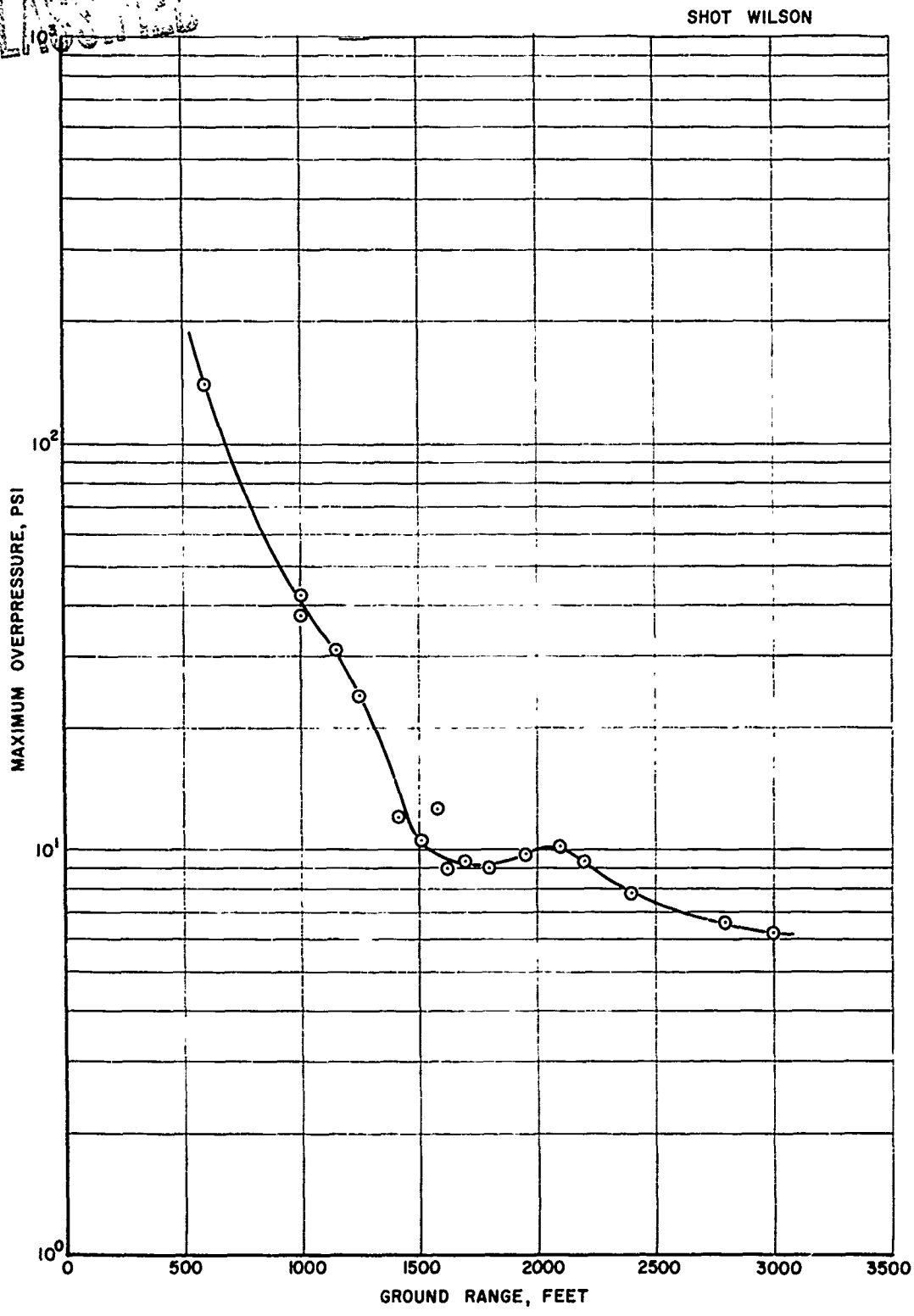

Figure 2.61 Maximum overpressure versus ground range, Shot Wilson.

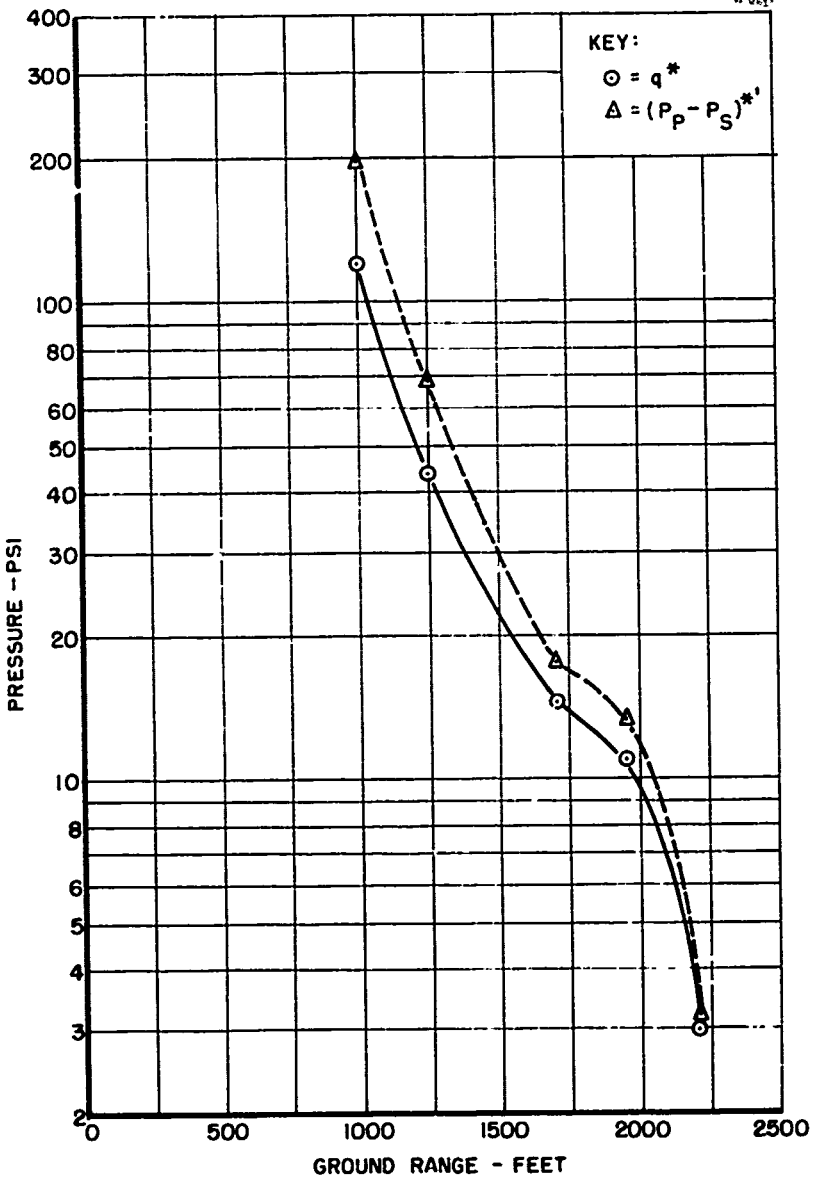

Figure 2.62 Maximum dynamic pressure versus ground range, Shot Wilson.

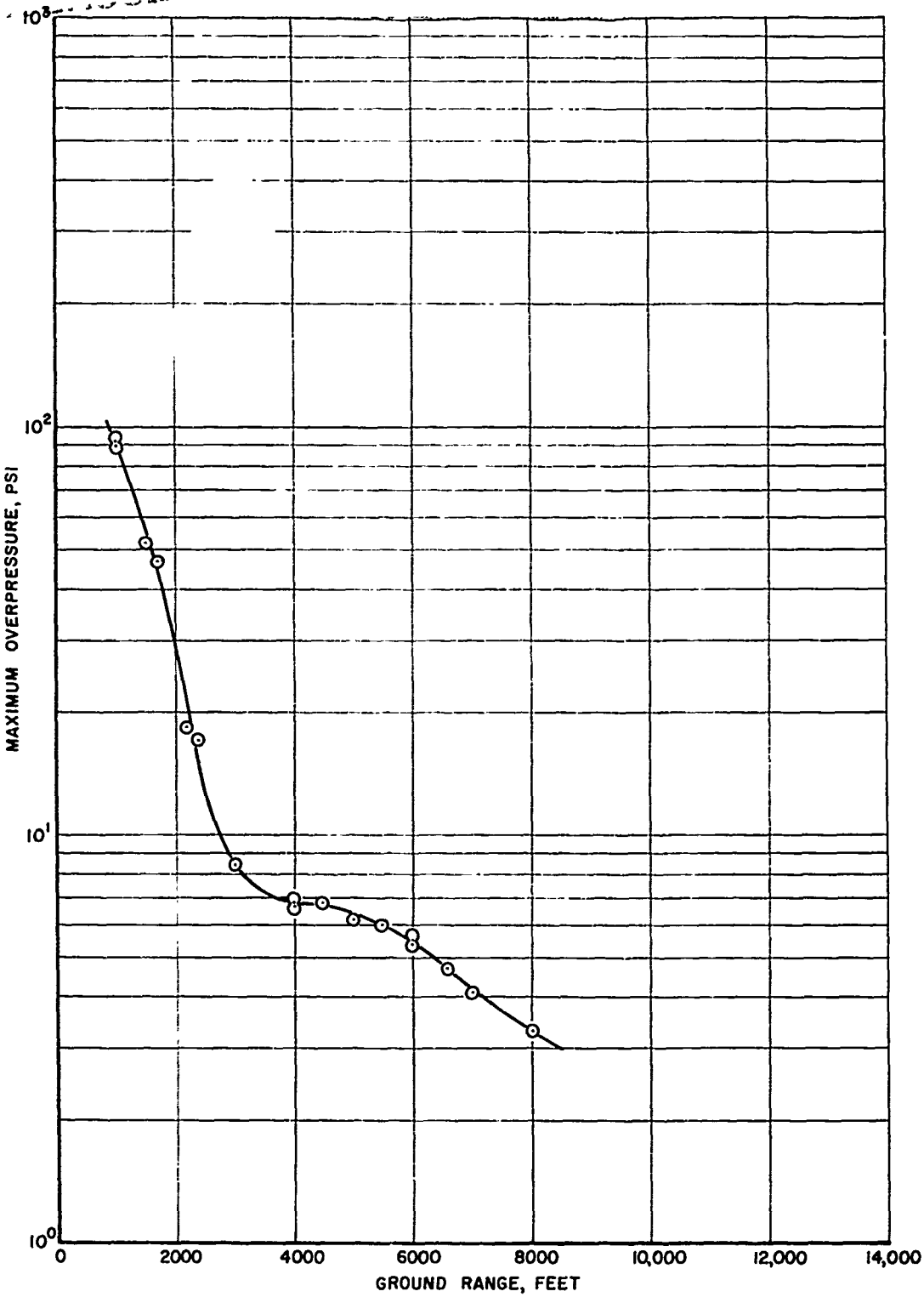

Figure 2.63 Maximum overpressure versus ground range, Shot Hood.

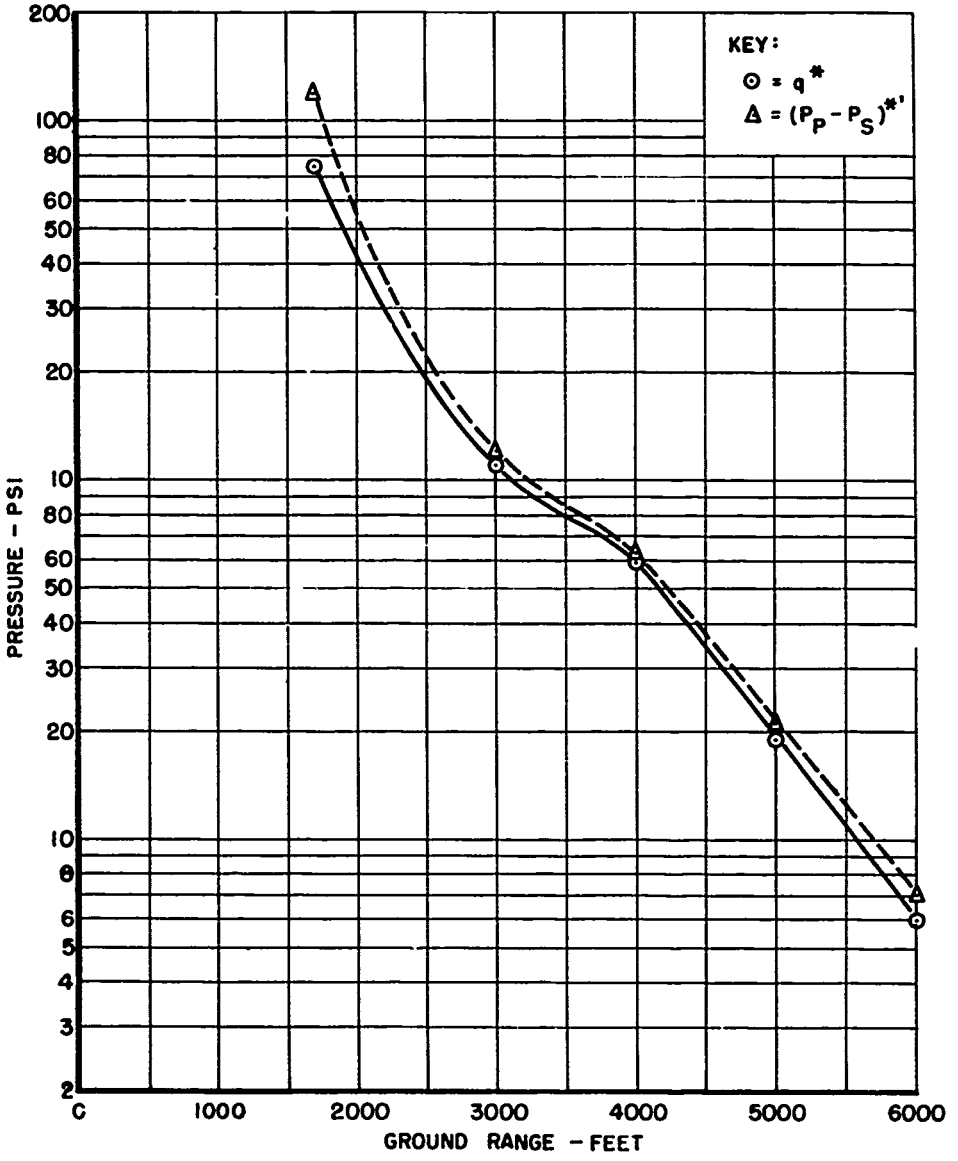

Figure 2.64 Maximum dynamic pressure versus ground range, Shot Hood.

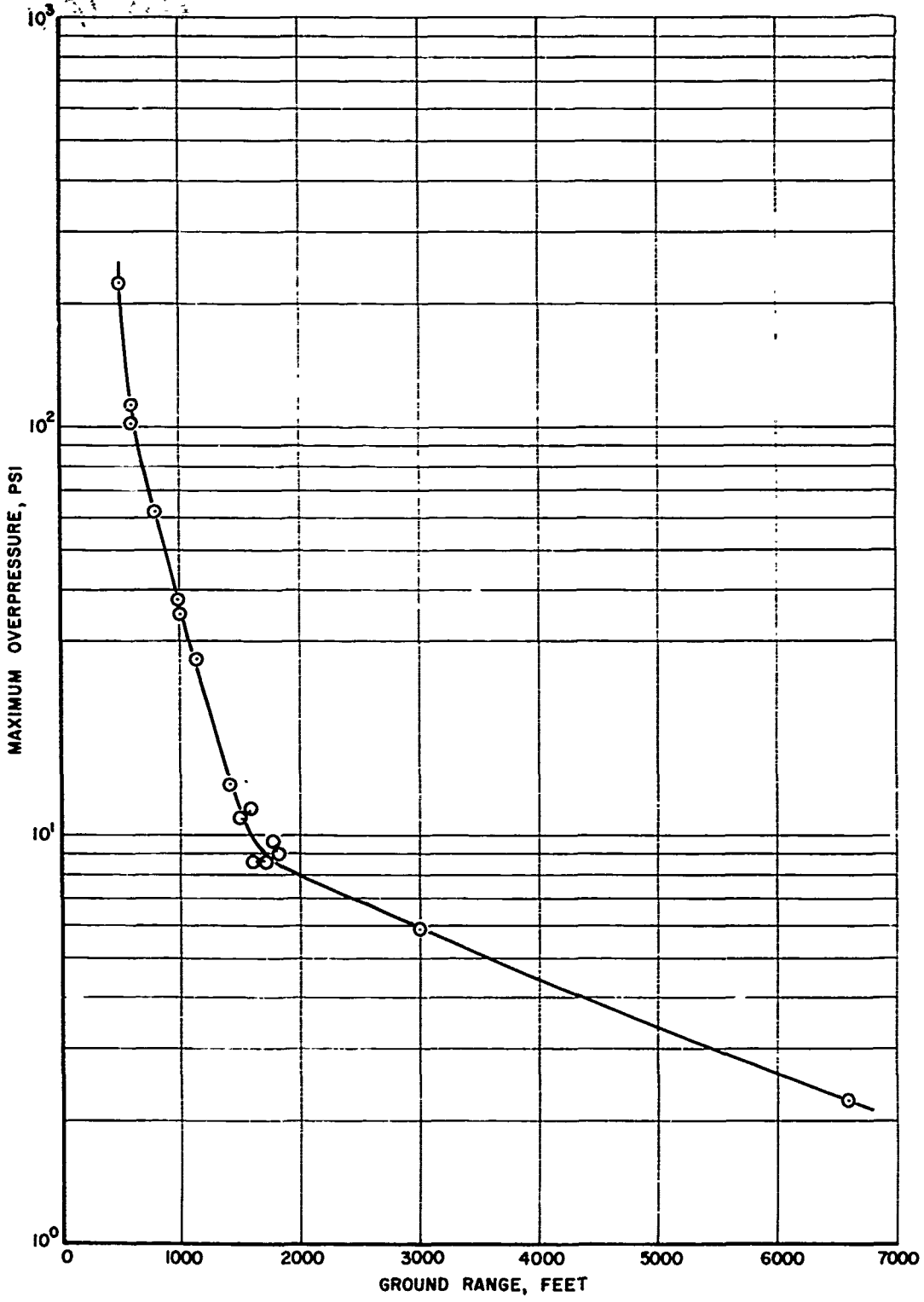

Figure 2.65 Maximum overpressure versus ground range, Shot Owens.

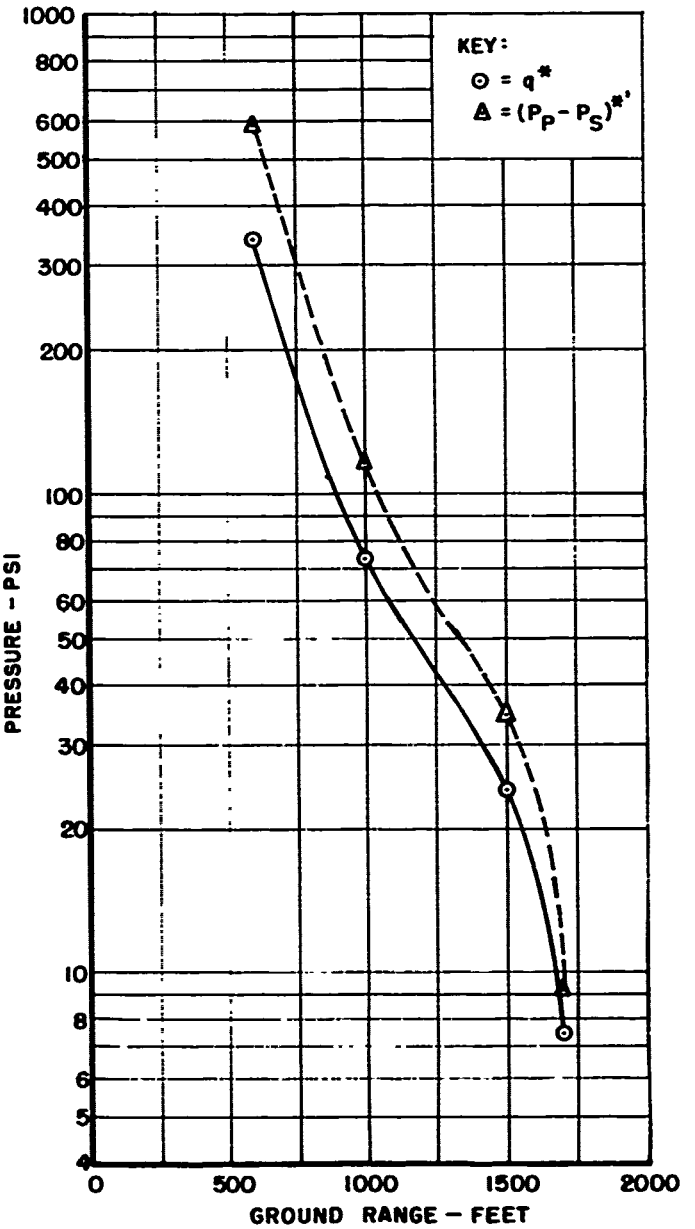

Figure 2.66 Maximum dynamic pressure versus ground range, Shot Owens.

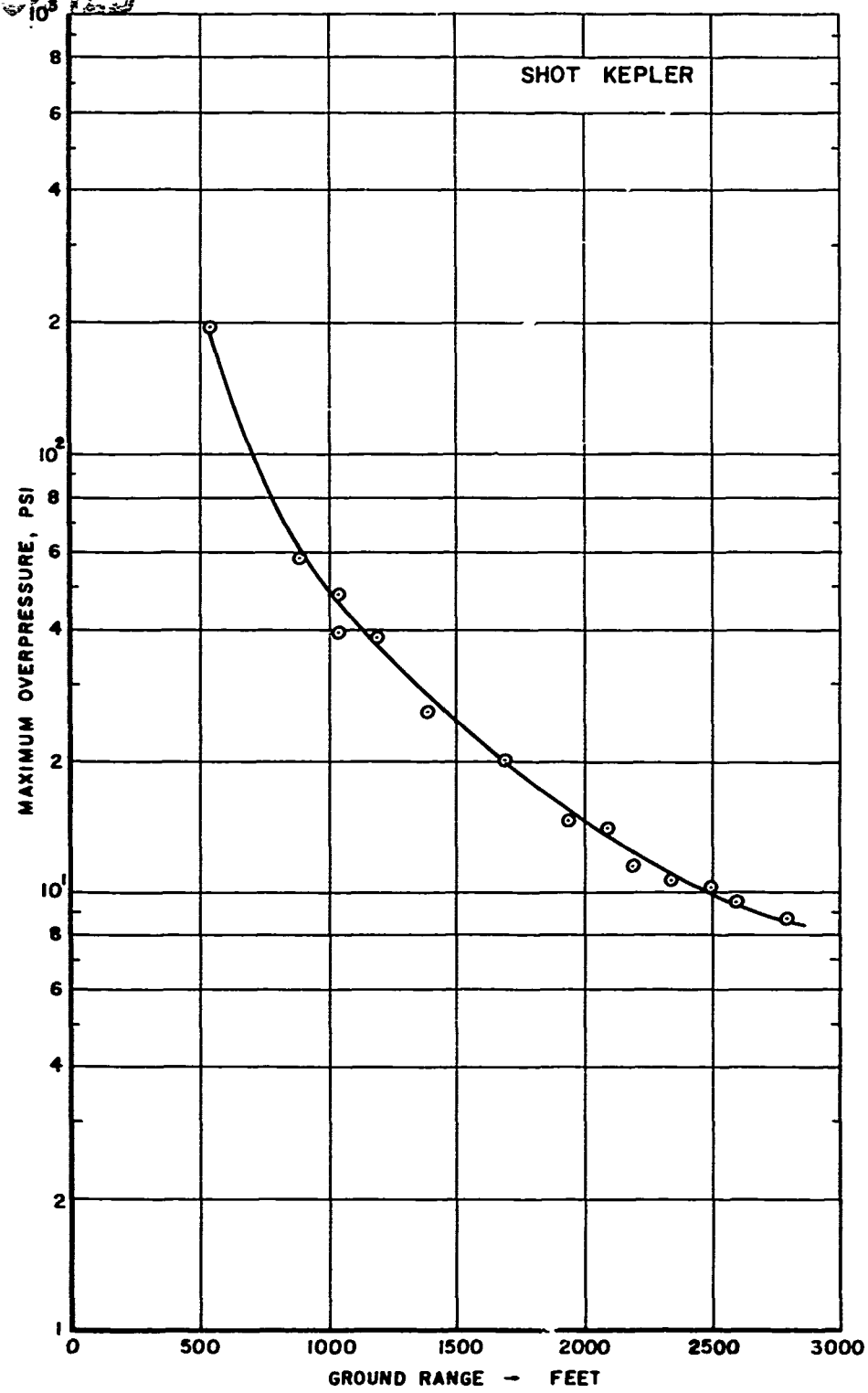

Figure 2.67 Maximum overpressure versus ground range, Shot Kepler.

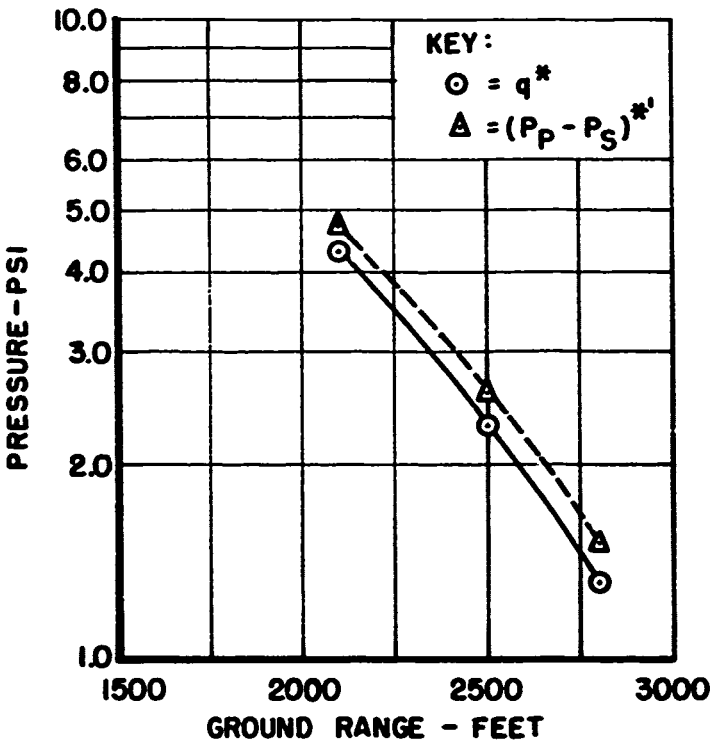

Figure 2.68 Maximum dynamic pressure versus ground range, Shot Kepler.

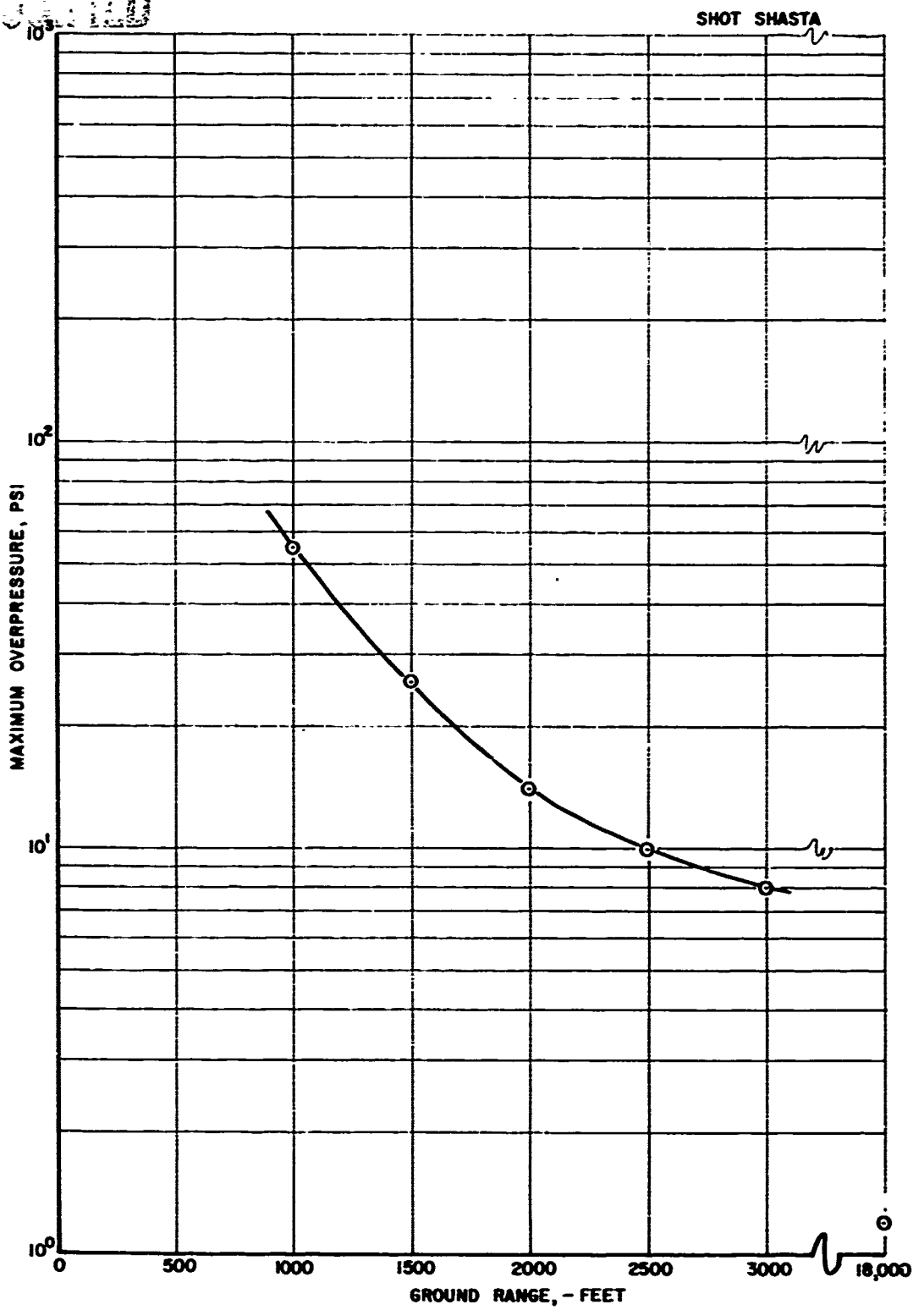

Figure 2.69 Maximum overpressure versus ground range, Shot Shasta.

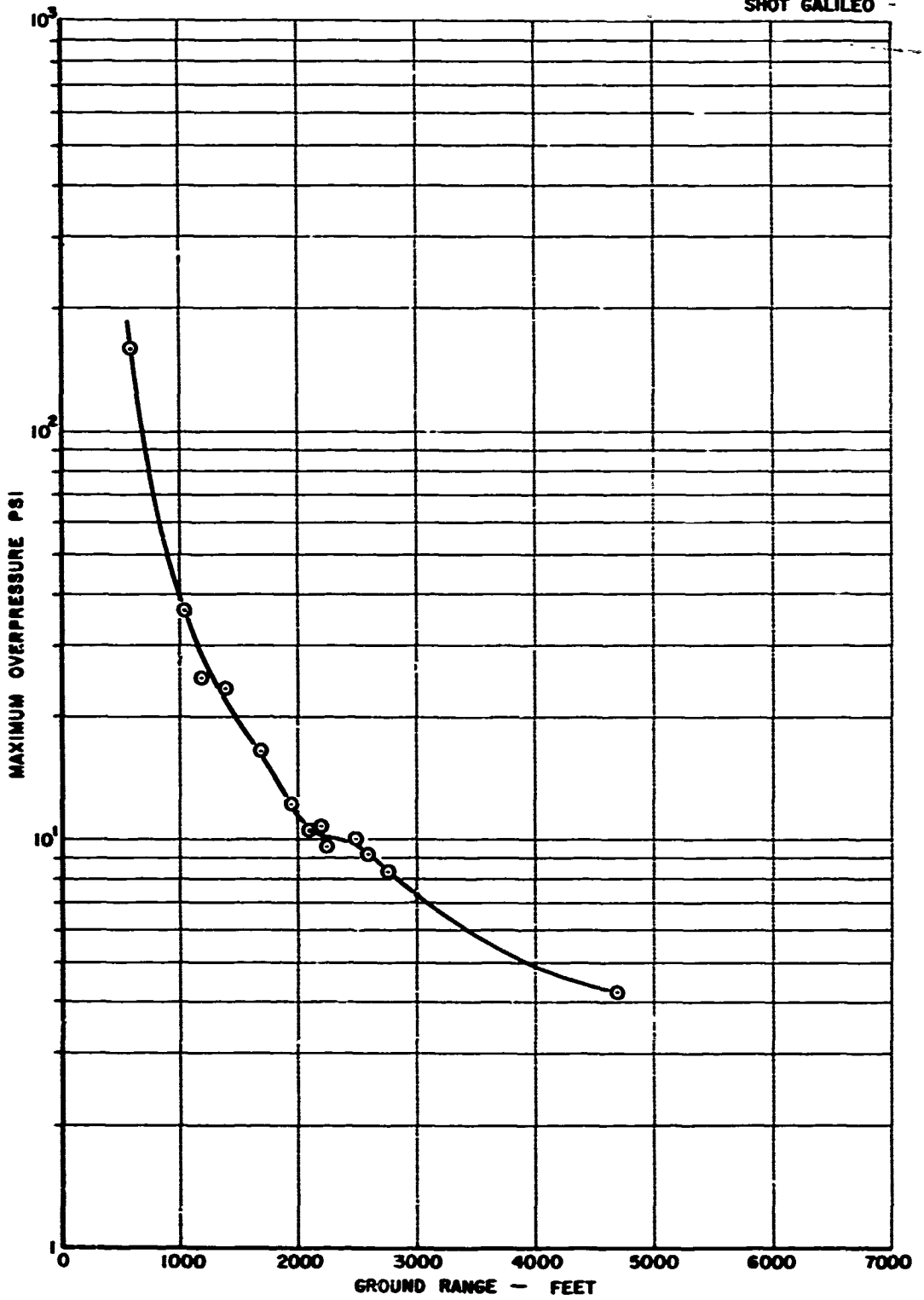

Figure 2.70 Maximum overpressure versus ground range, Shot Galileo.

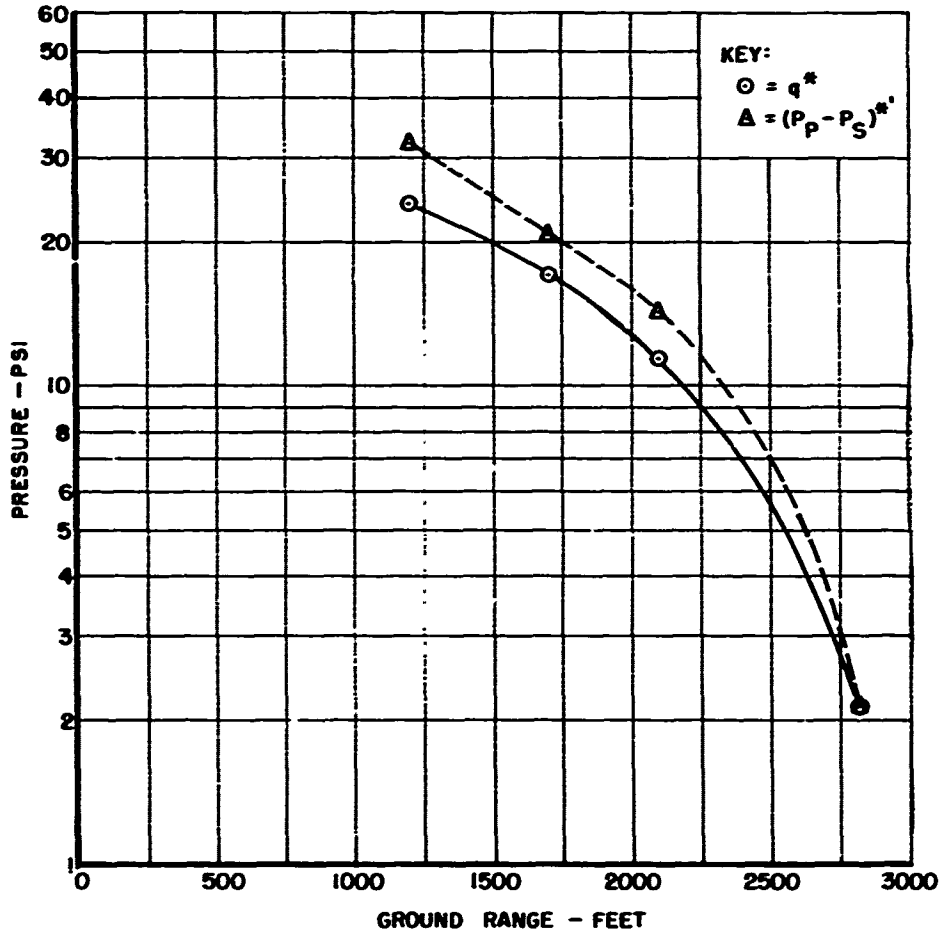

Figure 2.71 Maximum dynamic pressure versus ground range, Shot Galileo.

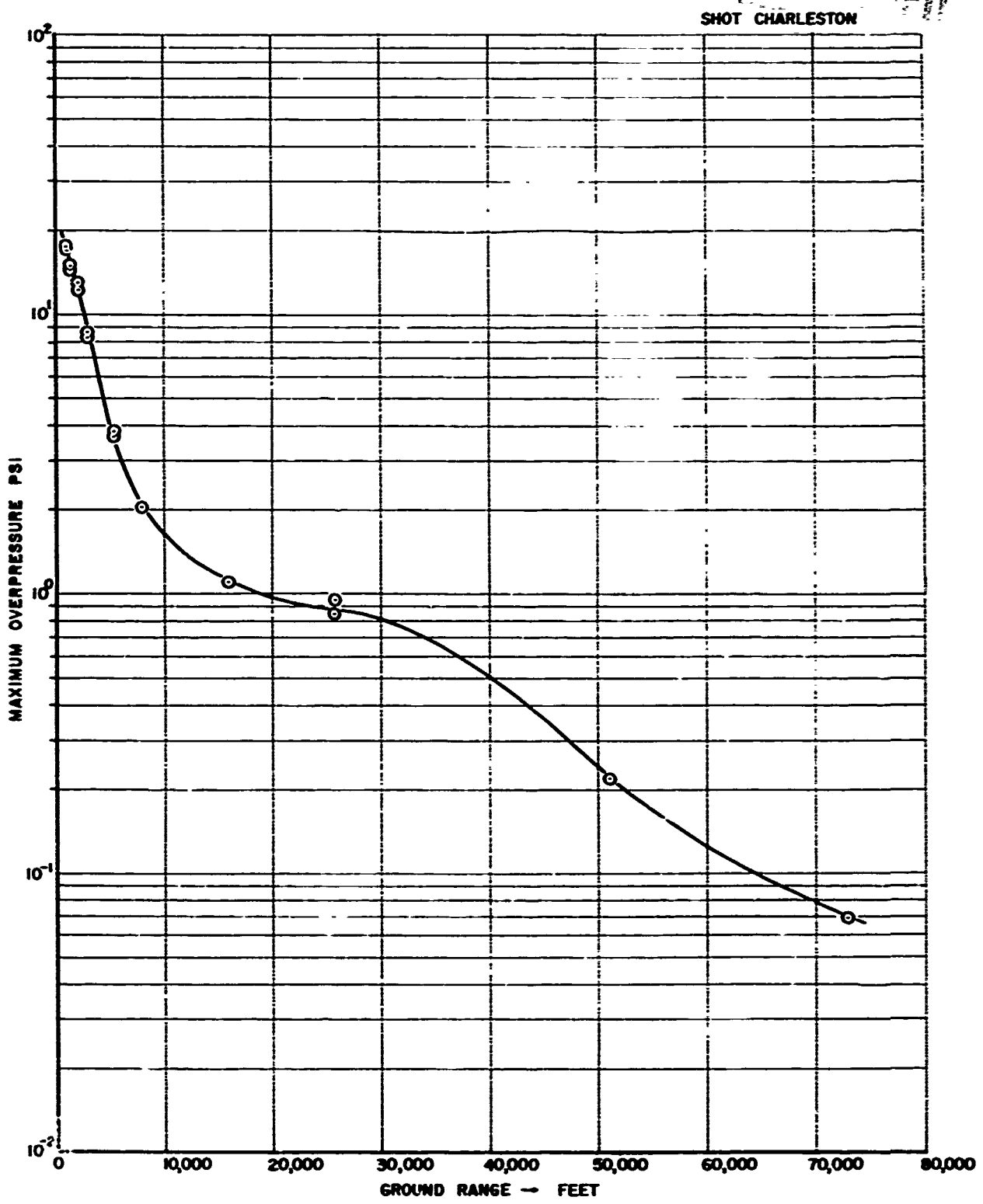

Figure 2.72 Maximum overpressure versus ground range, Shot Charleston.

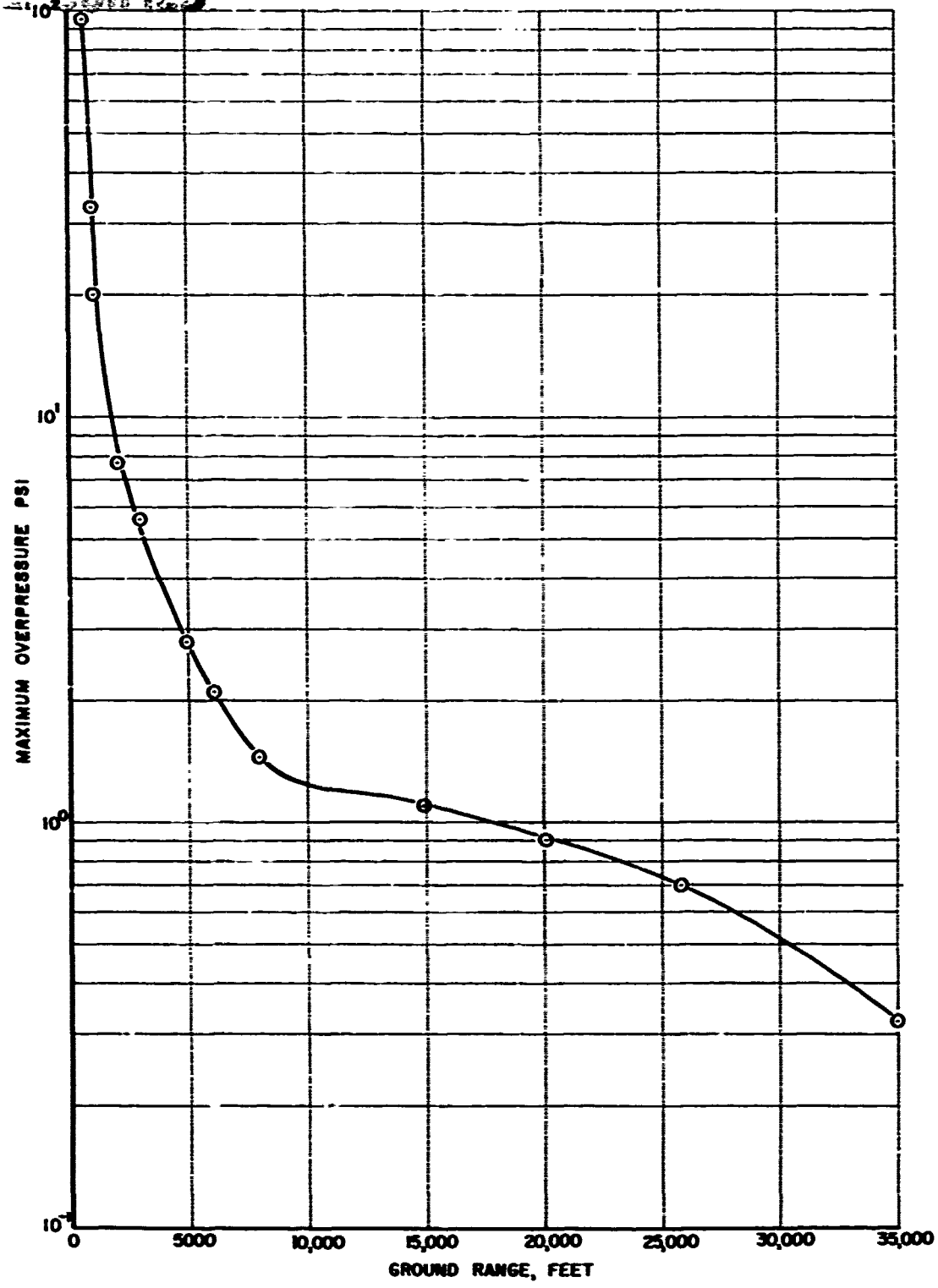

Figure 2.73 Maximum overpressure versus ground range, Shot Morgan.

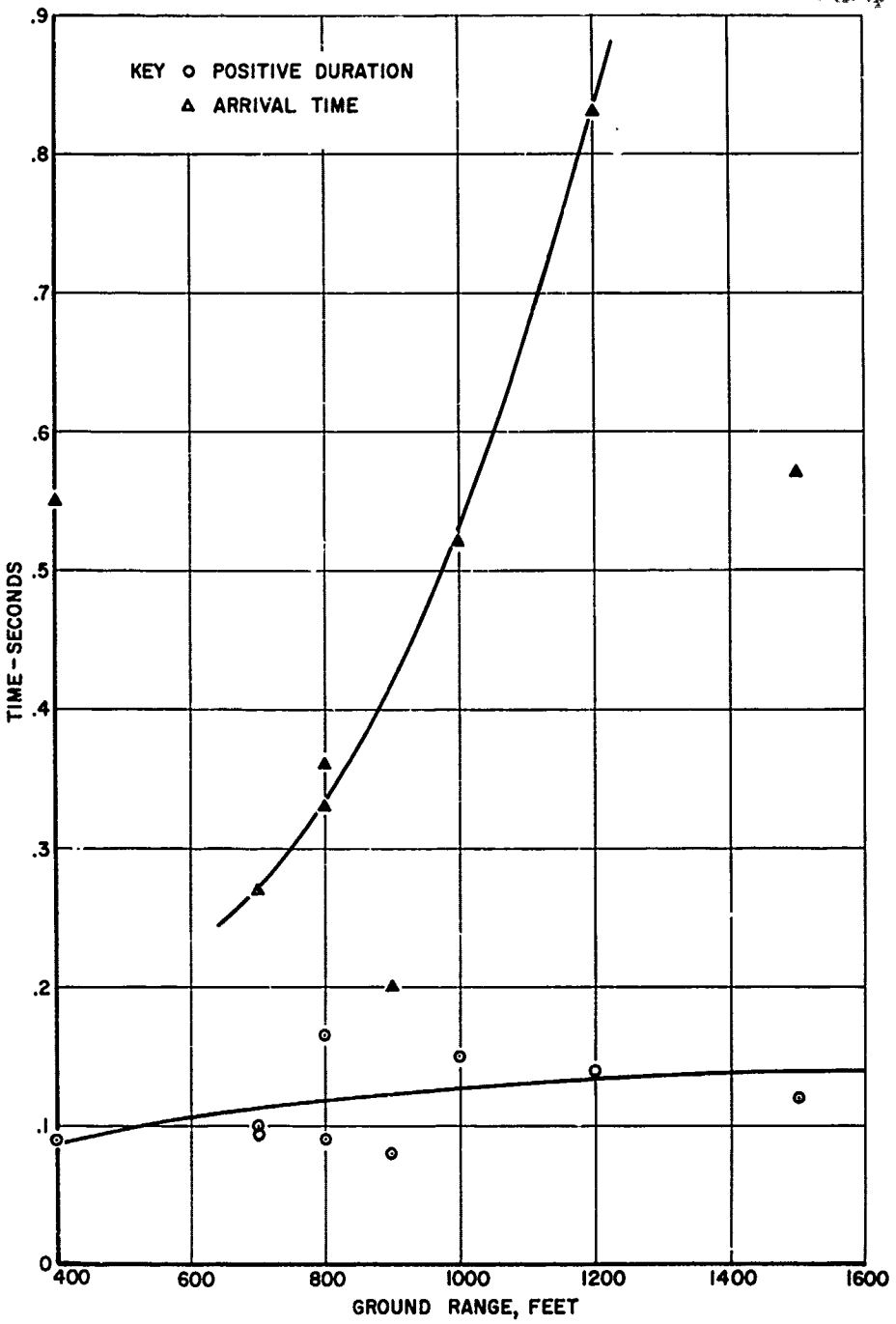

Figure 2.74 Arrival time and positive duration versus ground range, Shot Franklin.

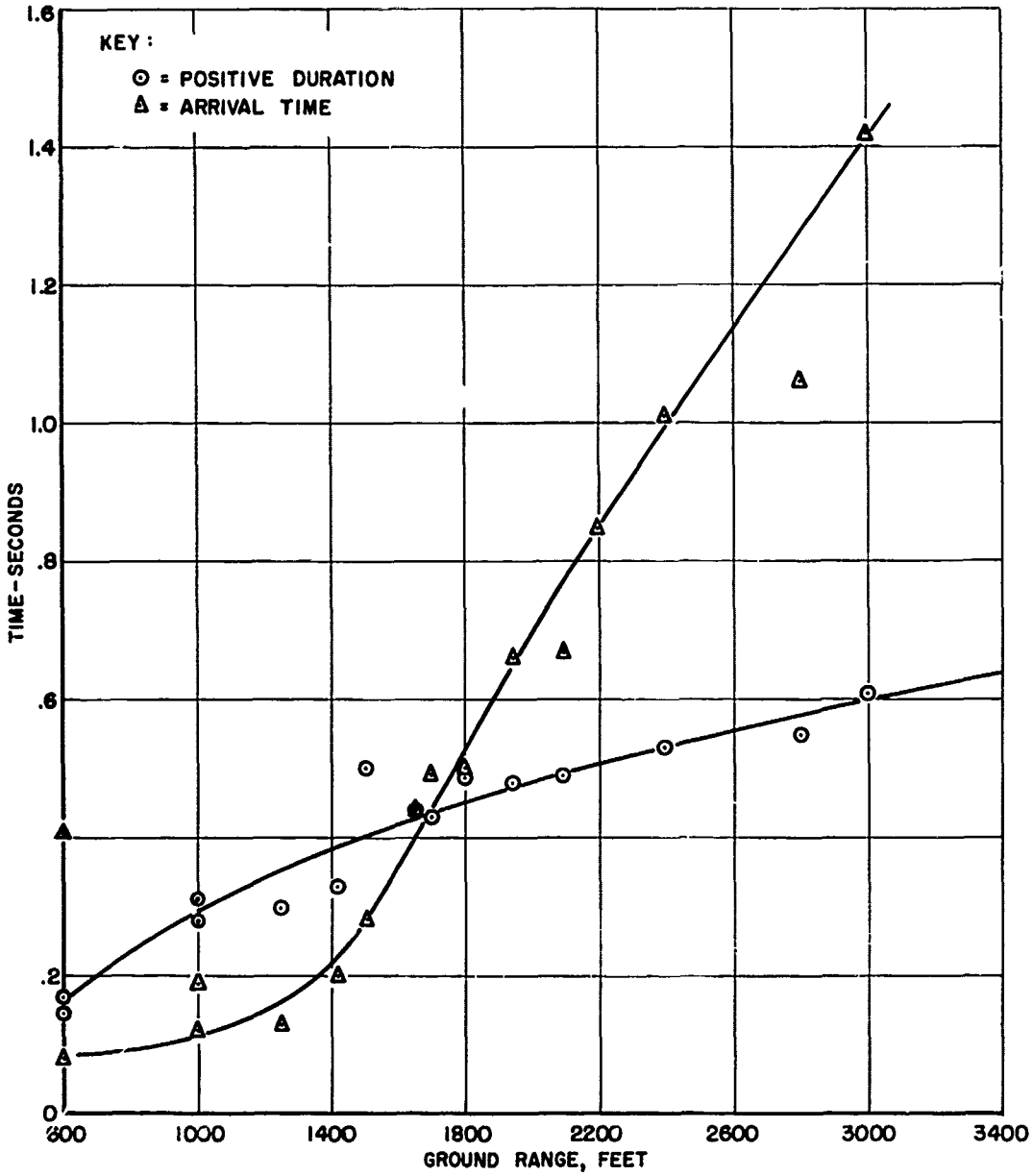

Figure 2.75 Arrival time and positive duration versus ground range, Shot Wilson.

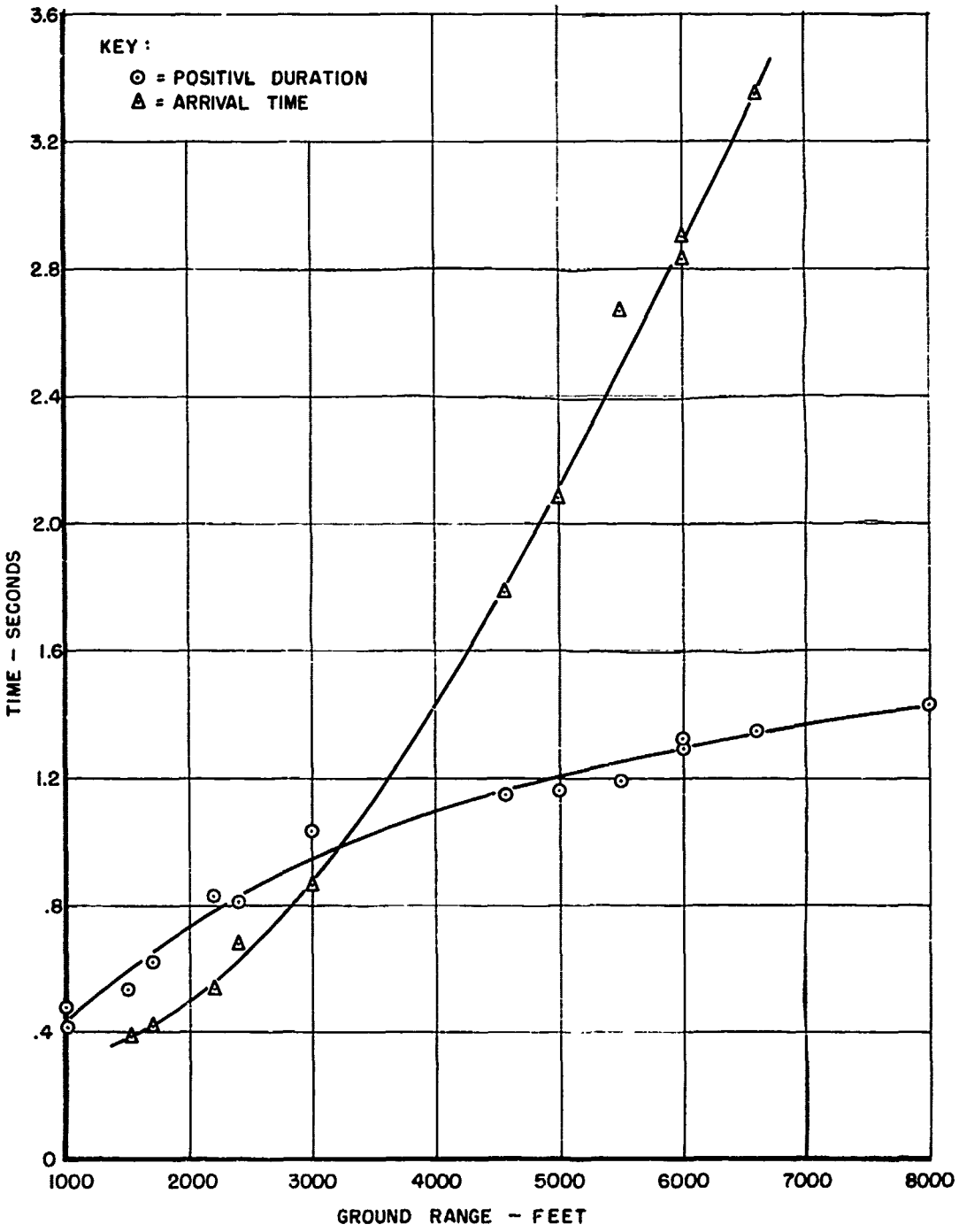

Figure 2.76 Arrival time and positive duration versus ground range, Shot Hood.

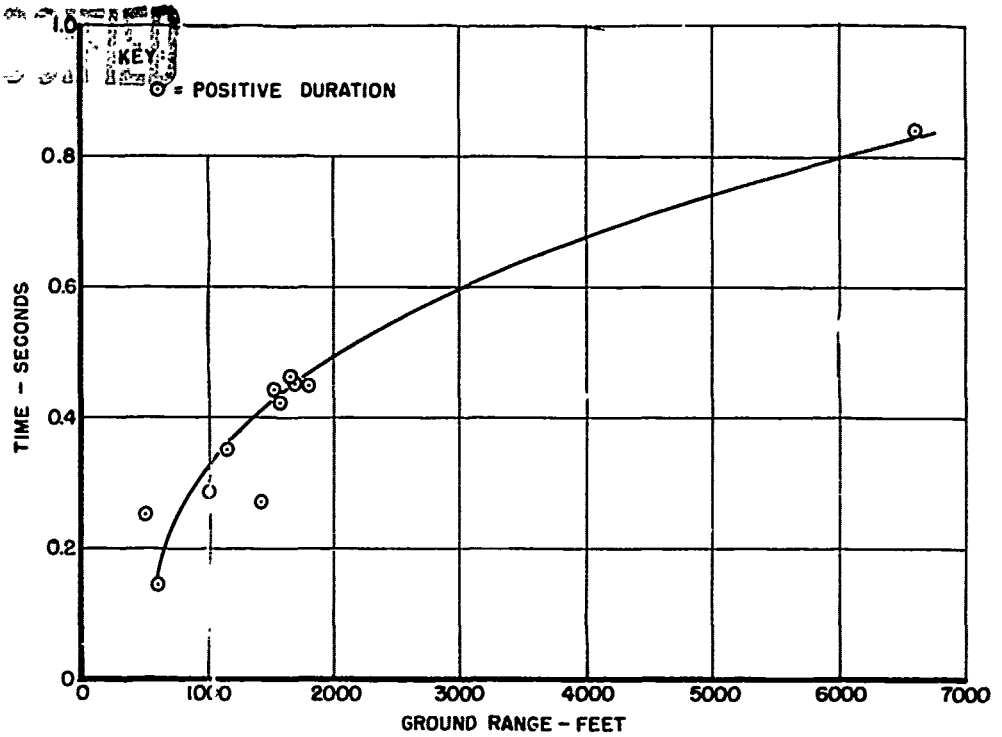

Figure 2.77 Positive duration versus ground range, Shot Owens.

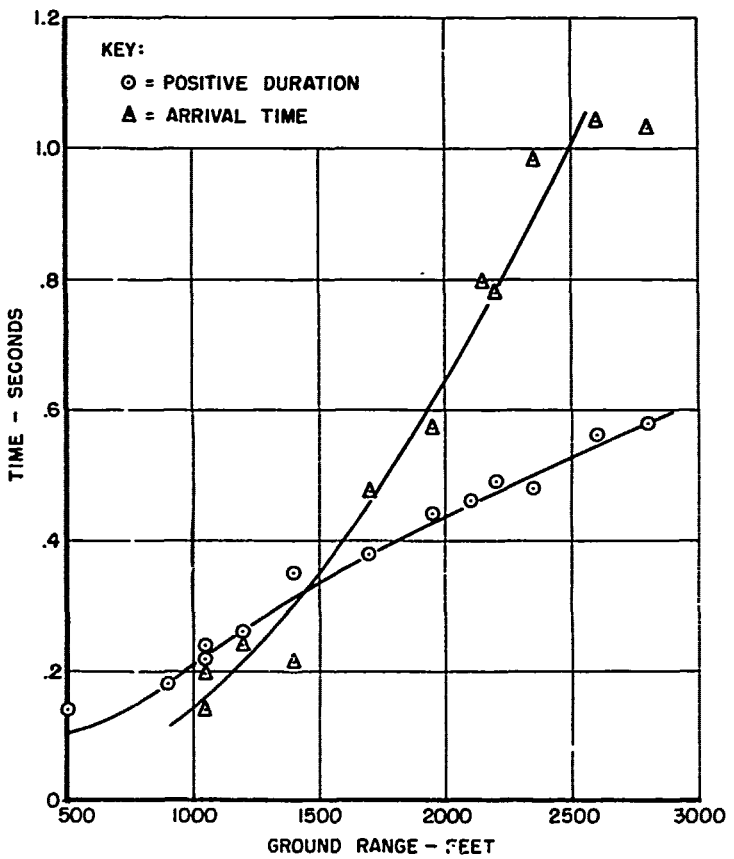

Figure 2.78 Arrival time and positive duration versus ground range, Shot Kepler.

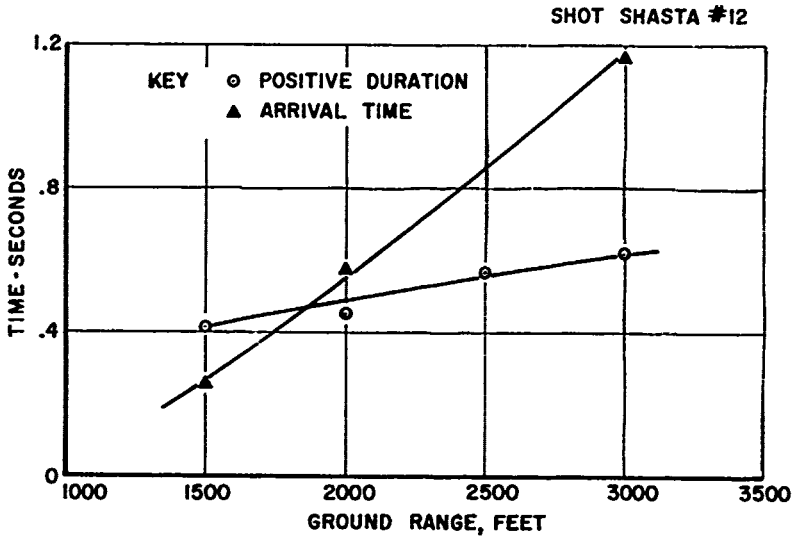

Figure 2.79 Arrival time and positive duration versus ground range, Shot Shasta.

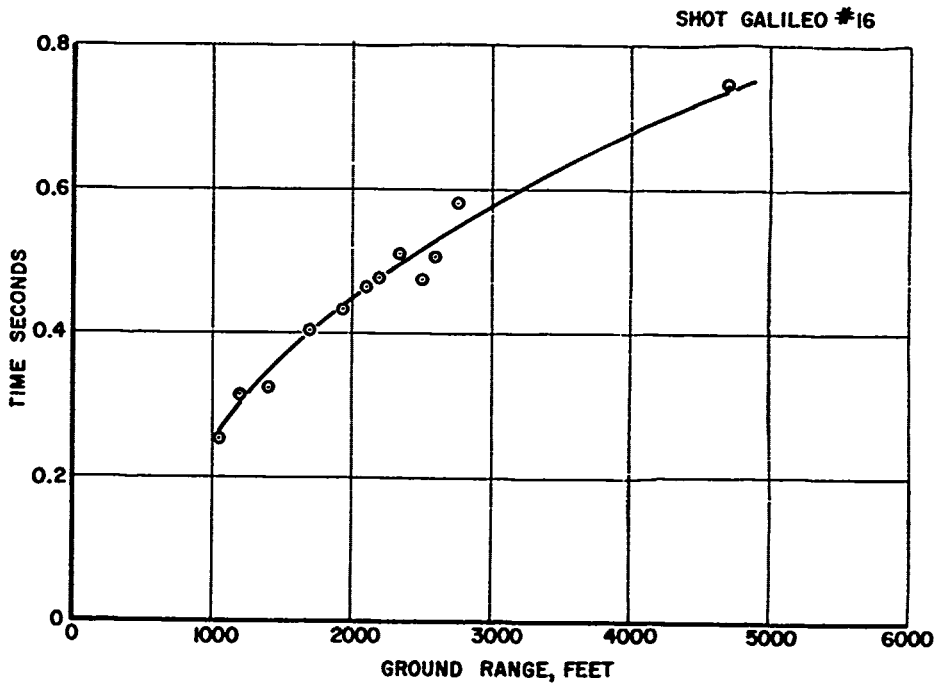

Figure 2.80 Positive duration versus ground range, Shot Galileo.

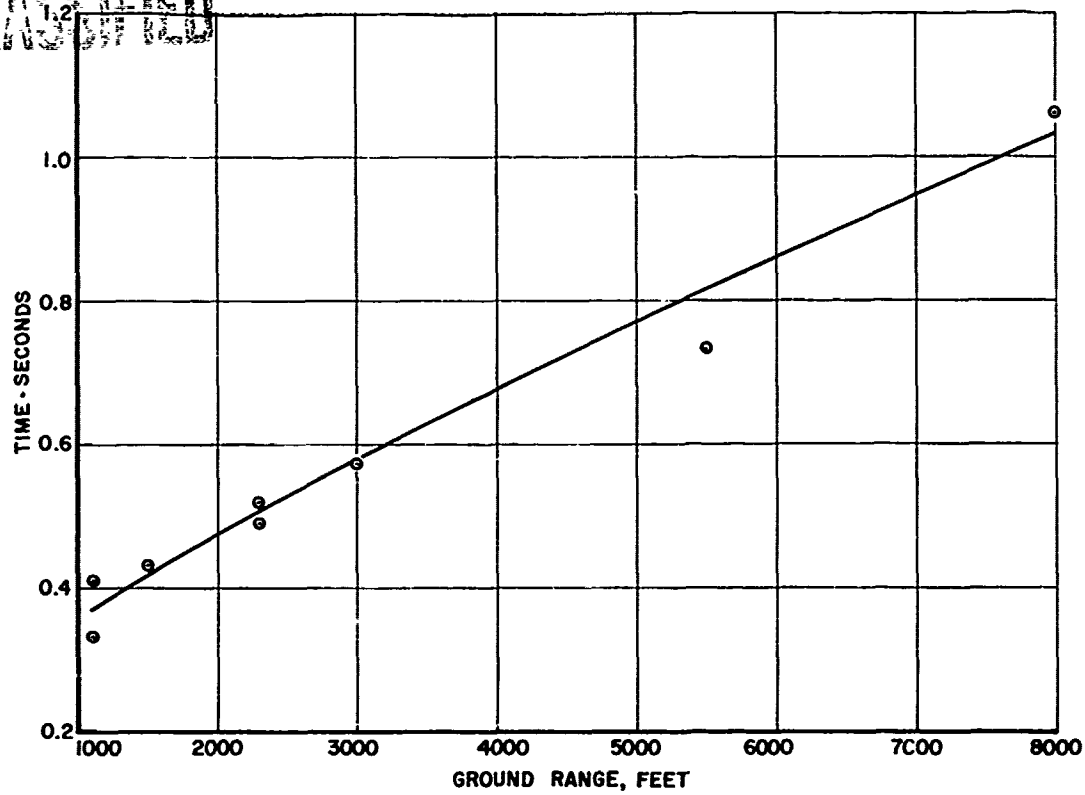

Figure 2.81 Positive duration versus ground range, Shot Charleston.

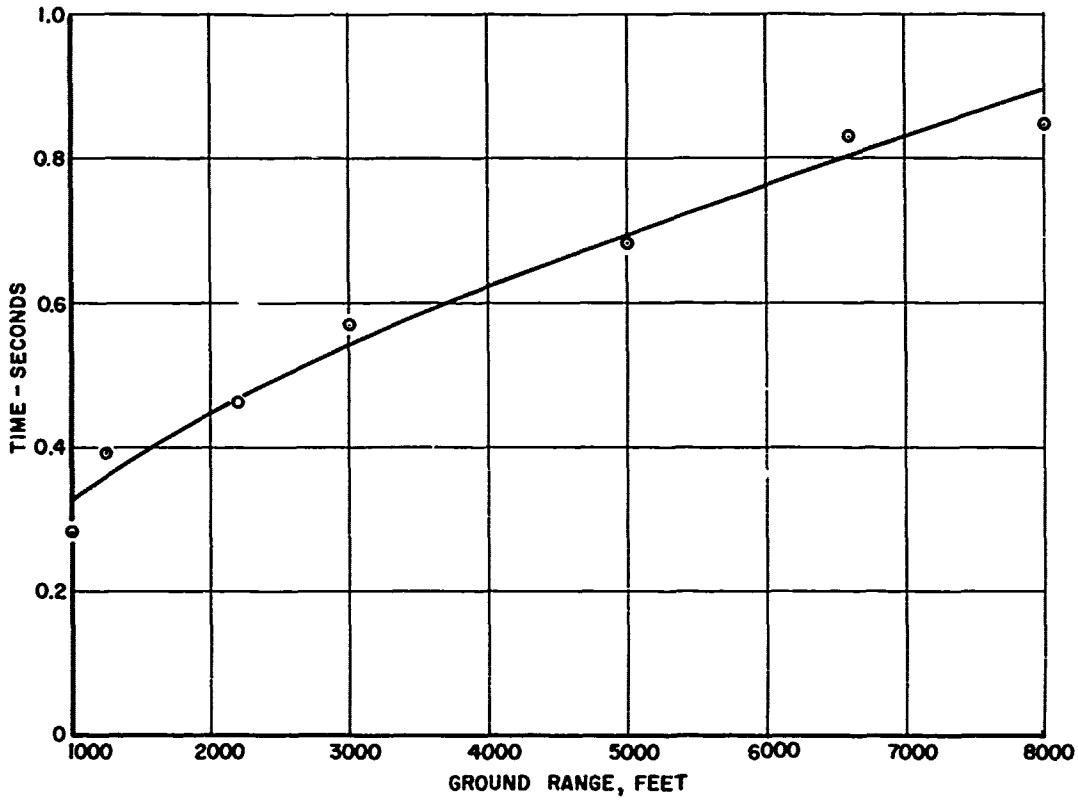

Figure 2.82 Positive duration versus ground range, Shot Morgan.

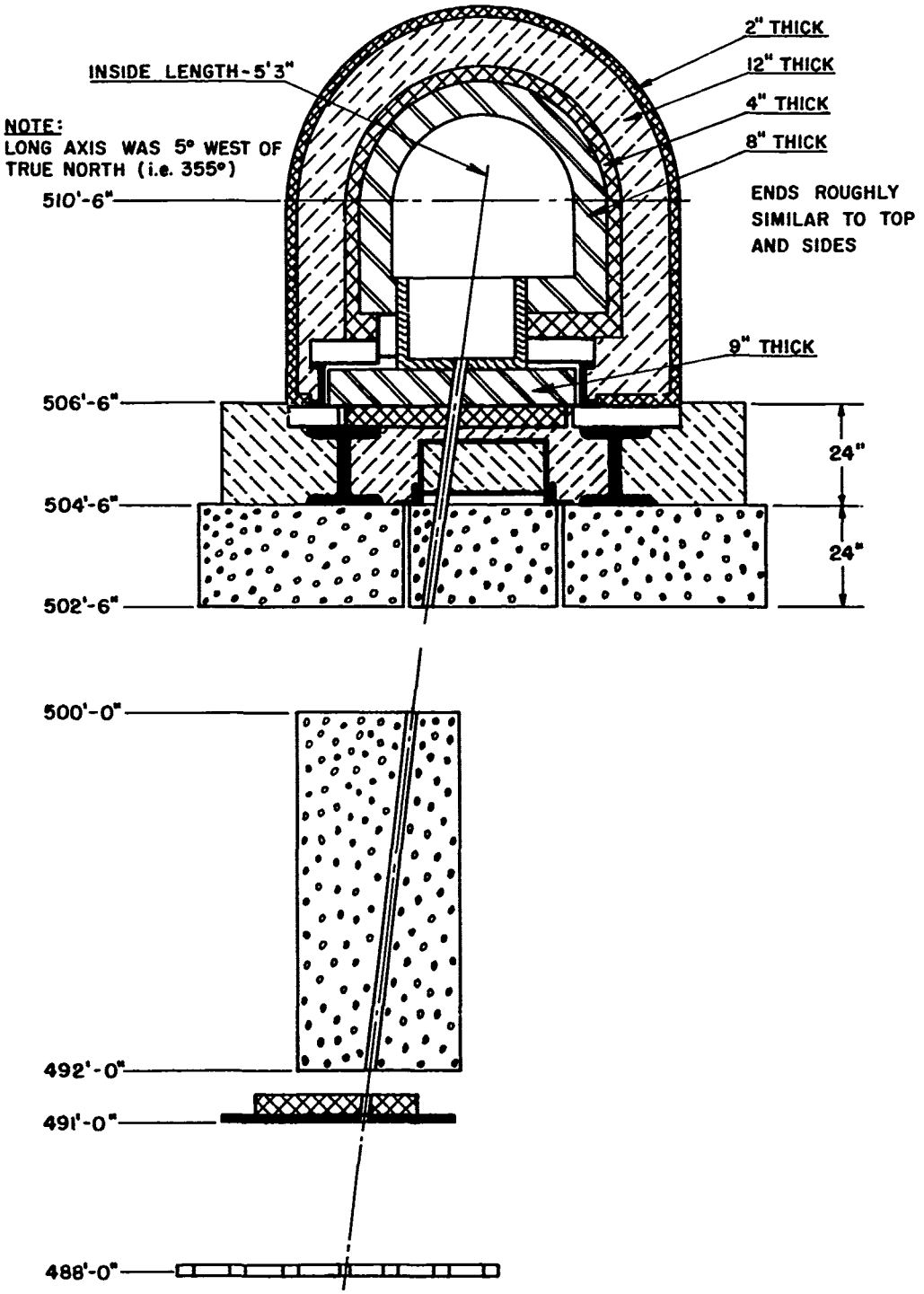

Figure 2.83 Layout of shield configuration, Shot Kepler.

NOTE:
MAIN AXIS OF SHIELD NE-SW WITH OPENING NE
SHELL DIMENSIONS - 63.2" HIGH, 5.2" WIDE, 117.6" LONG

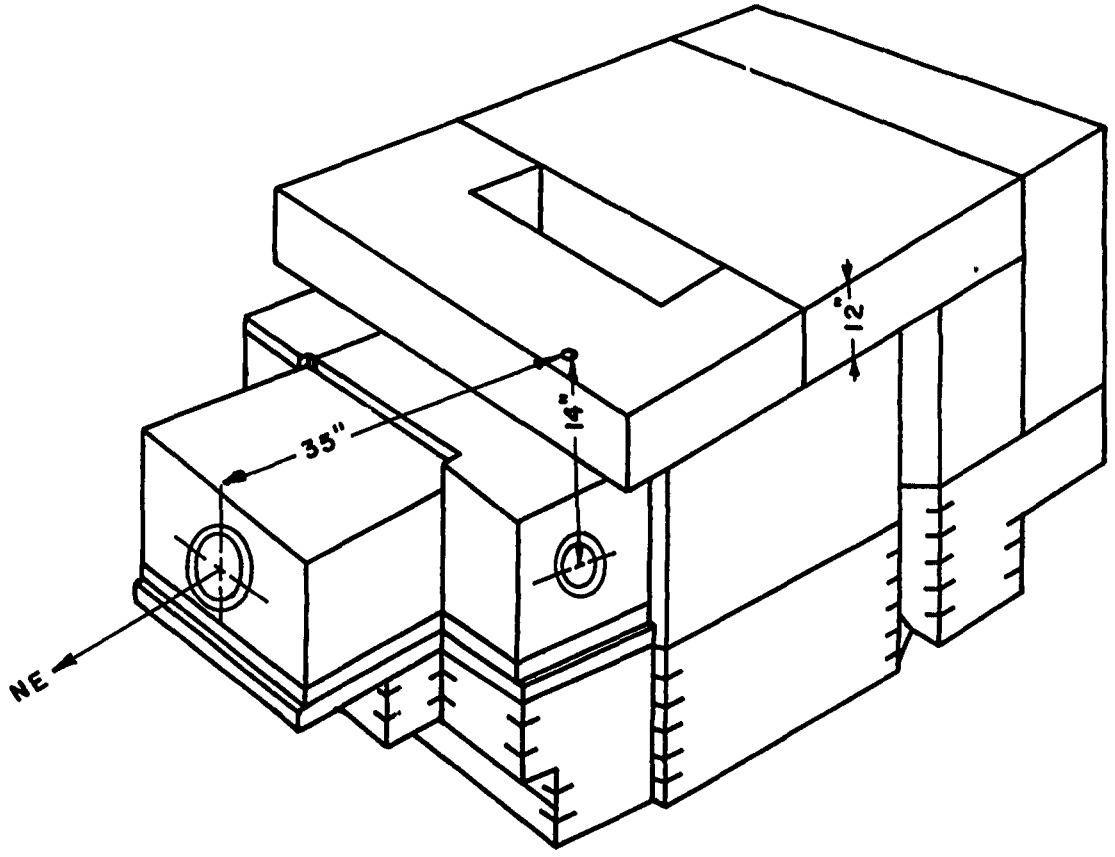

Figure 2.84 Layout of shield configuration, Shot Galileo.

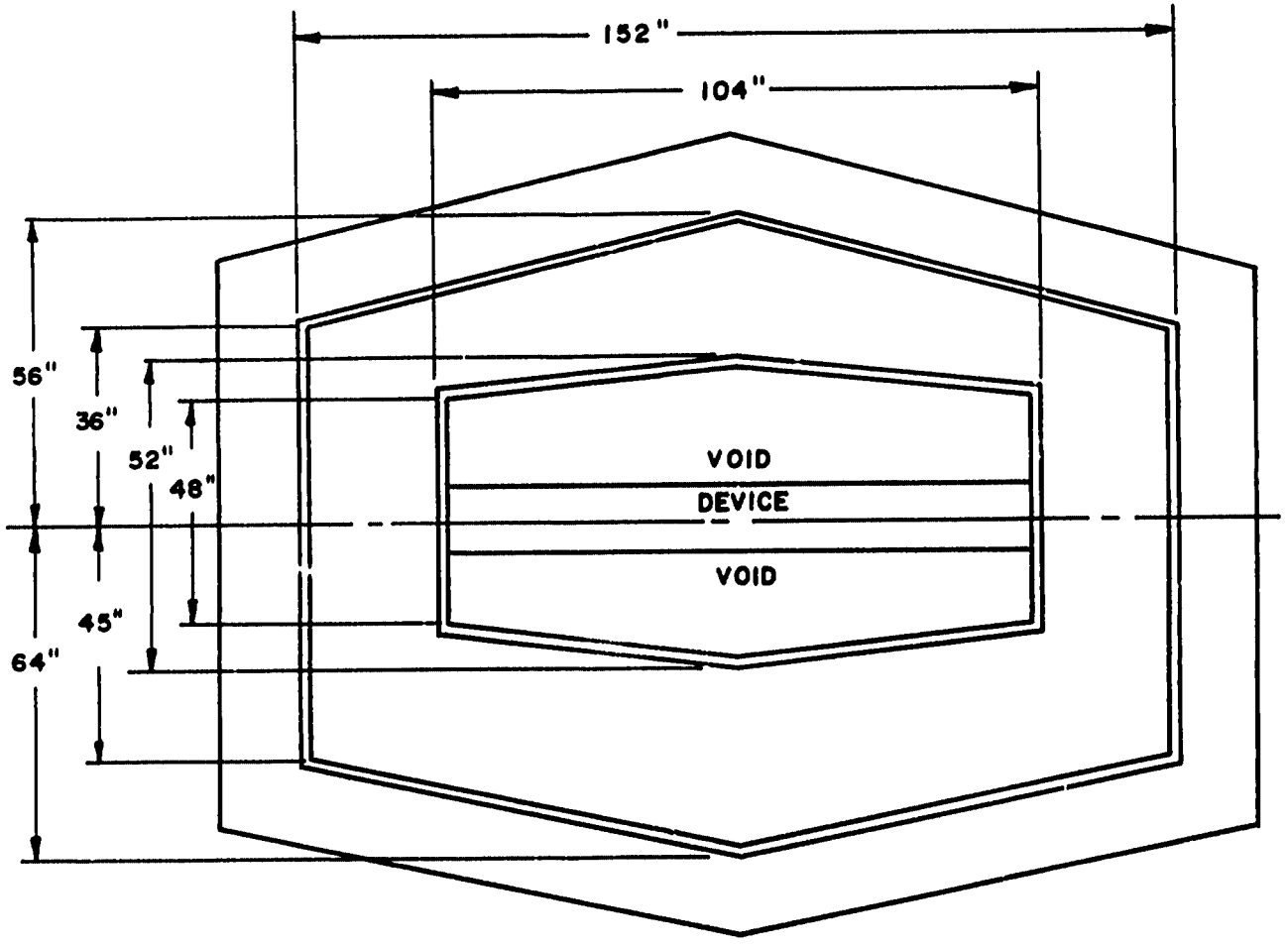

NOTE:
SIDEVIEW (FIG. IS APPROX. A
SOLID OF REVOLUTION)

Figure 2.85 Layout of shield configuration, Shot Shasta.

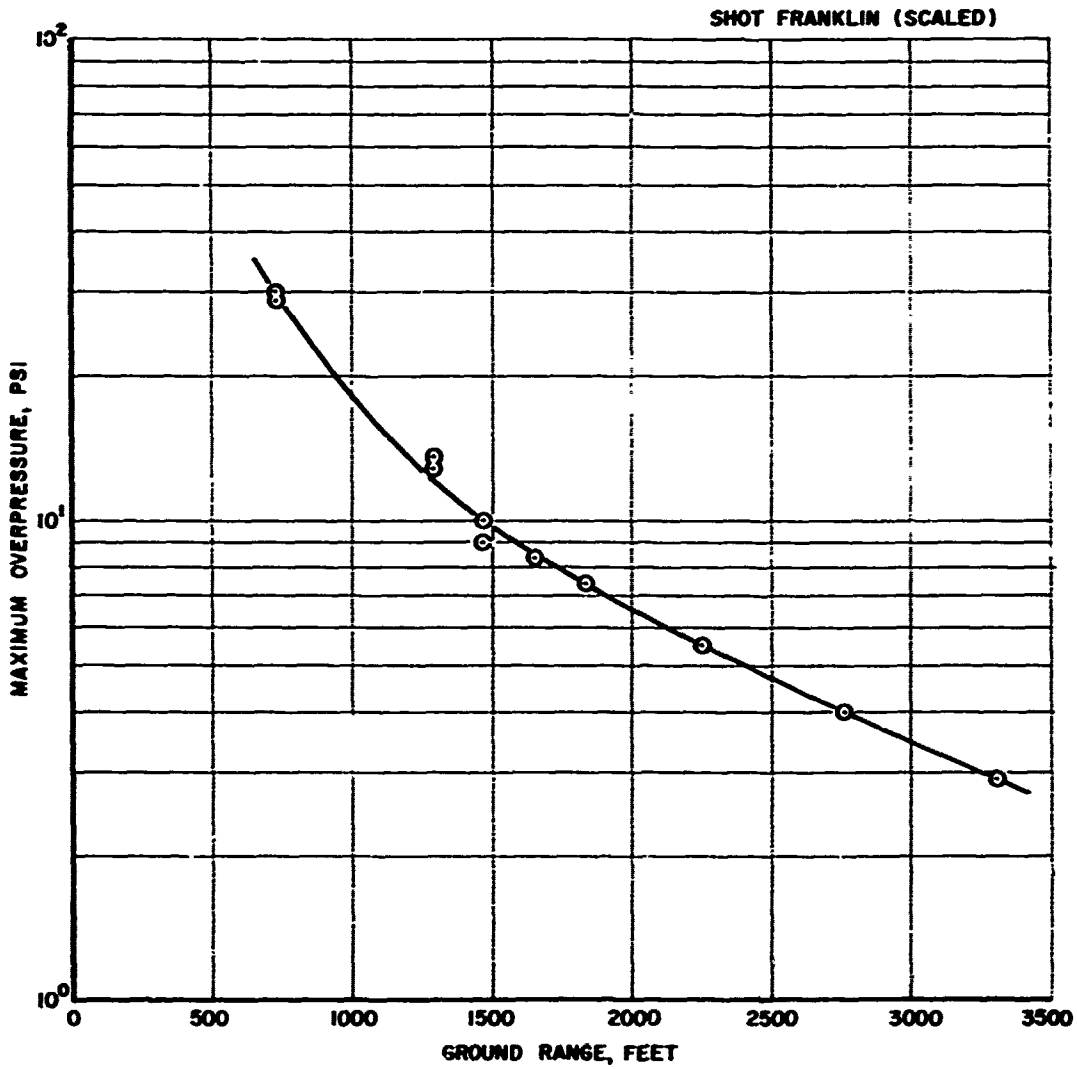

Figure 2.86 Maximum overpressure-distance versus ground range, scaled to 1 kt, Shot Franklin.

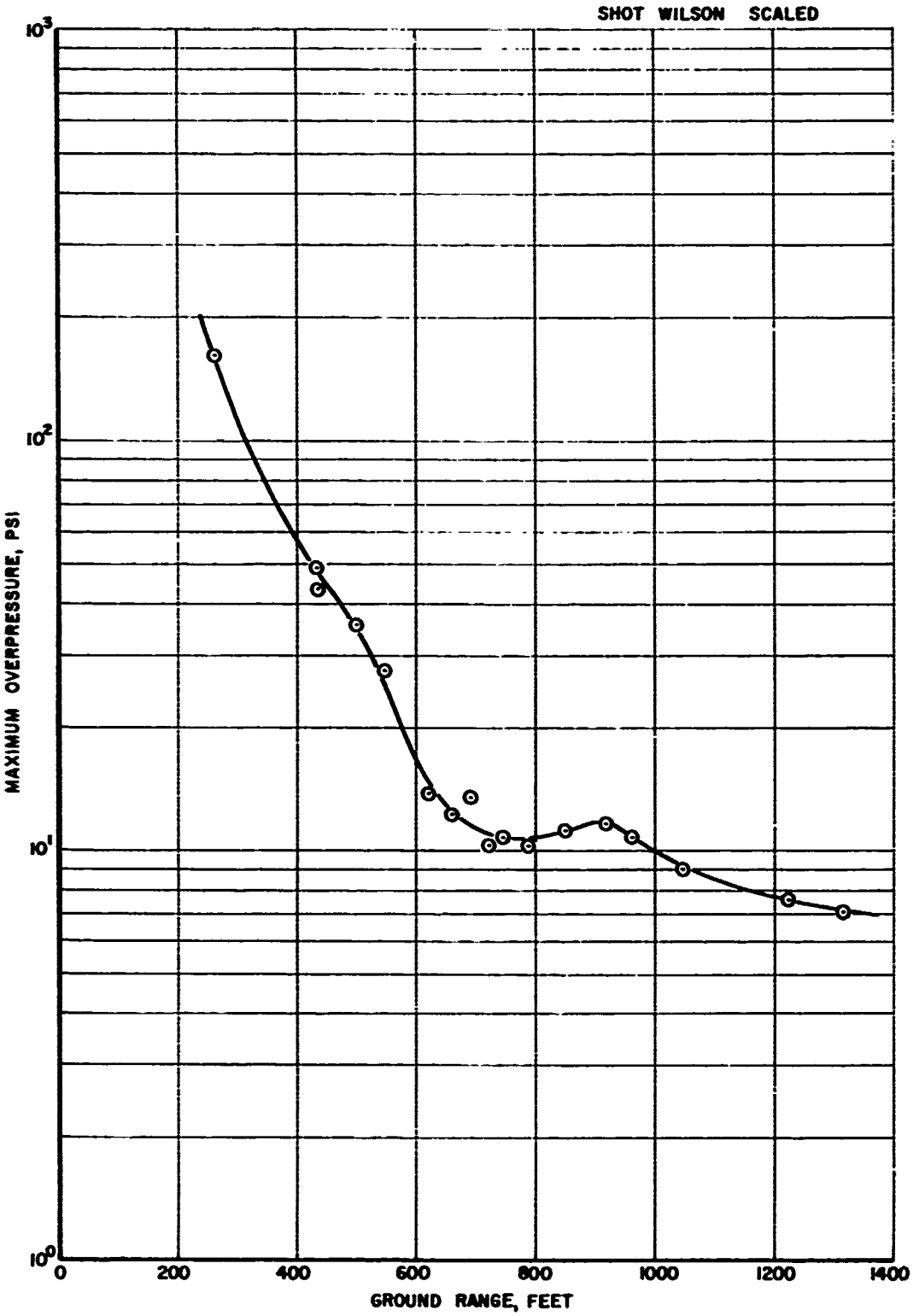

Figure 2.87 Maximum overpressure-distance versus ground range, scaled to 1 kt, Shot Wilson.

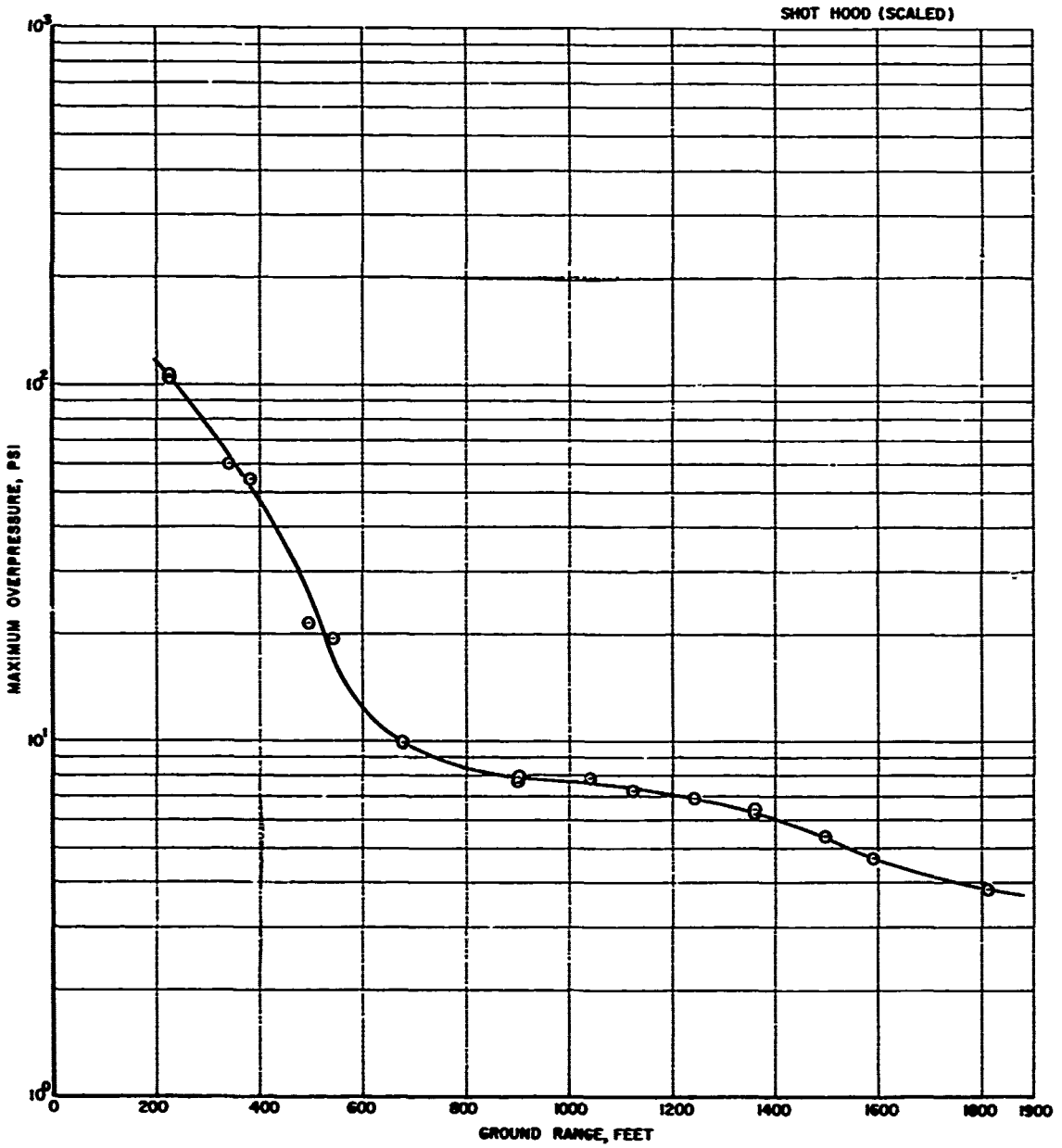

Figure 2.88 Maximum overpressure-distance versus ground range, scaled to 1 kt, Shot Hood.

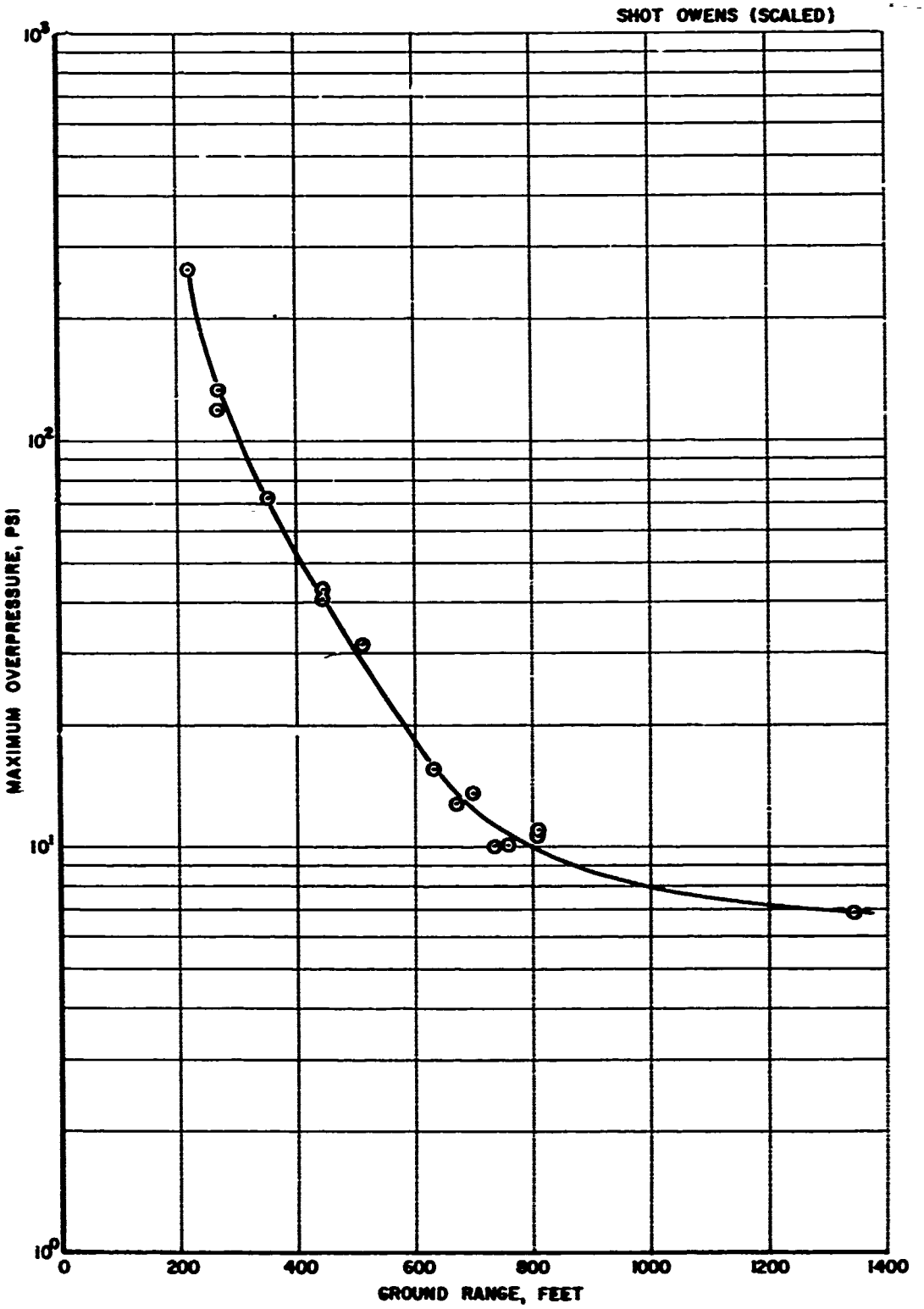

Figure 2.89 Maximum overpressure-distance versus ground range, scaled to 1 kt, Shot Owens.

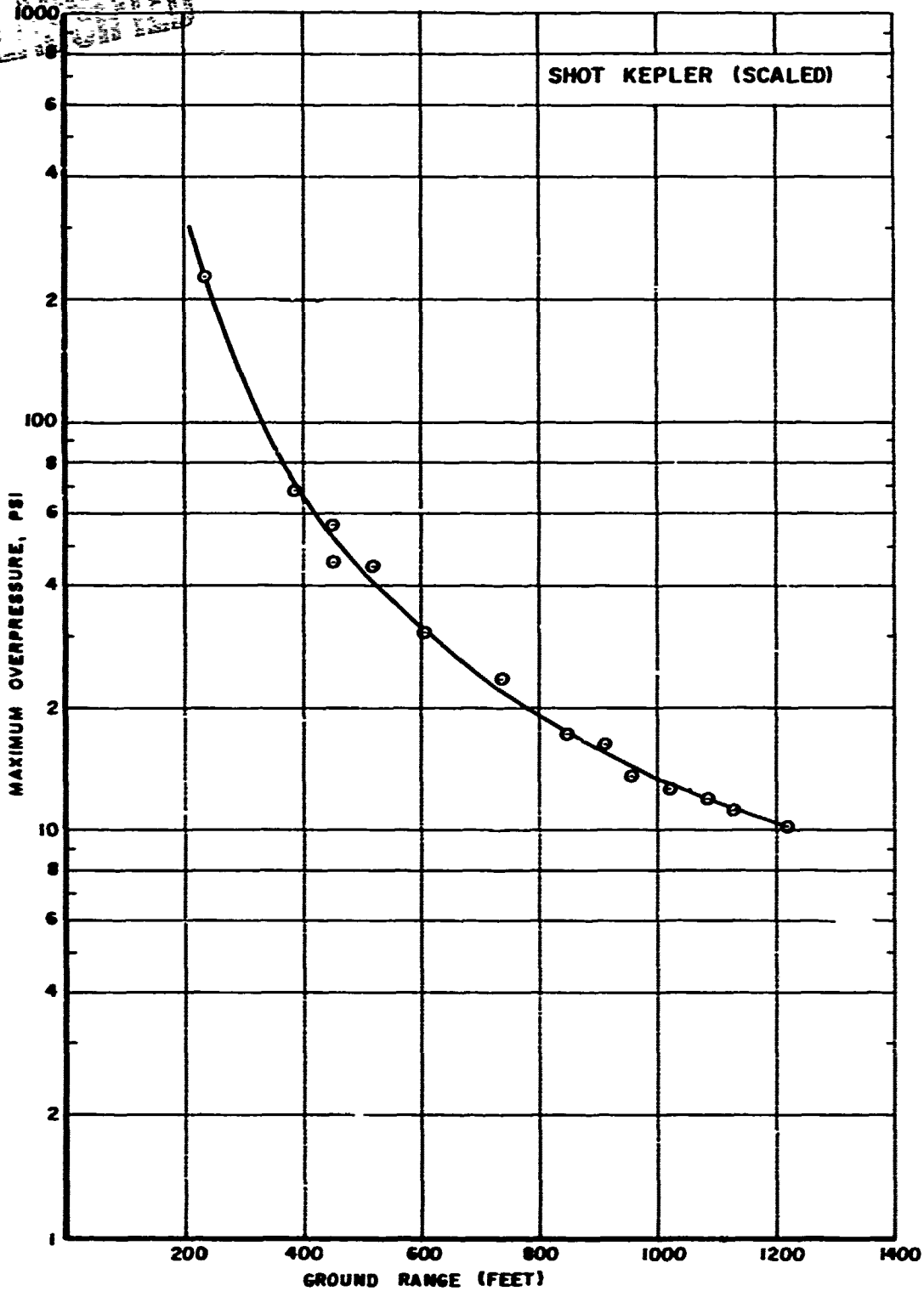

Figure 2.90 Maximum overpressure-distance versus ground range, scaled to 1 kt, Shot Kepler.

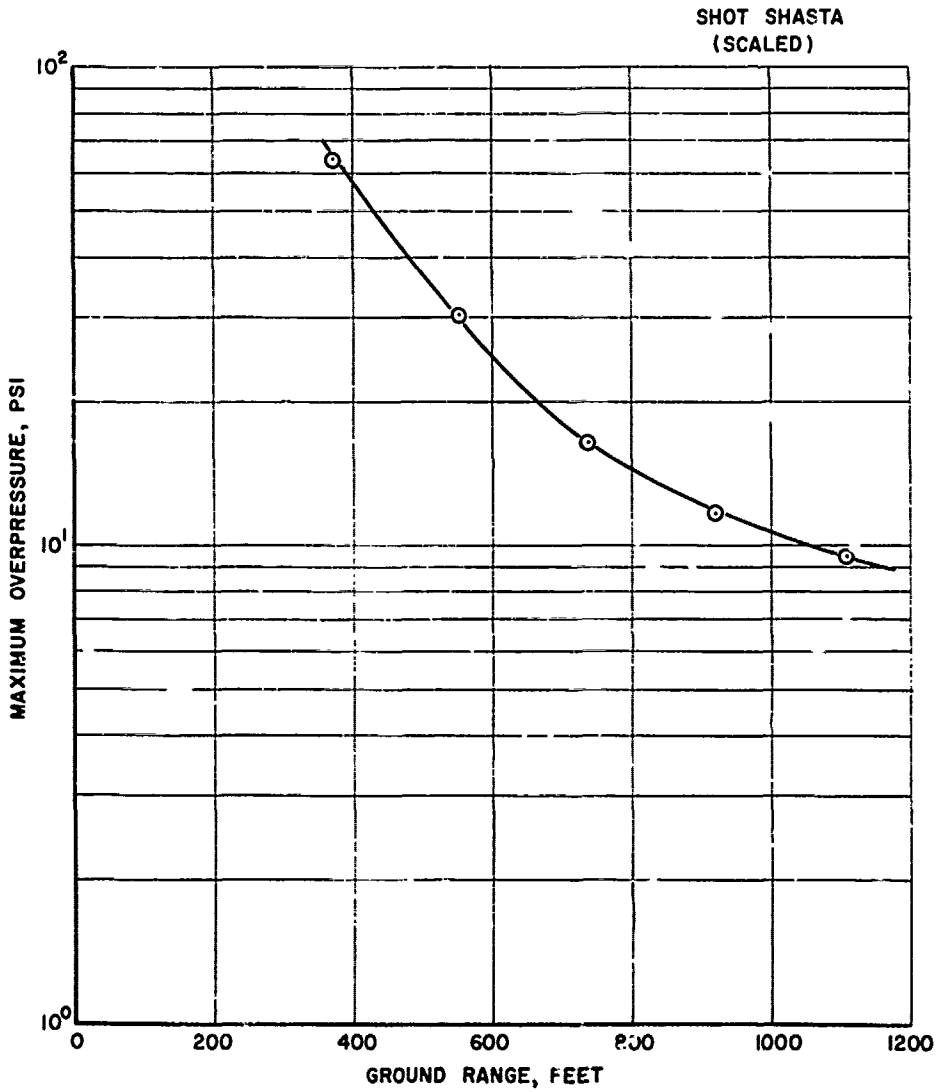

Figure 2.01 Maximum overpressure-distance versus ground range, scaled to 1 kt, Shot Shasta.

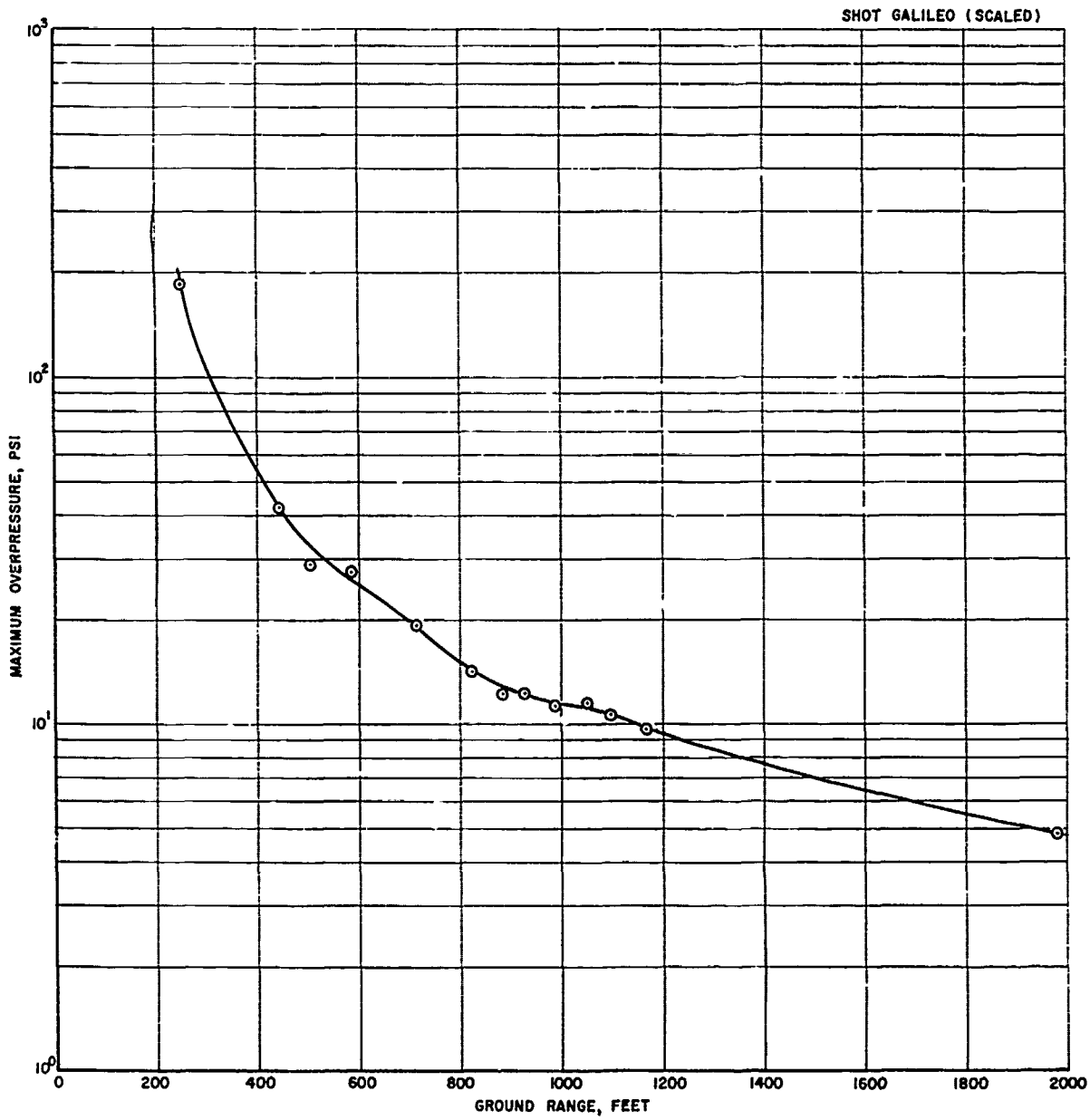

Figure 2.92 Maximum overpressure-distance versus ground range, scaled to 1 kt, Shot Galileo.

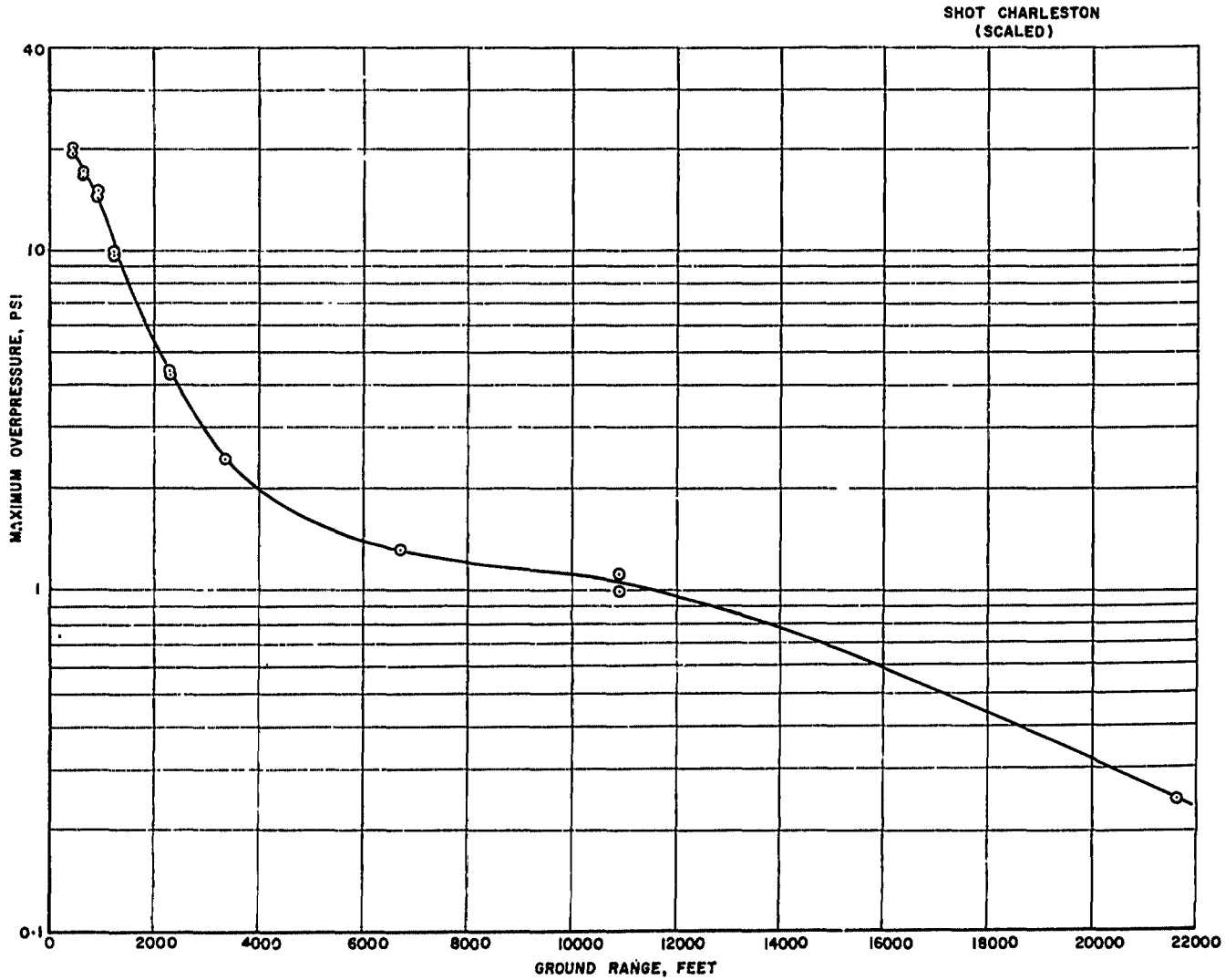

Figure 2.93 Maximum overpressure-distance versus ground range, scaled to 1 kt, Shot Charleston.

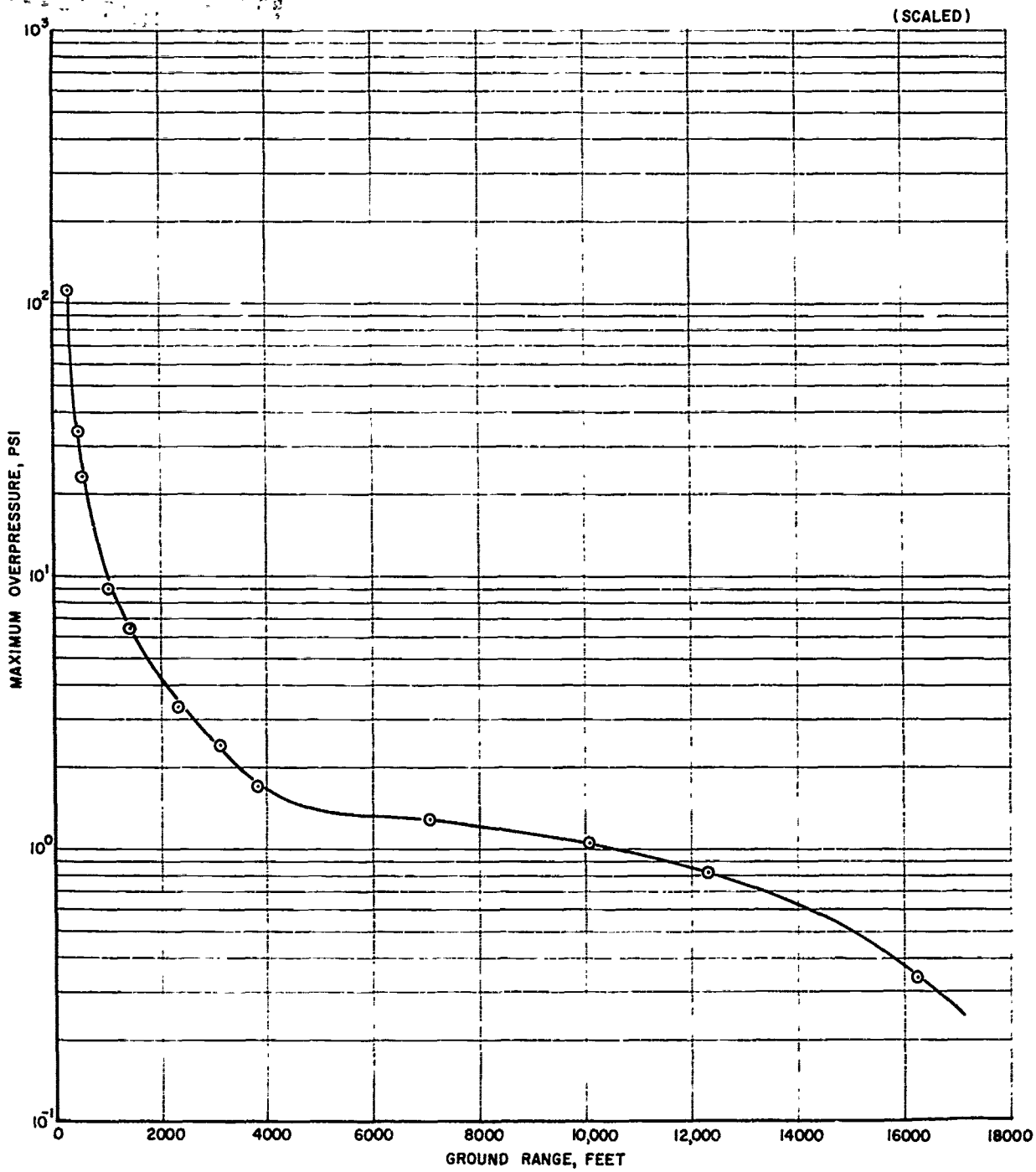

Figure 2.94 Maximum overpressure-distance versus ground range, scaled to 1 kt, Shot Morgan.

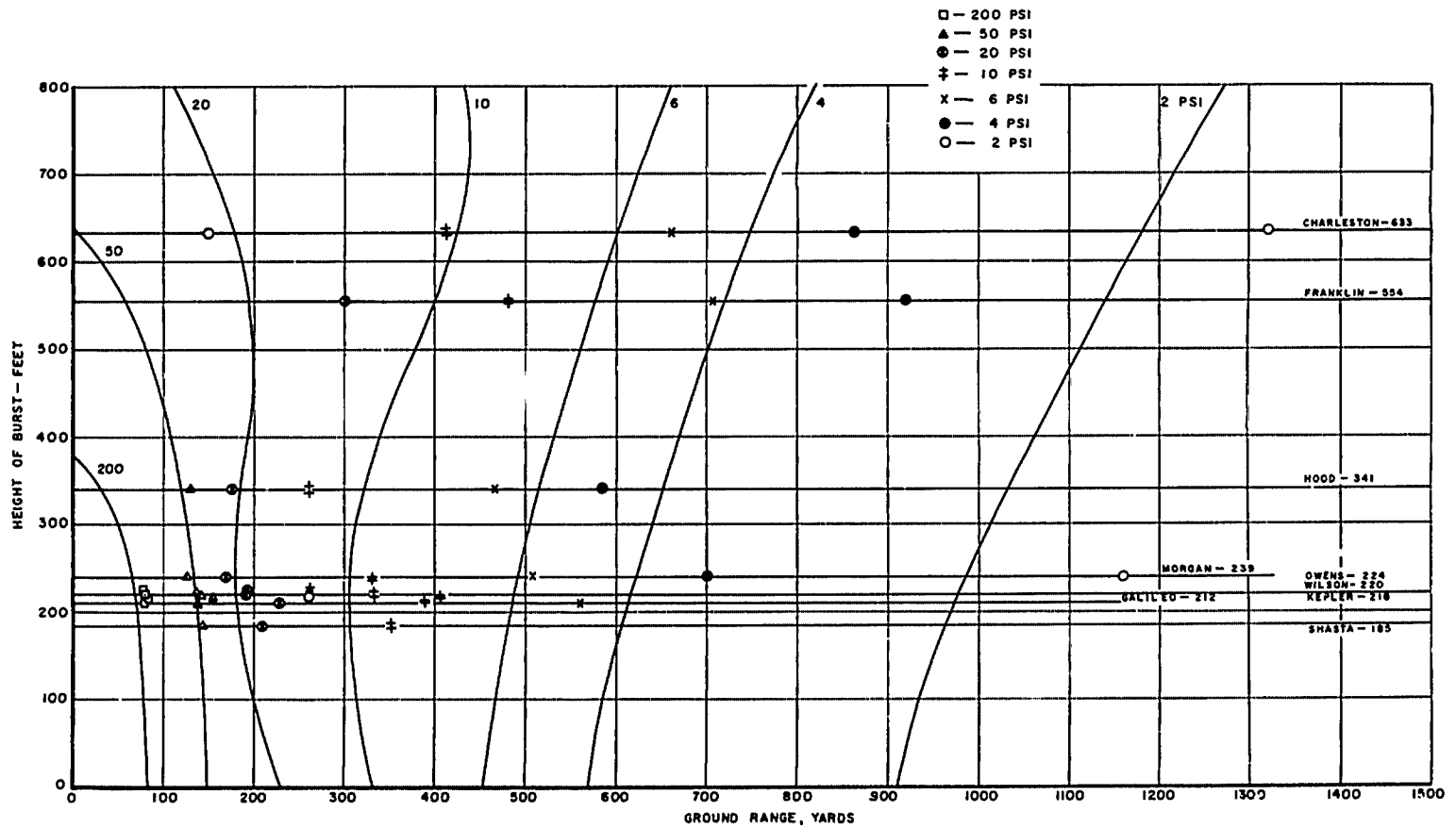

Figure 2.95 Height-of-burst curves versus ground range for isopressure contours.

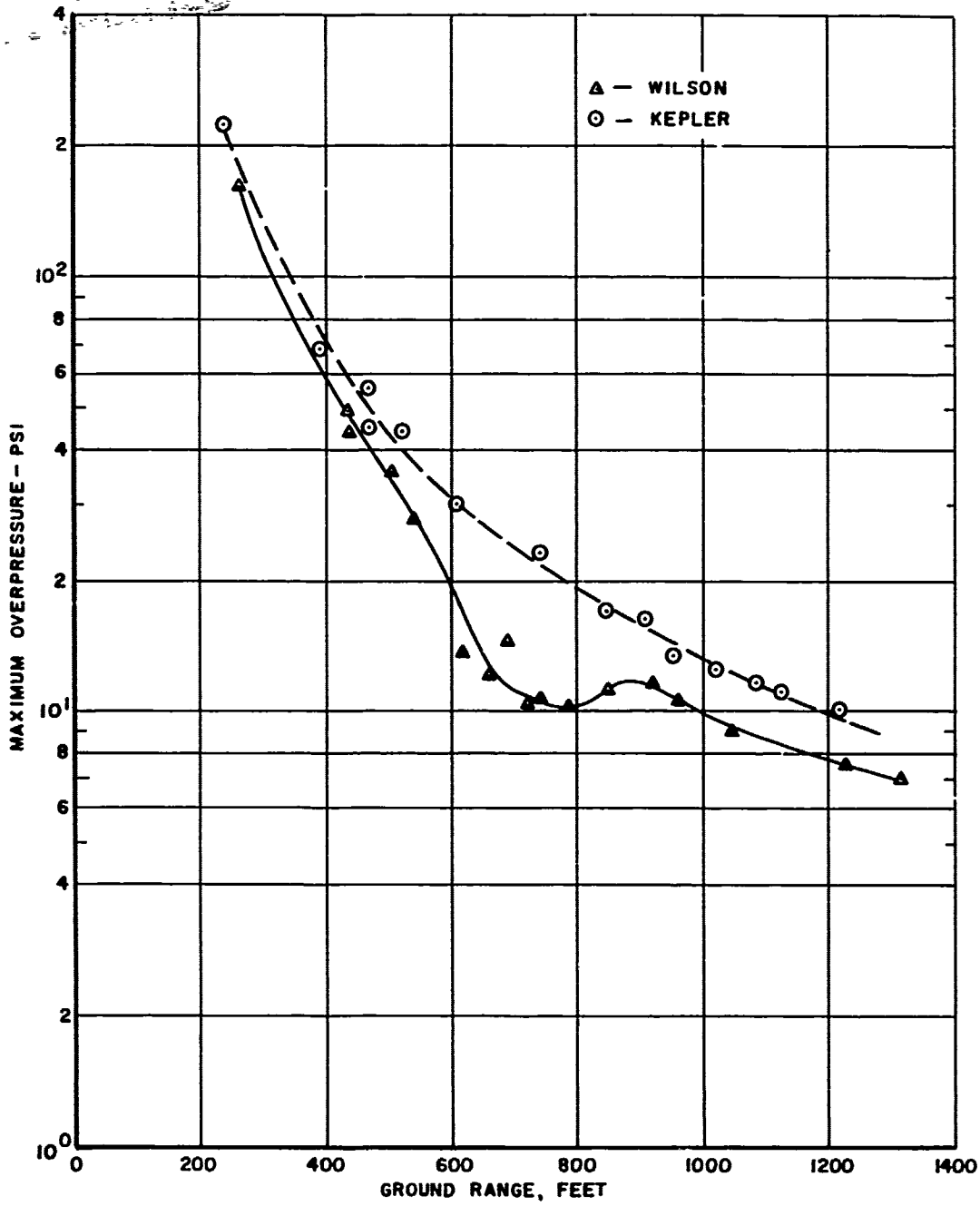

Figure 2.96 Comparison of overpressure, Shots Wilson and Kepler.

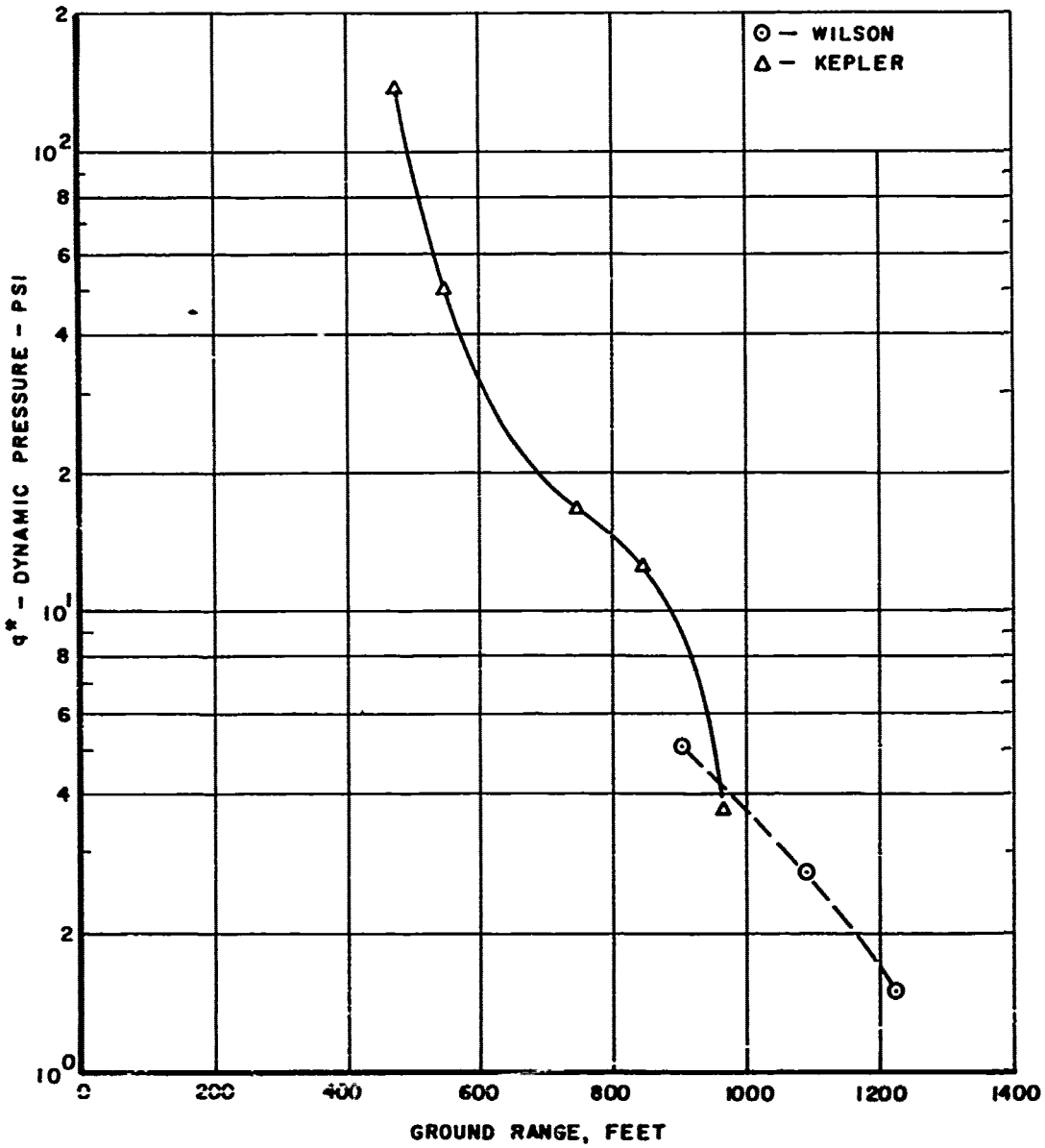

Figure 2.97 Comparison of dynamic pressure versus ground range, Shots Wilson and Kepler.

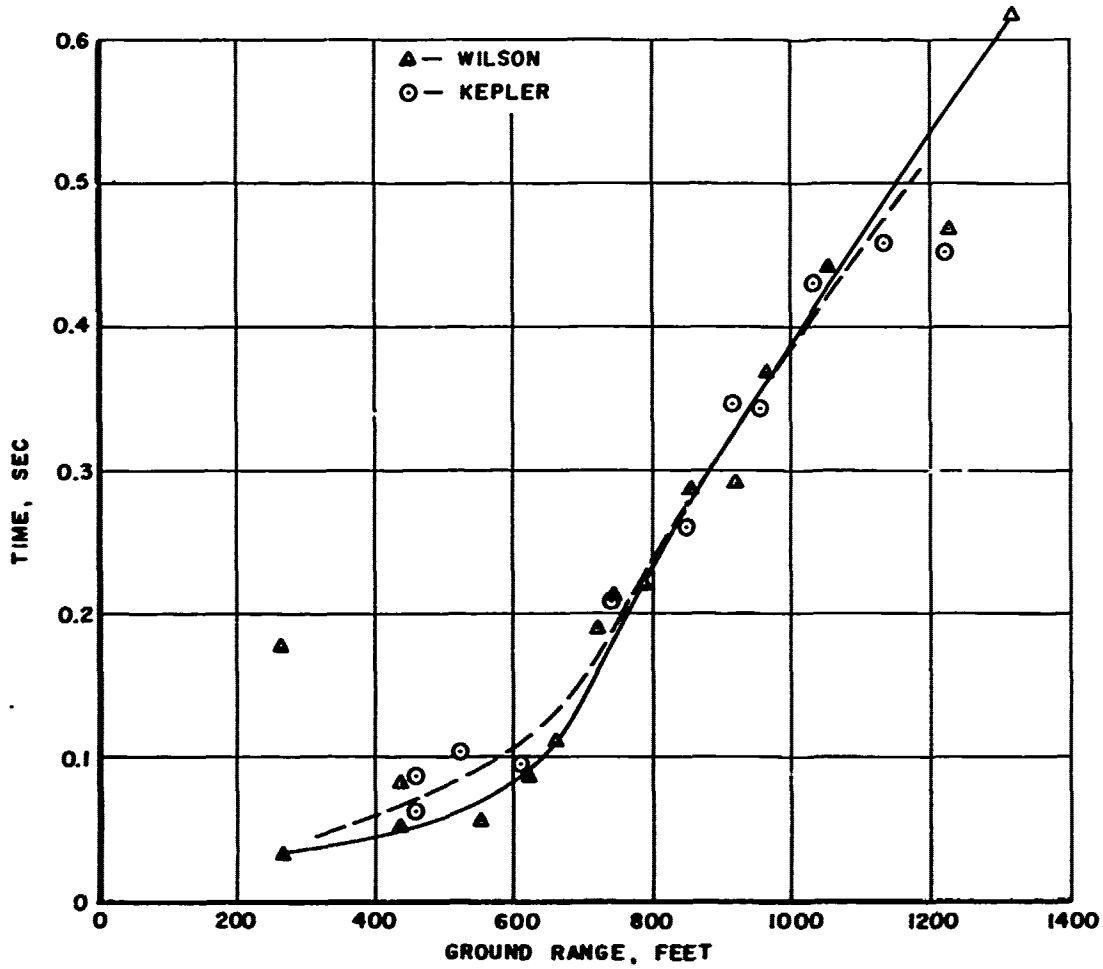

Figure 2.98 Comparison of arrival time versus ground range, Shots Wilson and Kepler.

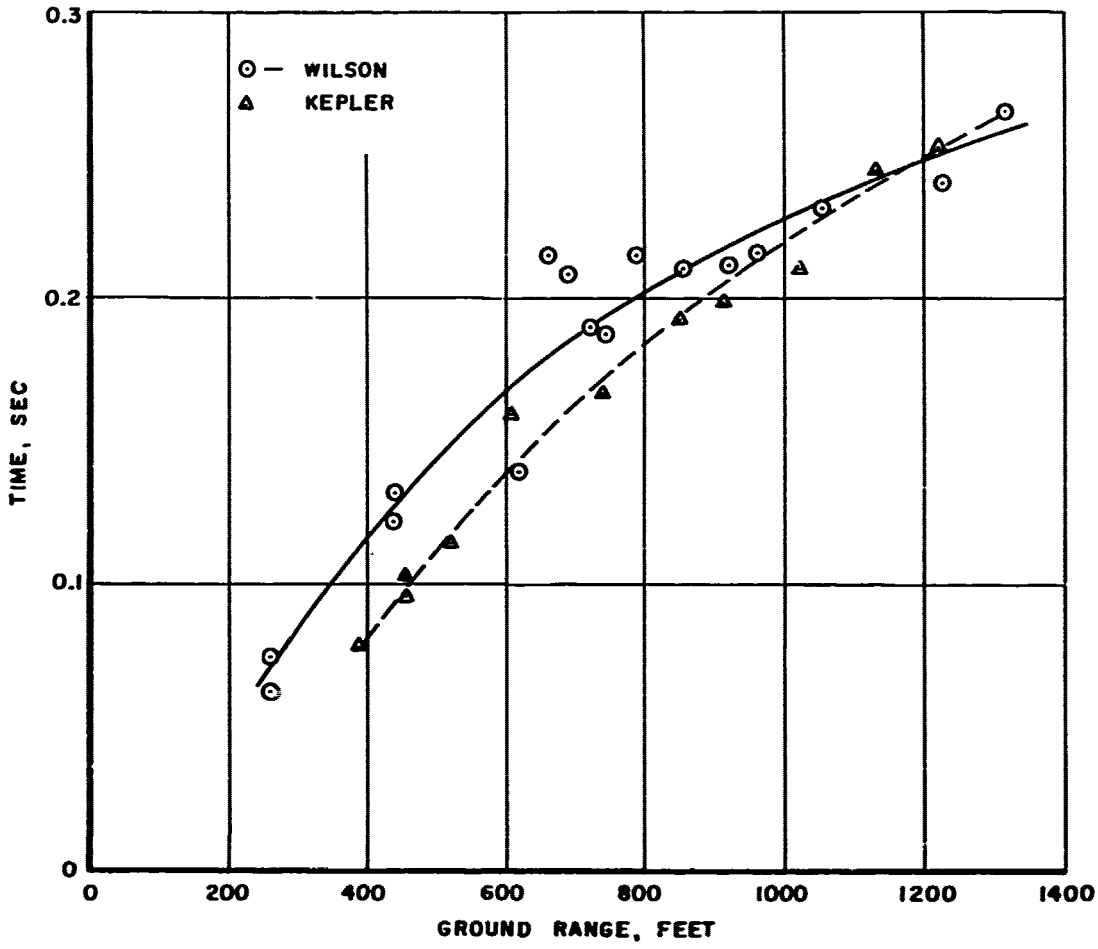

Figure 2.99 Comparison of positive duration versus ground range, Shots Wilson and Kepler.

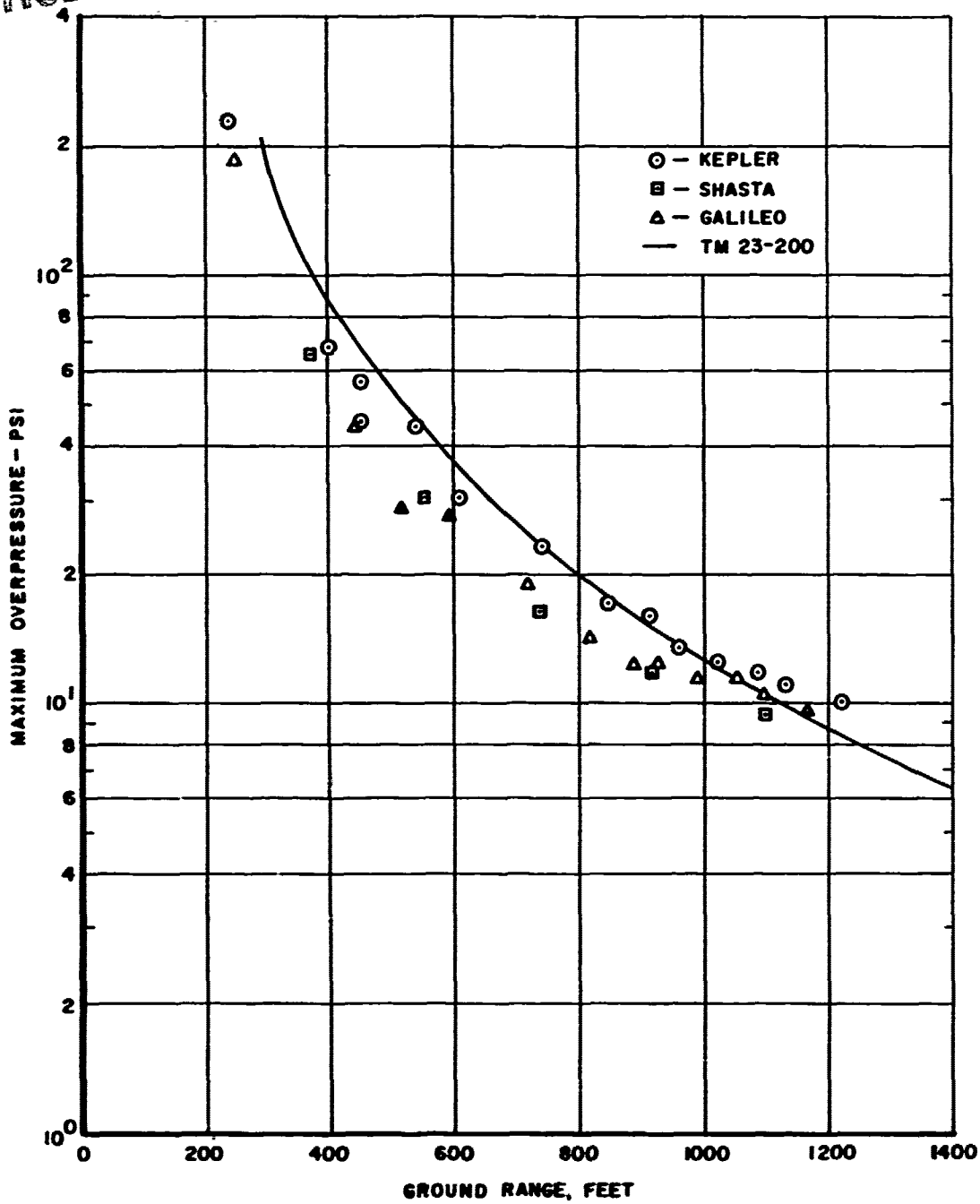

Figure 2.100 Comparison of overpressure from Shots Kepler, Shasta, and Galileo with the good surface height-of-burst curve of TM 23-200.

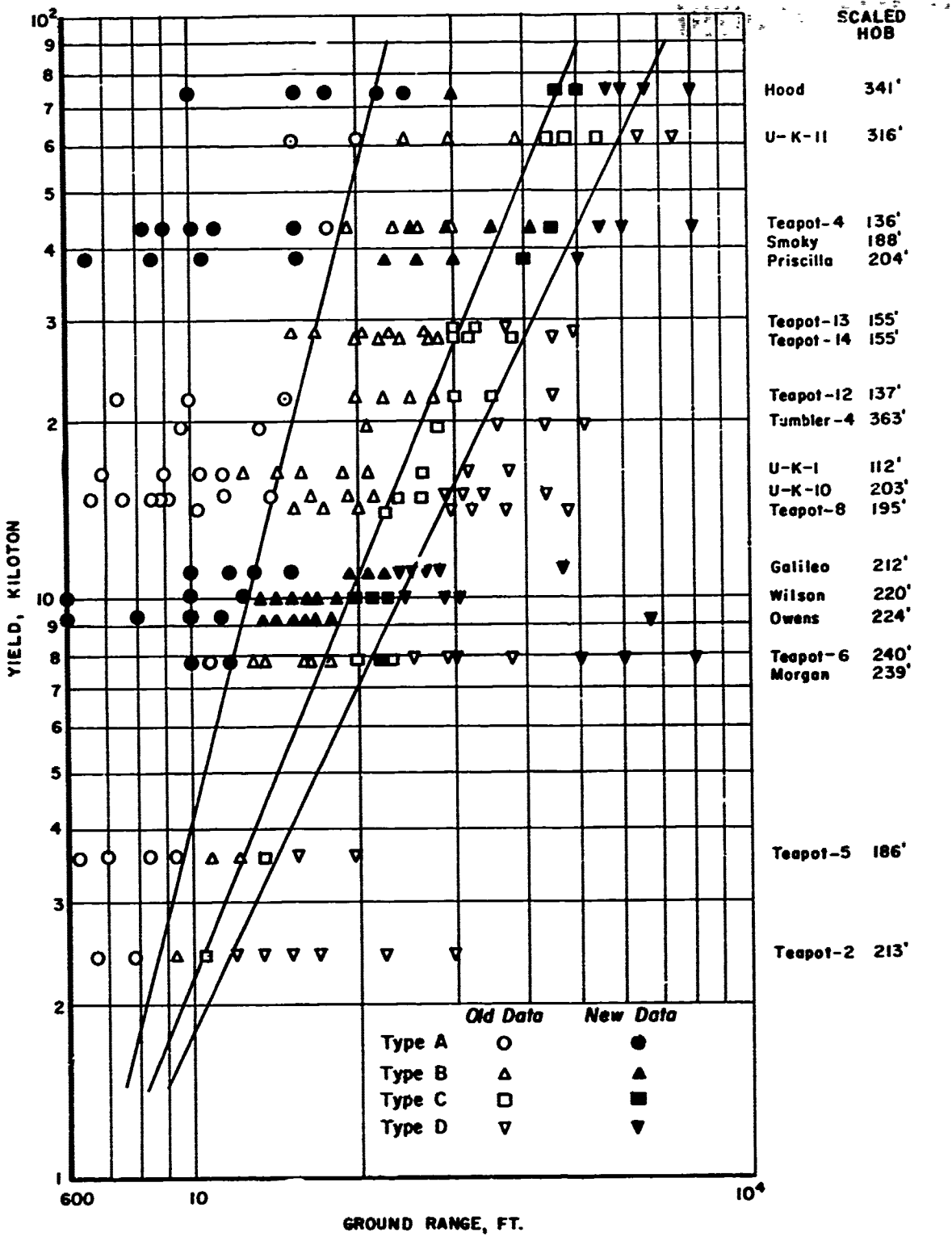

Figure 2.101 Wave types from Plumbbob versus ground distance and yield.

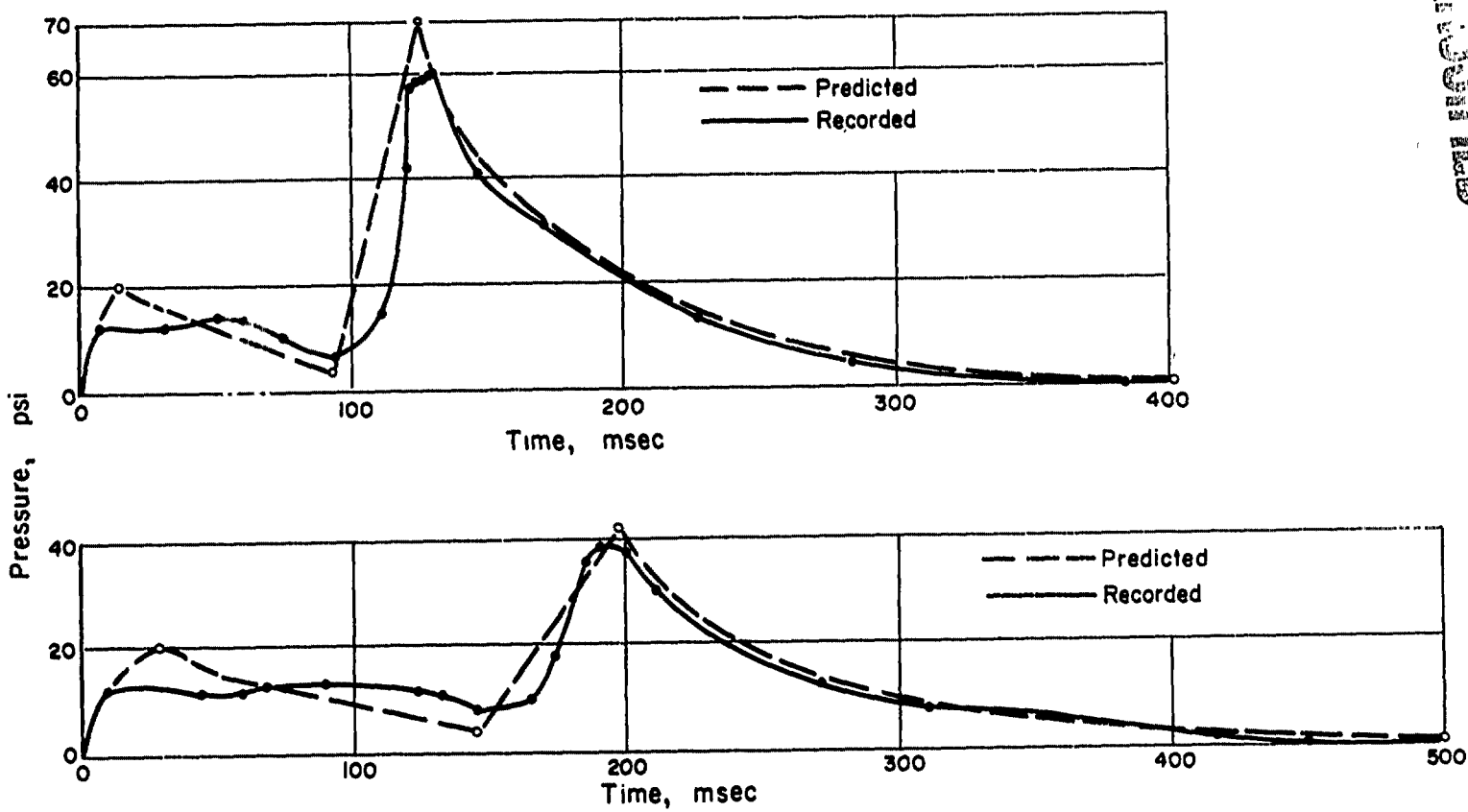

Figure 2.102 Comparison of predicted and measured waveforms, Shot Priscilla.

Chapter 3

BLAST PRESSURE, SHOT JOHN

Measurements of pressure waves at and near ground level resulting from nuclear bursts at high altitude can be used to determine proper scaling methods for overpressure, positive and negative phase durations, and time of arrival. Data from only one shot had been available for checking the procedures for high-altitude bursts. Additional data was required to substantiate the conclusions reached from these limited measurements. Shot John, burst at high altitude, provided some measurements.

3.1 OBJECTIVE

The objective of Project 1.1 was to obtain the overpressure-time history at various positions near and on the ground surface during Shot John. The data obtained was to corroborate further the scaling methods for free-air pressure and to determine the surface reflection of shock waves. The pressure measurements of interest were below the 1-psi region.

3.2 BACKGROUND AND THEORY

From the studies conducted (Reference 18) of a nuclear weapon burst at high altitude, it was shown that the blast efficiency of the detonation will decrease as the altitude of burst increases. A check of this phenomenon would require a blast line located at the same elevation as the burst point in order that the characteristics of shock-wave propagation as a function of distance could be determined through a homogeneous atmosphere. A pressure-distance curve obtained by this means could be compared to a free-air curve obtained from a burst at sea-level conditions to give an indication of the blast efficiency of the device.

As pointed out in Reference 19, measurements of pressure waves at and near the ground surface from a high-altitude shot could be used to check on the scaling laws, provided that the yield, blast efficiency, and free-air curve are known. The measurements taken during Operation Teapot (Reference 19) indicate that the modified Sachs scaling given in Equations 3.1, 3.2, and 3.3 is more appropriate for scaling overpressures, whereas the ordinary Sachs scaling is more appropriate for scaling the time parameters of the pressure wave.

To scale overpressures by modified Sachs scaling (Reference 20) from ambient pressure conditions at which measurements were taken to sea-level conditions, the following apply:

$$P_{so} = P_{sa}\left(\frac{P_o}{P_a}\right) \tag{3.1}$$

and the distance scaled to 1 kt at sea level is:

$$R_o = R_a\left(\frac{P_a}{P_o W}\right)^{1/3} \tag{3.2}$$

The time duration of the blast wave is scaled in accordance with the following:

$$t_o = t_a \left(\frac{P_a}{P_o W}\right)^{1/3} \left(\frac{T_a}{T_o}\right)^{1/2} \tag{3.3}$$

Where: P_s = overpressure
P = ambient pressure
R = slant distance
W = yield of weapon
t = time, duration of blast wave
T = absolute temperature

and the subscripts a and o refer to conditions at point of measurement and at sea level, respectively.

The ordinary Sachs scaling (Reference 21) for overpressure and time parameters of the shock wave take the same form, but P_a and T_a now are the ambient conditions at burst height.

3.3 PROCEDURE

The gages employed for measurement of the blast wave were self-recording very-low-pressure (VLP) gages (Reference 4). Basically, the VLP gage contains a diaphragm with a stylus attached to the center and a glass disk on which the motion of the diaphragm resulting from the pressure acting thereon is scribed by the stylus. The glass disk is on a turntable driven by a chronometrically governed motor. The initiation of the driving mechanism is accomplished at zero time (time of detonation) by photoelectric means.

Ten VLP gages were used to obtain the desired information. The gages were placed atop five poles 50 feet high and also at surface level. To check on the symmetry of the blast wave front, the gages were placed at ground zero and 10,000 feet from ground zero in four quadrants—north, south, east, and west (Figure 3.1).

3.4 DATA REDUCTION

The procedure for data reduction of the VLP records was similar to that used for P_t-gage records. However, a correction was applied to the VLP records that showed pressure values higher than those reported previously.

Calibration of the VLP gage in the past yielded a curve that showed deflection versus applied pressure. The pressure to the gage was statically applied with enough time lapse between step increases for temperature equilibrium to be reached. The air inside the scaled chamber of the gage then obeys Boyles law, i.e., PV = constant. For the case when the pressure applied is sudden, such as a shock wave, the gas inside the scaled chamber obeys the adiabatic compression law, PV^{γ} = constant. Furthermore, since the ratio of the volume of the scaled chamber to the area of the diaphragm is not large, the pressure inside the chamber was increased appreciably. These factors required that a new technique be devised for calibration of the VLP gage. A complete description of the calibration technique is given in Reference 22. The correction factor to be applied to the past data was determined to be 1×10^{-4} psi/mil deflection.

3.5 RESULTS

Of the 10 VLP gages used, good pressure-time records were obtained on 7, peak

pressures only were obtained on 2, and 1 failed to yield any information. The pressure measurements are given in Table 3.1. Traces of the pressure-time histories are given in Figures 3.2 through 3.5. The oscillations in the initial portion of each wave are due to lack of proper amount of damping. Dotted lines were drawn through these oscillations by averaging the top and bottom of each cycle. The maximum pressure was read from the smoothed curve. No attempt was made to determine the time of arrival or the positive duration of the blast wave.

3.6 DISCUSSION

The reflection factors derived from the pressure measurements are listed in Table 3.2. These were determined by calculating the ratio of pressure $(P_4 - P_3)$ to P_2. The P_1 point is shown in Figure 3.6. The average reflection factor was 0.90.

The reflected pressure P_R measured from the surface gage was converted to incident pressure P_1 by use of the relation $P_1 = P_R/1.90$. The value 1.90 was based on the average measured reflection factor of 0.90.

Table 3.3 lists the scaling factors used for the incident pressures at 50 feet and the ground. The scaled values of pressure and slant range, using the modified Sachs scaling and standard Sachs scaling, are given in Table 3.4. These scaled values are plotted in Figure 3.7 along with the scaled free-air curve from TM 23-200 (Reference 7). From the comparison of the measured scaled values with the free-air curve, the modified Sachs scaled values approach closer to the predicted free-air curve than the standard Sachs scaled values. However, the modified Sachs scaled values themselves do not fit this curve too well.

The predicted free-air curve was constructed based on data derived in Shot HA of Operation Teapot (Reference 19). Curves for Shots HA and John are shown in Figure 3.8. For the Shot HA points, only the SC data was used. In both methods of scaling the pressure, a considerable amount of spread in the data exists. The curves in Figure 3.8 do not indicate which scaling method is best suited for treatment of pressure data. To corrolate either of the scaling methods, additional information is needed. In particular, the information required is the partitioning of energy of detonations at various altitudes or a free-air pressure versus distance curve at co-altitude.

3.7 CONCLUSIONS AND RECOMMENDATIONS

During Shot John, the instrumentation was such that the scaling methods, Sachs or modified Sachs, were neither corroborated nor invalidated. For high-altitude bursts, pressure measurements should be made at co-altitude and lower altitudes for studying the partitioning of energy and propagation of shock waves through a nonhomogeneous atmosphere.

TABLE 3.1 PRESSURE MEASUREMENTS FROM VLP GAGES, SHOT JOHN

Ground Distance	Station	Position	Altitude of Station	Slant Range	Gage No.	P_1 Over-pressure	P_2 Incident Over-pressure	P_3 Minimum Pressure Before Reflection	P_4 Reflected Pressure
feet			feet	feet		psi	psi	psi	psi
774	Intended GZ	Ground	4,280	14,830	1*	0.450	–	–	–
		50-ft pole			5*	0.470	0.240	0.120	0.350
10,760	North	Ground	4,400	18,220	4*	0.410	–	–	–
		50-ft pole			8*	0.280	0.150	0.080	0.210
9,910	East	Ground	4,520	17,640	6†	–	–	–	–
		50-ft pole			9*	0.450	0.230	0.100	0.320
9,230	South	Ground	4,240	17,550	3‡	0.280	–	–	–
		50-ft pole			2‡	–	–	–	–
10,450	West	Ground	4,440	18,000	10*	0.420	–	–	–
		50-ft pole			7*	0.430	0.240	0.090	0.280

* Good pressure-time record.
† No record.
‡ Peak pressure only.

TABLE 3.2 PRESSURE REFLECTION FACTORS

Station	Gage Number	Incident Pressure	$P_4 - P_3$	Reflection Factor
Intended GZ	5	0.240	0.230	0.96
North	8	0.150	0.130	0.87
East	9	0.230	0.220	0.97
West	7	0.240	0.190	0.79
Average				0.90

TABLE 3.3 SCALING FACTORS

Station	Ambient Pressure, mb	Modified Sachs Scaling S_p	Modified Scaling S_d	Sachs S_p	Scaling S_d
Height of Burst	502	–	–	2.018	0.6631
Intended GZ	870	1.167	0.7961	–	–
North	868	1.172	0.7944	–	–
East	860	1.178	0.7934	–	–
South	869	1.166	0.7959	–	–
West	863	1.174	0.7942	–	–

TABLE 3.4 SCALED PRESSURE-DISTANCE DATA, SHOT JOHN

Station	Gage No.	Slant Range	Incident Pressure	Modified Sachs Scaling Slant Range	Modified Sachs Scaling Incident Pressure	Sachs Scaling Slant Range	Sachs Scaling Incident Pressure
		feet	psi	feet	psi	feet	psi
Intended Ground Zero	1	14,830	0.237	11,810	0.277	9,830	0.478
North	5	14,790	0.240	11,770	0.280	9,810	0.484
	4	18,220	0.216	14,470	0.253	12,080	0.436
	8	18,150	0.150	14,420	0.176	12,040	0.303
East	9	17,600	0.230	13,960	0.271	11,670	0.464
South	3	17,550	0.147	13,970	0.171	11,640	0.297
West	10	18,000	0.221	14,300	0.259	11,940	0.446
	7	17,560	0.240	13,950	0.282	11,640	0.484

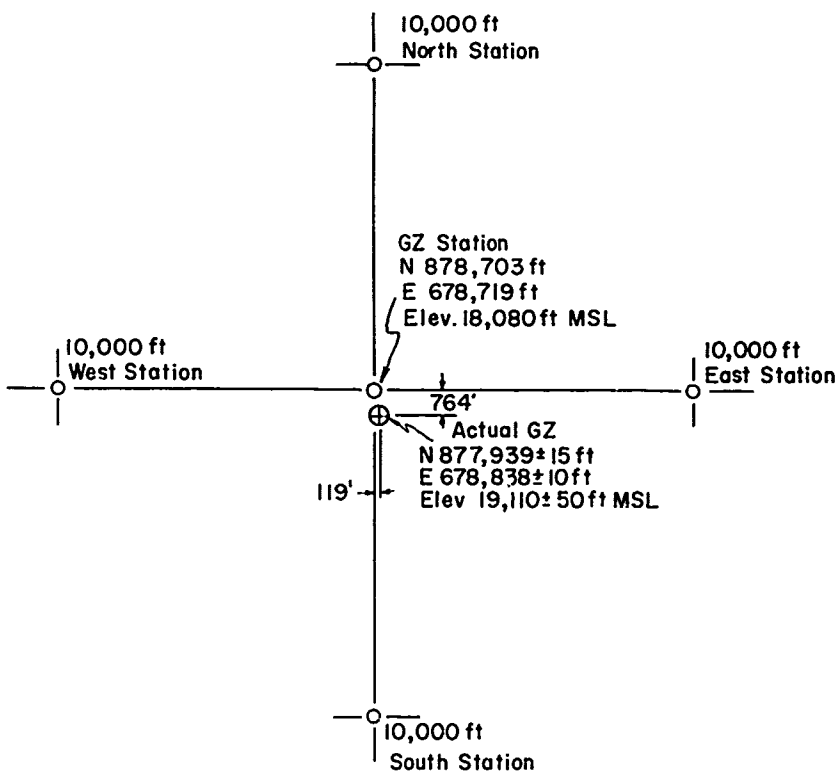

Figure 3.1 Field layout, Shot John.

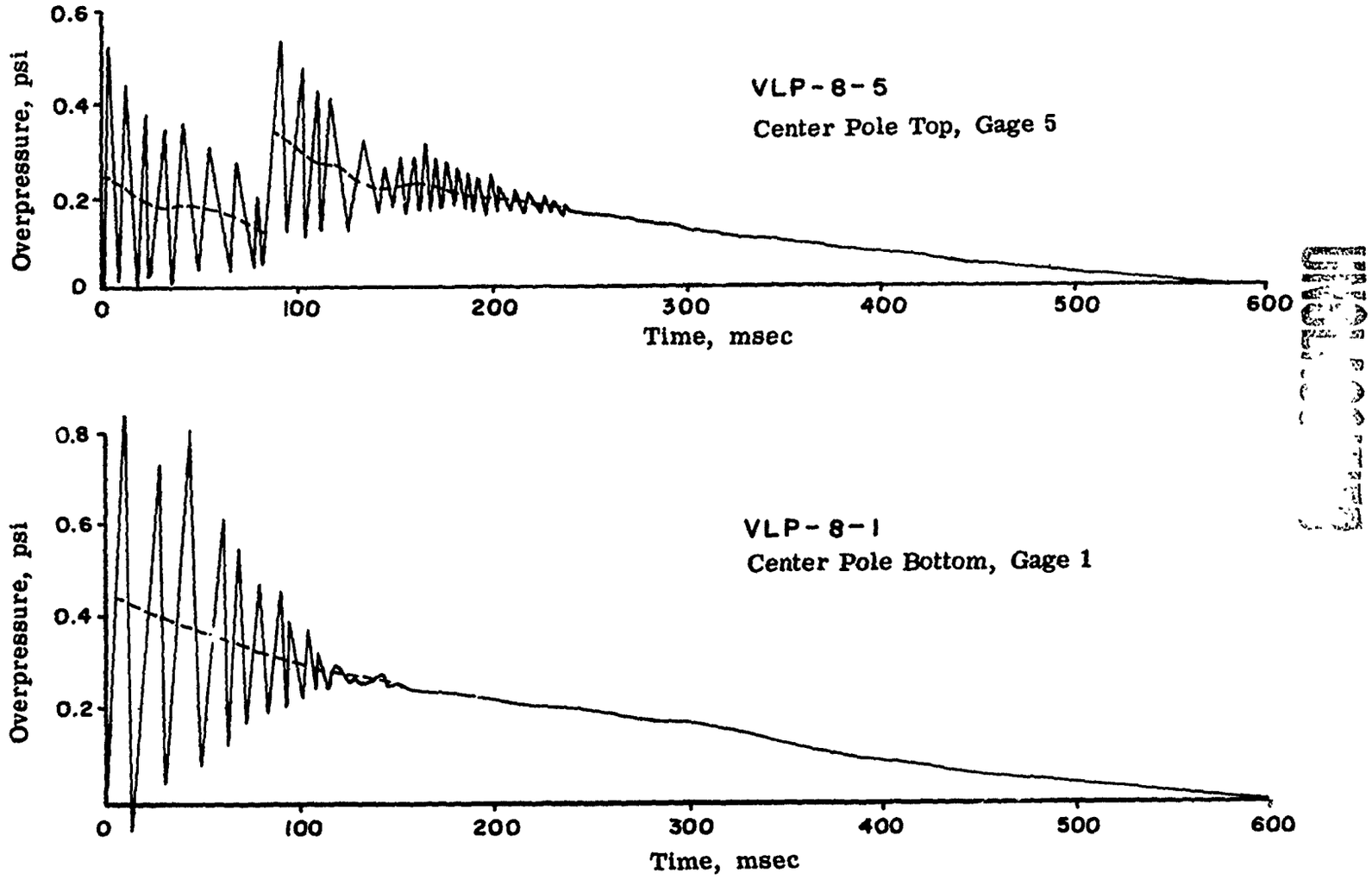

Figure 3.2 Pressure-time histories, VLP gages, ground zero, Shot John.

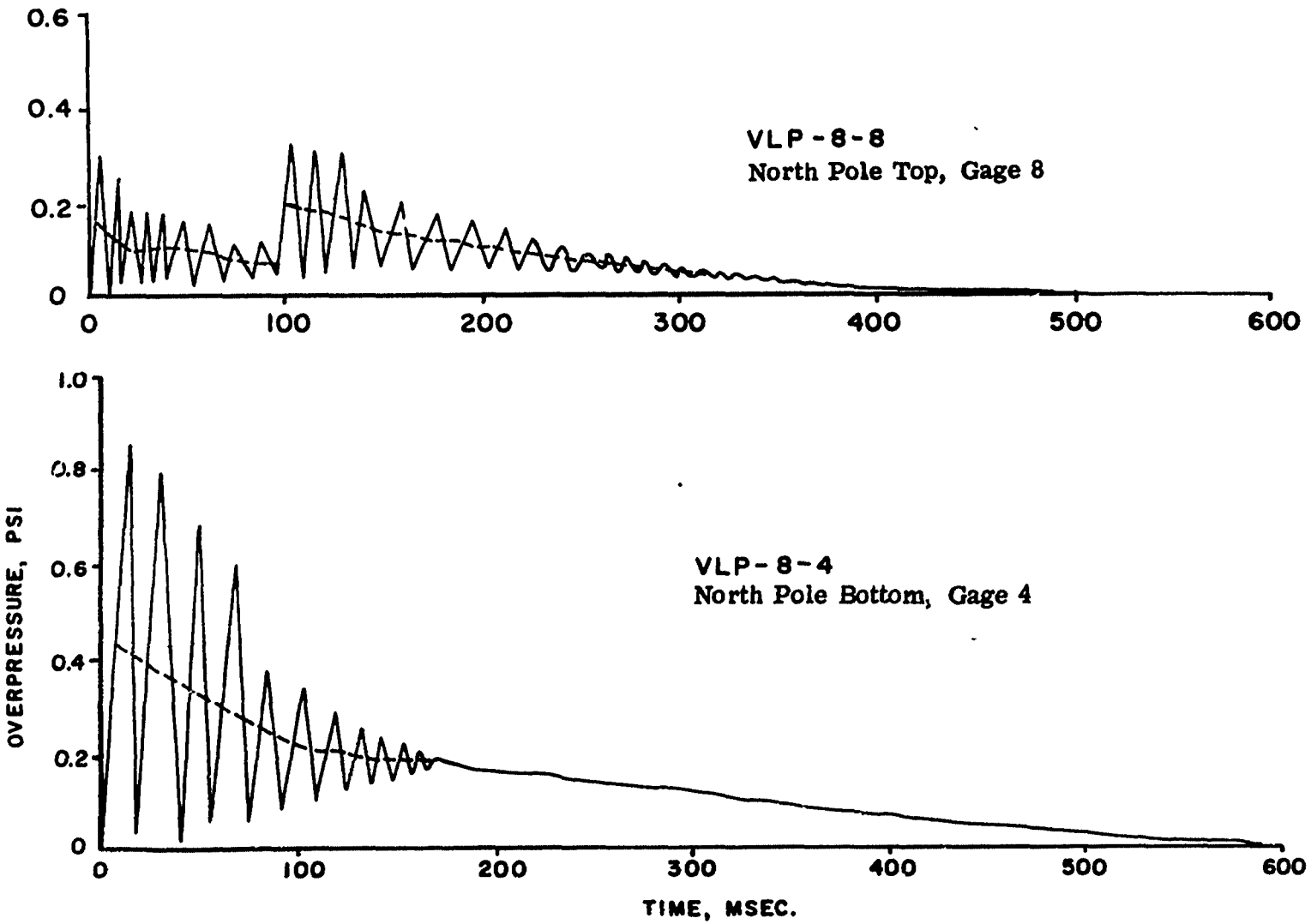

Figure 3.3 Pressure-time histories, VLP gages, north station, Shot John.

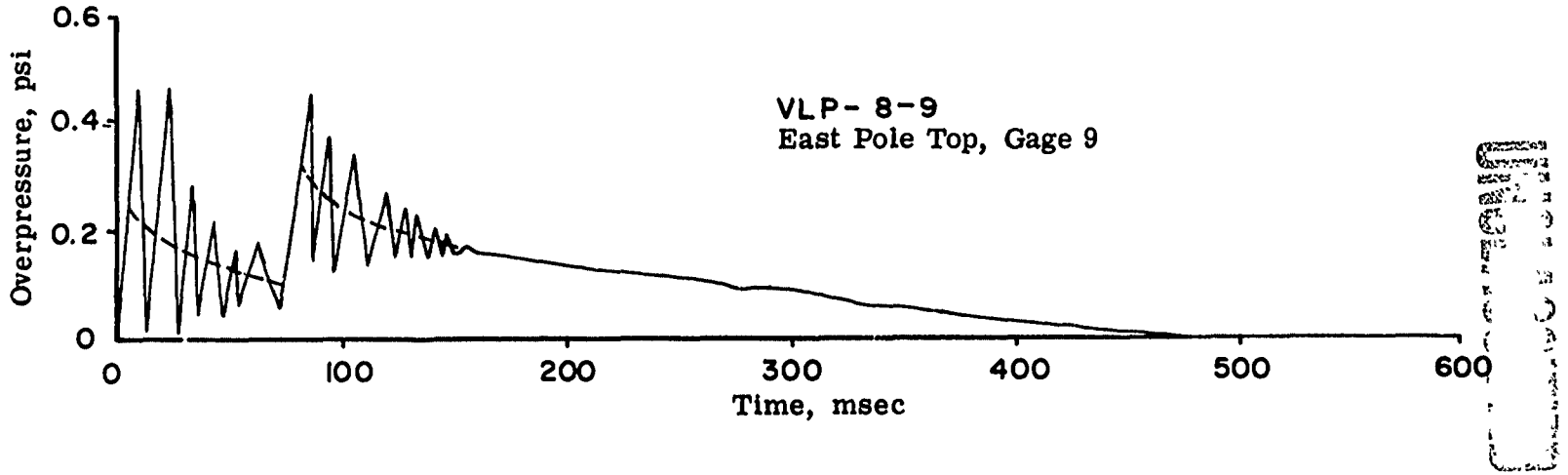

Figure 3.4 Pressure-time history, VLP gage, east station, Shot John.

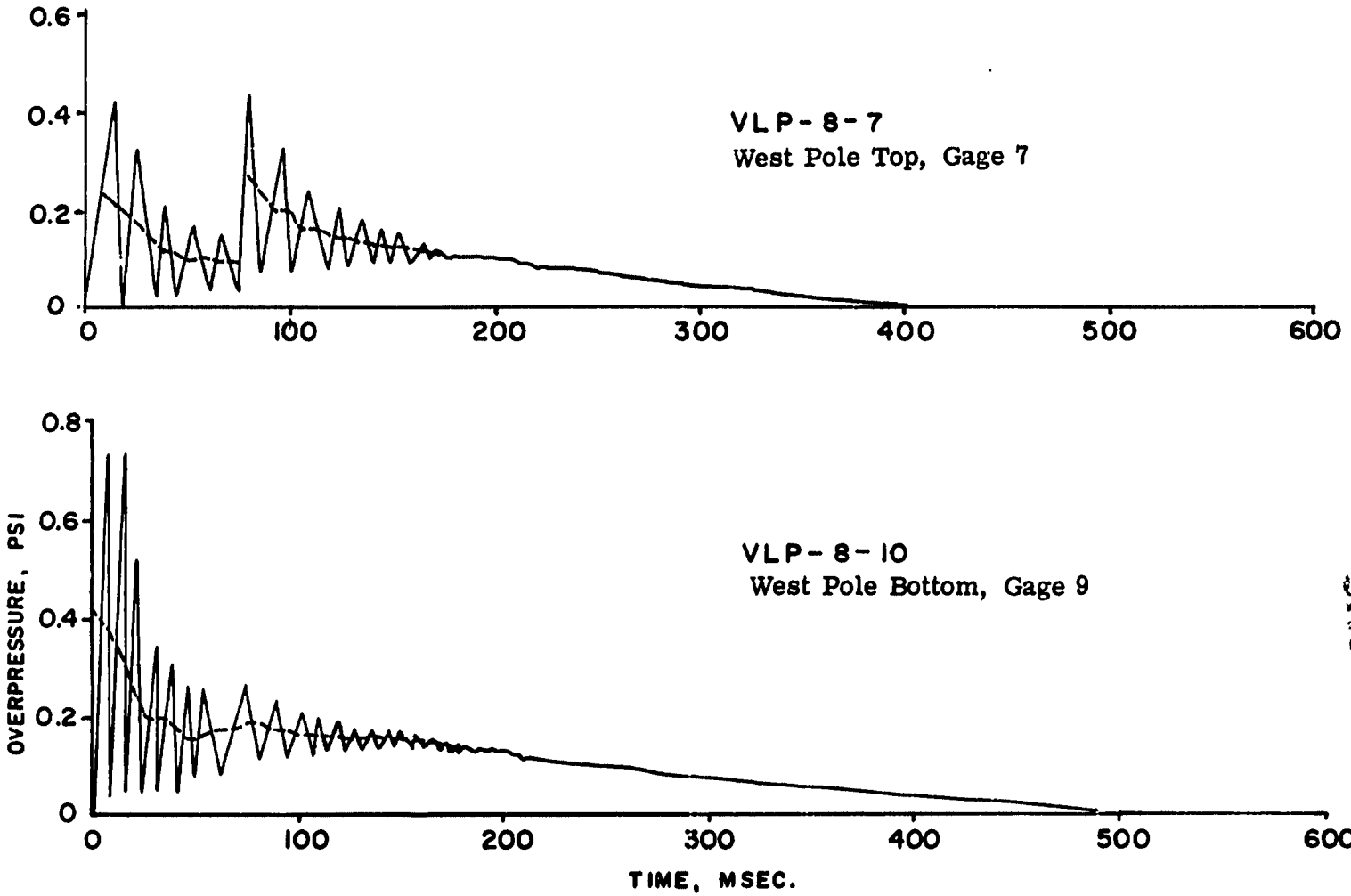

Figure 3.5 Pressure-time histories, VLP gages, west station, Shot John.

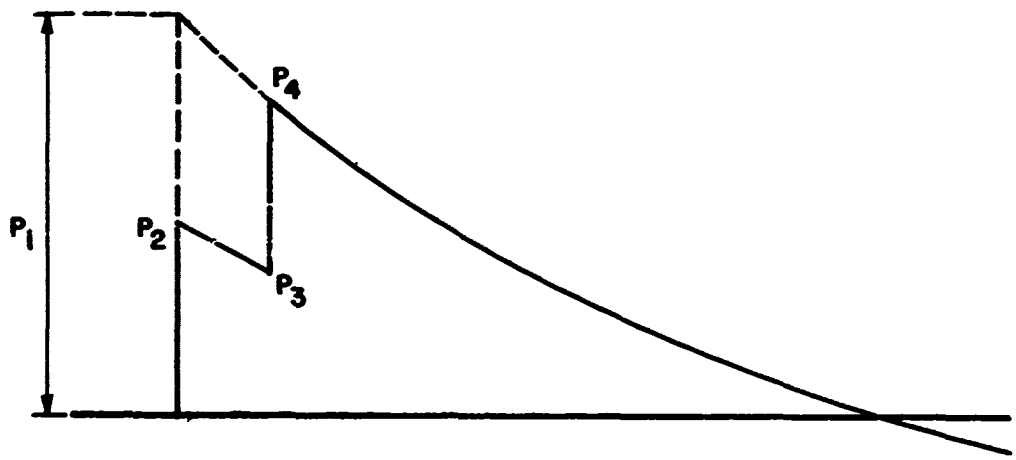

P_1 = reflected ground pressure
P_2 = incident pressure at gage
P_3 = pressure at gage before reflected pressure
P_4 = reflected pressure at gage

Figure 3.6 Pressure-time trace, 50 feet above surface.

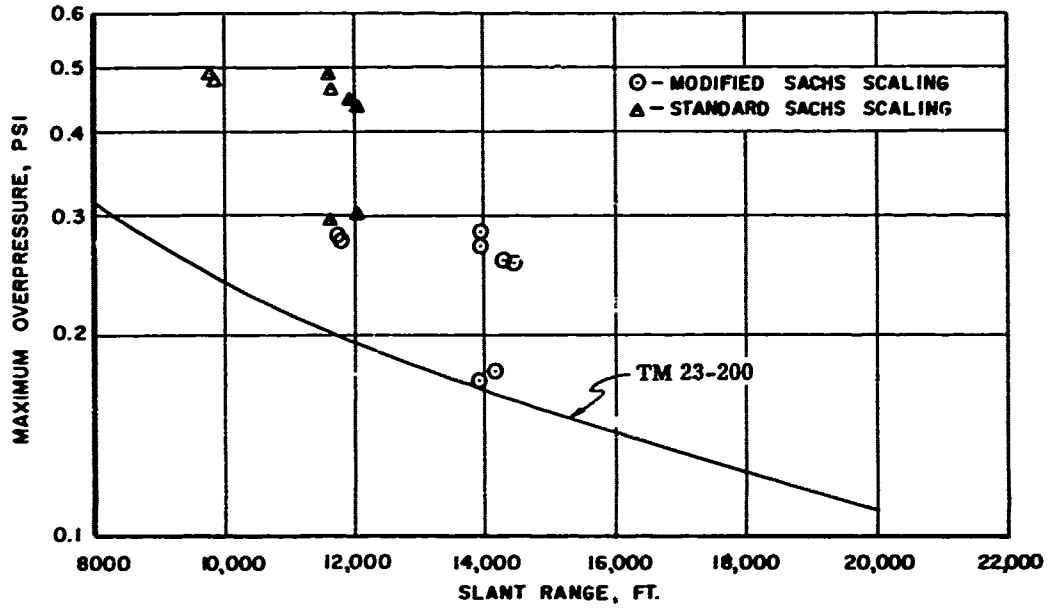

Figure 3.7 Comparison of maximum overpressure versus slant range, Shot John, with predicted curve, standard and modified Sachs scaling.

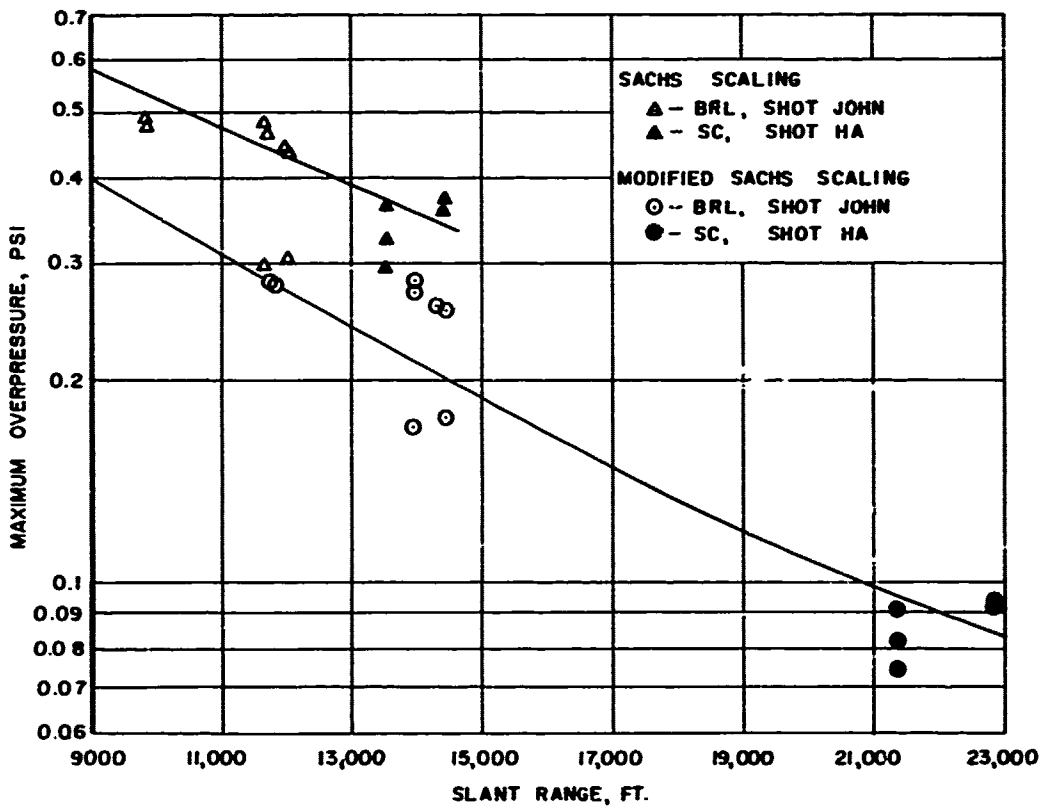

Figure 3.8 Maximum overpressure versus slant range, Shots John and HA, standard and modified Sachs scaling.

Chapter 4

VLP-GAGE MEASUREMENTS

At the beginning of Operation Plumbbob it became apparent, from the number of queries made concerning the predictions of pressure at large distances from the point of burst, that there was a paucity of data for which predictions of pressures could be made with a large degree of reliability. Several agencies were concerned about the effects that the pressures at large distances from point of burst may have on equipment and structures. These pressures were measured to provide the desired information to interested agencies.

4.1 OBJECTIVE

The objective of this portion of Project 1.1 was to obtain the pressure-time history of the blast at large distances from several nuclear bursts.

4.2 PROCEDURE

VLP gages were used for measurement of pressure at large distances from point of burst. The gages and the shots are given in Table 4.1. Some of the gages were used as backup to the instrumentation provided by Project 5.2.

These gages could be initiated either manually or by means of a photoelectric system. The standard method for initiation was manual and consisted of throwing a switch to complete the motor drive circuit and start the recording system. The photoinitiation system was used at stations when it was impossible for personnel to man the gage.

4.3 RESULTS

The shots and the pressure measurements obtained are given in Table 4.1. The distances given in the table are approximate. These were obtained by taking measurements from a map of the area prepared by the Corps of Engineers.

The measured values for all shots were scaled to 1 kt, sea level, and plotted in Figure 4.1. A large spread of the data exists, and the dotted curves indicate the variation in pressure that can be expected. The lack of instrumentation between burst point and location of gage, for determining atmospheric conditions, did not warrant further analysis of the terrain effects on the propagation of the shock waves.

The pressure-time histories of the records are given in Figures 4.2 through 4.8.

4.4 CONCLUSION

A large variation in maximum overpressures at large distances can be expected from nuclear detonations.

TABLE 4.1 VLP GAGE RESULTS

Shot	Station	Gage	Approximate Distance	Maximum Overpressure
			feet	psi
Hood	Radio Station, Yucca Lake	VLP-2	64,500	0.280
	Helicopter Pad	VLP-10	78,000	0.072
Kepler	Command Post	VLP-5	60,750	0.28
Owens	Command Post	VLP-4	73,000	0.085
	Command Post	VLP-5	73,000	0.078
	Airship, Yucca Lake	VLP-6	61,300	0.060
	Airship, Yucca Lake	VLP-9	61,300	–
Stokes	Airship, Yucca Lake	VLP-6	43,200	0.70
	Airship, Yucca Lake	VLP-9	43,200	0.50
Whitney	Command Post	VLP-5	76,800	0.029
Charleston	Yucca Well	VLP-2	51,200	0.31
	Command Post	VLP-8	73,000	0.03
	Mercury Junction, Y	VLP-10	25,900	0.32
Morgan	Yucca Well	VLP-2	51,200	0.28
	Yucca Well	VLP-10	51,200	0.27

[redacted]

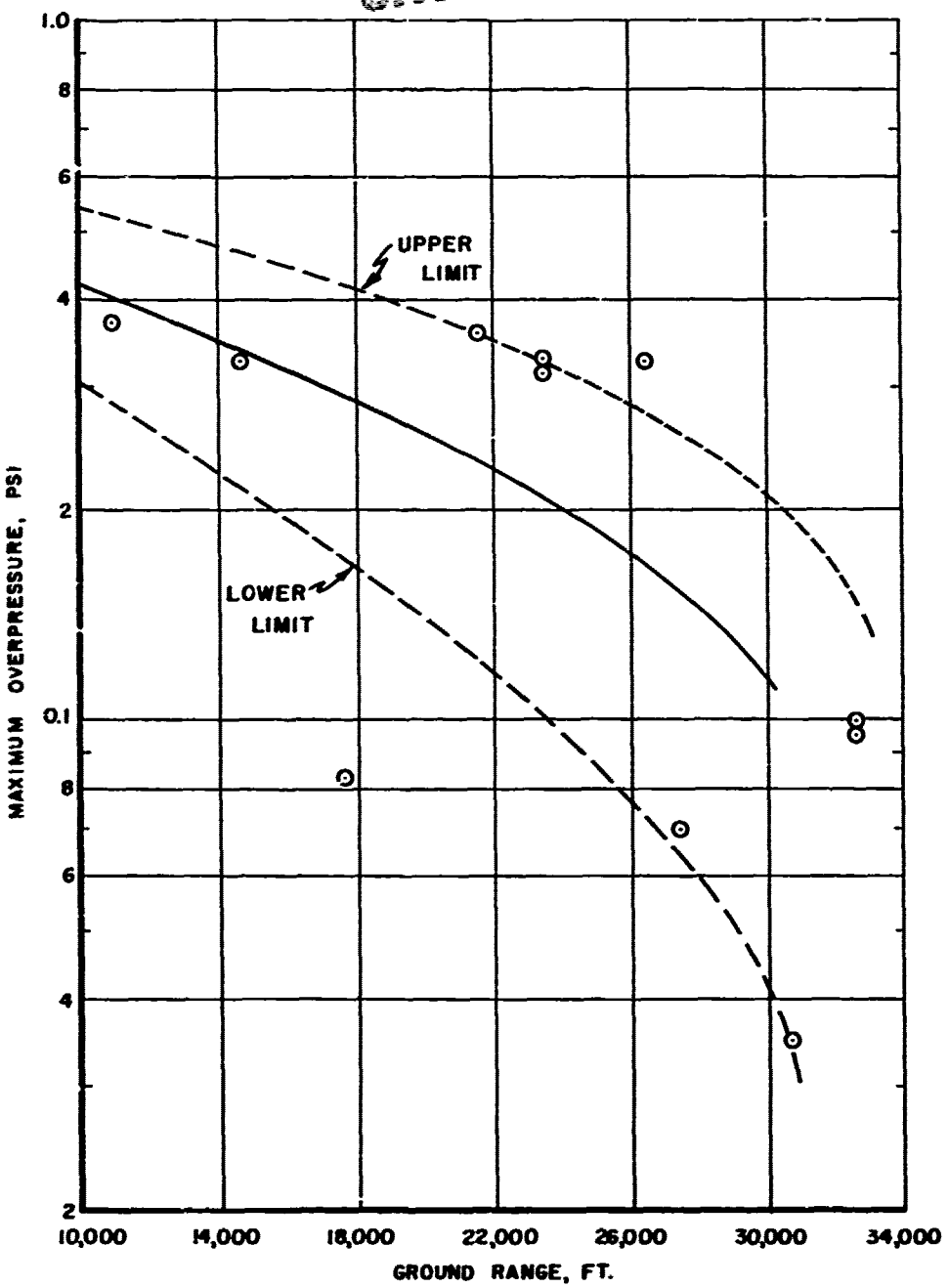

Figure 4.1 Maximum overpressure versus slant range, VLP gages, scaled to 1 kt, modified Sachs.

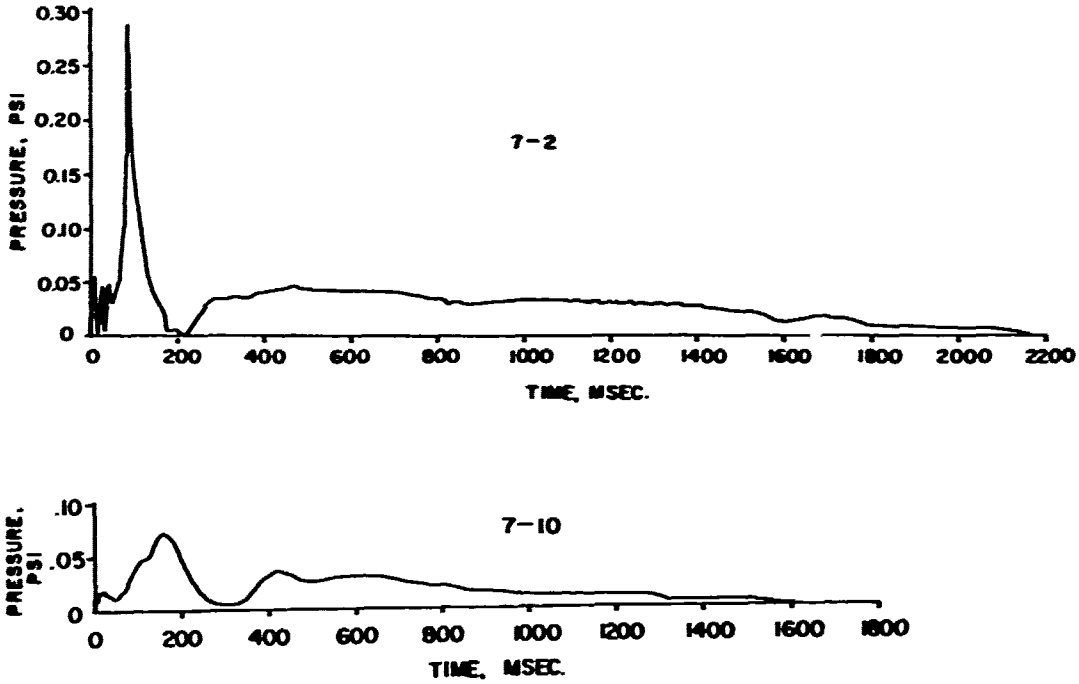

Figure 4.2 Overpressure-time histories, VLP Gages 2 and 10, Shot Hood.

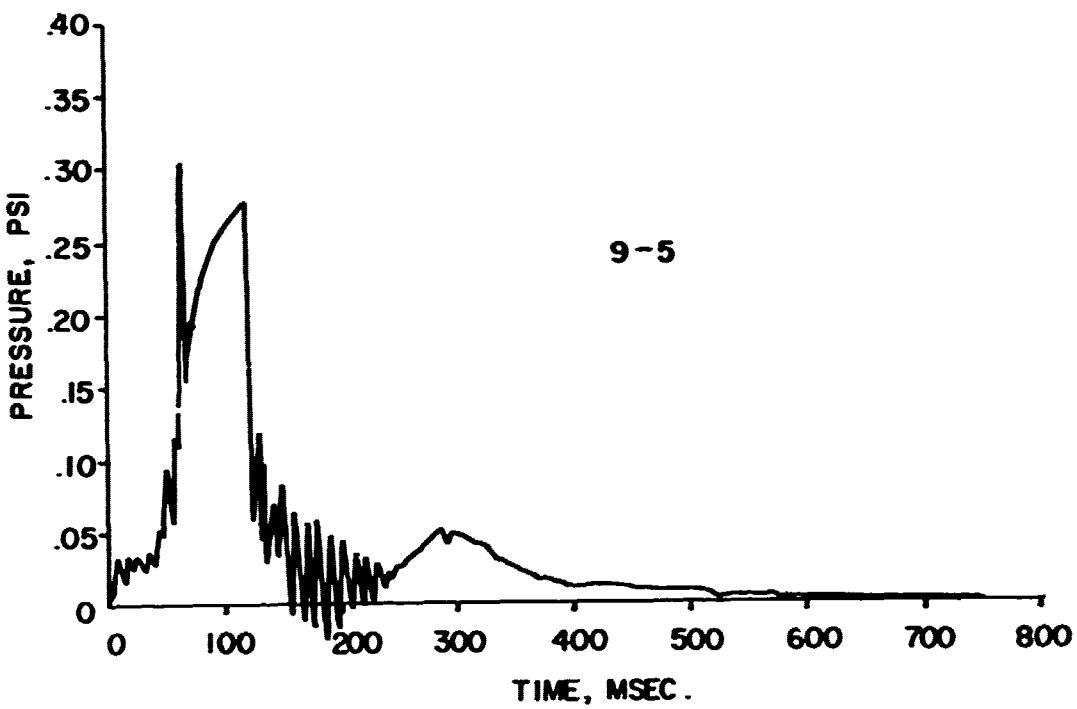

Figure 4.3 Overpressure-time history, VLP Gage 5, Shot Kepler.

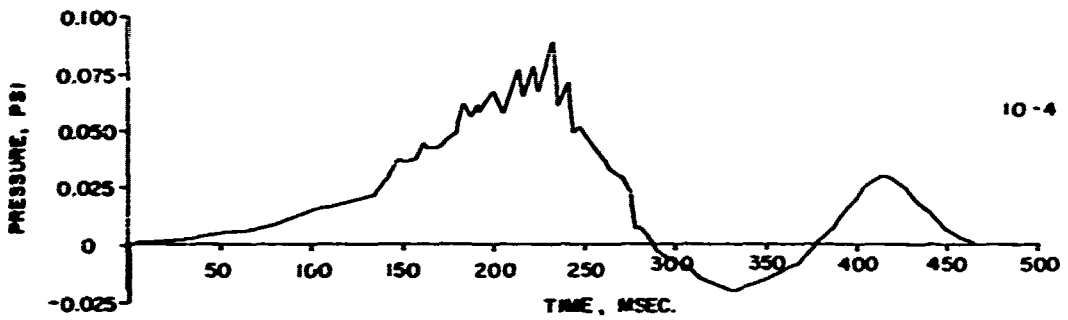

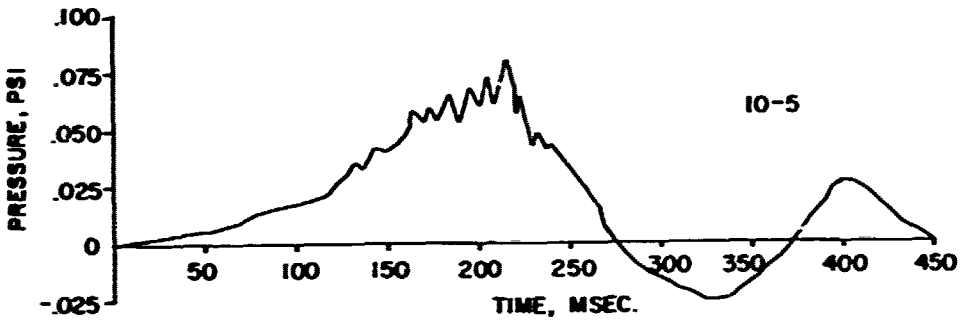

Figure 4.4 Overpressure-time histories, VLP Gages 4 and 5, Shot Owens.

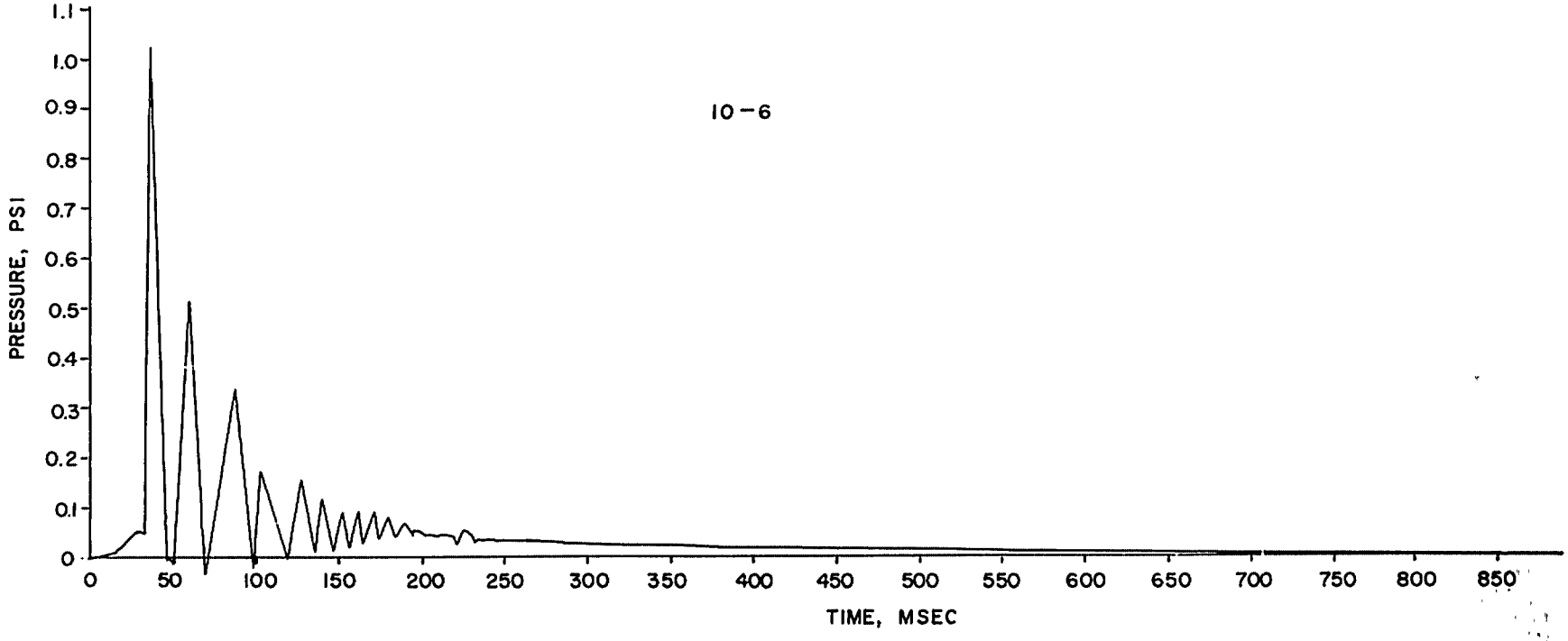

Figure 4.5 Overpressure-time history, VLP Gage 6, Shot Owens.

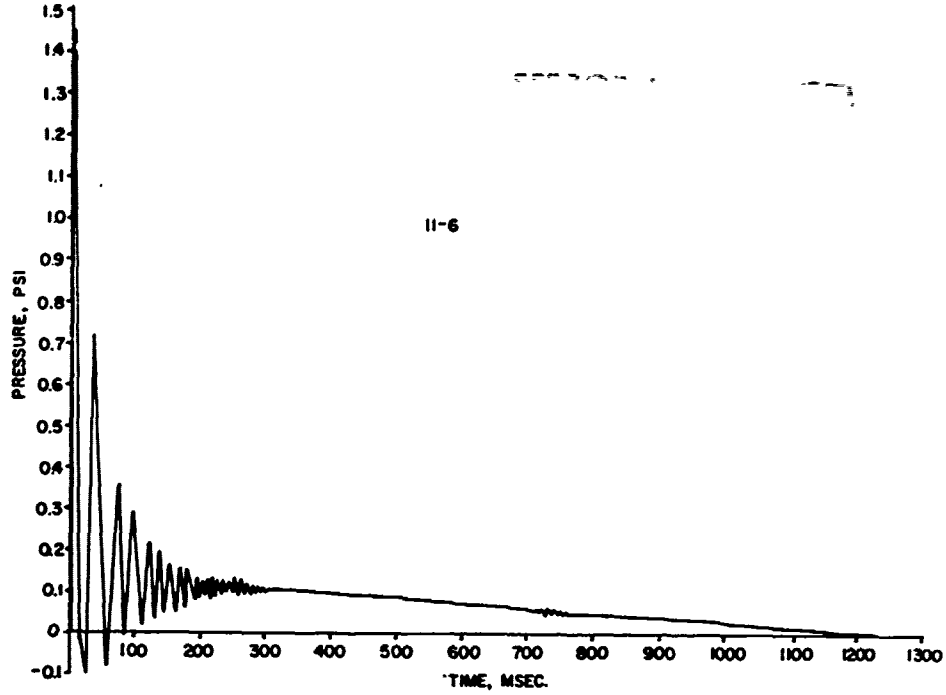

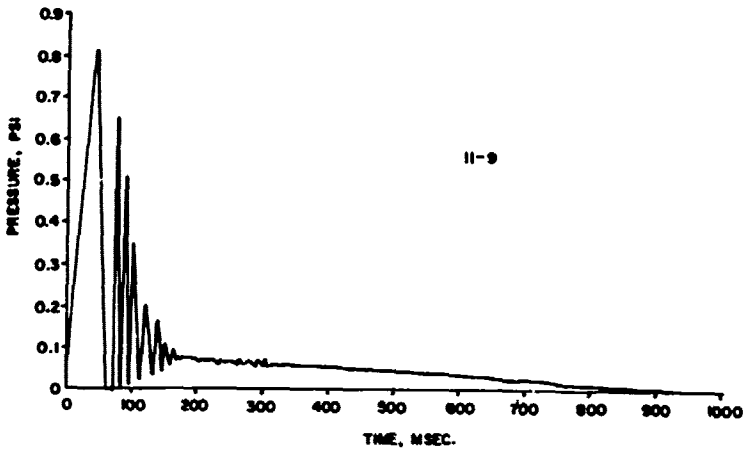

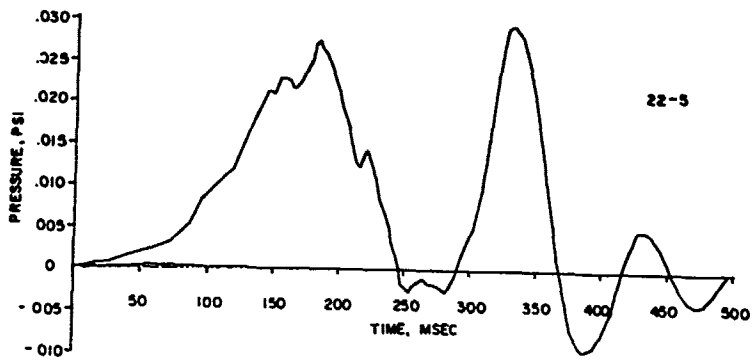

Figure 4.6 Overpressure-time histories, VLP Gages 6 and 9, Shot Stokes; VLP Gage 5, Shot Whitney.

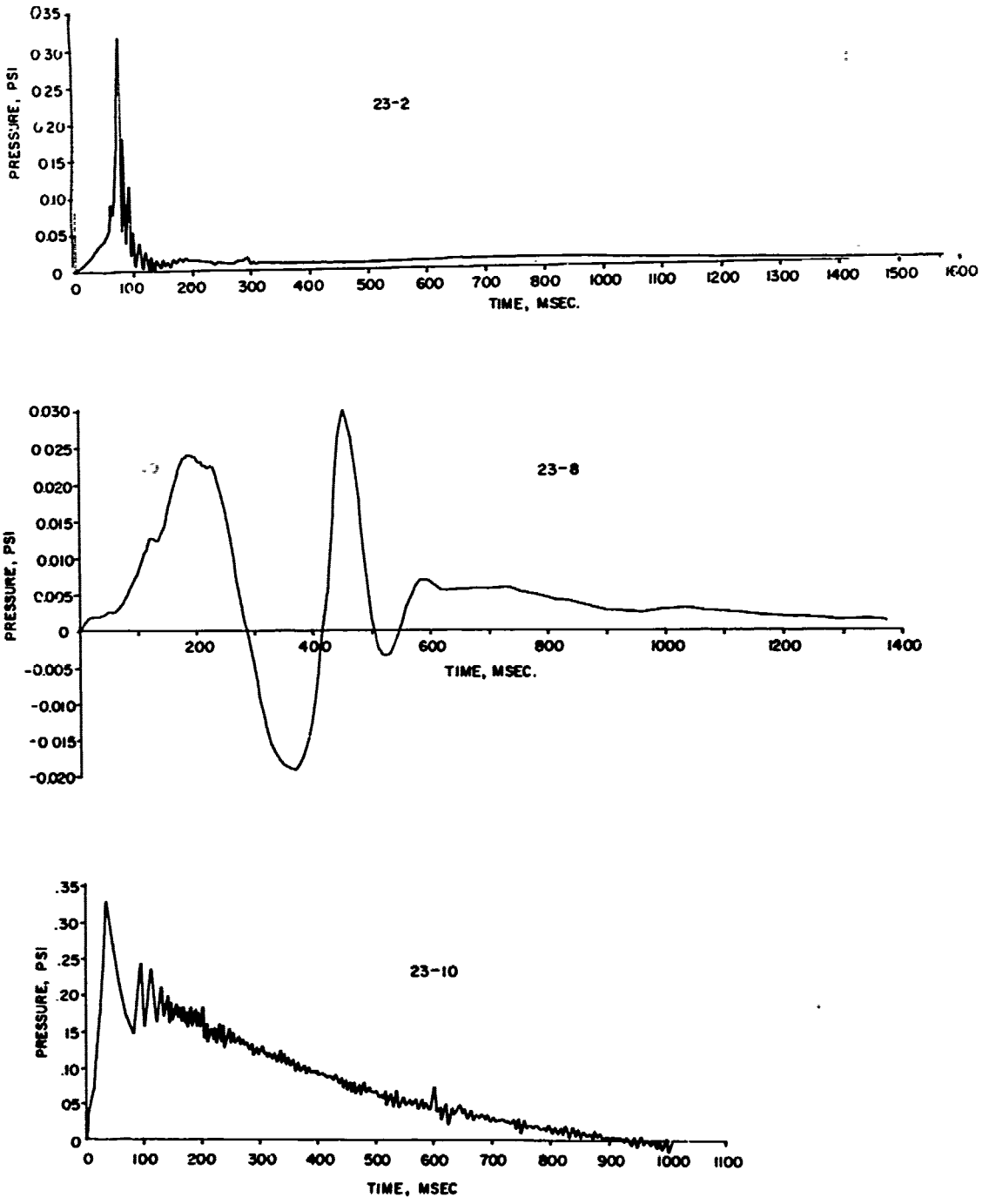

Figure 4.7 Overpressure-time histories, VLP Gages 2, 8, and 10, Shot Charleston.

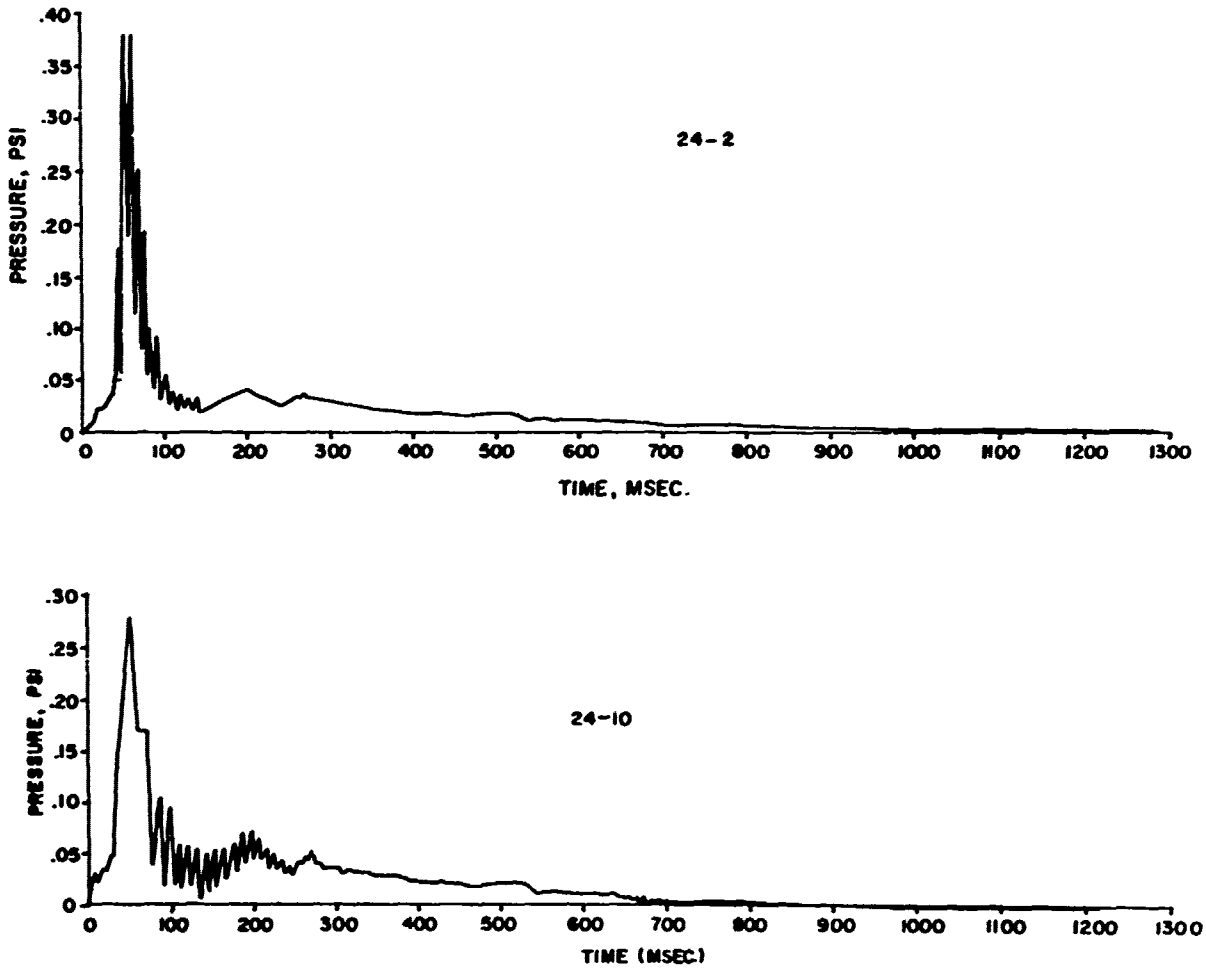

Figure 4.8 Overpressure-time histories, VLP Gages 2 and 10, Shot Morgan.

REFERENCES

1. C. D. Broyles; "Dynamic Pressure versus Time and Supporting Air Blast Measurements"; Project 1.1d, Operation Upshot-Knothole, WT-714, February 1954; Sandia Corporation, Albuquerque, New Mexico; Secret Formerly Restricted Data.

2. L. M. Swift and D. C. Sachs; "Air Pressure and Ground Shock Measurements"; Project 1.1b, Operation Upshot-Knothole, WT-711, January 1955; Stanford Research Institute, Menlo Park, California; Confidential Formerly Restricted Data.

3. W. E. Morris and others; "Air Blast Measurements"; Projects 1.1a and 1.2, Operation Upshot-Knothole, WT-710, August 1955; Naval Ordnance Laboratory Report 1180, U. S. Naval Ordnance Laboratory, White Oak, Silver Spring, Maryland; Confidential Formerly Restricted Data.

4. E. J. Bryant, N. H. Ethridge, and J. H. Keefer; "Measurements of Air-Blast Phenomena with Self-Recording Gages"; Project 1.14b, Operation Teapot, WT-1155, July 1959; Ballistic Research Laboratories, Aberdeen Proving Ground, Maryland; Confidential Formerly Restricted Data.

5. D. C. Sachs, L. M. Swift, and F. M. Sauer; "Airblast Overpressure and Dynamic Pressure over Various Surfaces"; Project 1.10, Operation Teapot, WT-1109, September 1957; Stanford Research Institute, Menlo Park, California; Confidential Formerly Restricted Data.

6. H. L. Brode; "Close-In H-Bomb Effects"; RM 1583; The RAND Corporation, Santa Monica, California.

7. "Capabilities of Atomic Weapons"; Department of the Army Technical Manual, TM 23-200; Department of the Navy, OPNAV Instruction 03400.1B; Department of the Air Force, Air Force Manual 136-1; Marine Corps Publication, NAVMC 1104; June 1955; Armed Forces Special Weapons Project, Washington 25, D. C.; Secret Restricted Data. (This document was revised November 1957; Confidential.)

8. F. B. Porzel; "Theoretical Blast Curves"; (Draft copy), J-17837, 25 May 1953; "Theoretical Blast Curves"; (Draft copy), J-19704, 20 August 1953; Los Alamos Scientific Laboratory, Los Alamos, New Mexico.

9. "Data Reduction Procedures for Nuclear Air Blast Instrumentation"; AFSWP-1084, (Appendix A), August 1959; Armed Forces Special Weapons Project, Washington 25, D. C.

10. "Nuclear Weapons Blast Phenomena", Chapter VI, Volume II, "Nuclear Height of Burst Charts"; DASA-1200, March 1960; Defense Atomic Support Agency, Washington 25, D.C.; Secret Formerly Restricted Data.

11. H. W. Liepmann and A. E. Puckett; "Introduction to Aerodynamics of a Compressible Fluid"; John Wiley and Sons, Inc., 1947.

12. C. H. Hoover; "Determination of Dust Registry Coefficient of BRL Self-Recording "q" Gages from SRI Wind Tunnel Shots"; Information Memo No. 13, Explosion Kinetics Branch, March 1959; Ballistic Research Laboratories, Aberdeen Proving Ground, Maryland.

13. "Wind Tunnel Tests of a Pitot-Static Blast Meter for the Sandia Corporation"; Report No. 384-015-01, April 1953; Cornell Aeronautical Laboratory, Inc.

14. C.N. Kingery, C.H. Hoover, and J.H. Keefer; "Ground Surface Air-Blast Pressure versus Distance"; Project 1.1, Operation Redwing, WT–1301, May 1960; Ballistic Research Laboratories, Aberdeen Proving Ground, Maryland; Secret Restricted Data.

15. E.J. Bryant and L.M. Swift; "Effects of Rough and Sloping Terrain on Airblast Phenomena"; Projects 1.8a and 1.8c, Operation Plumbbob, WT–1407; Ballistic Research Laboratories, Aberdeen Proving Ground, Maryland, and Stanford Research Institute, Menlo Park, California; Unclassified.

16. "Operation Plumbbob Fireball Data, Project 15.1"; 27 December 1957; Edgerton, Germeshausen and Grier, Inc., Boston, Massachusetts.

17. A.N. Julian; "In-Flight Structural Response of an FJ-4 Aircraft to Nuclear Detonations"; Project 5.3, Operation Plumbbob, WT–1432, February 1960; Bureau of Aeronautics, Washington 25, D.C., and North American Aviation, Inc., Columbus Division, Columbus, Ohio; Confidential.

18. F.H. Shelton; "Phenomenology of a High Altitude Atomic Explosion"; SC-3363 (TR), 28 April 1954; Sandia Corporation, Albuquerque, New Mexico.

19. J.W. Reed, J.R. Banister, and F.H. Shelton: "Ground-Level Microbarographic Pressure Measurements from a High-Altitude Burst"; Project 1.3, Operation Teapot, WT–1103; Sandia Corporation, Albuquerque, New Mexico; Confidential.

20. J.W. Bond; "Scaling of Peak Overpressure in a Nonuniform Atmosphere"; SC-1939 (TR), July 1951; Sandia Corporation, Albuquerque, New Mexico.

21. R.G. Sachs; "Dependence of Blast on Ambient Pressure and Temperature"; BRL-466, 15 May 1944; Ballistic Research Laboratories, Aberdeen Proving Ground, Maryland.

22. C.H. Hoover, G. Lovinger, and R.E. Reisler; "Preliminary Report on Low Pressure Gage Calibration—Phase II"; Information Memo No. 22, Explosion Kinetics Branch, Ballistic Research Laboratories, Aberdeen Proving Ground, Maryland.

DISTRIBUTION

Military Distribution Category 12

ARMY ACTIVITIES

1 Deputy Chief of Staff for Military Operations, D/A, Washington 25, D.C. ATTN: Dir. of SWAR
2 Chief of Research and Development, D/A, Washington 25, D.C. ATTN: Atomic Div.
3 Assistant Chief of Staff, Intelligence, D/A, Washington 25, D.C.
4 Chief of Engineers, D/A, Washington 25, D.C. ATTN: ENGNB
5 Chief of Engineers, D/A, Washington 25, D.C. ATTN: ENGEB
6 Chief of Engineers, D/A, Washington 25, D.C. ATTN: ENGTB
7- 8 Office, Chief of Ordnance, D/A, Washington 25, D.C. ATTN: ORDTN
9- 11 Commanding General, U.S. Continental Army Command, Ft. Monroe, Va.
12 Director of Special Weapons Development Office, Headquarters CONARC, Ft. Bliss, Tex. ATTN: Capt. Chester I. Peterson
13 President, U.S. Army Artillery Board, Ft. Sill, Okla.
14 President, U.S. Army Air Defense Board, Ft. Bliss, Tex.
15 Commandant, U.S. Army Command & General Staff College, Ft. Leavenworth, Kansas. ATTN: ARCHIVES
16 Commandant, U.S. Army Armored School, Ft. Knox, Ky.
17 Commandant, U.S. Army Artillery and Missile School, Ft. Sill, Okla. ATTN: Combat Development Department
18 Commandant, U.S. Army Aviation School, Ft. Rucker, Ala.
19 Commandant, U.S. Army Infantry School, Ft. Benning, Ga. ATTN: C.D.S.
20 Commandant, U.S. Army Ordnance and Guided Missile School, Redstone Arsenal, Ala.
21 Commanding General, Chemical Corps Training Comd., Ft. McClellan, Ala.
22 Commanding General, The Engineer Center, Ft. Belvoir, Va. ATTN: Asst. Cmdt, Engr. School
23 Director, Armed Forces Institute of Pathology, Walter Reed Army Med. Center, 625 16th St., NW, Washington 25, D.C.
24 Commanding Officer, Army Medical Research Lab., Ft. Knox, Ky.
25 Commandant, Walter Reed Army Inst. of Res., Walter Reed Army Medical Center, Washington 25, D.C.
26 Commanding General, QM R&E Comd., QM R&E Cntr., Natick, Mass. ATTN: Tech. Library
27- 28 Commanding Officer, Chemical Warfare Lab., Army Chemical Center, Md. ATTN: Tech. Library
29 Commanding General, Engineer Research and Dev. Lab., Ft. Belvoir, Va. ATTN: Chief, Tech. Support Branch
30 Director, Waterways Experiment Station, P.O. Box 631, Vicksburg, Miss. ATTN: Library
31 Commanding Officer, Picatinny Arsenal, Dover, N.J. ATTN: ORDBB-TK
32 Commanding Officer, Diamond Ord. Fuze Labs., Washington 25, D.C. ATTN: Chief, Nuclear Vulnerability Br. (230)
33- 34 Commanding General, Aberdeen Proving Grounds, Md. ATTN: Director, Ballistics Research Laboratory
35 Commanding General, Frankford Arsenal, Bridge and Tacony St., Philadelphia, Pa.
36 Commanding Officer, Watervliet Arsenal, Watervliet, New York. ATTN: ORDBF-RR
37 Commander, Army Rocket and Guided Missile Agency, Redstone Arsenal, Ala. ATTN: Tech Library
38 Commanding General, White Sands Missile Range, N. Mex. ATTN: ORDBS-OM
39 Commander, Army Ballistic Missile Agency, Redstone Arsenal, Ala. ATTN: ORDAB-HT
40 Commanding General, Ordnance Tank Automotive Command, Detroit Arsenal, Centerline, Mich. ATTN: ORDMC-RO
41 Commanding General, Ordnance Weapons Command, Rock Island, Ill.
42 Commanding General, U.S. Army Electronic Proving Ground, Ft. Huachuca, Ariz. ATTN: Tech. Library
43 Commanding General, USA Combat Surveillance Agency, 1124 N. Highland St., Arlington, Va.
44 The Research Analysis Corp., 6935 Arlington Rd., Bethesda 14, Md.
45 Commanding General, U. S. OSD Special Weapons-Ammunition Command, Dover, N.J.

NAVY ACTIVITIES

46- 47 Chief of Naval Operations, D/N, Washington 25, D.C. ATTN: OP-03EG
48 Chief of Naval Operations, D/N, Washington 25, D.C. ATTN: OP-75
49- 50 Chief of Naval Research, D/N, Washington 25, D.C. ATTN: Code 811
51- 53 Chief, Bureau of Naval Weapons, D/N, Washington 25, D.C. ATTN: DLI-3
54- 58 Chief, Bureau of Naval Weapons, D/N, Washington 25, D.C. ATTN: RAAD-25
59 Chief, Bureau of Ordnance, D/N, Washington 25, D.C.
60 Chief, Bureau of Ships, D/N, Washington 25, D.C. ATTN: Code 423
61 Chief, Bureau of Yards and Docks, D/N, Washington 25, D.C. ATTN: D-440
62 Director, U.S. Naval Research Laboratory, Washington 25, D.C. ATTN: Mrs. Katherine H. Cass
63- 64 Commander, U.S. Naval Ordnance Laboratory, White Oak, Silver Spring 19, Md.
65 Director, Material Lab. (Code 900), New York Naval Shipyard, Brooklyn 1, N.Y.
66 Commanding Officer and Director, Navy Electronics Laboratory, San Diego 52, Calif.
67 Commanding Officer, U.S. Naval Mine Defense Lab., Panama City, Fla.
68- 69 Commanding Officer, U.S. Naval Radiological Defense Laboratory, San Francisco, Calif. ATTN: Tech. Info. Div.
70- 71 Commanding Officer and Director, U.S. Naval Civil Engineering Laboratory, Port Hueneme, Calif. ATTN: Code L31
72 Commanding Officer, U.S. Naval Schools Command, U.S. Naval Station, Treasure Island, San Francisco, Calif.
73 Superintendent, U.S. Naval Postgraduate School, Monterey, Calif.
74 Commanding Officer, U.S. Fleet Sonar School, U.S. Naval Base, Key West, Fla.
75 Commanding Officer, U.S. Fleet Sonar School, San Diego 47, Calif.
76 Officer-in-Charge, U.S. Naval School, CEC Officers, U.S. Naval Construction Bn. Center, Port Hueneme, Calif.
77 Commanding Officer, Nuclear Weapons Training Center, Atlantic, U.S. Naval Base, Norfolk 11, Va. ATTN: Nuclear Warfare Dept.
78 Commanding Officer, Nuclear Weapons Training Center, Pacific, Naval Station, San Diego, Calif.
79 Commanding Officer, U.S. Naval Damage Control Tng. Center, Naval Base, Philadelphia 12, Pa. ATTN: ABC Defense Course
80 Commanding Officer, Air Development Squadron 5, VX-5, China Lake, Calif.

[redacted]

81 Commanding Officer, Naval Air Material Center, Philadelphia 12, Pa. ATTN: Technical Data Br.
[illegible] Commanding Officer U.S. Naval Air Development Center, Johnsville, Pa. ATTN: NADC Librarian
[illegible] Commanding Officer, U.S. Naval Medical Research Institute, National Naval Medical Center, Bethesda, Md.
[illegible] Commanding Officer and Director, David W. Taylor Model Basin, Washington 7, D.C. ATTN: Library
[illegible] Commanding Officer and Director, U.S. Naval Engineering Experiment Station, Annapolis, Md.
[illegible] Commander, Norfolk Naval Shipyard, Portsmouth, Va. ATTN: Underwater Explosions Research Division
[illegible] Commandant, U.S. Marine Corps, Washington 25, D.C. ATTN: Code A03H
[illegible] Director, Marine Corps Landing Force, Development Center, MCS, Quantico, Va.
[illegible] Commanding Officer, U.S. Naval CIC School, U.S. Naval Air Station, Glynco, Brunswick, Ga.
[illegible] Chief, Bureau of Naval Weapons, Navy Department, Washington 25, D.C. ATTN: RRRE
[illegible] Commander-in-Chief, U.S. Pacific Fleet, Fleet Post Office, San Francisco, Calif.
[illegible] Commanding General, Fleet Marine Force, Pacific, Fleet Post Office, San Francisco, Calif.

AIR FORCE ACTIVITIES

[illegible] Air Force Technical Applications Center, Hq. USAF, Washington 25, D. C.
[illegible] Hq. USAF, ATTN: Operations Analysis Office, Office, Vice Chief of Staff, Washington 25, D. C.
[illegible] Director of Civil Engineering, HQ. USAF, Washington 25, D.C. ATTN: AFOCE-ES
[illegible] HQ. USAF, Washington 25, D.C. ATTN: AFCIN-3D1
[illegible] Director of Research and Development, DCS/D, HQ. USAF, Washington 25, D.C. ATTN: Guidance and Weapons Div.
[illegible] The Surgeon General, HQ. USAF, Washington 25, D.C. ATTN: Bio.-Def. Pre. Med. Division
111 Commander, Tactical Air Command, Langley AFB, Va. ATTN: Doc. Security Branch
112 Commander, Air Defense Command, Ent AFB, Colorado. ATTN: Operations Analysis Section, ADOOA
[illegible] Commander, Hq. Air Research and Development Command, Andrews AFB, Washington 25, D.C. ATTN: RDRWA
[illegible] Commander, Air Force Ballistic Missile Div. HQ. ARDC, Air Force Unit Post Office, Los Angeles 45, Calif. ATTN: WDSOT
115 Commander, Second Air Force, Barksdale AFB, La. ATTN: Operations Analysis Office
116-117 Commander, AF Cambridge Research Center, L. G. Hanscom Field, Bedford, Mass. ATTN: CRQST-2
118-122 Commander, Air Force Special Weapons Center, Kirtland AFB, Albuquerque, N. Mex. ATTN: Tech. Info. & Intel. Div.
123-124 Director, Air University Library, Maxwell AFB, Ala.
125 Commander, Lowry Technical Training Center (TW), Lowry AFB, Denver, Colorado.
[illegible] Commandant, School of Aviation Medicine, USAF Aerospace Medical Center (ATC), Brooks AFB, Tex. ATTN: Col. G. L. Hekhuis
127-129 Commander, Wright Air Development Center, Wright-Patterson AFB, Dayton, Ohio. ATTN: WCACT (For WCOSI)
[illegible] Director, USAF Project RAND, VIA: USAF Liaison Office, The RAND Corp., 1700 Main St., Santa Monica, Calif.
[illegible] Commander, Rome Air Development Center, ARDC, Griffiss AFB, N.Y. ATTN: Documents Library, RCSSL-1
[illegible] Commander, Air Technical Intelligence Center, USAF, Wright-Patterson AFB, Ohio. ATTN: APCIN-4B1a, Library
[illegible] Assistant Chief of Staff, Intelligence, HQ. USAFE, APO 633, New York, N. Y. ATTN: Directorate of Air Targets
135 Commander-in-Chief, Pacific Air Forces, APO 953, San Francisco, Calif. ATTN: PFCIS-MB, Base Recovery

OTHER DEPARTMENT OF DEFENSE ACTIVITIES

[illegible] Director of Defense Research and Engineering, Washington 25, D.C. ATTN: Tech. Library
[illegible] Chairman, Armed Services Explosives Safety Board, DOD, Building T-7, Gravelly Point, Washington 25, D.C.
[illegible] Director, Weapons Systems Evaluation Group, Room 1E880, The Pentagon, Washington 25, D.C.
[illegible] Chief, Defense Atomic Support Agency, Washington 25, D.C. ATTN: Document Library
[illegible] Commander, Field Command, DASA, Sandia Base, Albuquerque, N. Mex.
[illegible] Commander, Field Command, DASA, Sandia Base, Albuquerque, N. Mex. ATTN: FCTG
[illegible] Commander, Field Command, DASA, Sandia Base, Albuquerque, N. Mex. ATTN: FCWT
147 Administrator, National Aeronautics and Space Administration, 1520 "H" St., N.W., Washington 25, D.C. ATTN: Mr. R. V. Rhode
148 Commander-in-Chief, Strategic Air Command, Offutt AFB, Neb. ATTN: OAWS
149 U.S. Documents Officer, Office of the United States National Military Representative - SHAPE, APO 55, New York, N.Y.

ATOMIC ENERGY COMMISSION ACTIVITIES

150-152 U.S. Atomic Energy Commission, Technical Library, Washington 25, D.C. ATTN: For DMA
153-154 Los Alamos Scientific Laboratory, Report Library, P.O. Box 1663, Los Alamos, N. Mex. ATTN: Helen Redman
155-159 Sandia Corporation, Classified Document Division, Sandia Base, Albuquerque, N. Mex. ATTN: H. J. Smyth, Jr.
160-169 University of California Lawrence Radiation Laboratory, P.O. Box 808, Livermore, Calif. ATTN: Clovis G. Craig
170 Division of Technical Information Extension, Oak Ridge, Tenn. (Master
171-200 Division of Technical Information Extension, Oak Ridge, Tenn. (Surplus)

[redacted]ATA

USAEC Division of Technical Information Extension, Oak Ridge, Tennessee